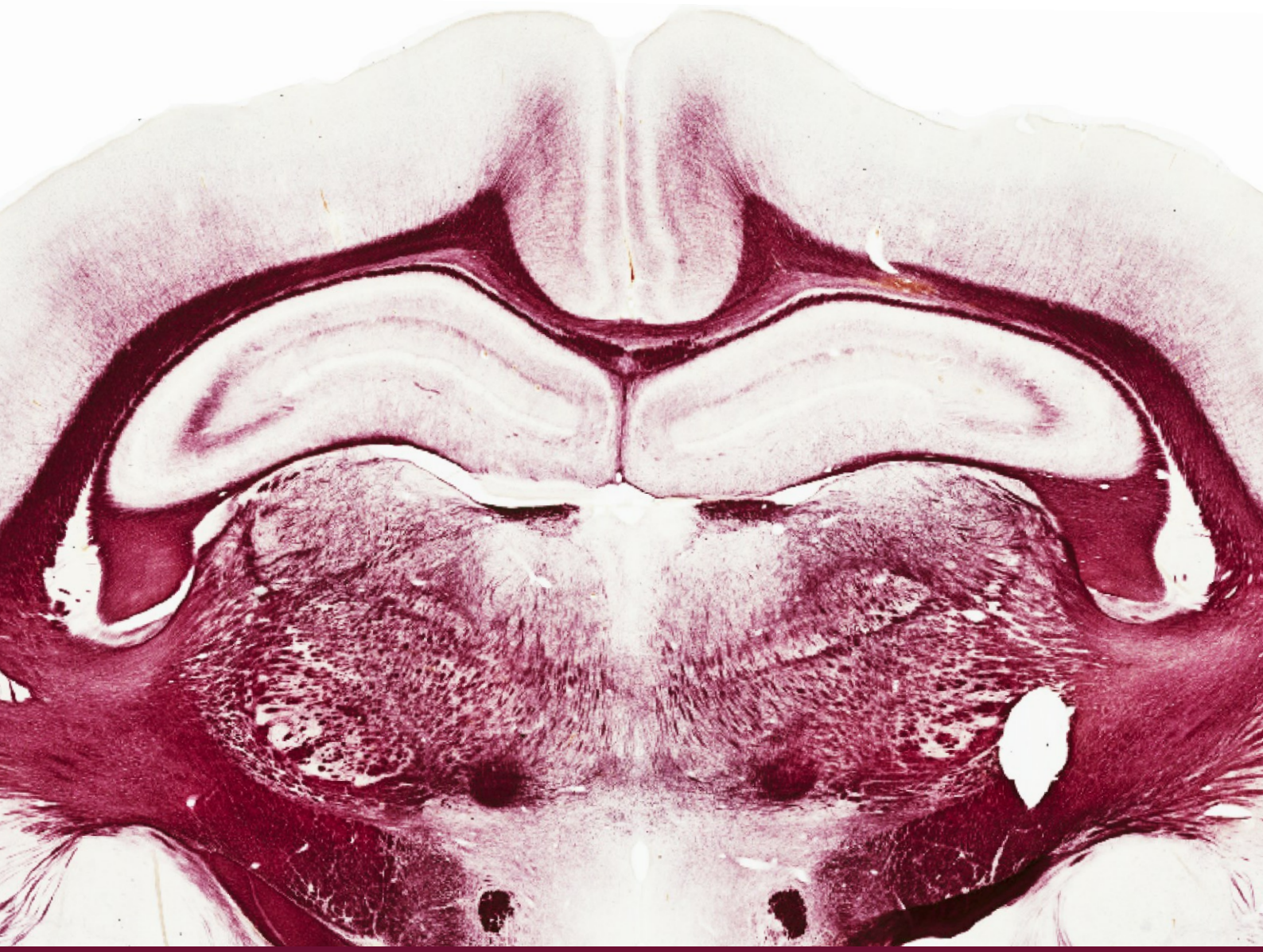

Diogo Miguel Matos Vila Verde

Seizure activity and brain damage: a tale of two hippocampi

PhD thesis in Biomedical Sciences

December 2020

UNIVERSITÀ
DI PAVIA

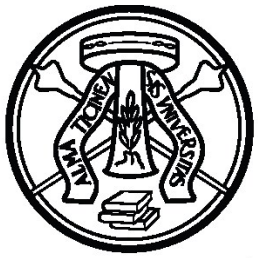

UNIVERSITÀ
DI PAVIA

PhD IN BIOMEDICAL SCIENCES
DEPARTMENT OF BRAIN AND BEHAVIORAL SCIENCES
UNIT OF NEUROPHYSIOLOGY

Seizures activity and brain damage: a tale of two hippocampi

PhD Tutor: Marco de Curtis
PhD Supervisor: Gerardo Biella

PhD dissertation of
Diogo Miguel Matos Vila Verde

a.a: 2019/2020

For Otília

Acknowledgements

First and foremost, I would like to acknowledge Marco de Curtis for believing in me when few did and taking me under his wing. For all the help, mentoring and always pushing me to do better. If it was not for you none of this would be possible so for that, and much more, a big thank you.

To my mom, my wonderful goofy mom. You drive me insane most of the time, but I love you to death. Thank you for being you and always treating me like I am 10 years old even though I am close to 30 now. For all the difficulties and hardships that you endured, thank you for making me who I am.

To the rest of my family, for being present by my side at all times and giving me the support and care I always needed, especially you Félix and my little dork brother Tomás.

To all the people in my laboratory, especially Laura Librizzi, Laura Uva, Alessandro, Francesca and Gerardo, for being my Italian family and always making me feel welcome and helping me in everything that I need.

To all the EU-Glia PhD family consortium, especially Josien, Toni and Giorgio, for being my partners in crime in this EU-Glia journey and making me laugh more times than I can remember. For all the patience and good times, thank you. It would not be the same without you guys.

To all my friends, you know who you are. Thank you for being on my side at all times and making my life a living hell most of the time! I wouldn't trade you for the world.

To my rock, my safe haven, my everything, Marlene. Thank you for moving to another country for me, thank you for your patience, thank you for your love, friendship, laughs and, most of all, thank you for putting yourself in second place time and time again for me. Without you none of this would make any sense. You're my wonderwall. Amo-te.

This work has received funding from the European Union's Horizon 2020 research and innovation programme under the Marie Sklodowska-Curie grant agreement No 722053

Table of Contents

Abbreviations

AQP4	Aquaporin 4
ANOVA	Analysis of variance
BBB	Blood-brain barrier
CA1	*Cornu ammonis 1*
CA3	*Cornu ammonis 3*
CNS	Central nervous system
COX-2	Cyclo-oxygenase-2
Cy3	Cyanine 3
DG	Dentate gyrus
DZP	Diazepam
EEG	Electroencephalography
FJ	Fluoro-Jade
FSGSE	Focal, secondary generalized *Status Epilepticus*
GAPDH	Glyceraldehyde 3-phosphate dehydrogenase
GFAP	Glial fibrillary acidic protein
HO-1	Heme oxygenase-1
Iba-1	Ionized calcium-binding adapter molecule-1
IgG	Immunoglobulin G
IL-1β	Interleukin-1 beta
ILAE	International league against epilepsy
KA	Kainic Acid
K_{ir} 4.1	Inward-rectifier potassium channel 4.1
MAP2	Microtubule-associated protein 2
NCSE	Non-convulsive *Status Epilepticus*
NeuN	Neuronal nuclei
PILO	Pilocarpine
ROI	Region of interest
SD	Standard deviation
SE	*Status Epilepticus*
SSSE	Self-sustained *Status Epilepticus*
TLS-HS	Temporal lobe epilepsy with hippocampal sclerosis

Abstract

Objective: Focal non-convulsive *status epilepticus* (ncSE) is a relatively common emergency condition that in most cases presents itself as first epileptic manifestation. In recent years it became increasingly clear that *de novo* focal ncSE should be promptly treated to improve post-*status* outcome. Whether the presence of seizures during this condition contributes to ensuing brain damage is not unequivocally demonstrated and is here addressed. **Methods:** We used continuous video-EEG monitoring to characterize an acute experimental focal ncSE model induced by unilateral intrahippocampal injection of kainic acid (KA) in guinea pigs. Immunohistochemistry, morphological reconstruction and mRNA expression analysis were used as markers to detect and quantify brain injury at 3 days and 1 month post focal ncSE. To distinguish between the effects of seizure activity *vs* excitotoxic properties of KA, another cohort of animals was generated and i.p. injected with diazepam. **Results:** Seizure activity during focal ncSE involved both hippocampi and neuronal loss was limited to the KA-injected hippocampus. Diazepam treatment reduced both ncSE duration and local KA-induced neuropathological damage. Transient and possibly reversible astro and microgliosis associated with upregulation of astrocytic-specific aquaporin-4 and $K_{ir}4.1$ genes was observed mainly in the hippocampus contralateral to KA injection. Ipsilaterally, permanent gliosis was present and neuronal loss as well as blood-brain barrier dysfunction were not averted. **Interpretation:** Seizures at the site of injection of KA worsen tissue damage. We also show that focal ncSE induces a transient and possibly reversible activation of astro and microglia in regions remote from KA injection, suggesting that seizure activity without a local pathogenic co-factor does not promote detrimental changes in the brain. These findings demonstrate that focal damage remains circumscribed to the lesional region during focal ncSE and that the propagation of seizure activity to regions remote from the primary site of injection did not seem to exert a harmful effect, in this model. Lastly, our study emphasizes the need of antiepileptic treatment to contain the local epileptic focus during focal ncSE.

Keywords: Epilepsy, hippocampus, brain damage, focal non-convulsive *status epilepticus*, seizures

Chapter 1

Introduction

1.1 Status Epilepticus

One of the biggest unanswered questions in the epileptology field for years has been weather seizures are a cause or consequence of brain damage. *Status Epilepticus* (SE) is a neurological emergency with considerable morbidity and mortality[1], characterized by continuous epileptic seizures and epileptic activity that persists without remission for more than 5 min. SE may occur in patients with a pre-existing epileptic disorder, or can be caused by a *de novo,* acute etiology. The newer classification of the International League Against Epilepsy (ILAE) sets two conceptual timelines for SE: a) differentiation between a first threshold beyond which seizures are unlikely to stop (5 min for generalized convulsive seizures, 10 min for focal seizures); b) period of time in which SE can have long-term consequences[2]. For generalized convulsive SE this period of time has been estimated, mostly based on animal studies, at 30 min[2]. Moreover, clinical and imaging studies revealed focal structural alterations in the brain of patients shortly after convulsive SE resolution[3]. While there is increasing experimental evidence that generalized convulsive SE produces long-lasting neuropathologic detrimental changes in the brain of rodents and humans[4–6], non-convulsive *status epilepticus* (ncSE) is one of the greateast diagnostics and therapeutic challenges in modern neurology.

1.1.2- non-convulsive Status Epilepticus

The newer ILAE classification[2] initially categorizes SE semiology into convulsive or non-convulsive, according to the most prominent clinical manifestation (Table 1). The term ncSE includes SE conditions associated with seizures that do not generate motor (mostly, but not exclusively tonic-clonic) movements, and may feature a vast diversity of symptoms depending on the cortical region recruited during SE. This condition can be characterized by very subtle clinical features, such as a change in behavior, mental status or minimal motor symptoms lasting longer than 10 min – often several hours/days. Since the clinical features may be very discrete and sometimes hard to distinguish from normal behavior without EEG monitoring, ncSE is usually overlooked and consequently not treated properly with its long-term effects largely undetermined and controversial among the scientific community.

Table 1- Semiology classification of SE according to ILAE [2]

Main category	Sub-categories	Details
A – Prominent motor symptoms		
A.1 Convulsive SE (a.k.a. tonic-clonic SE)	**A.1.1** Generalized convulsive **A.1.2** Focal onset evolving into bilateral convulsive SE **A.1.3** Unknown focal or generalized	- Focal origin - Difficult to assess clinically - Patient clinical history is of great help
A.2 Myoclonic SE (prominent epileptic myoclonic jerks)	**A.2.1** With coma **A.2.2** Without coma	Generalized SE
A.3 Focal motor SE	**A.3.1** Repeated focal motor seizures **A.3.2** Epilepsia partialis continua **A.3.3** Adversive status **A.3.4** Oculoclonic status **A.3.5** Ictal paresis (focal inhibitory SE)	-
A.4 Tonic SE	-	- Generalized SE - Rare - Mostly present in patients with developmental retardation
A.5 Hyperkinetic SE	-	- Extremely rare - Focal origin
B – No prominent motor symptoms		
B.1 Non-convulsive SE with coma (a.k.a. subtle SE)	-	- May be focal or generalized
B.2 Non-convulsive SE without coma	**B.2.1** Generalized **B.2.1.1** Typical absence status **B.2.1.2** Atypical absence status **B.2.1.3** Myoclonic absence status	
	B.2.2 Focal **B.2.2.1** Without impairment of consciousness **B.2.2.2** Aphasic status **B.2.2.3** With impaired consciousness	In **B.2.2.1**: - Aura continua - Autonomic, sensory, visual, olfactory, gustatory, emotional,

		physic or auditory symptoms
	B.2.3 Unknown focal or generalized **B.2.3.1** Autonomic SE	- Focal origin - Very rare

NCSE can be of generalized or focal origin[2]. Primary generalized ncSE typically occurs in patients with genetic (idiopathic) epilepsy (*e.g.*, absence SE) and seems to carry few, if any, long-term morbidities with no evidence of neuropathology[2]. Absence SE, indeed, may occur several times in patients without obvious *sequelae*[7]. SE may also present itself as focal ncSE due to a localized brain dysfunction and focal epileptiform EEG activity; this may or may not secondarily develop into tonic-clonic seizures with diffuse epileptiform EEG discharges. Therefore, patients with focal ncSE may also suffer from generalized seizures (focal, secondarily generalized *status epilepticus* – FSGSE). Recent epidemiological assessments of SE, applying the newer ILAE definition[2], indicate a prevalence of focal ncSE in 36 % of all SE cases; When FSGSE arising from an initial focal ncSE is included in the statistics, its prevalence increases to 65-85%, suggesting that focal ncSE represents the most frequent form of human SE[8,9].

The majority of focal ncSE etiologies are related to acute cortical injuries (such as cerebrovascular diseases, brain trauma, infections) or progressive conditions (e.g., tumor, neurodegenerative diseases), which are always related to focal alterations in the brain. Furthermore, several studies suggest that the underlying etiology, age of onset, and pre-existing comorbidities represent the most important determinants of SE prognosis, long term consequences and pathology[10–12]. Additionally, clinical studies have shown that ncSE produces blood biomarkers of neuronal damage even without an acute brain injury[4,13,14] and that patients suffering from focal ncSE have a higher mortality than patients with the same underlying disease (stroke, anoxic-hypoxic encephalopathy, etc.) that did not experience a focal ncSE[15–17]; all cohorts, however, analyzed patients with focal ncSE and FSGSE together. On the other hand, other data suggests that focal ncSE may be associated with a transient brain cognitive/neurological decline, followed by complete resolution and clinical remission within hours/days/weeks[18,19] with no evidence of long-term cognitive, memory or behavioral abnormalities[20–23]. Also, neuropsychological examinations performed before and after focal ncSE (both focal and FSGSE) in patients with pre-existing epilepsy did not show any differences in these studies[24,25].

A chronic epileptic condition can be the consequence of both focal ncSE and FSGSE. The most common type of chronic focal epilepsy, temporal lobe epilepsy with hippocampal sclerosis (TLE-HS), is proposed to recognize repeated or prolonged febrile seizures[26] or a focal ncSE as initial precipitating factors. This condition is characterized by focal uni or bilateral seizure activity associated with gliosis, major neuronal loss in *cornu ammonis* (CA)1, CA3 and the hilus as well as occasional mossy fiber sprouting and granule cell dispersion in the dentate gyrus[27,28]. Generally, it is preceded by an initial precipitating event in early life (trauma, infection, prolonged febrile seizure, etc.) with or without an obvious SE condition. Spontaneous epileptic seizures in TLE ensue after a highly variable latent period from the initial acute episode, during which alterations leading to epileptogenesis and HS occur[29].

Available clinical data is not clear enough to discriminate the specific actions of the underlying SE etiologies from that exerted by prolonged epileptiform activity. This information is clinically relevant, since complete seizure control is commonly enforced to prevent long-term consequences, in spite of the fact that aggressive anti-seizure treatment protocols may expose patients to potentially dangerous side effects[22,30]. Due to the intrinsic limitations of the studies performed on patient cohorts, animal studies have proven to be a fundamental tool.

1.2 Animal models

Several experimental protocols have been used to induce SE in rodents, and they can mainly be divided into two main groups: injection of chemotoxins (either systemic or intracerebral) or electrical stimulation. Also, new models such as the lateral-fluid percussion injury[31] and SSP-saporin[32] have emerged in recent years but are still not as widely used as the previous models.

1.2.1- Systemic application of chemoconvulsants

Systemic pilocarpine (PILO) or kainic acid (KA) are commonly used, inducing acute convulsive SE with widespread multifocal damage[33–36] and for these reasons cannot be considered as sheer models of focal ncSE[37]. In various animal species (rat, mouse, cat)

these treatments induce SE within an hour and result in multifocal lesions of cortical and subcortical brain structures. Moreover, SE promoted by systemic KA and PILO initiates with multi-focal epileptiform discharges that rapidly evolve into secondarily convulsive generalized seizures[38]. The presence of prolonged convulsive seizures and the possible diffusion of the systemic-applied convulsant in specific brain regions (such as brainstem nuclei) induces a diffuse neuropathology and is associated with a high rate of mortality[39]. The chronic alterations induced by systemic PILO and KA include typical temporal-limbic pathology that partly mimics the findings in human TLE-HS[40], but generally the neuropathology is widespread in brain areas that are usually not affected in patients with TLE-HS. Therefore, systemic KA and PILO post-SE models have been inaccurately identified as models of mesial TLE and focal ncSE, due to the multifocal and bilateral alterations[37] present in this model that are not found in human TLE-HS[41,42].

1.2.2- Intracerebral drug application

Intracerebral KA injection offers a better approach to focal induction of ictogenesis and epileptogenesis[43]. This includes intra-hippocampal[44–47], intra-amygdala[48–50] and intra-cortical microinjections[51] of KA resulting in pathological alterations that closely resemble TLE-HS. Some studies propose that the acute SE promotes secondary epileptogenesis and alterations in brain regions remote to the KA injection site[45,48,49,52,53]. Nevertheless, intracerebral KA injection may cause either focal ncSE or FSGSE, depending on the protocol (dose, site of injection, etc.) and animal species[44,46–48,54]. A small volume of KA (typically 50 nl- 0.5 µL depending on the brain area) at a concentration that varies between 7 ng up to 0.4 µg is slowly injected through a cannula inserted in the target region, usually CA1 or CA3 hippocampal regions[43] (amygdala is another common area of injection[53]). An extended overview of the current literature in regard to the intra-hippocampal KA animal model can be found in Figure 1. If the protocol includes video-EEG monitoring of the SE, KA injection is followed within few minutes by EEG-seizure activity in the injected region. SE may spontaneously recede or can be blocked by intraperitoneal injection of a benzodiazepine, commonly diazepam[55].

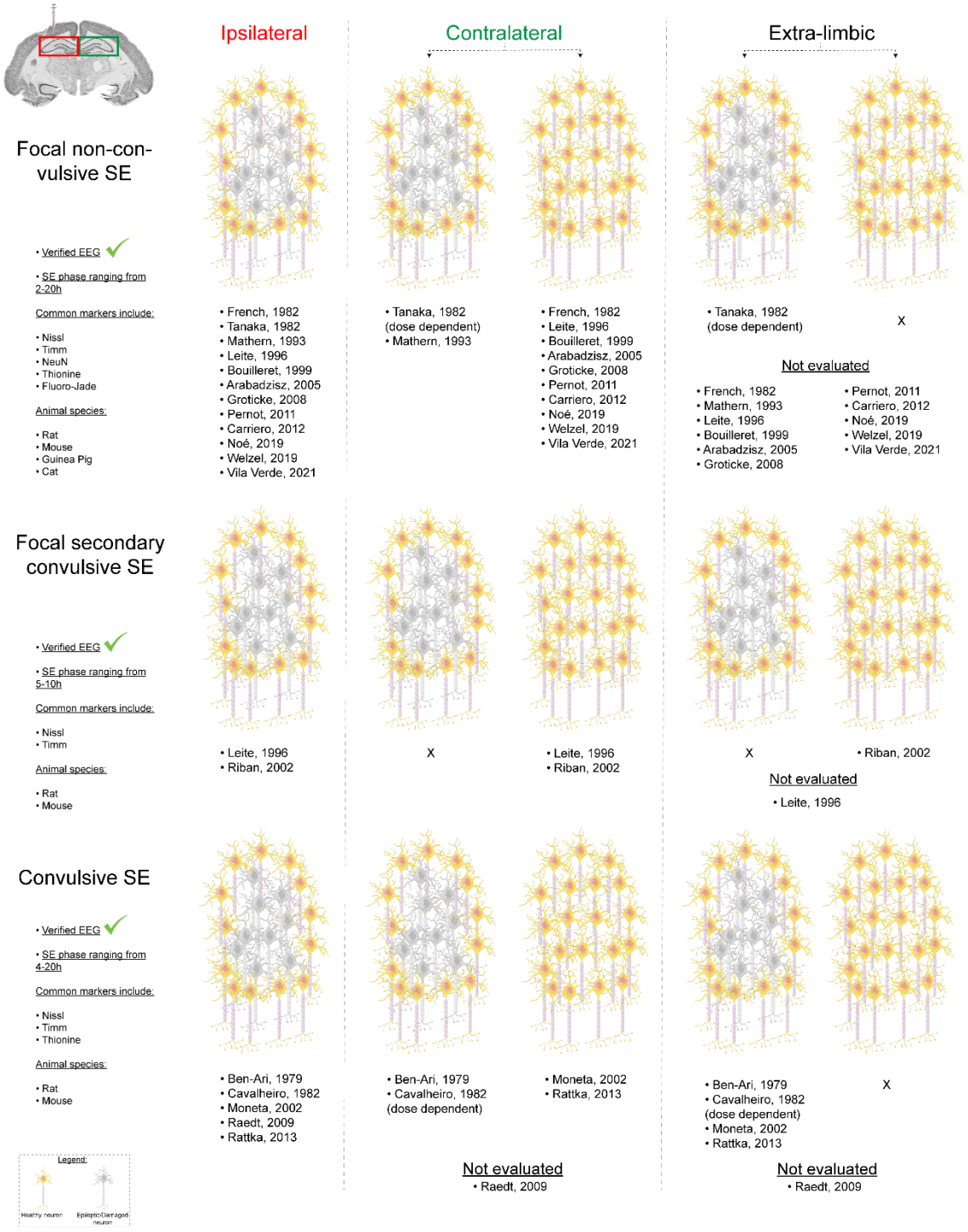

Figure 1- Overview of relevant literature for the intra-hippocampal KA animal model. Details such as SE duration, common markers analyzed and animal species are given to better understand in which specific papers neuronal damage was found ipsilateral (first column), contralateral (middle column) to KA injection and, also, in extra-limbic regions (last column). Literature is also divided by which type of SE was observed: focal non-convulsive SE (focal ncSE – first row), focal secondary convulsive SE (FSGSE – second row) and convulsive generalized SE (third row). Only literature where EEG/video-EEG was employed was included in order to properly classify which SE animals developed. X represents no studies found fitting that category. Not evaluated indicates that in those particular papers, that evaluation was not carried out.

As previously mentioned, since most protocols involve temporal lobe areas, a focal TLE-HS develops following a variable latent period after the initial SE in the majority of animals. Seizure semiology include a combination of reduced consciousness, oral/facial automatisms and repeated secondary generalization with tonic-clonic movements in some cases[43,56–58]. Seizure behavior has often been graded according to a motor symptom-oriented severity scale (Racine scale[59]). Seizure semiology and electrographic activity (focal ncSE *vs* FSGSE) during SE may explain the variation of reported pathophysiology after focal ncSE[44,60–62] and thereby represents a substantial confounder when distinguishing SE-induced and subsequent spontaneous seizure-related pathophysiology. In principle, a proper focal ncSE model (comparable to B2.2 sub-category in Table 1) should correlate with focal seizures with a minimal (if any) number of convulsive seizures. This aspect is crucial, since generalized seizures associated with FSGSE have been demonstrated to correlate with extensive brain damage[53,54].

1.2.3- Intracerebral electrical stimulation

Alternatively, focal electrical stimulation of the perforant path or other limbic structures can also induce either focal or secondary convulsive SE, with or without damage beyond the area of stimulation[56,57,63–65]. Since stimulation can be timely stopped in these models, the severity of the SE is often better controlled compared to the pharmacological models (KA, PILO, etc.). Two main stimulation protocols are commonly used: high frequency (>20 Hz) tetanic stimulation for max 60-90[58] min with or without low frequency (<2Hz) prolonged stimulation, leading to a self-sustained *status epilepticus* (SSSE). Even though the perforant path is the most often used region for the stimulation, the amygdala stimulation is often employed as well[66,67].

In the electrical rodent models, animals are implanted with isolated stainless-steel electrodes into the desired region and 1-2 weeks later, thresholds for electrographic after discharges are assessed, followed by electrical stimulation. The stimulation induces a subsequent self-sustained continuous electrographic seizure activity measured by the implanted electrodes. The SE was originally described to self-terminate after around 8 h[68], but has in several subsequent studies been interrupted after ± 2 h with pentobarbital or benzodiazepines (diazepam). SSSE seizure semiology varies between animals and, typically, 3 distinct behavioral types of SSSE can be observed: a) continuous focal

seizures; b) continuous focal seizures, repeatedly interrupted by generalized convulsive seizures; and c) continuous generalized convulsive seizures[69].

Similar to the intracerebral models, a classification into two different SE types was defined in this model: a predominant (>90% of the time) focal ncSE with focal seizures featuring ambulatory, explorative behavior, orofacial movements, salivation and chewing with impaired consciousness and a FSGSE (>70%) characterized by long-lasting convulsive tonic-clonic movements (secondary generalized from a focal origin)[70]. The brain pathology following these different focal SE is very diverse. Histological analysis of rat brains after the different SSSE types indicated that neuronal loss after focal SSSE was much more regionally restricted and less severe compared to neuronal damage after SSSE with generalized convulsive seizures, which was similar to the brain damage seen in the KA and PILO models of TLE-HS[69]. For example, Mohapel and colleagues observed 1 week post-SE for both focal ncSE and FSGSE increased programmed cell death/apoptosis within the dentate gyrus of the hippocampus, and exclusively in FSGSE was still present after 1 month[70]. In these models, local pathology at the site of stimulation is invariably observed and the contralateral hippocampus may also express damage markers, in particular when the SE is characterized by convulsive seizures.

Overall, regardless of the model, animal data has revealed important aspects of focal ncSE and its consequences but have not proven to be conclusive, since the large majority of these studies do not accurately represent a model of focal ncSE without a secondary generalization, and to this day there is still scientific debate on how much these focal ncSE seizures, and their associated spontaneous recurrent seizures are “provokers or bystanders” to neuronal loss and glial dysfunction, producing long-lasting harmful consequences to the brain.

1.3 Neuronal injury in focal ncSE

As previously mentioned, intracerebral administration of drugs has major advantages to study the effects of a focal ncSE in comparison to systemic overall brain-damaging models that are aimed most of the time at the induction of a convulsive SE. However, the question of how much seizure activity during focal ncSE (without secondary generalization) and subsequently during spontaneous seizures contribute

directly to neuronal loss is still debatable. Even though the majority of authors seem to agree that at the local site of injection neuronal loss is a common feature during SE, no consensus has been found regarding the impact of seizure activity on other regions away from the injection site that are producing seizure activity as well. Regarding the intracerebral injection in the hippocampus for example, while some authors show that neuronal injury during ncSE is restricted to the injected hippocampus, with few alterations in the contralateral hippocampus[45,52,65,71–74], other have reported neuronal loss not only contralaterally but also in extra-hippocampal regions such as the amygdala and cortex[47,62,75]. Moreover, concerning chronic epileptic seizures, data have shown in the past that further seizures after the initial epileptogenic insult do not necessarily lead to progressive cell loss. Whereas some authors argue that both the initial insult as well as recurrent seizures contribute to damage development[75], others show a lack of clear association between the number of lifetime seizures and the severity of neuronal loss in the hilus [67] with a follow-up study demonstrating the ongoing neuronal damage 8 months after ncSE with fluoro-jade positive cells in the hippocampus present in only 1 of 8 rats, even though all animals had recurrent spontaneous seizures[76]. This and similar findings in both rats and humans suggest that further seizures after the initial epileptogenic insult do not necessarily lead to progressive cell loss[77–79].

One major aspect of neuronal loss evaluation that should be taken into account and creates discrepancy between studies (besides dosage, animal species and protocol) is how case dependent this evaluation is. The interpretation of the data should be done differently depending on which region is being evaluated (ipsilateral *vs* contralateral *vs* extra-hippocampus) as well as at different time points after focal ncSE to consider the development of cell loss in a time-dependent manner (Figure 2).

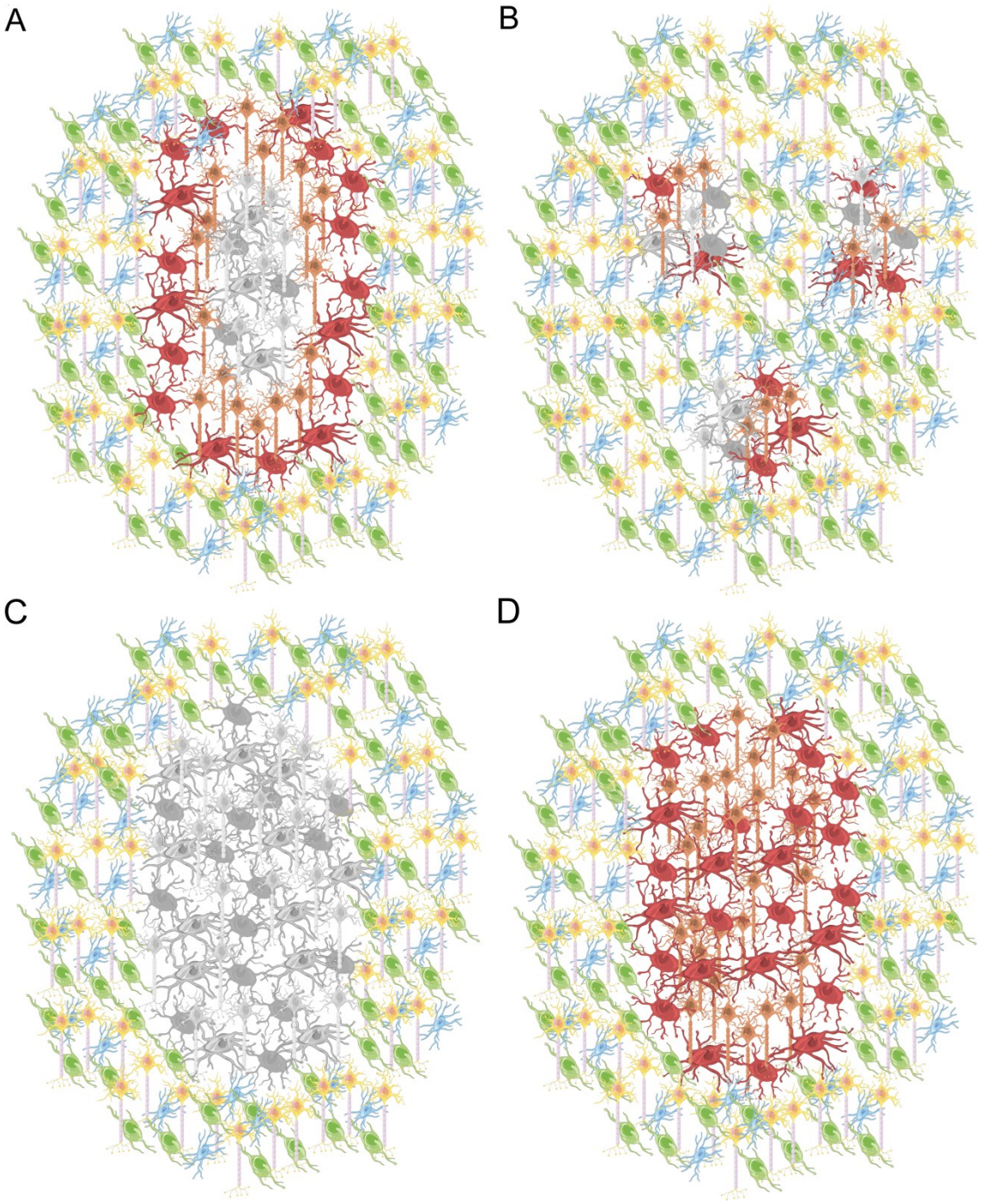

Figure 2- Scheme of hypothetical relationships of neuronal and glial populations after focal ncSE induced neuronal death. In all figures: green cells: resting astrocytes; blue cells: resting microglia; yellow cells: normal neurons; orange cells: epileptogenic neurons; red cells: reactive astrocytes and microglia; grey cells: dead neurons/astrocytes/microglia. **(A)** Focal neuronal and glial loss. A small cluster of dead neurons and glial cells is shown to be clumped together within a network of normal cells. Between these 2 completely different populations is the group of neurons that are hypothetically epileptogenic surrounded by astro and microgliosis. **(B)** Diffuse neuronal loss. This scheme illustrates scattered neuronal and glial loss as well as epileptogenic neurons enclosed by gliosis spread across different areas. **(C)** Neuronal and glial death without generation of epileptogenic neurons and gliosis. **(D)** Absence of neuronal/glial death with the presence of a cluster of epileptogenic neurons and gliosis.

When considering neuronal loss in models of intracerebral focal ncSE, different situations can arise that should be considered: typically, what happens after the chemoconvulsant injection into the brain is the development of an injection zone that has the normal excitotoxic death of neurons and glia (grey cells in hypothesis A in Figure 2) associated to the properties of the chemoconvulsant substance. At the same time, an outer-near region develops, with all the inflammatory processes induced by activated astro and microglia (red glia in hypothesis A in Figure 2) causing neurons to become dysfunctional and epileptogenic (orange in hypothesis A in Figure 2) generating seizure activity and most likely recurrent spontaneous seizures. However, other scenarios should be considered as well: it can also happen that after injection, a diffuse neuronal loss occurs generating a dispersed gliosis and neuronal loss/epileptic neurons across different brain regions (hypothesis B in Figure 2). This obviously requires analysis not only of the injected area but across different regions remote to the injection zone (contralateral hippocampus, amygdala, etc.) that might be disregarded if the evaluation of these extra-injection regions is not carried out. Furthermore, it can also occur (as depicted in hypothesis C in Figure 2) that the injection induces a zone where all glial cells and neurons (epileptic or not) enter apoptosis in a time dependent manner. If the analysis is carried too early, this region might be still developing apoptotic processes and show levels of neuronal loss that do not properly reflect the final outcome. A good example of this situation could be when the hippocampus is injected and develops seizure activity during focal ncSE, but no chronic spontaneous seizure activity arises after the latent phase due to the absence of dysfunctional epileptogenic neurons and, in consequence, epileptogenesis does not occur. Lastly, in hypothesis D of Figure 2, a scenario could befall where no cell loss is observed but the epileptogenic zone is formed, and seizure activity is being generated. This situation can potentially evolve into scenario A or C from Figure 1 or, on the other hand, can be a transient effect and after a period of time all glial cells return to their resting states and epileptic neurons remain generating spontaneous seizure activity with no cell loss. A prime example of this situation occurs (in some studies[72–74]) when you have the contralateral hippocampus that generates seizure activity, but no cell loss is observed. Of note, it should be mentioned that these hypotheses are not static, and one hypothesis can evolve and become another one with the passage of time.

Another fundamental aspect of evaluating cell loss (and many other processes) in focal ncSE is to take into account how glial cells, that innately affect neuronal network proper functioning, are responding to the experimental conditions.

1.4 Glial homeostasis in focal ncSE

Glial cells are highly complex cells that are considered the "glue" of the brain since they have a multitask housekeeping function that requires them to not only sense but also respond to many signals, including alterations in energy supply, neuronal activity, extracellular ion concentrations, osmolarity, among many others. Their dysfunction has been for decades associated to epilepsy mainly through hyperexcitability and inflammatory-related processes (see extensive reviews[80,81]). Inflammation in the brain is triggered by reactive astrocytes, microglia and endothelial cells of the blood-brain barrier (BBB) that induce activation and synthesis of pro-inflammatory cytokines and enzymes that are able to cause major neuronal dysfunction, death and seizure induction (Figure 3). Furthermore, brain inflammation is able to affect the permeability of the BBB directly via cytokine-mediated activation[82]. Studies have shown a quick inflammatory response to acute seizures that largely implicates interleukin-1β (IL-1β) signaling pathway, promoting chronic neuronal hyper excitability and synaptic reorganization, contributing to the pathophysiologic process of epileptogenesis[80,83]. In turn, seizure activity is able to trigger the production of inflammatory molecules that affect seizure severity and recurrence[84], creating a loop that perpetuates brain damage (Figure 3). Profound gliosis has been observed in models of intrahippocampal focal ncSE in the injected hippocampus[46,52,72,74,85]. However, similar to the neuronal loss evaluation, contralateral or extra-hippocampal gliosis in these models has been inconsistently described: while in some studies, no gliosis was found in regions remote to injection[46,72,73], others have reported GFAP immunoreactivity also contralateral to KA injection[52,85–87], with one of these studies reporting a reactive astrogliosis that is maintained over time in the ipsilateral hippocampus, but decreases to control levels on the contralateral side[52].

Interestingly, it has been shown that astro and microgliosis associated with inflammation can have neuroprotective roles[88,89]. In fact, data shows that for instance microglia can be either neuroprotective or harmful depending on their activation status,

which in turn is dependent on the inflammatory mileau[88,90]. This balance, together with the extent of gliosis (persistent *vs* transient effect), might explain why there is a relatively low incidence of seizure activity in other neurological disorders associated with brain inflammation.

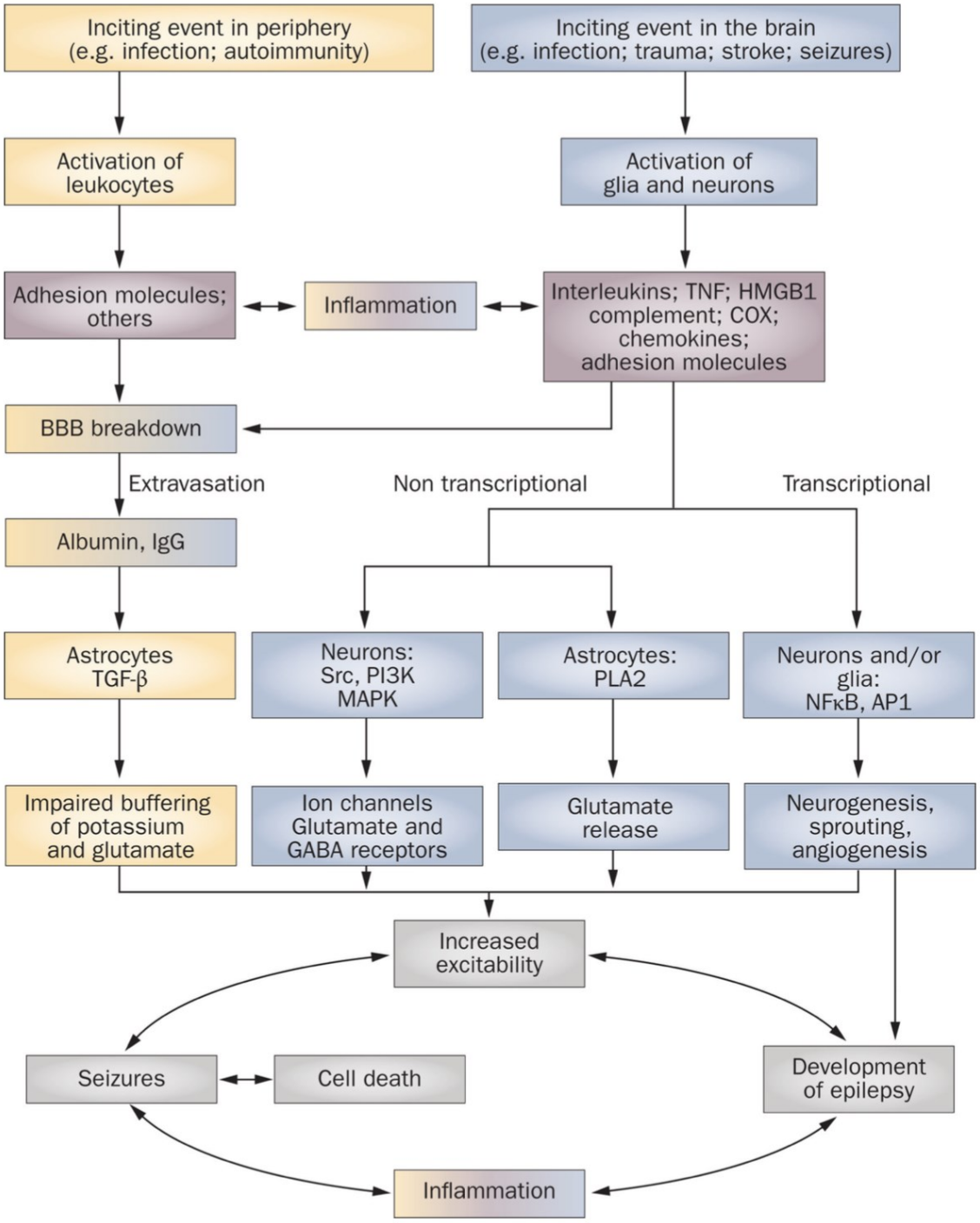

Figure 3- Pathophysiological scheme of inflammatory events linked to epilepsy. These events can be initiated in the central nervous system (CNS) by local injuries or peripherally following infections or autoimmune disorders that lead to activation of glia/neurons or leukocytes, respectively. These cells release

inflammatory mediators into the brain or blood, thereby provoking a cascade of inflammatory processes that cause a spectrum of damaging outcomes. The effects of brain inflammation contribute to the generation of seizures and cell death, which, in turn, activates further inflammation, thereby establishing a circle of events that contributes to the development of epilepsy. Peripheral pathway is shown in yellow; CNS pathway is in blue; inflammatory molecules are shown in pink. Merged colors indicate the contribution of each pathway to inflammation and blood-brain barrier (BBB) damage. Adapted from[91].

In summation, studies have not unequivocally resolved whether seizure activity alone occurring during focal ncSE have an impact on the extent, severity and distribution of brain damage since this damage has been mainly evaluated in models that either do not accurately represent a proper focal ncSE condition without secondarily convulsive generalization or do not focus on the role of seizure activity in regions remote to the local injection zone.

With all this in mind, our present study is focused on how much seizure activity *per se* affects the development of both localized and remote brain damage in a model of focal ncSE without secondary generalization.

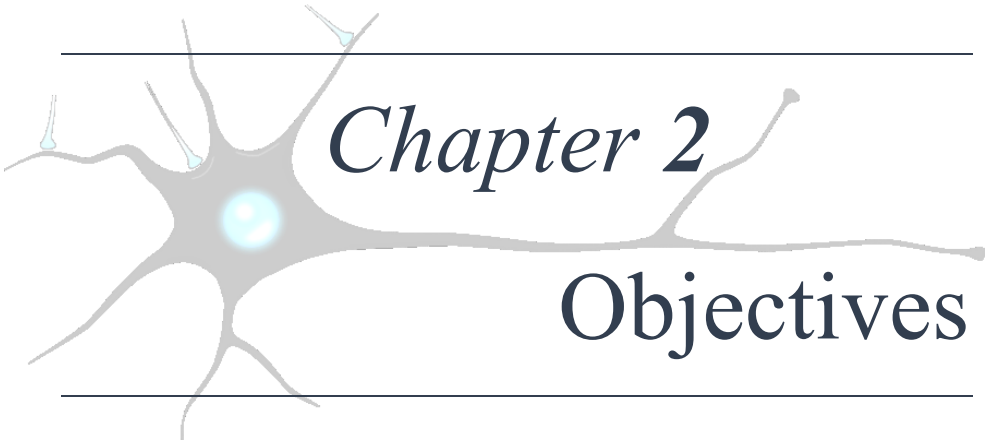

Chapter 2

Objectives

2.1 Aim of the work

With the present study we sought to better clarify the role of seizure activity alone in the development of brain damage and epileptogenesis not only in the local region of injection but also in a remote region where there is no direct excitotoxic effect of the injected chemoconvulsant. In order to do, we used a previously characterized intrahippocampal kainic acid (KA) animal model of focal ncSE without secondary generalization, defined as a model in which non-convulsive focal seizures occur during the SE acute phase that, after a latent period, mimics human TLE-HS with the development of hippocampal sclerosis and spontaneous chronic seizures[72–74].

Following this rational, we injected KA in the right hippocampus of guinea pigs and after proper video-EEG evaluation, we examined the molecular changes that occurred in the injected hippocampus (ipsilateral) to assess the local damage produced by KA + seizure activity. Moreover, in order to study a remote region that was not affected by the excitotoxic effect of KA but was generating seizure activity independently (as verified with EEG recordings) we also examined the contralateral hippocampus to understand how much seizure activity *per se* was able to promote long-lasting brain alterations.

Accordingly, the hippocampus of each guinea pig ipsilateral and contralateral to KA injection were separately analyzed in 3 main experimental conditions, with 3 different reasonings for each cohort:

Acute SE phase: In this group, our aim was to evaluate the more intense acute damage provoked by the focal ncSE phase and likewise animals were followed for 3 days post-KA injection to encapsule the main acute changes in this model (as previously described[72]).

Chronic epileptic phase: Taking into consideration that the proper evaluation of brain damage should be done at various time-points, since cell loss can develop in a time-dependent manner, we produced another animal cohort that was similarly injected and developed focal ncSE as the previous group, but were followed for 1-month post-KA injection (previously shown as the average time to develop a chronic condition in this animal model[72–74]). Moreover, in this group, not only we followed cell loss over time, but we were also able to evaluate if recurrent spontaneous seizure activity would be responsible for the exacerbation of the already established damage assessed in the 3-days

post-injection animal group. With this information we were able to understand how much seizure activity *per se* would be responsible for the development of brain damage without the contribution of all the damaging processes occurring in parallel with seizure activity during SE.

Diazepam treated group: By injecting diazepam systemically before KA injection, we were able suppress most of seizure activity (as previously shown[55]) and generate an acute 3-days animal group in which the only damage observed was due to the cytotoxic effects of KA. By comparing this group (KA damage) against the acute 3 days focal ncSE animal cohort (KA + seizures) we were able to indirectly observe how much local damage was produced by KA alone and how much seizure activity "on top" of KA would exacerbate this damage. This knowledge was critical to understand if, in a clinical point of view, the presence of seizures during focal ncSE would be able to induce a higher degree of brain damage sequalae compared to the underlying cause (trauma, infection, etc.) that triggered the focal ncSE would do alone without seizure activity.

In order to accomplish our goals, after generating our experimental groups and validating our video-EEG data, several molecular parameters were investigated: to assess neuronal loss, we measured neuronal markers NeuN and MAP2 as well as apoptosis with Fluoro-Jade and TUNEL. Stress related HO-1 and activity-dependent c-Fos gene expression was measured with qPCR. Furthermore, we investigated how astrocytes were responding to our experimental conditions by measuring the levels of GFAP and astrocytic-specific aquaporin-4 and K_{ir} 4.1 mRNA levels as well as inflammatory associated genes IL-1β and COX-2. Additionally, to examine how microglia was responding in our study, we did an in-depth profile of their reactive states with morphological reconstruction of these cells using IBA-1. Finally, blood-brain barrier alterations were measured with the assessment of blood-borne molecule immunoglobulin G (IgG).

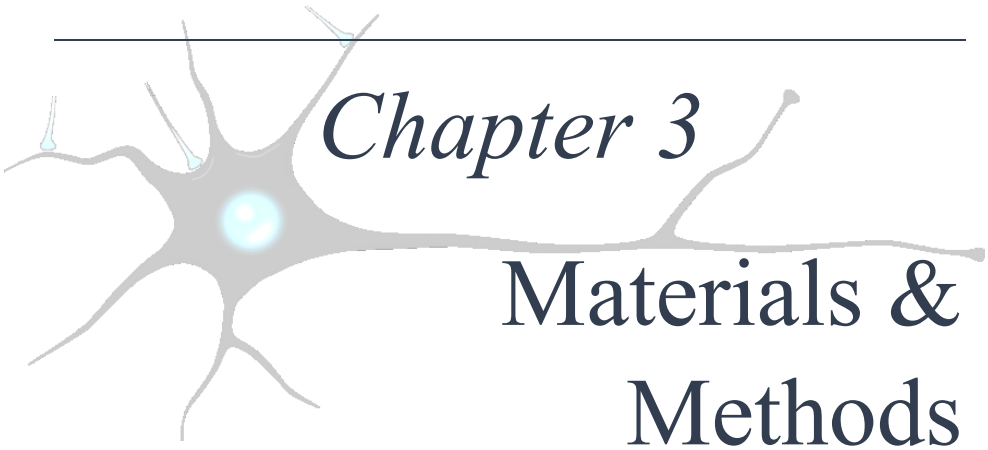

Chapter 3

Materials & Methods

3.1- Animal model

The study is based on a representative population of 49 adult female Hartley guinea pigs (250-300 g weight, 3 postnatal weeks of age; Charles River, Calco, Italy) housed in a 12h light/dark controlled cycle environment with *ad libitum* food and water supply. The experimental protocol was reviewed and approved by the Animal Welfare Office of the Italian Health Ministry (Authorization n. 36/2016-PR, January 18th, 2016), in accordance with the European Committee Council Directive (2010/63/EU) and with the 3Rs principle. Efforts were made to minimize the number of animals used and their suffering. Of the 49 animals, 34 were developed for the molecular examination and 15 were produced for the mRNA expression analysis.

3.1.1- Implantation of electrodes and injection cannula

Forty-four guinea pigs were surgically implanted with bilateral depth (intrahippocampal) and superficial (epidural) EEG recording electrodes. Briefly, 30 min before surgery, animals were subcutaneously treated with 4.2 mg/kg carprofen (Finadyne; Schering Ploug, Kenilworth, NJ, US). Subsequently, animals were deeply anesthetized with 5% isoflurane (Furane; Abbott Laboratories, Abbott Park, IL, US) and were fixed on a stereotaxic frame (SR-6; Narishige, Japan, Tokyo) adapted with guinea pig ear bars (EB-2; Narishige) and a mask (GM-3; Narishige) to maintain gaseous isoflurane anesthesia. During surgery, isoflurane levels were maintained at 1.5-2.0 %. After exposing and drilling the skull, 4 stainless steel screws of 1.1 mm diameter soldered to stainless steel wires with golden plug at the opposite tip were used as epidural, reference and ground electrodes (Figure 1A, B). Two epidural electrodes were placed bilaterally over the somatosensory cortex, whereas reference and ground electrodes were implanted into the bone above cerebellum. Two polyamide-coated stainless-steel wires (0.175 mm diameter; Advent, Eyn- sham, Oxford, United Kingdom) used as depth electrodes were placed in the dorsal *cornu ammonis* 1 (CA1) regions of both hippocampi [stereotaxic coordinates: anteroposterior -3 mm, mediolateral ± 3 mm, dorsoventral -3.25 mm relative to Bregma according to Luparello (1967)] (Figure 1C). The electrode in the right hippocampus was glued to a stainless-steel guide cannula (23 gauge; Cooper Needle Works Ltd, Birmingham, United Kingdom) for intrahippocampal injection, closed off using a bent cannula (30 gauge; Cooper Needle Works Ltd). The distance between the electrode tips and the cannula was 3.25 mm. The cannula ended just above the neocortex,

preventing any damage to the hippocampus (Figure 2A). All electrodes were inserted in a pedestal connector (Plastic One, Roanoke, VA, U.S.A.) and fixed on the skull with acrylic cement (Paladur; Heraeus, South Bend, IN, U.S.A.). After surgery, animals were hosted in individual cages and treated with subcutaneous injection of 5 mg/kg enrofloxacin (Baytril; Bayer, Leverkusen, Germany) and carprofen (4.2 mg/kg) for 5 days and with intramuscular dexamethasone (1 mg/kg) every 12 h for 48 h. All implanted animals survived the surgery procedure.

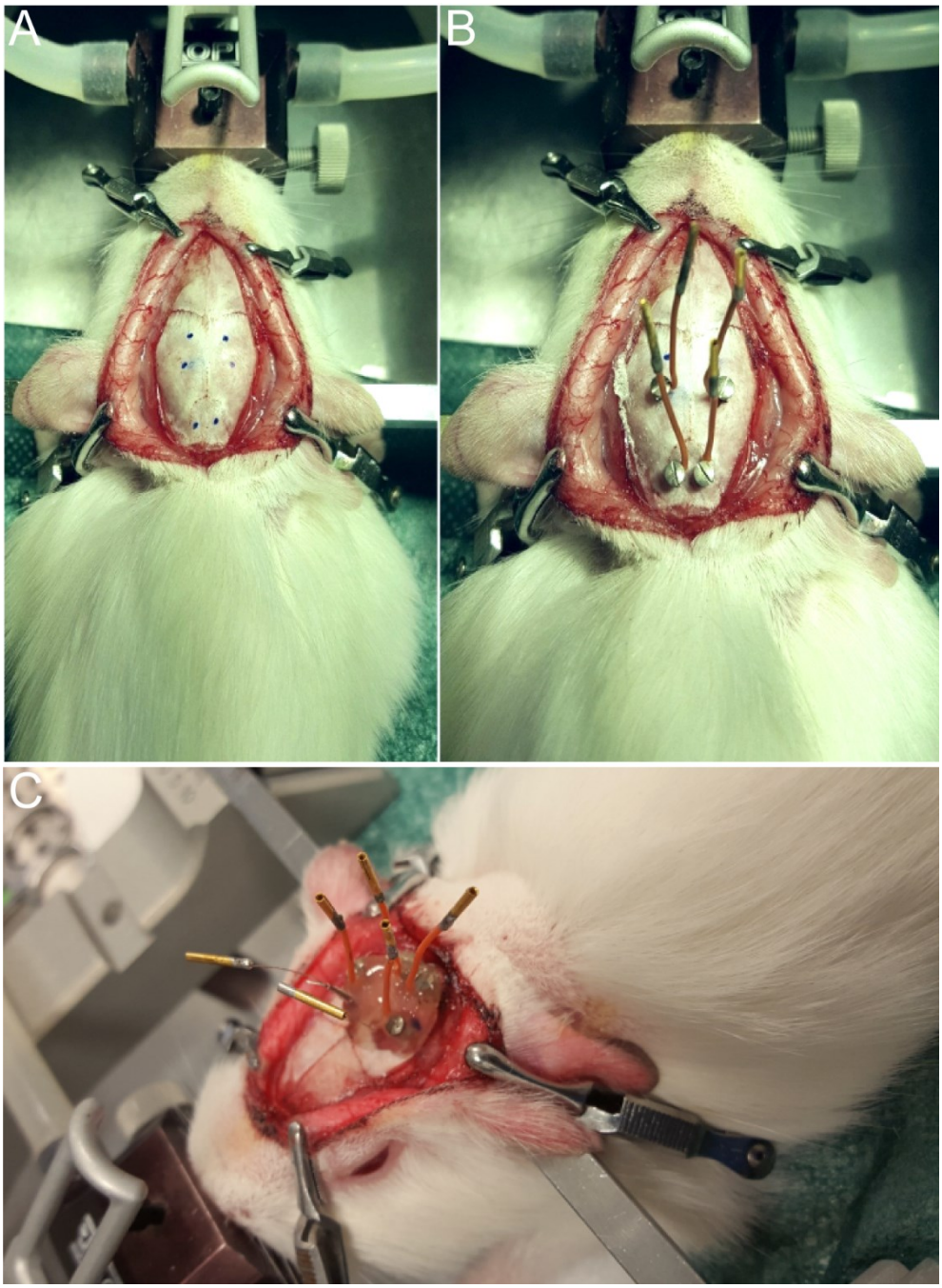

Figure 1- Implantation procedure. **(A)** opening of the skull. **(B)** Epidural electrode implantation. **(C)** Final headset structure with epidural and deep electrodes.

3.1.2- Unilateral intrahippocampal KA/saline injection and diazepam administration

Seven days after electrode implantation, all 44 animals were injected in the dorsal CA1 area of the right hippocampus (ipsilateral) with either kainic acid (KA; *n*=34) or 0.9% NaCl saline solution (sham operated animals; *n*=10) under continuous video-EEG recording. A 30-gauge needle, connected to 5 µl Hamilton syringe via a polyethylene tube, was lowered through the guide cannula in the right hippocampus (Figure 2A). After brain adjustment, animals were injected unilaterally with a volume of 1 µl 0.9% NaCl solution with 1 µg KA (Sigma, St. Louis, MO, U.S.A.) over a period of 2 min. Then, the needle was kept in place for 2 min to prevent backflow of the injected solution and subsequently pulled out of the brain over the course of 1 min. Within 10 min following KA injection, epileptiform activity typical of a non-convulsive *status epilepticus* (ncSE) was recorded in all animals. For the diazepam (DZP) group, 30 min before KA administration, animals were interperitoneally injected with diazepam (7-8 µg depending on animal weight); 3-4 µg diazepam was repeated 30 min after KA to terminate seizure activity. Sham animals were injected in the right hippocampus with 1 µl 0.9% NaCl following the same protocol. None of the sham operated/injected guinea pigs showed epileptiform activity in the EEG recordings. Acute phase animals were recorded for 3 days post-KA injection; chronic animals were video-EEG recorded 7 days every other week for no less than 4 weeks after focal ncSE, to verify the presence of spontaneous epileptiform discharges and seizures (Figure 2B).

Five different experimental groups were used: naïve (*n*=5; not video-EEG monitored); sham-operated/treated (Sham: *n*=10; 5 of those for mRNA analysis) animals; KA-injected guinea pigs sacrificed either 3 days after KA injection (acute KA: *n*=14; 5 of them used for mRNA studies) or 4 weeks post-injection (chronic KA: *n*=14; 5 utilized for mRNA investigation); KA-injected animals treated with diazepam and sacrificed 3 days post-KA injection (acute DZP + KA: *n*=6). The animals used for the study of mRNA expression were video-EEG monitored but were not included in the EEG analysis. Nevertheless, they were carefully monitored to insure they had a focal ncSE similar to the rest of the cohort.

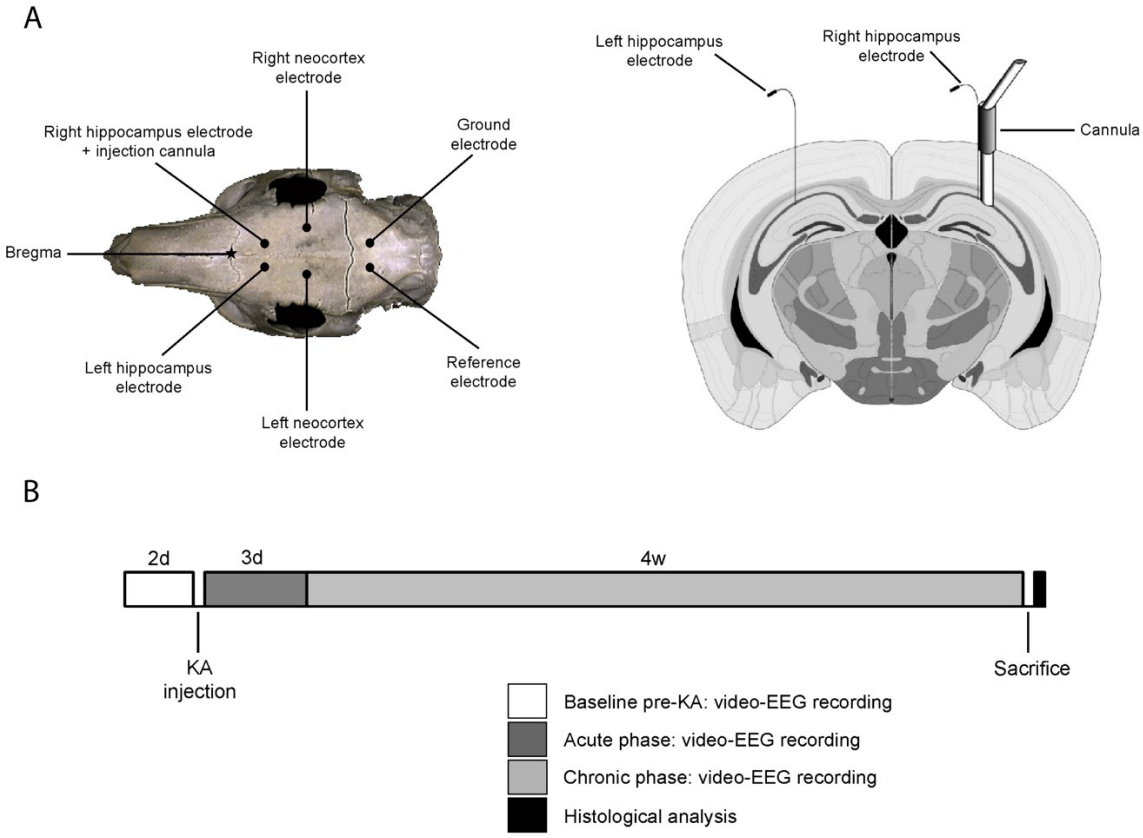

Figure 2- Implantation scheme and timelines. **(A)** Skull electrode implantation areas for epidural and deep electrodes. **(B)** Timeline for KA animal groups.

3.1.3- Video-EEG recording

Continuous video-EEG monitoring began 1 week after surgery; implanted pedestals were connected to a cable mounted on a swivel coupled to the preamplifier stage of a BrainQuick EEG System (Micromed, Mogliano Veneto, Italy). Synchronized video-EEG was continuously recorded 48h before injection (baseline), during the induction of focal ncSE and for the following 3 days in the acute phase animals (KA and DZP + KA) and for 4 weeks in the chronic KA animal group (Figure 2B). EEG data were recorded at 0.1-1.0 kHz, 2064 Hz sampling rate, with 16-bit precision and high-pass filter at 0.1 Hz, using the System Plus Evolution (Micromed). Video signals were simultaneously acquired with 2 digital cameras positioned with different viewpoints to detect minimal motor events during focal ncSE and chronic epileptic phase. Acute seizures were defined as seizures occurring within 72h post-KA injection. Video-EEG was analyzed offline and hippocampal EEG patterns during/after KA injection were identified and quantified for each animal. EEG activity recorded in the frontal cortex was

utilized to identify the presence of a diffuse EEG pattern (associated most of the time to a convulsive phenotype). Seizure events during KA-induced focal ncSE were defined as large amplitude spiking activity with clear and tonic bursting phases longer than 20 s, followed by post-ictal depression coupled with continuous rhythmic 1-3 Hz spiking. Seizures were also automatically counted with a software developed by Vadym Gnatkovsky to analyze long EEG recording periods with a compressed time scale[92]. In these animals, spontaneous seizures were identified with 7 days video-EEG recordings performed every other week for 4 weeks (Figure 2B). Seizure discharges were identified as focal unilateral or bilateral as well as convulsive or non-convulsive, based on the EEG pattern distribution and video analysis.

3.2- Molecular analysis

3.2.1- Immunohistochemistry

At the end of video-EEG recording sessions, animals were anesthetized with sodium thiopental (125 mg/kg i.p., Farmotal; Pharmacia, Milano, Italy) and transcardially perfused with 0.9% NaCl for 4 min. Subsequently, perfusion was done with 4% paraformaldehyde in phosphate buffer 0.1 M for 5 min. After fixation, intracranial recording electrodes and guide cannula were carefully removed. Brains were removed and immersed in 4% paraformaldehyde for 48h before cutting into coronal section (50 μm) for immunohistochemical processing. Two serial coronal sections *per* animal rostral and caudal to the local damage induced by KA injection were selected and blindly analyzed by independent researchers. A standardized protocol was used for histochemical staining. Briefly, after endogenous peroxidase inactivation (3% H2O2 in PBS) and non-specific antigen binding sites blocking (1% BSA/0.2% Triton-X 100 in PBS), free-floating sections were incubated overnight at 4° C with the desired primary antibodies (Table 1) in 0.1% BSA/0.2% Triton-X 100. The tissue was washed in PBS and processed for 75 min with avidin-biotin-peroxidase protocol (ABC; Vector Laboratories, Burlingame, CA, US). Visualization of labeling was achieved using 3,3'-diaminobenzidine tetra hydrochloride (DAB; Sigma, Milano, Italy). Slices were rinsed, mounted, dehydrated and cover-slipped with distyrene plasticizer xylene (DPX; BDH Lab Supplies, Leicestershire, UK). For endogenous guinea-pig IgG immunostaining,

slices were treated only with the secondary antibody. The IgG immunostaining and the amplification of the primary antibody labeling were obtained by 75 min incubation with biotinylated goat anti-guinea pig IgG. Immuno-stained sections were visualized using the Scanscope software (Aperio Technologies, CA, US). Staining for NeuN, MAP2, GFAP and IgG were analyzed in five different experimental conditions (naïve, sham-treated, acute KA, acute DZP + KA and chronic KA). Quantitative field fraction estimates were carried out in both hippocampi using Image-Pro Plus 7 software (Media Cybernetics, Inc. MD, US). Specific immunostaining density was estimated at 5x magnification in 3 regions of interest (ROIs) positioned in CA1, CA3 and dentate gyrus (DG) with respect to background signal (Figure 3). For each ROI densitometry was automatically calculated by the software on 2 adjacent slices in each hippocampal subfield (18 ROIs *per* brain slice; 3 ROIs *per* subfield) ipsilateral (right) and contralateral (left) to KA injection, after symmetry between hippocampi was verified. Densitometric ROIs were positioned at least 0.5 mm away from the electrode tracks to avoid inclusion of electrode-related tissue alterations in the analysis. For tridimensional reconstruction of microglial cells, immunohistochemistry using Iba-1 and DAPI conjugated to Cy3 was performed on 50 µm thick coronal sections using the previously mentioned protocol.

Table 1- Antibodies used in immunostainings

Antibodies	Supplier	Host	Type	Dilution
Cyanine 3 (Cy3)	Merck Millipore	Mouse	Polyclonal	1:500
DAPI	Sigma-Aldrich	Mouse	Polyclonal	1:5000
Glial fibrillary acidic protein (GFAP)	Agilent Dako	Rabbit	Polyclonal	1:500
Immunoglobulin G (IgG)	Merck Millipore	Goat	Polyclonal	1:200
Ionized calcium-binding adapter molecule 1 (Iba-1)	Abcam	Goat	Polyclonal	1:200
Microtubule-associated protein 2 (MAP2)	Invitrogen	Mouse	Monoclonal	1:1000
Neuronal nuclei (NeuN)	Merck Millipore	Mouse	Monoclonal	1:1000

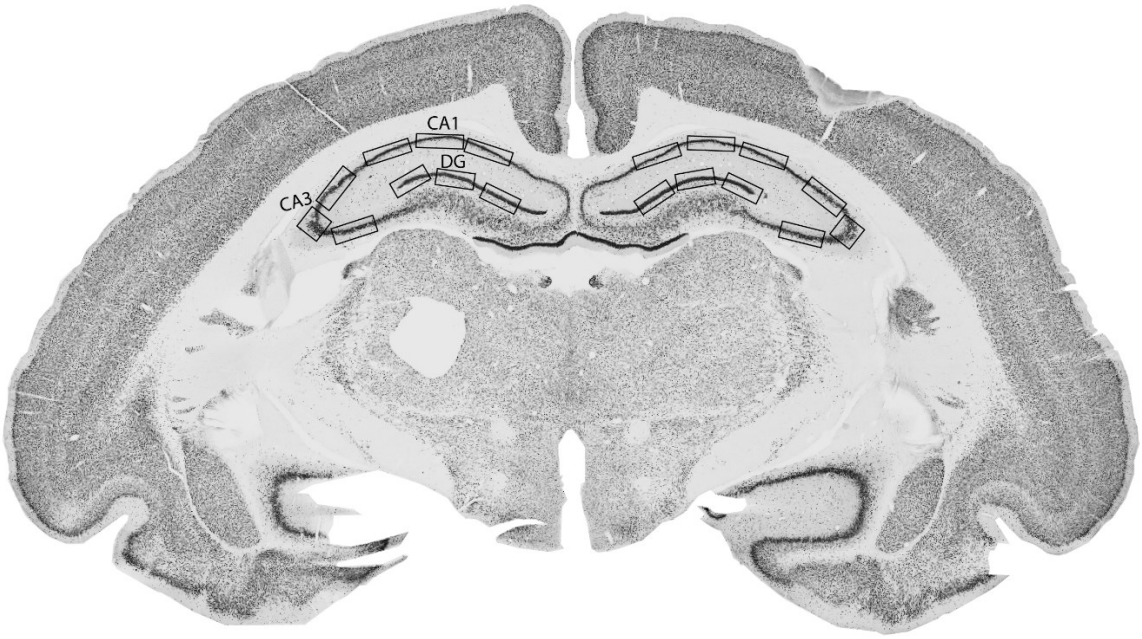

Figure 3- Representation of the ROIs employed in the immunostaining density analysis of the ipsi and contralateral CA1, CA3 and DG hippocampal regions.

3.2.2- Fluoro-Jade and TUNEL

Regarding Fluoro-Jade (FJ) staining, 2 sections away from the electrode tracks for each guinea pig were mounted in distilled water on glass slides, air-dried, immersed in a series of graded ethanol (50, 75, 100, 75, 50%, 3 min each step) and washed in distilled water for 3 min. Sections were then treated with 0.06% potassium permanganate for 15 min, washed, immersed in 0.001% FJ (Histo-Chem, Inc., Jefferson, Arkansas, USA) in 0.1% acetic acid for 30 min and rinsed in distilled water. After drying, slides were clarified in xylene and cover slipped with DPX. To quantify FJ^+ cells, cell counting was performed in CA1, CA3 and *hilus* areas of both ipsi and contralateral hippocampus for each experimental group (at least two section/each animal). For each section, at least 2 adjacent non-overlapping fields *per* area were captured under identical conditions at 40x magnification (290 µm x 290 µm) with a Leica TCS SP8 microscope. All FJ^+ cells were then counted using FIJI-ImageJ (v2.0.0) independently by two investigators and values averaged to a single value *per* area in both ipsi and contralateral hippocampus and compared to their corresponding controls.

To determine the apoptotic cell density the DeadEnd™ Fluorometric TUNEL System (Promega, Madison, WI, USA) was used. Briefly, 2 sections away from the electrode marks for each animal were mounted in distilled water on glass slides, air-dried,

and were digested with 20 mg/ml proteinase K at room temperature for 10 min, washed twice in PBS and then fixed with PFA 4% for 5 min. Each section was then incubated with TUNEL detection mixture according to the manufacturers instructions for 1 h at 37°C. Slides were then rinsed in PBS, air-dried and cover slipped with DPX. The acquirement and analysis were done in the same fashion as previously mentioned in the FJ experiments.

3.2.3- Morphometry analysis of microglia

Regarding the tridimensional reconstruction of microglial structure, coronal brain sections with 50 µm thickness were used and stained for Iba-1 and DAPI (cell nuclei) as described above. Sections were visualized using a Leica SP8 confocal microscope equipped with AOBS, resonant scanner and motorized stage x-y-z as well as DM camera for widefield acquisition (Leica Microsystems, Germany), applying the LASX software with navigator (version 3.1). Previews of the whole section in widefield (10X/0.3 dry) using the DAPI channel were taken in order to choose areas of interest, namely dorsal CA1 *stratum radiatum* and DG (Figure 4), that were further acquired at a higher resolution in the confocal mode (2 sections *per* animal, 0.5 mm away from the electrode tracks). Two channel (Iba-1 and DAPI) Z-stack images (Z-step intervals of 0.3 µm) were acquired using a 63X/1.4 oil objective and a DFC365 FX CCD Camera (Leica) with a x-y sampling of 72 nm. After acquisition, cells were eligible for reconstruction if the following criteria were met: a) Iba-1-positive cell was surrounding a single DAPI-stained nucleus; b) cell did not present truncated processes; c) cell was sufficiently individualized to ensure the correct reconstruction of the processes. A total of 180 cells, 90 for CA1 and 90 for DG, were selected for reconstruction performed using simple neurite tracer (SNT) plugin available in FIJI-ImageJ software (v2.0.0), an open-source tool previously described to successfully assess tridimensional morphology of neurons and glial cells [93,94]. Microglial morphometric properties were evaluated by quantifying the number of processes, total length (in µm), average number of intersections and Sholl analysis (number of intersections at radial intervals of 2 µm starting from the central point of the soma).

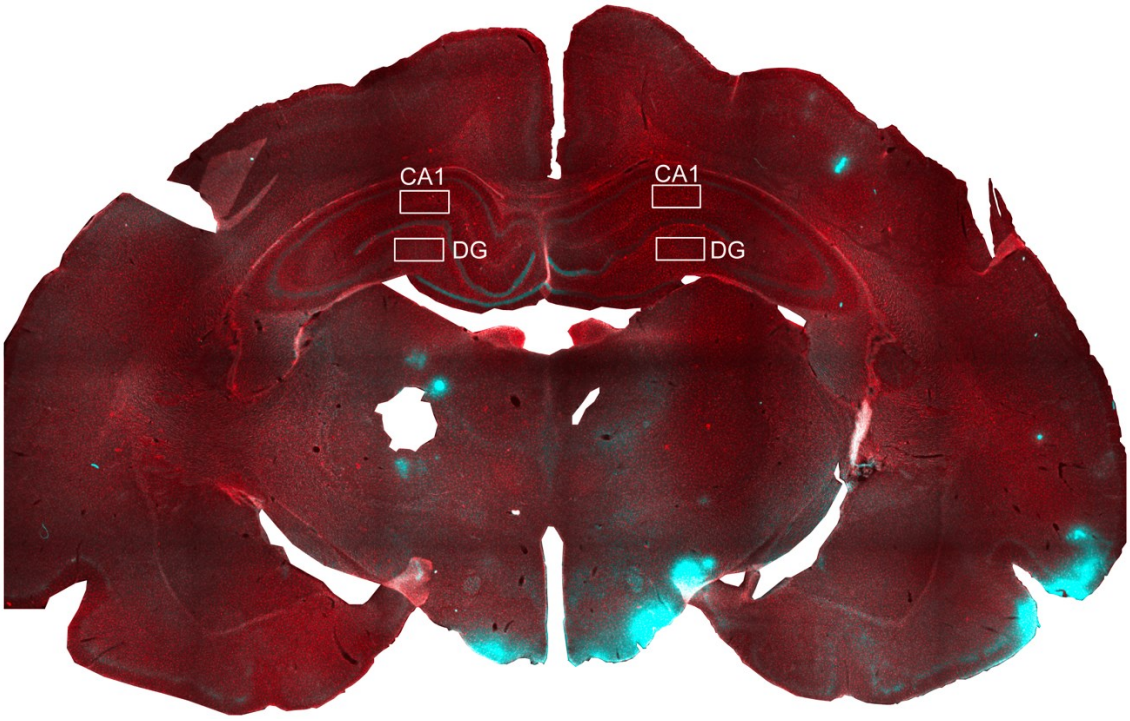

Figure 4- Representation of the ROIs used for the morphological reconstruction of microglia in the ipsi and contralateral CA1 and DG hippocampal regions. Iba-1 in red and DAPI in blue. 3 cells *per* ROI were reconstructed.

3.2.4- RNA isolation and quantitative real-time PCR

Fresh hippocampal brain tissue for mRNA analysis was obtained from a group of 5 sham-operated and KA-injected guinea pigs either 3 days (n=5) or 4 weeks (n=5) post-KA injection. Brains were removed and the whole hippocampus dissected out on a cold Petri dish and dorsal CA1 and DG ipsilateral and contralateral to KA injection were further dissected (Figure 5) and separately stored at -80ºC. For RNA isolation, frozen brain tissue was homogenized in 700 µL Qiazol Lysis Reagent (Qiagen Benelux, Venlo, Netherlands). Total RNA was isolated using the miRNeasy Mini kit (Qiagen Benelux, Venlo, Netherlands) according to the manufacturer instructions. Concentration and purity of RNA was determined at 260/280 nm using a Nanodrop 2000 spectrophotometer (Thermo Fisher Scientific, Waltham, MA, USA). To evaluate mRNA expression, 1 µg tissue-derived total RNA were reverse-transcribed into cDNA using oligo-dT primers. PCRs were run on a Roche Lightcycler 480 thermocycler (Roche Applied Science, Basel, Switzerland) using reference genes actin and glyceraldehyde 3-phosphate dehydrogenase (GAPDH) (see Table 2 for primer sequences). PCR mix contained 1 µL cDNA, 2.5 µL SensiFAST SYBR Green NoROX kit (Bioline Reagents Limited, London, UK), 0.4 µM

of forward/reverse primers plus water to a final volume of 5 µL/well. PCR reactions were run in duplicates and a negative control containing water instead of cDNA was included for each gene in each run. Cycling conditions were as follows: initial denaturation at 95 °C for 5 min, followed by 45 cycles of denaturation at 95 °C for 15 s, annealing at 65 °C for 5 s and extension at 72 °C for 10 s. Fluorescence of the sample was measured via single acquisition mode at 72 °C after each cycle. Primer specificity was assessed using melt curve analysis after each run. To study potentially relevant pathogenic elements (inflammation, glial function, activity-dependent changes) associated to brain damage, the following genes were analyzed: a) interleukin-1 beta (IL-1 β); b) cyclo-oxygenase-2 (COX-2); c) heme oxygenase-1 (HO-1); d) c-FOS; e) aquaporin 4 (AQP4) and f) inwardly rectifying potassium channel 4.1 (K_{ir} 4.1). Quantification of data was performed using LinRegPCR in which linear regression on the Log (fluorescence) *per* cycle number data was employed to determine the amplification efficiency *per* sample. The starting concentration of each marker was divided by the starting concentration of the reference genes (GAPDH and Actin) and this ratio was compared between all groups.

Table 2- Primer sequences used for quantitative real-time PCR

Gene	Forward primer	Reverse primer
IL-1β	CACAGTGGAATTTGAATCC	GACACTAGTTCTAACTTGAAG
COX-2	CTTCCTGCGCAATGCAATCA	GGCTTCCCAGCTTTTGTAGC
HO-1	ATGGAGATGGAGACGGGGAC	AGTGAGGAACTGAGGGGTCG
c-FOS	CCTGACTGTCGCTGATCCTC	AAATCTCAGGTCCCCAACG
AQP4	CACTAAATCGAGGCCACAGC	CCATGATGTCCTCTCTGGTGC
K_{ir} 4.1	CCACTGTACCTGGGACACAA	CCATTATGGGCCGGCTTTCT
Actin	CTACCTTCAACTCCATCA	GGAGCAATGATCTTGATC
GAPDH	CTCGTCATCAATGGAAAG	GTGGATTCCACTACATAC

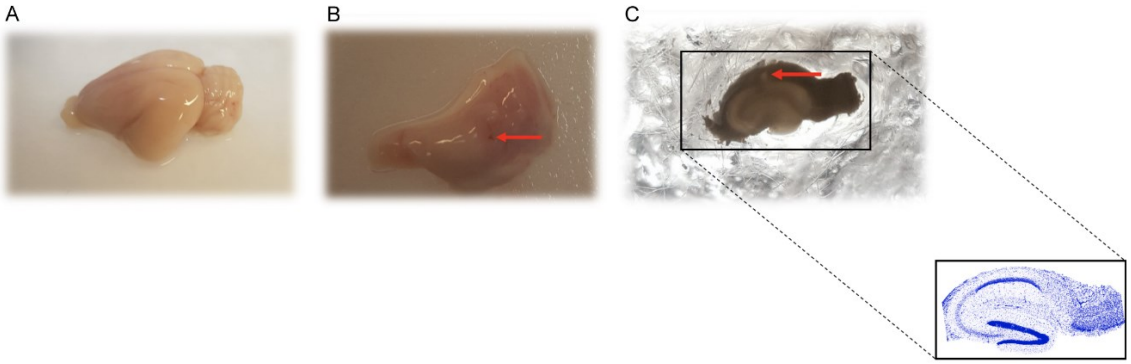

Figure 5- Representation of hippocampal dissection for the mRNA analysis. **(A)** Whole brain removal. **(B)** Whole hippocampus. **(C)** Slice of hippocampus right before being dissected into CA1, CA3 and DG regions. Red arrow corresponds to injection needle mark.

3.3- Statistical analysis

All statistical analysis was performed in Graph-Pad Prism 8.2 (GraphPad Software Inc., San Francisco, CA, US). Prior to any analysis, identification of outliers was performed using the ROUT method. Afterwards, the Shapiro–Wilk normality test was performed to access normal distribution. When normal distribution was met, one-way analysis of variance (ANOVA) was used to compare 4 independent groups and a paired or unpaired Student *t*-test to match 2 groups directly, for dependent or independent data respectively. Moreover, when data was not normally distributed, the non-parametric Kruskal-Wallis test followed by a Mann-Whitney U post-hoc test was employed to compare 4 independent groups and a paired Wilcoxon signed-rank test to relate 2 dependent groups against each other. In the morphology data, results are expressed as means ± standard deviation (SD) for the number of independent experiments (*n*). The remaining graphical data is illustrated with boxplots with min., max., median and quartiles shown. The confidence interval (1- α) was set as 95% (0.95) so that the difference between means was considered statistically significant at p values of less than 5% (0.05), 1% (0.01), 0.1% (0.001) and 0.01% (0.0001) of significance level (α).

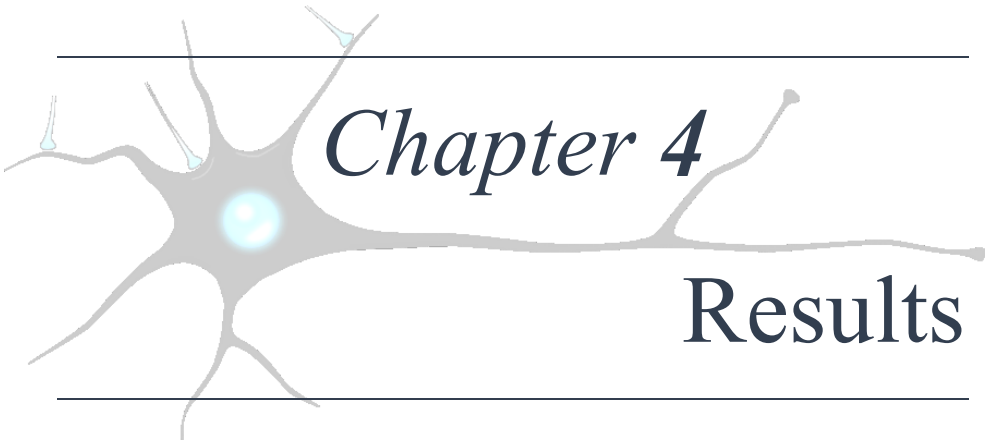

Chapter 4

Results

4.1. Video-EEG

Focal non-convulsive *status epilepticus* (ncSE) was induced by a unilateral intra-hippocampal injection of 1 µg in 1µl of kainic acid (KA) in the right (ipsilateral) dorsal CA1 area of 34 guinea pigs. Of these, 14 were sacrificed 3 days post-KA injection (acute post-ncSE phase) to assess the peak phase of brain damage, as it was shown before in publications from our group in the same animal model[72,74,85]. Considering that time may also be a key factor in the generation/progression of damage, a different group of animals (*n*=14; KA chronic) were sacrificed 4 weeks post-KA injection, which has been the previously established timepoint for these animals to develop chronic spontaneous seizures[72,74,85]. To unravel if seizure activity during focal ncSE exacerbates the damage established by KA, we treated another group of animals (*n*=6; DZP + KA) with intraperitoneal diazepam (DZP). These 3 groups were compared against sham-operated animals (*n*=10) that experienced the same protocol as all the other cohorts but were injected with a 0.9% NaCl saline solution instead of KA. All these animals were separated into 2 large groups: 1 was used for video-EEG, immunohistochemical and morphological analysis (Naïve *n*=5; Sham *n*=5; 3 days post-KA *n*=9; KA chronic *n*=9; DZP + KA *n*=6) and the other for gene expression studies (Sham *n*=5; 3 days post-KA *n*=5; KA chronic *n*=5).

4.1.1- Acute 3-days post-KA

Within 5 min after KA injection, focal ncSE began in the injected right hippocampus (ipsilateral KA in Figure 1A). Subsequent seizures during focal ncSE propagated to the contralateral hippocampus and both hippocampi generated seizures 79.7 ± 11.9 % of the time (mean ± SD; Figure 1H) with no cortical EEG involvement. Seizure activity was defined as large amplitude spiking with clear and tonic bursting phases longer than 20 s, followed by post-ictal depression coupled with continuous rhythmic 1-3 Hz spiking (Figure 1 A, B). Spikes and sharp waves were a common interictal feature (not shown). Animal behavior during seizure activity was analyzed using synchronized video-EEG recordings; seizures occurring during focal ncSE were classified as non-convulsive or secondarily convulsive according to the Racine scale (stages 1-3 correspond to non-convulsive and 4/5 to convulsive phenotype with bilateral

and diffuse EEG discharges)[59]. Regarding the KA groups, seizures during focal ncSE were 89.1 ± 12.9 % non-convulsive (Figure 1G), with the most common animal behavior observed being exploration, immobility and mouth/head myoclonus with an occasional head nodding (Figure 3). A total of 115 focal secondarily convulsive seizures lasting less than 20 s were found among 1071 seizures analyzed (10.8 ± 12.9 %) occurring during the focal ncSE of all 18 animals. The time spent in secondarily convulsive seizures was minimal compared to the duration of the focal ncSE (not shown). In only 4 animals 10-15 convulsive seizures were observed (out of 353), while the remaining 14 animals had 1-3 (Figure 1F). The inclusion of the 4 animals with >10 convulsive seizures did not modify the overall immunostaining densitometric results (see below). None of the animals processed for the mRNA expression analysis showed more than 1 convulsive seizure during focal ncSE. When the spectrogram software to automatically detect seizures was employed to be certain each seizure was correctly counted, clear bursts for each seizure were easily observed (Figure 2). Furthermore, preceding each seizure, a fast-activity event was frequently detected (Figure 2 – bottom blue arrows in zoomed portion). No epileptiform activity was detected in sham animals recorded for 6 h after intrahippocampal NaCl saline solution injection (not shown).

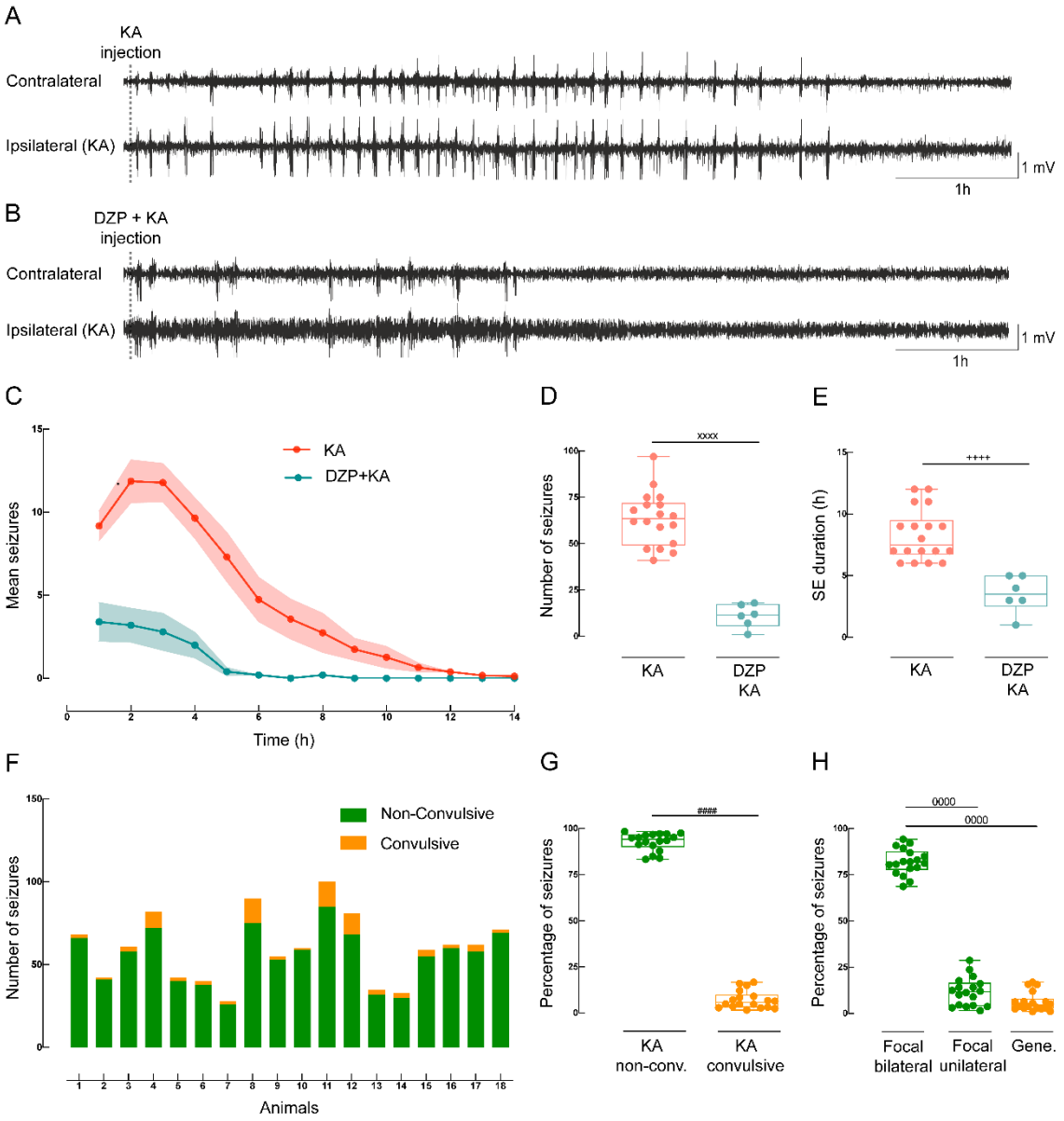

Figure 1 - EEG and seizure features during ncSE induced by unilateral intrahippocampal KA injection in KA and diazepam (DZP) + KA animals. EEG analysis was performed in 18 KA animals (9 processed 3 days after SE onset, and 9 chronic KA animals recorded/analyzed in acute phase - *n*=18) and in 6 DZP + KA animals (*n*=6). **(A)** Compressed 7h EEG recording from left (contralateral) and right [ipsilateral (KA)]) hippocampus after KA injection in CA1 area of right hippocampus (vertical dotted line on both traces). **(B)** Compressed 7h EEG recording from left (contralateral) and right [ipsilateral (KA)] hippocampus after intraperitoneal administration of DZP followed by intrahippocampal KA injection. **(C)** Mean seizures *per* hour after KA injection (red trace) and KA preceded by DZP (blue trace). **(D)** Number of seizures *per* animal treated with KA injection (red) *vs* DZP + KA (blue). (^{xxxx}): p<0.0001 (unpaired *t*-test). **(E)** *Status epilepticus* duration in hours *per* animal after KA injection (red) *vs* DZP + KA (blue). ($^{++++}$): p<0.0001 (Mann-Whitney U test). **(F)** Number of convulsive (yellow) and non-convulsive (green) seizures for each animal. **(G)** Percentage of seizures characterized by a convulsive (yellow) *vs* non-convulsive phenotype (green). ($^{####}$): p<0.0001 (Wilcoxon signed-rank test). **(H)** Percentage of seizures *per* animal defined as focal bilateral (green) *vs* focal unilateral (green) *vs* generalized (yellow). (^{0000}): p<0.0001 (paired *t*-test).

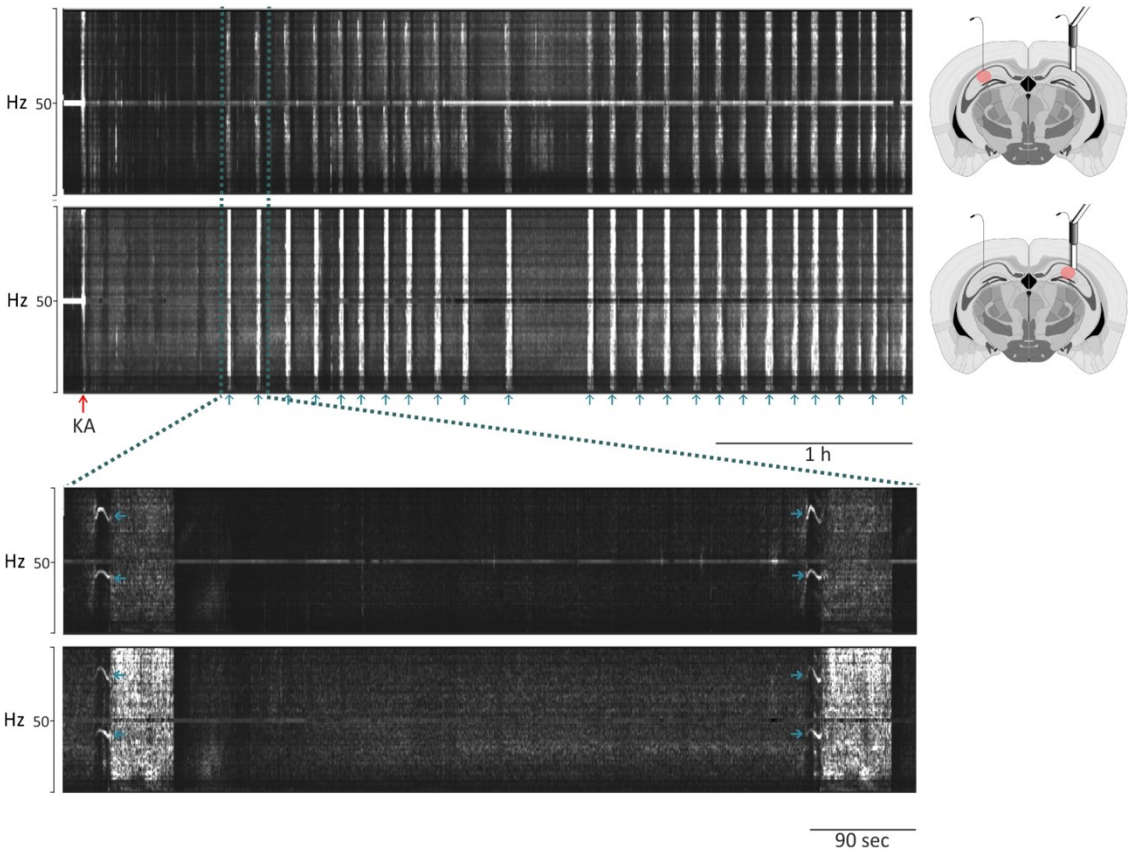

Figure 2 – EEG spectrogram analysis. Top 2 spectrograms represent both hippocampi recordings 4h post-KA injection. Bottom 3 spectrograms represent a zoomed view of 2 seizure events with a trademark fast activity burst preceding each seizure highlighted with blue arrow. On Top: red arrow indicates KA injection and blue arrows represent each seizure. Software developed by Vadym Gnatkovsky[92].

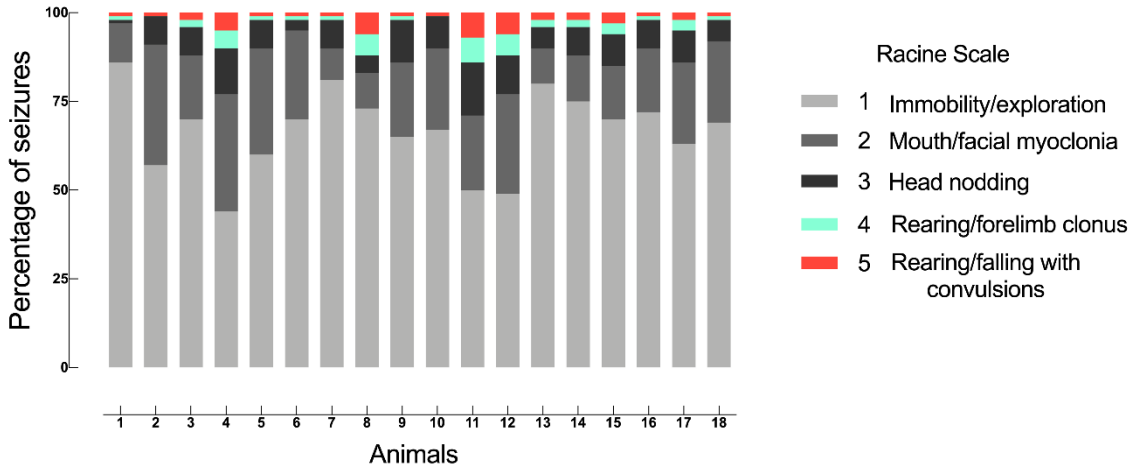

Figure 3 - Animal phenotype characterization. In total, 18 KA animals were video-EEG monitored and their behavior while seizing characterized and divided in 1 of 5 stages of the Racine scale[59]. For each animal, the percentage of seizures *per* Racine stage is represented in colors. In each stage, animals could also develop phenotypic characteristic of previous stages.

4.1.2- Diazepam + KA

Furthermore, when KA animals were compared to DZP-treated animals, focal ncSE duration was 8.3 ± 2.0 h in KA-injected animals and was higher in regard to the DZP + KA group (3.5 ± 1.5 h; Figure 1E). Additionally, the number of seizures *per* animal was higher in the KA group (63.5 ± 14.3 seizures *per* animal) in comparison to DZP + KA animals (11 ± 6.3 seizures Figure 1C, D). Concerning the DZP + KA animal cohort, the few residual seizures that these animals experienced had its origin in the injected hippocampus and 64.6% of the time remained focal in the ipsilateral hippocampus (focal unilateral) but could also spread to the contralateral hippocamps (focal bilateral – 35.4%) (Figure 4A). All seizures observed in this group, were of a non-convulsive nature (Figure 4B), with only subtle behaviors such as immobility and mouth chewing being observed.

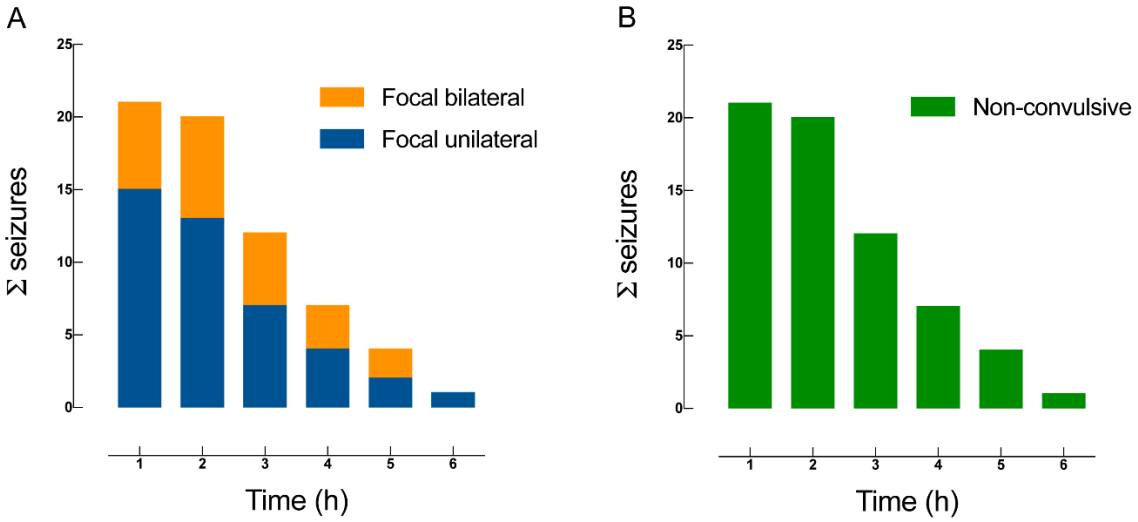

Figure 4 – DZP + KA animal EEG characterization. In total, 6 DZP + KA animals were video-EEG monitored for 3 days post-KA injection and their phenotype analyzed. **(A)** Sum of seizures classified as focal unilateral (blue) *vs* focal bilateral (orange) *per* hour post-KA injection. **(B)** Sum of seizures *per* hour characterized by a non-convulsive behavior.

4.1.3- Chronic 1-month post-KA

As previously mentioned, KA chronic animals were video-EEG monitored for 4 weeks post-KA not only to detect subtle behaviors but also the development of spontaneous chronic seizures. In all animals analyzed, a chronic epileptic condition developed with recurrent spontaneous seizures occurring and ipsilateral hippocampal sclerosis developing (see below). On average, animals had a latent phase of 8.7 ± 1.2 days

until the first chronic spontaneous seizure was registered (Figure 5 B). Isolated spikes and short bursts were also commonly observed (not shown). Seizure activity was mostly focally restricted to the injected hippocampus (78.6% of the time; Figure 5 A, C) and spread to the contralateral hippocampus on some occasions (21.4%). Similar to the DZP + KA animal cohort, these animals had almost no noticeable behaviors while experiencing spontaneous seizure activity, re-enforcing the concept that it is absolutely necessary a constant EEG monitoring to be able to properly study the chronic epileptic phase in epileptic animal models.

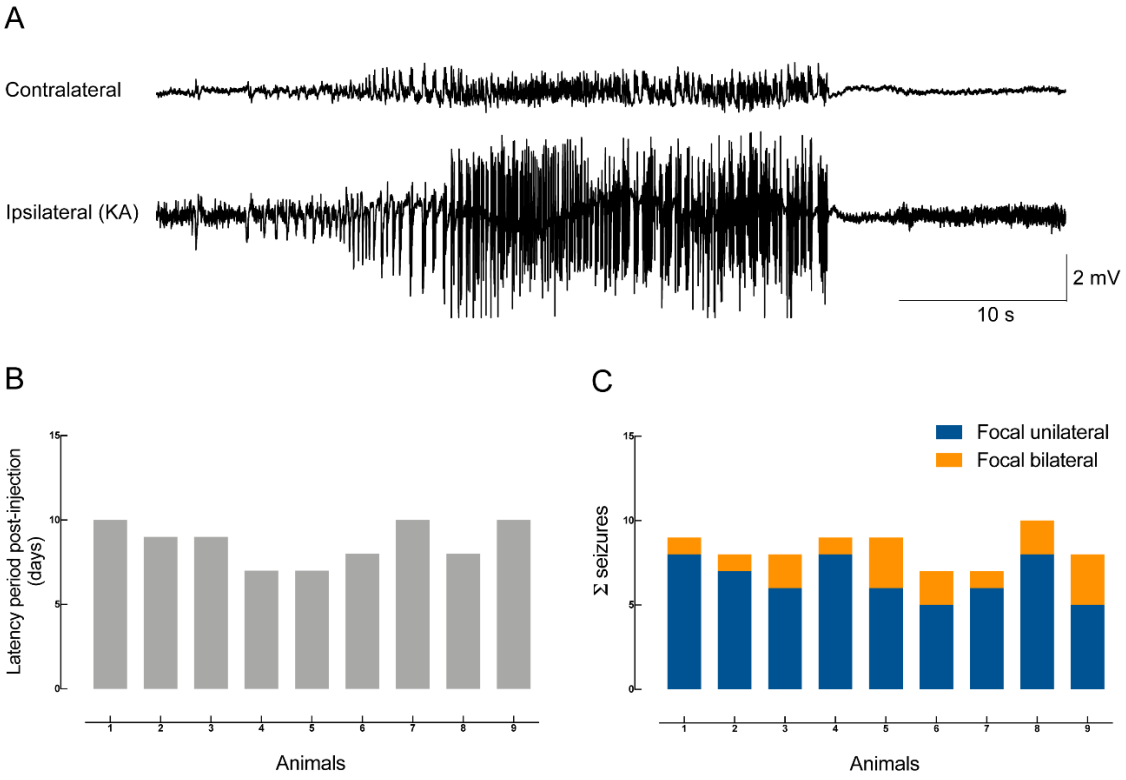

Figure 5 – KA chronic animal EEG characterization. In total, 9 KA chronic animals were video-EEG monitored for 4 weeks post-KA. **(A)** EEG recording of a spontaneous chronic seizure from left (contralateral) and right [ipsilateral (KA)]) hippocampus 4 weeks post-KA injection. **(B)** Latency period in days from the end of SE until the onset of the first spontaneous seizure *per* animal **(C)** Sum of seizures *per* animal described as focal unilateral (blue) *vs* focal bilateral (orange).

4.2. Immunostaining and apoptotic analysis

After video-EEG monitoring, animals were sacrificed either 3 days or 4 weeks post injection and coronal sections were cut and immunostained to evaluate neuronal cell loss (NeuN and MAP2; representative microphotographs in Figure 9), astrogliosis (GFAP; Figure 12) and blood-brain barrier disruption (IgG; Figure 12). Initially, we started by evaluating if the surgery procedure and the insertion of electrodes in the hippocampus could have been potentially provoking some type of damage with densitometric analysis of NeuN, MAP2, GFAP and IgG immunostaining in CA1, CA3, DG and of naïve animals (*n*=5) compared to sham-operated animals (*n*=5). No statistical differences were found by comparing these 2 groups (Figure 6 A-D); therefore, the sham group was used as our control condition throughout the study.

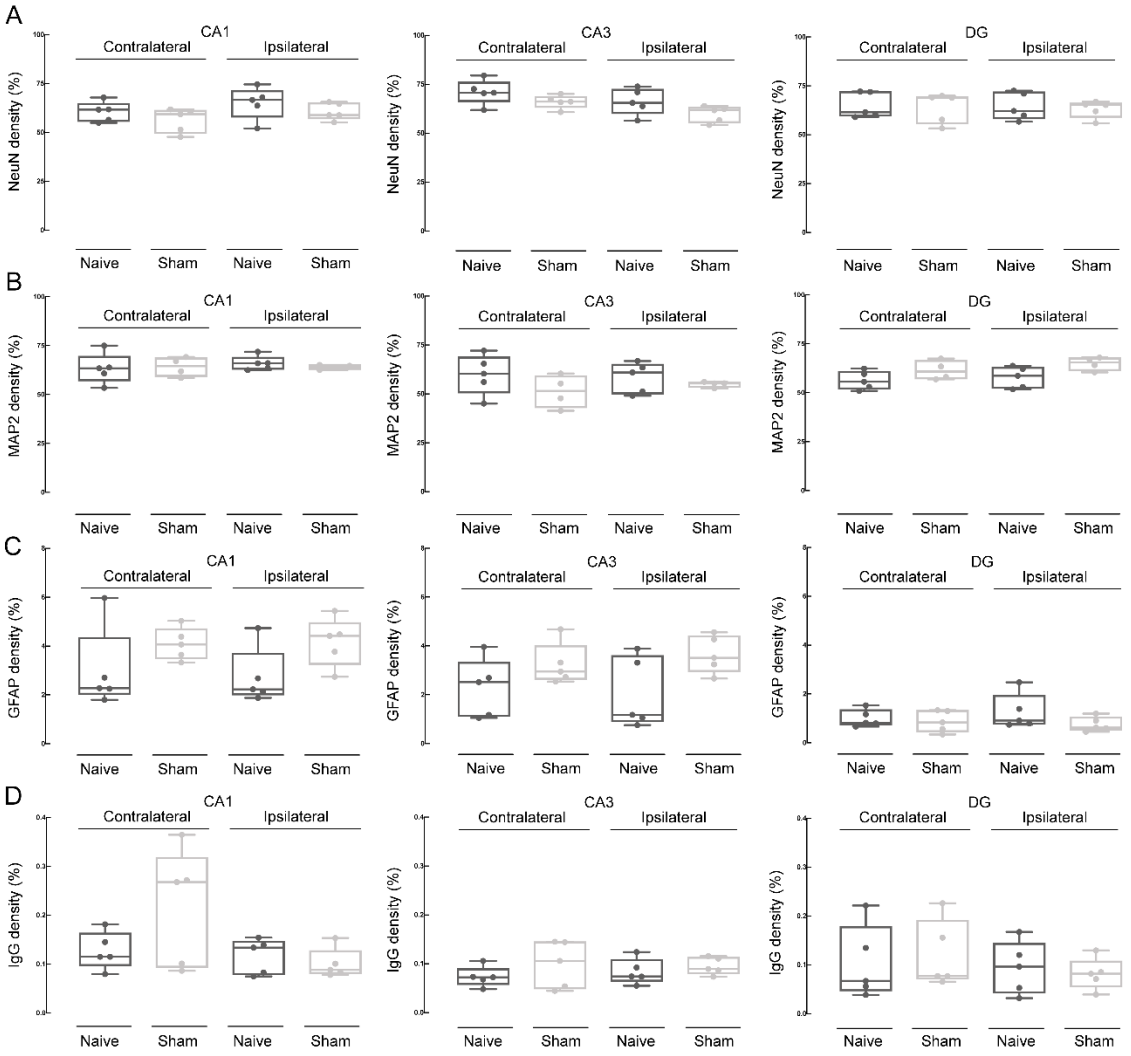

Figure 6 – Semi-quantitative analysis of NeuN, MAP2, GFAP and IgG densitometry in control (naïve) and sham-operated animals. Percentage of densitometric changes in NeuN **(A)**, MAP2 **(B)**, GFAP **(C)** and IgG **(D)** stainings in the contra and ipsilateral CA1 (left column), CA3 (middle column) and DG (right column) subregions. Densitometric values were obtained from the same areas of naïve (*n*=5) and sham-operated (*n*=5) control animals.

4.2.1- NeuN and MAP2

Densitometric measurements separately performed in the hippocampus ipsilateral (KA + seizures) and contralateral (seizures only) to KA injection were compared to their respective regions in sham-operated animals and DZP + KA group (Figures 7 and 12). As shown in a preliminary study performed in a different set of animals[73], 3 days post-KA decrease in NeuN and MAP2 densitometric values were observed in the ipsilateral CA1, CA3 and DG (only NeuN) with respect to the homologous subfields of sham-operated animals (Figure 7; also representative panel in Figure 9). The observed neuronal loss in the KA-injected CA1, CA3 and DG persisted in the KA chronic group, except for DG in NeuN when compared to the sham animal group (Figure 7). Remarkably, densitometric NeuN and MAP2 values in the DZP + KA animal group (Figure 7) were higher than the 3-days KA group for all subfields and were similar to sham-guinea pigs for NeuN (CA1 and DG) and for MAP2 (DG). Moreover, in the DZP + KA group, the values in CA3 for NeuN and in CA1 and CA3 for MAP2 were lower compared to the sham groups but higher than the 3-days post-KA animal cohort (Figure 7). No densitometric NeuN or MAP2 changes were detected in the contralateral hippocampus of KA (both 3 days and 4 weeks) and DZP + KA animals when compared to their respective sham-controls (Figure 7).

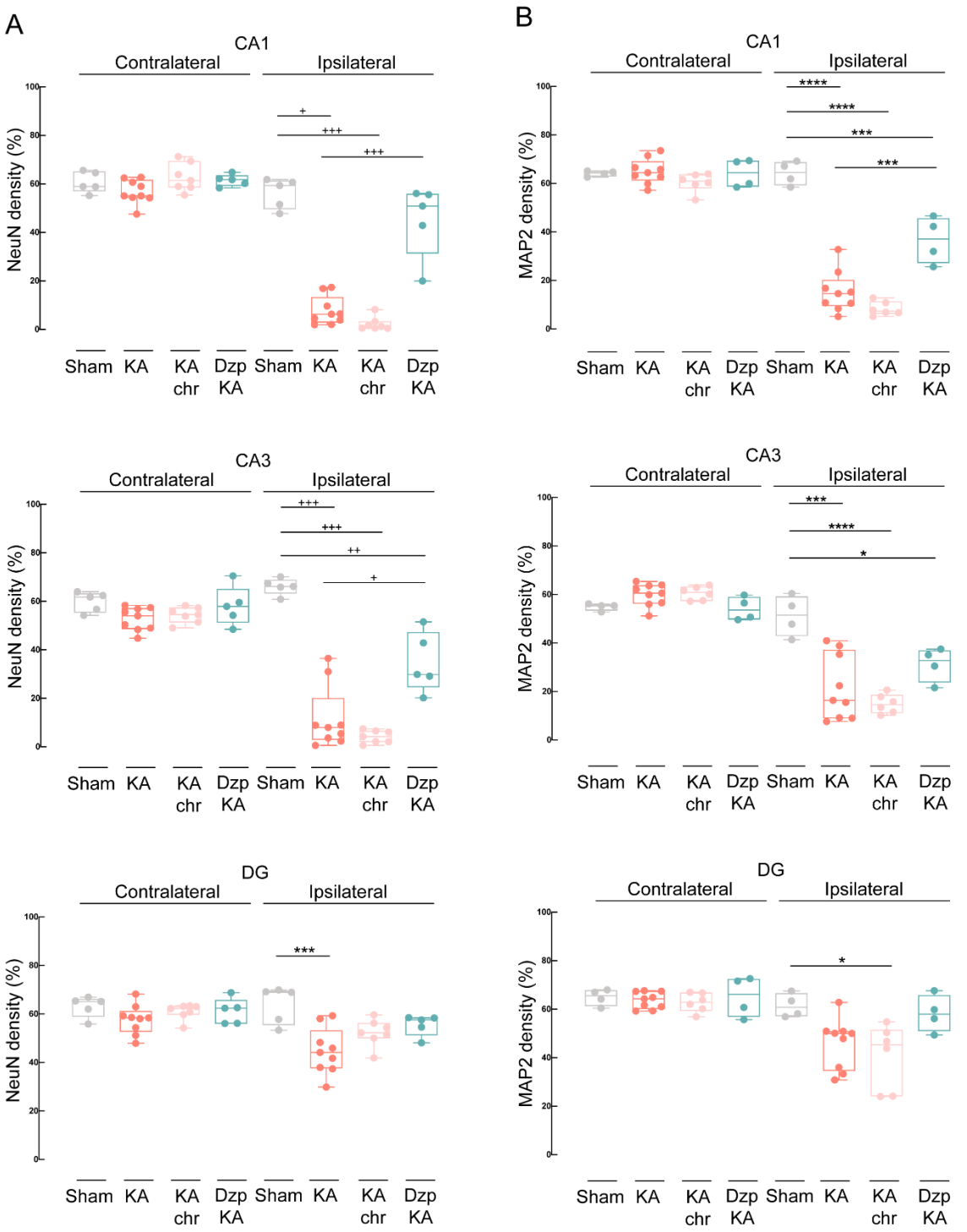

Figure 7 – NeuN and MAP2 semi-quantitative densitometry analysis. For **(A)** and **(B)**: Grey columns: sham-operated animals. Red columns: 3 days post-KA injection (KA). Pink columns: 1-month post-KA injection animals (KA chronic). Green columns: animals treated with DZP and KA injected (DZP + KA). Average percentage of densitometric changes in the KA-injected (ipsilateral) and contralateral hippocampal CA1 (first row), CA3 (middle row) and DG (last row) subregions are illustrated. **(A)** NeuN densitometric values obtained from sham (n=5), KA (n=9), KA chronic (n=7) and DZP + KA (n=5) guinea pigs. ($^{+}$): $p<0.05$; ($^{++}$): $p<0.01$; ($^{+++}$): $p<0.001$ (Mann-Whitney U test); (***): $p<0.001$ [one-way analysis of variance (ANOVA)]. **(B)** MAP2 densitometric changes from the same areas of sham (n=4), KA (n=9), KA chronic (n=6) and DZP + KA injection (n=4) guinea pigs. (*): $p<0.05$; (***): $p<0.001$; (****): $p<0.0001$ (ANOVA).

As previously mentioned, even though we defined our animal model as focal ncSE, we found that roughly 10.8 ± 12.9 % of all seizures analyzed were defined as convulsive seizures. The large majority of this convulsive seizures were present in 4 animals of the 3-days post-KA cohort (animals 4,8,11 and 12 in Figure 1F). Likewise, to investigate how much 10% ± of convulsive seizures would influence the evaluation of damage (with NeuN, MAP2; and below GFAP and IgG) we divided the 9 acute 3 days post-KA cohort into animals with < 2% of convulsive seizures (KA^-) *vs* animals with 10% ± convulsive seizures (KA^+) and found no difference when the 2 groups were compared against each other (Figure 8).

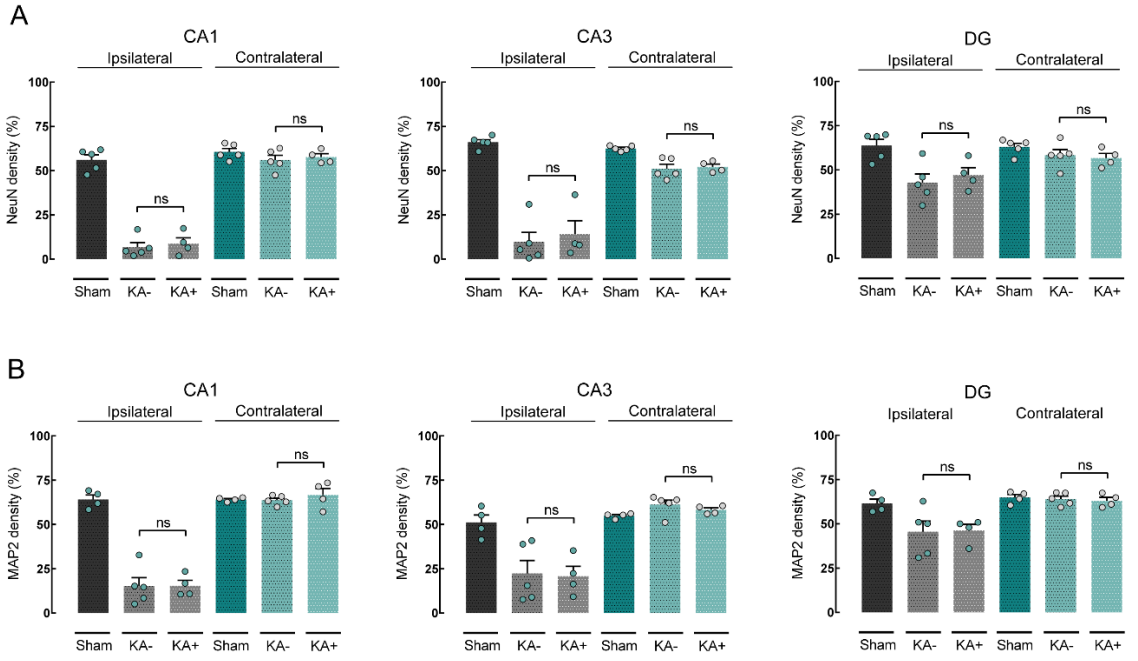

Figure 8 – NeuN and MAP2 semi-quantitative densitometry analysis. Average percentage of densitometric changes in the KA-injected (ipsilateral - grey shading) and contralateral (green shading) hippocampal CA1 (left panels), CA3 (middle panels) and DG (right panels) subregions are illustrated. **(A)** NeuN densitometric values obtained from sham (*n*=5) and 3 days-post KA animals divided into: KA^- (<2% of convulsive seizures; *n*=5), KA^+ (±10% convulsive seizures; *n*=4). Ns = non-significant. **(B)** MAP2 densitometric values obtained from sham (*n*=5) and 3 days-post KA animals divided into: KA^- (<2% of convulsive seizures; *n*=5), KA^+ (±10% convulsive seizures; *n*=4). Ns = non-significant.

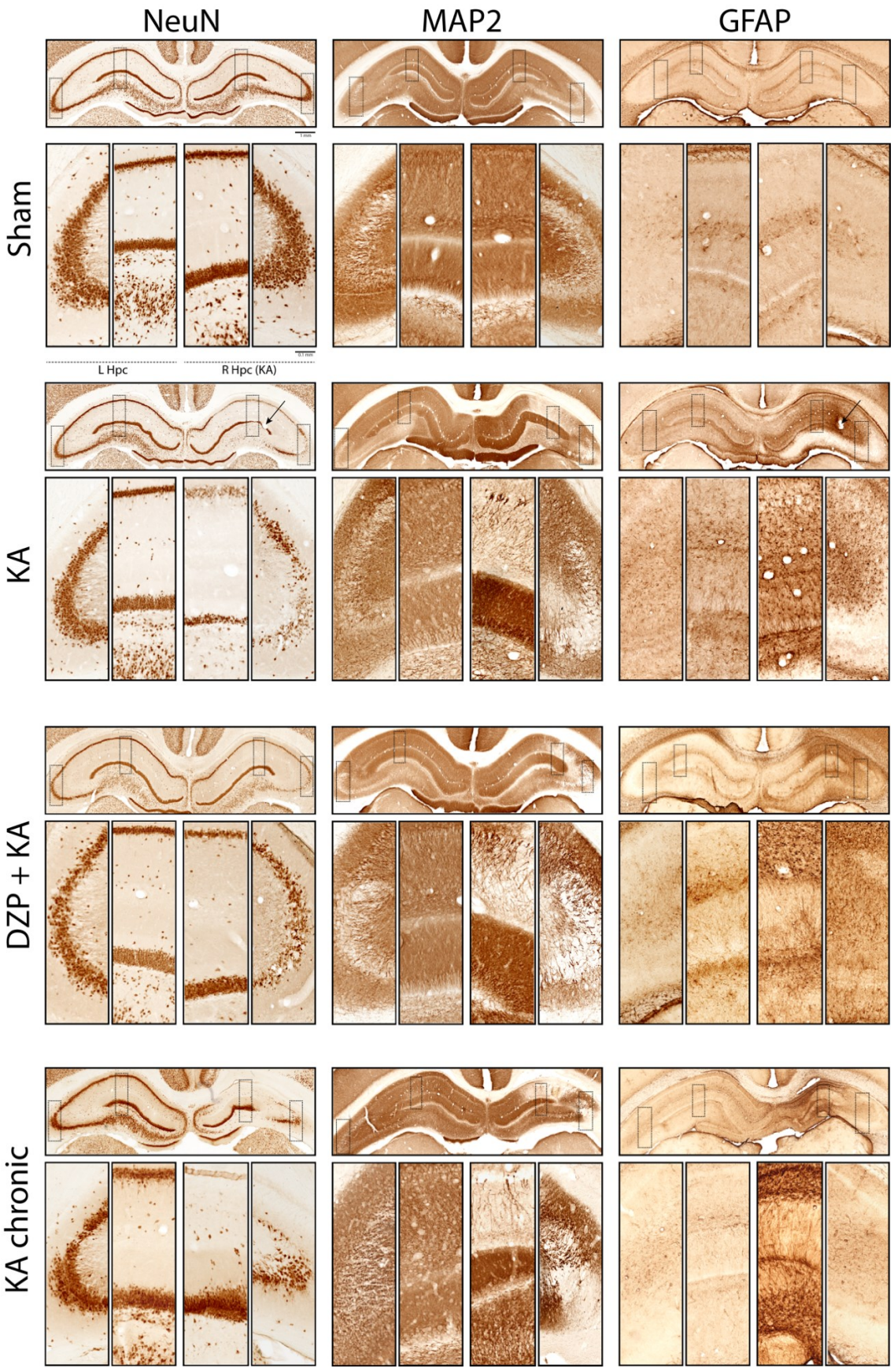

Figure 9 – NeuN, MAP2 and GFAP representative micrographs. NeuN, MAP2 and GFAP immunostained coronal sections represented at low (upper pictures) and high magnification (lower pictures; dotted area

outlined in the upper photographs) for sham (first row), 3 days KA (second row), DZP + KA (third row) and KA chronic animals (last row). KA was injected in the right dorsal CA1 region (injection cannula artifact marked by arrowhead). Left and right hemispheres contralateral and ipsilateral to hippocampal KA injection, respectively, are illustrated. Calibration bars in higher magnification = 0.1 mm and in lower magnification = 1 mm.

4.2.2- Fluoro-Jade and TUNEL

To complement the neuronal loss evaluation, we investigated the ongoing degeneration of neurons with Fluoro-Jade (FJ). Accordingly, FJ^+ cells were observed restrictedly and consistently in the ipsilateral hippocampus in CA1, CA3 and DG in the 3-days post-KA and DZP + KA groups only (Figure 10A, B). FJ^+ cells were not detected neither at 4 weeks post-KA nor in the contralateral hippocampus of any animal group (Figure 10B).

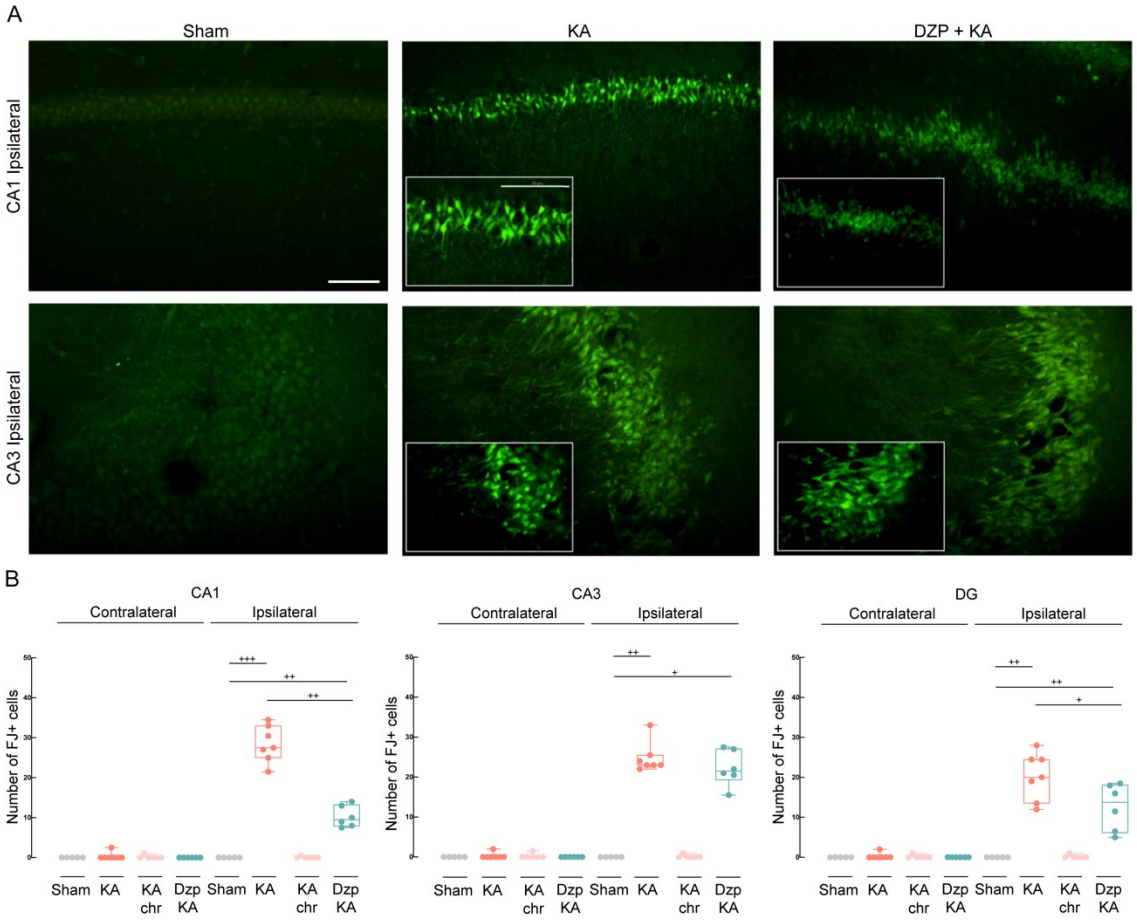

Figure 10 – Fluoro-Jade (FJ) immunostaining and quantification in CA1, CA3 and DG subregions. **(A)** Representative photographs of CA1 (first row) and CA3 (second row) subregions in the right hippocampi ipsilateral to KA injection of sham-operated (left column), 3-days post-KA injection (middle column) and DZP + KA injection (right column) guinea pigs. Higher magnification photos are illustrated in the inserts.

Calibration bars at higher magnification = 50 µm and at lower magnification = 100 µm. **(B)** Comparison between number of FJ^+ cells in the KA injected (ipsilateral) and contralateral hippocampal subregions. In all graphics, grey, red, pink and green plots show counts from sham (*n*=5), KA 3 days after ncSE (*n*=7), KA chronic (*n*=6) and DZP + KA (*n*=6) guinea pigs, respectively. ($^+$): p<0.05; ($^{++}$): p<0.01; ($^{+++}$): p<0.001 (Mann-Whitney U test).

Moreover, taking in consideration that all FJ^+ cells observed were present in the 3-days acute phase, we measured the DNA fragmentation levels with the TUNEL assay in CA1, CA3 and DG of the 3 days post-KA animal group. Similar to the FJ findings, $TUNEL^+$ cells were found exclusively and commonly in the injected hippocampus only (Figure 11).

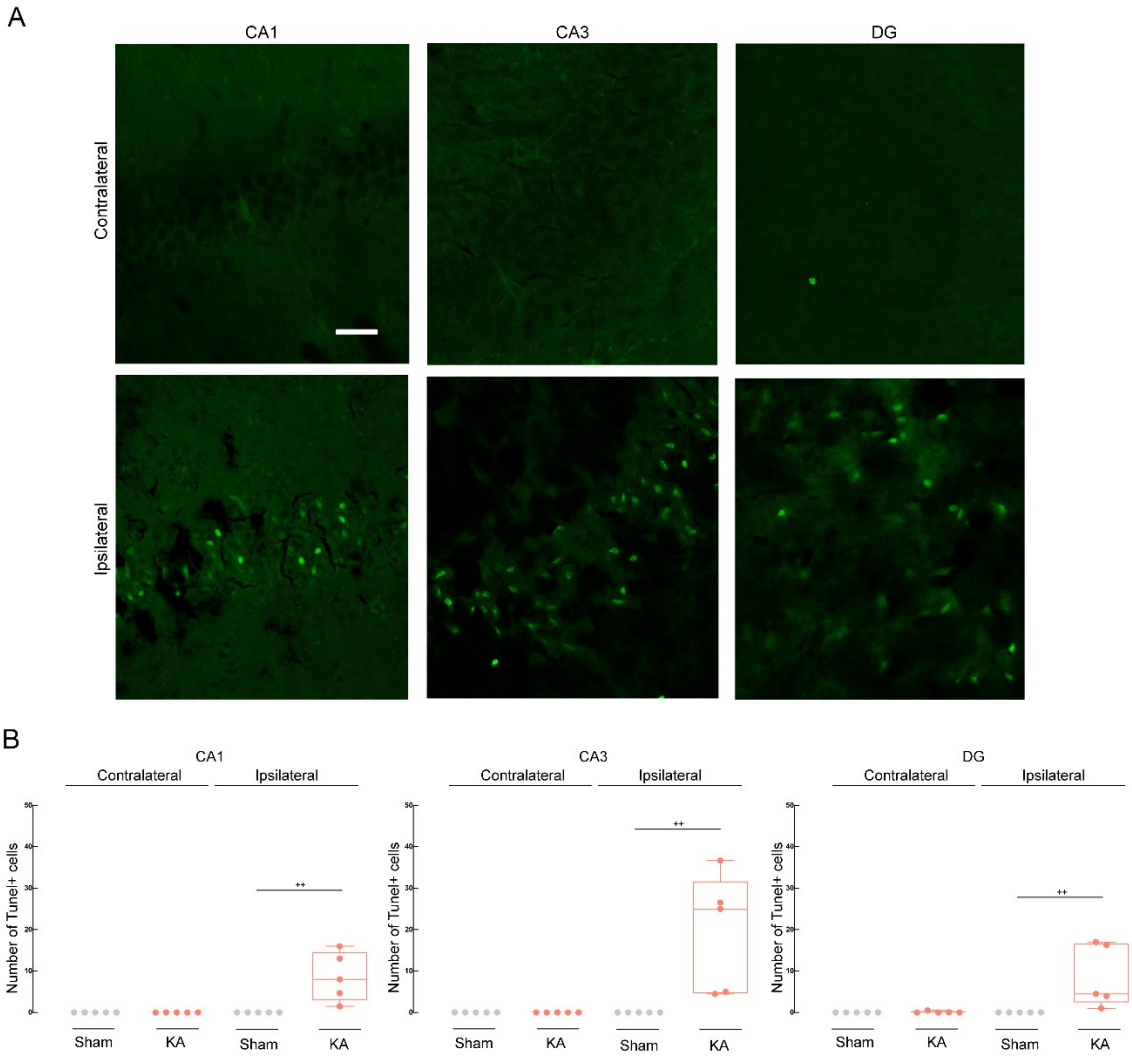

Figure 11 – TUNEL immunostaining and quantification in CA1, CA3 and DG subregions. **(A)** Representative photographs of CA1 (first column), CA3 (middle column) and DG (last column) subregions of the ipsilateral and contralateral hippocampi of 3-days post-KA guinea pigs. Calibration bars = 50 µm. **(B)** Comparison between number of $TUNEL^+$ cells in CA1, CA3 and DG of ipsilateral and contralateral

hippocampal subregions. In all graphics, grey and red plots show counts from sham (*n*=5) and KA 3 days after ncSE (*n*=5) guinea pigs, respectively. ($^{++}$): $p<0.01$ (Mann-Whitney U test).

4.2.3- GFAP and IgG

Subsequently, we examined astrocytic reactive state in the same animal groups. As illustrated in Figure 12A (see also Figure 9) astrogliosis was induced by KA treatment. The densitometric values were significantly higher in all subfields ipsilateral to KA injection at 3-days post-KA when matched to the sham-operated guinea pigs (Figure 12A; representative panel in Figure 9). High GFAP immuno-density was sustained in CA1 and DG of the KA chronic guinea pigs (Figure 12A). DZP + KA treated animals had the same high densitometric profile of the 3-days post-KA injected guinea pigs when compared to their respective sham-groups (Figure 12A). Contrasting to our previous preliminary study[73], an increase in GFAP densitometry was also detected in the contralateral hippocampus of both KA (CA1, CA3 and DG) and DZP + KA guinea pigs (CA3 and DG) in comparison with their corresponding sham-operated animals (Figure 12A). These values decreased in the 4 weeks post-KA animal cohort and differences were no longer observed when matched against the sham operated animals (Figure 12A).

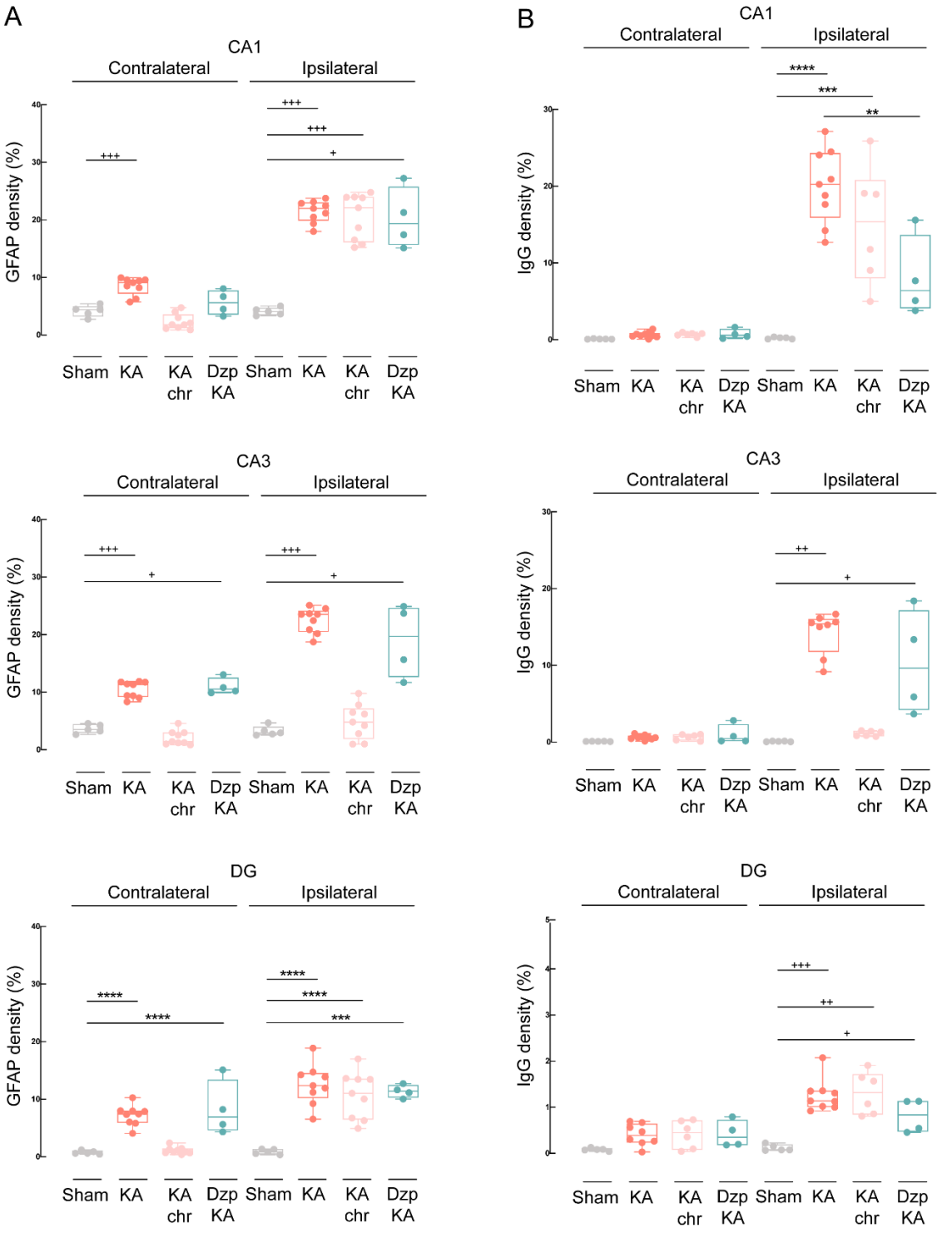

Figure 12 – GFAP and IgG semi-quantitative densitometry analysis. Average percentage of densitometric changes in the KA injected (ipsilateral) and contralateral hippocampal CA1, CA3 and DG subregions. Grey plots: sham-operated animals. Red plots: 3-days post-KA injection guinea pigs (KA). Pink plots: 1-month post-KA injection animals (KA chronic). Green plots: animals treated with DZP and KA injected (DZP + KA). **(A)** GFAP densitometric changes from sham (n=5), KA (n=9), KA chronic (n=9) and DZP + KA (n=4) guinea pigs. ($^{+}$): p<0.05; ($^{+++}$): p<0.001 (Mann-Whitney U test); (***): p<0.001; (****): p<0.0001 (ANOVA). **(C)** Average percentage of densitometric IgG staining in sham (n=5), KA (n=9), KA chronic (n=6) and DZP + KA (n=4) guinea pigs. ($^{+}$): p<0.05; ($^{++}$): p<0.01; ($^{+++}$): p<0.001 (Mann-Whitney U test); (**): p<0.01; (***): p<0.001; (****): p<0.0001 (ANOVA).

Lastly, we evaluated the percentage of IgG immunostaining density in CA1, CA3 and DG as a measure of blood-brain barrier (BBB) extravasation into the brain. Higher IgG densitometry values were observed in the ipsilateral hippocampus at 3 days post-KA injection in all regions compared to their respective controls (Figure 12B; representative panel in Figure 13); these values were sustained in CA1 and DG 4 weeks post-KA injection (Figure 12B). Additionally, in the DZP + KA group, CA3 and DG values were higher compared to sham-operated animals (Figure 12B). No changes in IgG densitometry were observed in the contralateral hippocampus in any group (Figure 12B). Overall, these data seem to indicate that KA induced a local increase in BBB permeability exclusively in the KA-injected hippocampus.

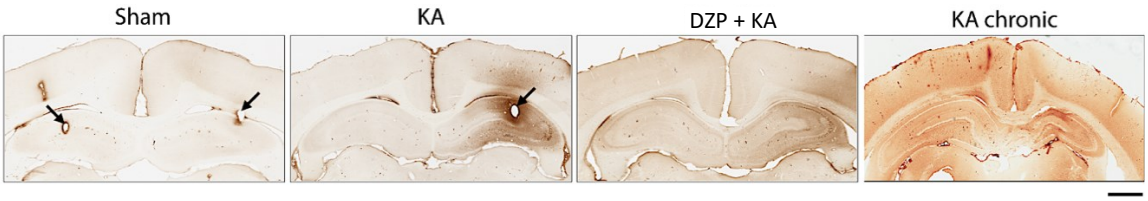

Figure 13 – IgG representative micrographs. IgG immunostained coronal sections represented for sham (first), 3-days post-KA (second), DZP + KA (third) and KA chronic animals (last). KA was injected in the right dorsal CA1 region (injection cannula artifact marked by arrowhead). Calibration bar= 1 mm.

Similar to the NeuN and MAP2 analysis, we also evaluated how the aforementioned 4 animals that developed a higher % of convulsive seizures would match against the remaining animals from the same 3-days post-KA cohort in the GFAP and IgG immunodensitometry analysis (Figure 14). Identical to NeuN and MAP2, GFAP and IgG analysis between these two groups showed no differences between animals with roughly 10% ± of convulsive seizures *vs* animals that experience < 2% of convulsive seizures, demonstrating that in our model the few convulsive seizures observed in a small number of animals had no relevant contribution to the development of brain damage markers as previously shown in preceding studies[72–74].

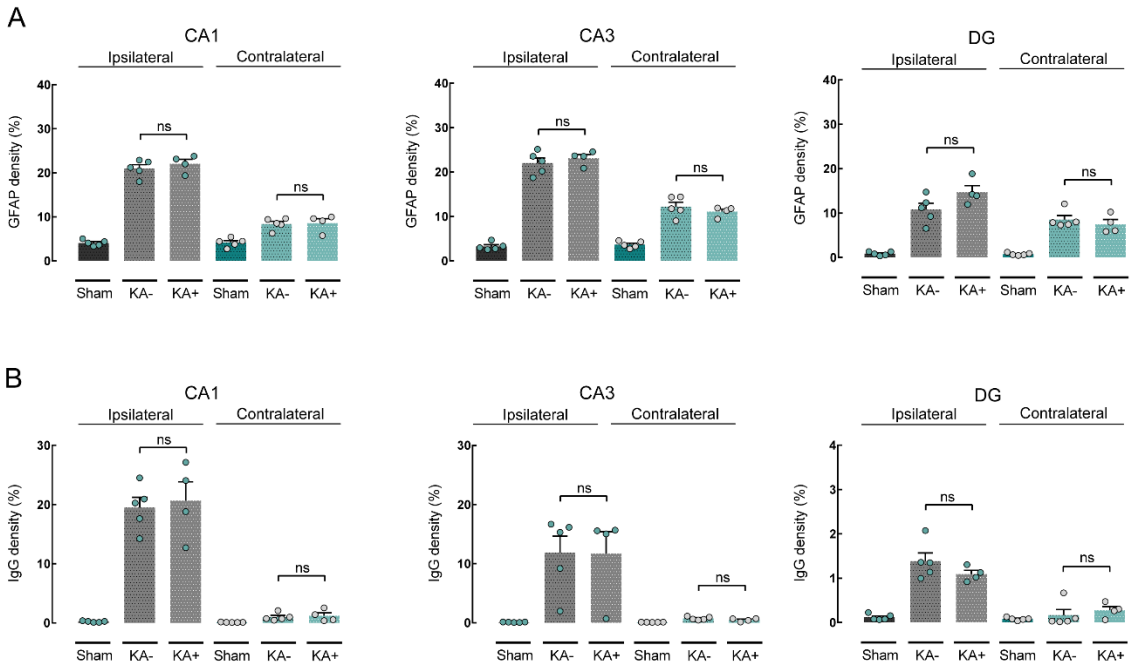

Figure 14 – GFAP and IgG semi-quantitative densitometry analysis. Average percentage of densitometric changes in the KA-injected (ipsilateral - grey shading) and contralateral (green shading) hippocampal CA1 (left panels), CA3 (middle panels) and DG (right panels) subregions are illustrated. **(A)** GFAP densitometric values obtained from sham (*n*=5) and 3 days-post KA animals divided into: KA^- (< 2% of convulsive seizures; *n*=5), KA^+ (±10% convulsive seizures; *n*=4). Ns = non-significant. **(B)** IgG densitometric values obtained from sham (*n*=5) and 3 days-post KA animals divided into: KA^- (< 2% of convulsive seizures; *n*=5), KA^+ (±10% convulsive seizures; *n*=4). Ns = non-significant.

4.3. Morphological analysis of microglia

To further study glial involvement in KA-induced focal ncSE, we also examined the morphological changes of microglia cells in the hippocampus ipsilateral and contralateral to KA injection, analyzed with Iba-1 immunofluorescent sections (Figure 15A, F). Sholl analysis was used to quantify the number of intersections at radial intervals of 2 µm starting from the soma (Figure 15B, C, D, E) and showed smaller values in the ipsi (CA1 and DG) and contralateral (CA1) hippocampus of KA animals matched against sham-their respective sham-operated guinea pigs (Figure 15D, E). Concerning the chronic group, Sholl analysis showed microglia changes towards an activated-phenotype occurring in both CA1 and DG in KA-injected ipsilateral hippocampus (Figure 15D, E), whereas values similar to sham group were observed in the contralateral hippocampus (Figure 15D, E).

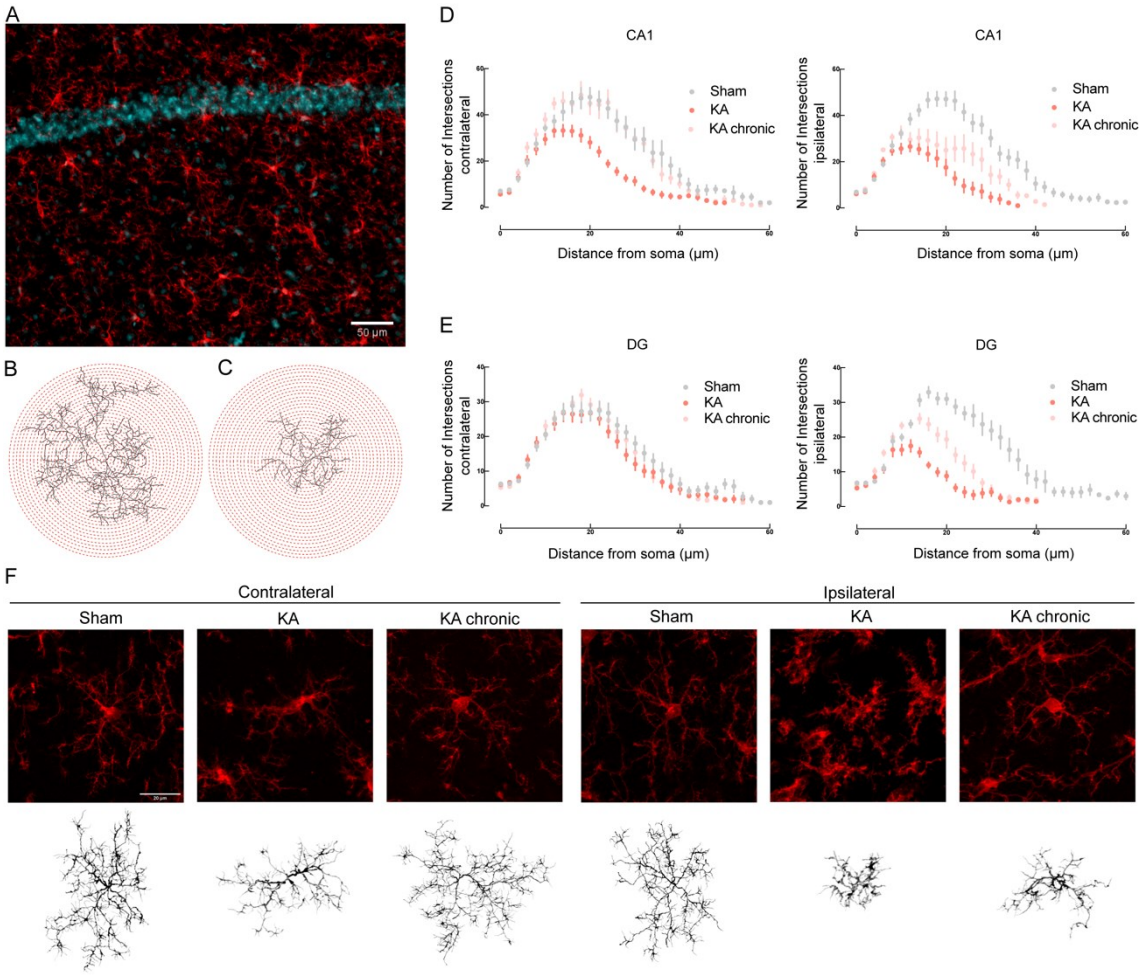

Figure 15 – Morphological analysis and reconstruction of microglial cells in hippocampal CA1 and DG. **(A)** Representative immunofluorescence of a hippocampal coronal section of CA1 pyramidal layer: neurons marked by DAPI in blue, microglia stained with Iba-1 in red. Calibration bar = 50 µm. **(B)** Representative Sholl analysis setting of a manually reconstructed microglia cell from a KA animal (contralateral hippocampus) and **(C)** from the ipsilateral hippocampus of the same animal. The circles centered around the soma are separated by at radial intervals of 2 µm. **(D)** Number of intersections *per* 2 µm radius plotted against the distance from the cell soma in the contralateral (left) and ipsilateral (right) CA1 hippocampal region. Grey line: sham-operated animals. Red line: 3-days post-KA injection (KA). Pink line: 1-month post-KA injection (KA chronic). **(E)** Number of intersections *per* 2 µm radial steps in the contralateral (left) and ipsilateral (right) DG region. For **(D)** and **(E)** *n*=15 cells; 3 cells *per* animal. **(F)** Representative morphologies of microglial cells in Iba-1 immunofluorescence coronal sections in the CA1 hippocampal regions are shown for sham, KA and KA chronic animals.; the correspondent reconstruction of the microglial cell is illustrated in the lower part of the panel. Left and right (KA-injected) hippocampus is marked by contralateral and ipsilateral, respectively. Calibration bar = 20 µm.

Moreover, by directly comparing the Sholl analysis between the ipsilateral and contralateral hippocampus of 3 days post-KA animals (Figure 16A) and 1-month post-KA guinea pigs (Figure 16B), we observed a consistent decrease in the number of intersections in both CA1 and DG and consequently in complexity (towards a more microgliosis-like phenotype i.e. amoeboid shape) of microglia in the ipsilateral hippocampus of 3 days post-KA animals when compared to their respective contralateral

hippocampus (Figure 16A) that was maintained over time as demonstrated by the chronic KA animal group (Figure 16B).

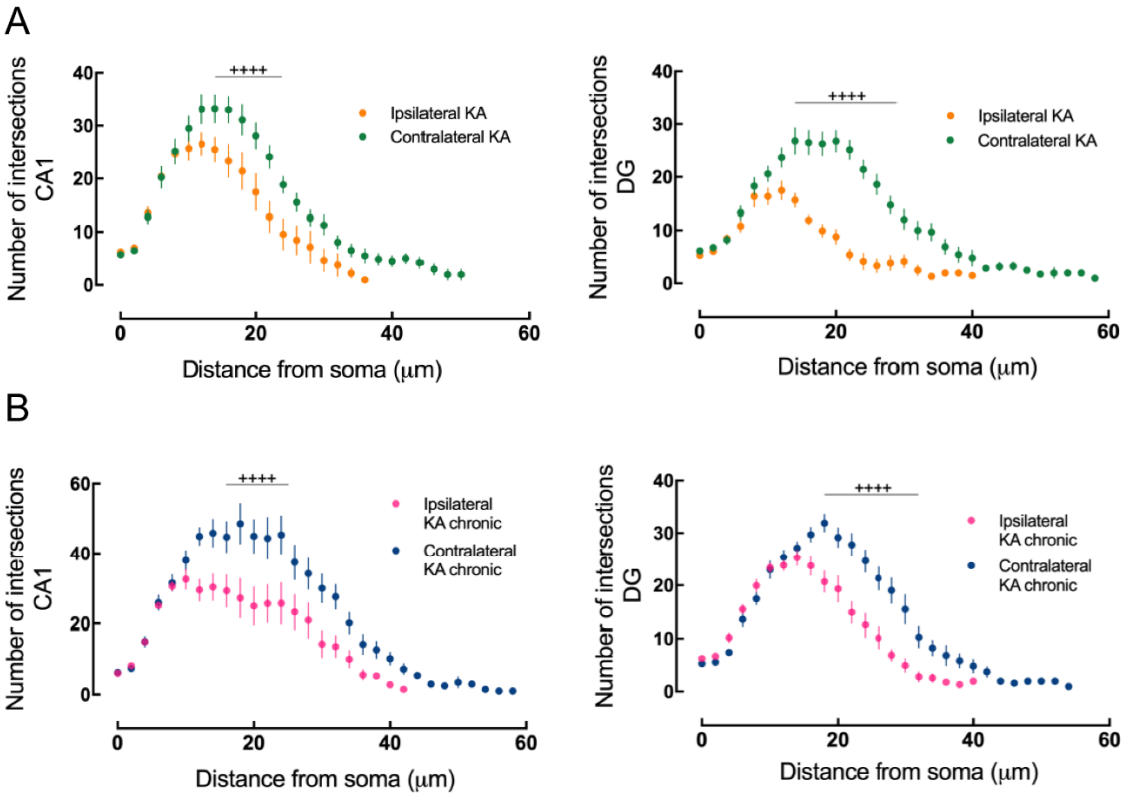

Figure 16 – Sholl analysis of microglial cells in hippocampal CA1 and DG. **(A)** Number of intersections *per* 2 µm radius plotted against the distance from the cell soma in the contralateral and ipsilateral CA1 and DG hippocampal regions of 3-days post-KA injected guinea pigs. Green line: contralateral hippocampus. Orange line: ipsilateral hippocampus. ($^{++++}$): $p<0.001$ (Mann-Whitney U test). **(B)** Number of intersections *per* 2 µm radius plotted against the distance from the cell soma in the contralateral and ipsilateral CA1 and DG hippocampal regions of 1-month post-KA injected guinea pigs. Green line: contralateral hippocampus. Orange line: ipsilateral hippocampus. ($^{++++}$): $p<0.0001$ (Mann-Whitney U test). For **(A)** and **(B)** n=15 cells; 3 cells *per* animal.

Furthermore, microglia cells had a significantly reduction in the number of number of processes (firs row), total length (second row) and average intersections (last row) at 3 days post-KA in ipsilateral CA1 and DG when compared to their respective sham-animals (Figure 17; see also Figure 15F). The same profile was observed in the contralateral hippocampus 3-days post KA (except average number of intersections in DG; Figure 17). Curiously, while in the ipsilateral hippocampus these changes were sustained over time (except average intersections in CA1), in the contralateral hippocampus they all returned to basal levels in the KA chronic group and showed no difference when compared to their correspondent sham-groups (Figure 17).

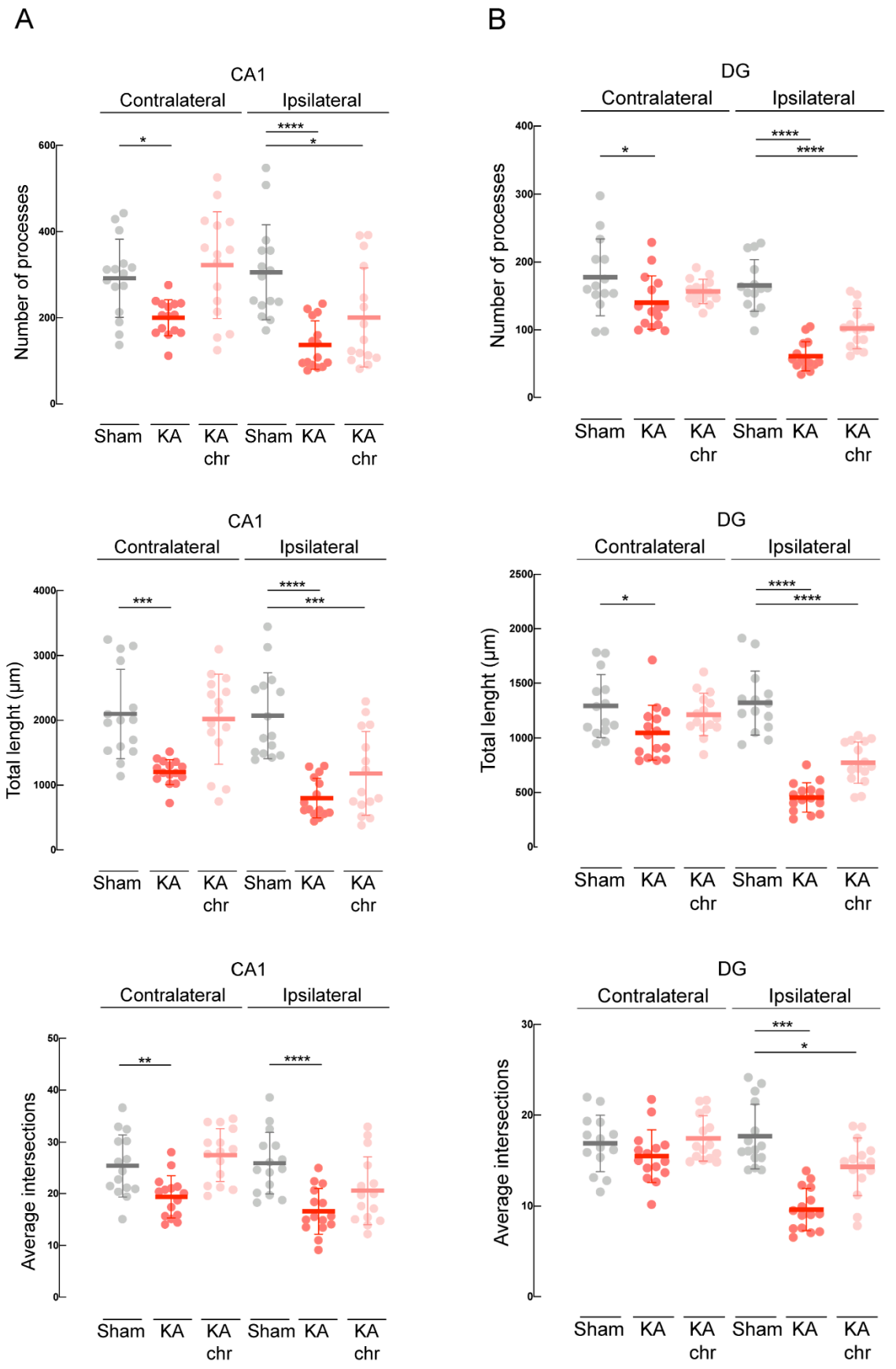

Figure 17 – Comparative analysis of microglial tridimensional morphology based on Sholl analysis. Grey plots: sham-operated animals. Red plots: 3 days post-KA injection guinea pigs (KA). Pink plots: 1-month

post-KA injection animals (KA chronic). **(A)** Number of processes *per* 2 μm radius, total length and average number of intersections of microglia cells in CA1 hippocampal formation from sham (*n*=15 cells), KA (*n*=15 cells) and KA chronic (*n*=15 cells) guinea pigs (3 cells *per* animal). (*): p<0.05; (**): p<0.01; (***): p<0.001; (****): p<0.0001 (ANOVA). **(B)** Number of processes *per* 2 μm radius, total length and average number of intersections of microglia cells in DG from sham (*n*=15 cells), KA (*n*=15 cells) and KA chronic (*n*=15 cells) animals (3 cells *per* animal). (*): p<0.05; (***): p<0.001; (****): p<0.0001 (ANOVA).

4.4. Gene expression analysis

4.4.1- IL1-β, Cox-2, HO-1 and c-FOS

In light of the observed transient and perchance reversible glial activation coupled with a general neuronal preservation in the hippocampus contralateral to KA injection, we complemented the morphological analysis with the study of gene expression (through mRNA relative expression) in CA1 and DG using quantitative real-time PCR (Figure 18 and 19). Initially, we measured the mRNA levels of pro-inflammatory genes IL1-β and COX-2 (Figure 18A, B, respectively). Similar to the densitometry analysis, we observed a significant increase in mRNA levels in the ipsilateral CA1, 3 days post-KA with respect to their sham-operated animals (Figure 18A, B); expression was higher also in DG, with statistical significance only for COX-2 (Figure 18B). One month following KA injection, these genes were no longer upregulated when compared to their respective sham-operated groups (Figure 18A, B). Contralaterally, no increase in the aforementioned genes was observed in any group (Figure 18A, B). Stress-induced gene HO-1 and activity-dependent c-Fos expression were upregulated in the ipsilateral side at 3 days post-KA injection compared against sham-animals in CA1 and DG (Figure 18C, 19A, respectively). No increment on mRNA expression levels were observed in the KA chronic group in the ipsilateral side as well as all contralateral hippocampi groups matched against their respective sham-operated groups in both CA1 and DG (Figure 18, 19A).

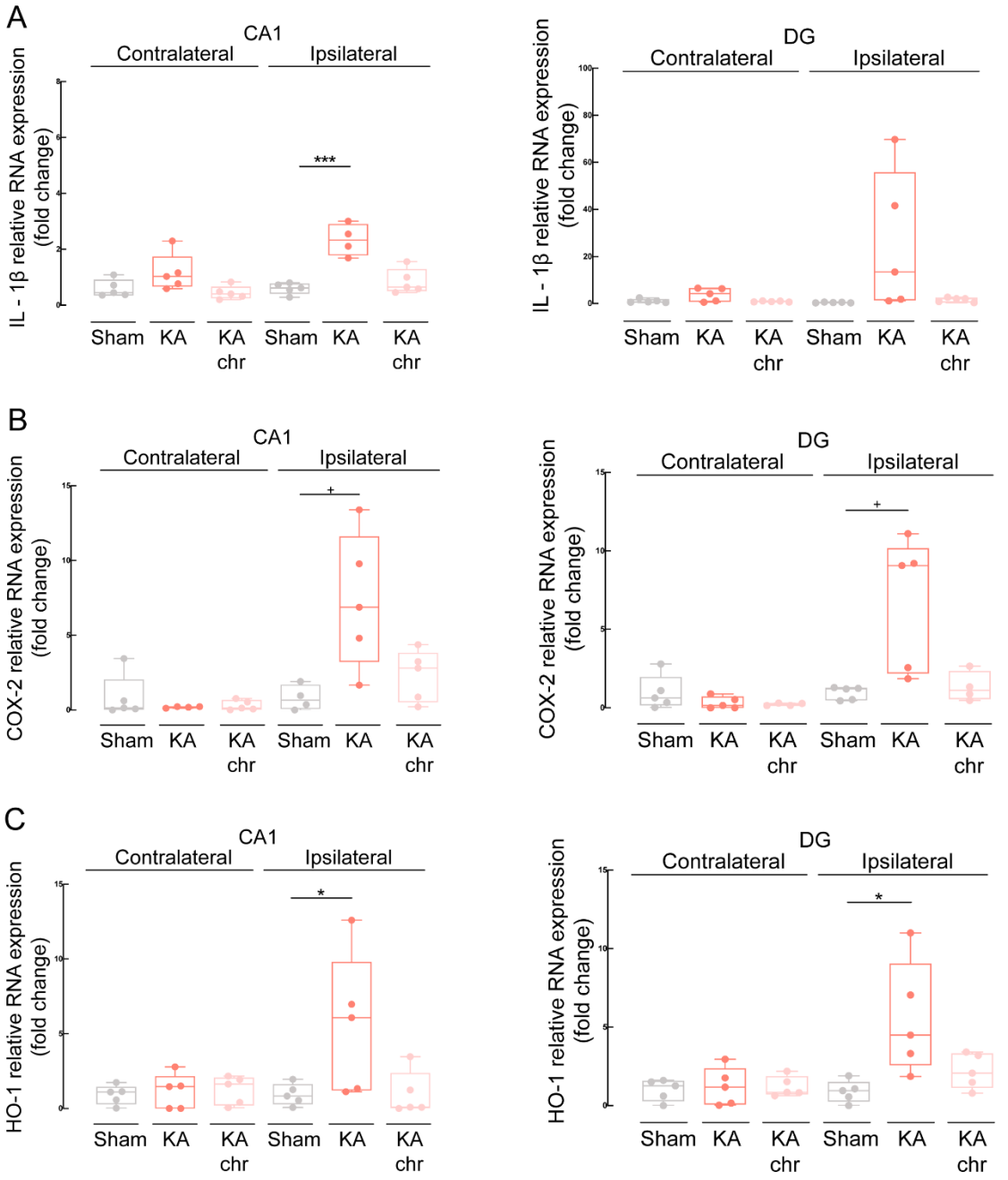

Figure 18 – Quantitative real-time PCR gene expression analysis of IL-1β, COX-2 and HO-1 genes. Grey plots: sham-operated animals. Red plots: 3-days post-KA injection guinea pigs (KA). Pink plots: 1-month post-KA injection animals (KA chronic). Average relative mRNA expression (fold change) in the hippocampal CA1 and DG subregions ipsi- and contralateral to KA injection are represented. The mean value of 5 animals for each of the 3 groups is reported, unless indicated. All values were normalized to housekeeping genes (Actin and GADPH) as well as to their respective sham-operated animal groups. **(A)** IL-1β RNA expression obtained from sham, KA and KA chronic guinea pigs in CA1 (left) and DG (right). (***): $p<0.001$ (ANOVA). **(B)** COX-2 mRNA expression levels obtained from the same areas of sham (n=4-5), KA and KA chronic (n=4-5) guinea pigs in CA1 (left) and DG (right). ($^{+}$): $p<0.05$ (Mann-Whitney U test). **(C)** HO-1 RNA expression levels obtained from the same areas of sham, KA and KA chronic guinea pigs in CA1 (left) and DG (right). (*): $p<0.05$ (ANOVA).

4.4.2- AQP4 and K_{ir} 4.1

Finally, astrocyte specific AQP4 and K_{ir} 4.1 gene expression was evaluated (Figure 19B, C). AQP4 mRNA levels were upregulated in DG ipsilaterally at 3 days post-KA injection compared sham animals, but not in KA chronic animals (Figure 19B). Intriguingly, an increase in the expression levels of AQP4 in CA1 and DG and K_{ir} 4.1 in DG was observed in the contralateral hippocampus compared to sham guinea pigs (Figure 19B, C) suggesting a seizure activity-mediated upregulation of both genes that are selectively expressed in astrocytes[95]. These increased levels in mRNA expression reverted to sham-operated values in the animals 1-month post-KA injection (Figure 19B, C). This seems to suggest that, in the contralateral hippocampus, the increased expression in GFAP and morphological change in microglia was accompanied with an upregulation of AQP4 and K_{ir} 4.1 genes at 3 days post-KA but no correlation towards neuronal death or BBB leakage was observed (based upon the NeuN, MAP2, FJ, TUNEL and IgG results).

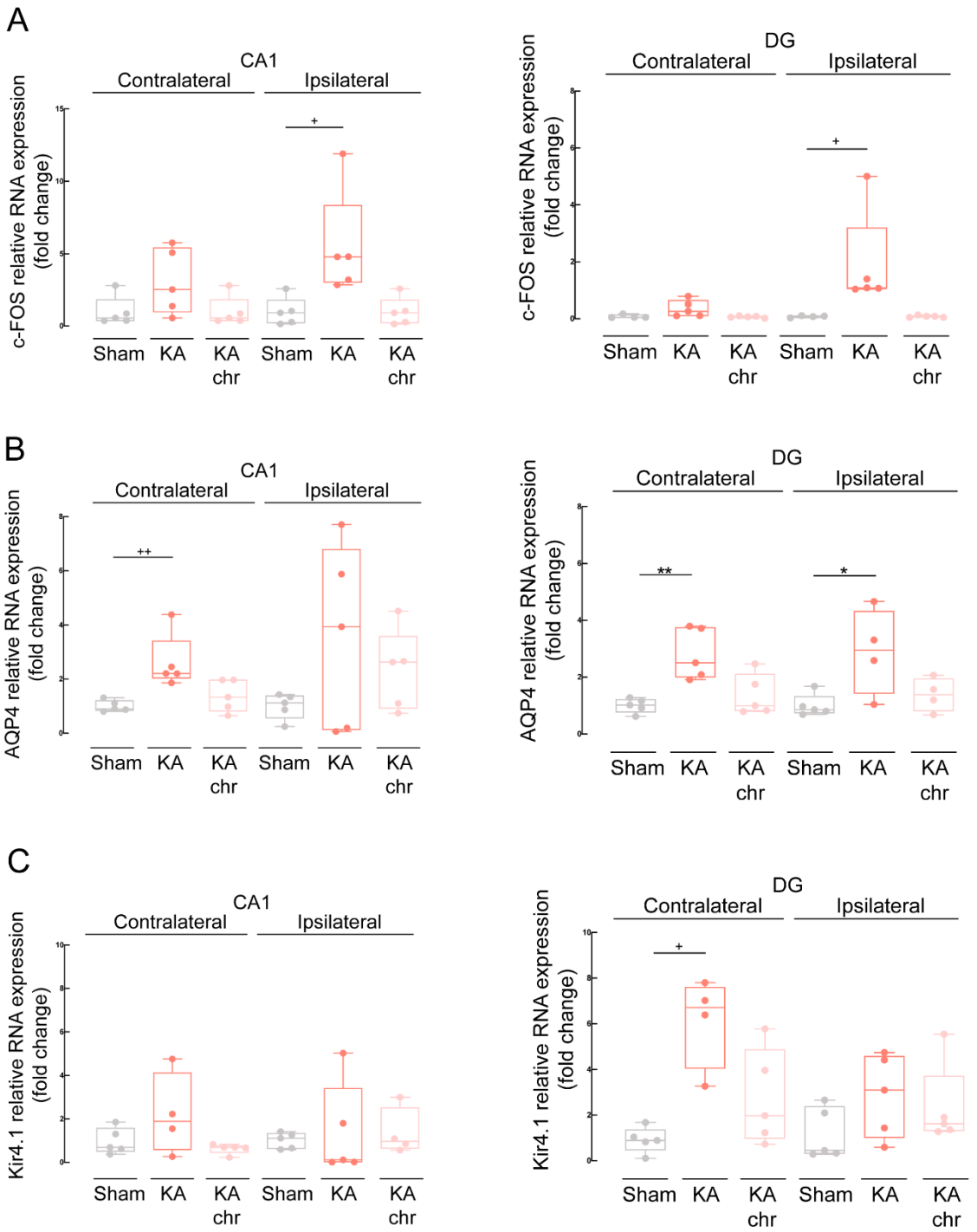

Figure 19 – Quantitative real-time PCR gene expression analysis of c-FOS, AQP4 and K_{ir} 4.1 genes. Grey plots: sham-operated animals. Red plots: 3-days post-KA injection guinea pigs (KA). Pink plots: 1-month post-KA injection animals (KA chronic). Average relative mRNA expression (fold change) in the hippocampal CA1 and DG subregions ipsi- and contralateral to KA injection are represented. The mean value of 5 animals for each of the 3 groups is reported, unless indicated. All values were normalized to housekeeping genes (Actin and GADPH) as well as to their respective sham-operated animal groups. **(A)** c-FOS mRNA expression levels obtained from the same areas of sham, KA and KA chronic guinea pigs in CA1 (left) and DG (right). ($^{+}$): $p<0.05$ (Mann-Whitney U test). **(B)** AQP4 mRNA expression levels obtained from the same areas of sham, KA and KA chronic (n=4-5) guinea pigs in CA1 (left) and DG (right). ($^{++}$): $p<0.01$ (Mann-Whitney U test); (*): $p<0.05$; (**): $p<0.01$ (ANOVA). **(C)** K_{ir} 4.1 mRNA expression levels obtained from the same areas of sham, KA and KA chronic (n=4-5) guinea pigs in CA1 (left) and DG (right). ($^{+}$): $p<0.05$ (Mann-Whitney U test).

Chapter **5**

Discussion

5.1 Discussion

The present study focusses on a model of focal non-convulsive *status epilepticus* (ncSE) without secondary generalization that mimics one of the most common and unproperly treated types of human *status epilepticus* (SE). Our data supports the notion that focal non-convulsive seizures recorded during the course of focal ncSE, when occurring without the contribution of any other harmful insult to the brain [kainic acid (KA) in our case], might not be as detrimental as we once thought. Furthermore, we show for the first time to our knowledge that in this model of focal ncSE without secondary generalization, when analyzing a remote secondary seizing structure that experiences no cytotoxic effect of KA (i.e. contralateral hippocampus), glial cells seem to have a mild transient and possibly reversible activation with intrinsic defense mechanisms that might help neurons cope with seizure activity and therefore do not translate into neuronal loss or blood-brain barrier (BBB) leakage.

As previously mentioned, the majority of animal models that use intracerebral KA injection report focal secondarily generalized seizures[48,49,62]. The presence of prominent convulsive generalized seizures in these studies is a major confounder for the analysis of tissue pathology, since convulsive seizures have been demonstrated for years to cause brain damage via complex generalized and systemic pathogenic mechanisms (for reviews, see[4,5]). In our model, we were able to induce a primary epileptogenic focus in one hippocampus with the intrahippocampal KA injection, that consequently spreads to the contralateral hippocampus in less than a minute. For this reason, we were able to analyze a remote secondary region that was characterized by having independent seizure activity during focal ncSE with no other underlying cytotoxic damaging event occurring in parallel. Additionally, the separate activity patterns and occasional desynchronization of the two hippocampi observed in the EEG analysis suggested that these structures, in fact, undergo a different spatiotemporal evolution following the initial SE. As shown in our group before[73], the unilateral EEG recording observed at focal ncSE onset excludes that the bilateral activation is due volume-conducted activity from the injected hippocampus.

For the data to be as coherent as possible, all animals included in this study developed a focal ncSE with focal non-convulsive seizures entraining both hippocampi; focal seizures could, on occasion, secondarily evolve into diffusely propagated cortical

epileptiform discharges that correlated with a generalized motor behavior. With the exception of 4 animals that presented 10-15 secondarily convulsive seizures during focal ncSE, the number of brief (<30 s) convulsive seizures in our experimental group was minimal and results did not change when these 4 animals were removed from the analysis (further addressed below).

As aforementioned, the reasoning for the inclusion of a chronic condition in this study was twofold: a) the intent of characterizing its electrobehavioural features as well as establish if epileptogenesis had occurred in all animals with features that faithfully mimic human mesial temporal lobe epilepsy with hippocampal sclerosis (mTLE-HS), as previously described[72,74]; b) understand if the damage developed in the acute 3 days KA animal cohort could progress/worsen in a time dependent manner or if, on the contrary, the main damaging event in this model was the ncSE phase and time/spontaneous seizures had no significant impact in further harming the brain. Moreover, seizure suppressor diazepam (DZP) was employed with the intent of indirectly analyzing how much seizure activity could exacerbate the damage already established by KA, by comparing the 3 days KA animal group that in the ipsilateral hippocampus experienced KA injection together with seizures activity *vs* the ipsilateral hippocampus of DZP animals that only underwent the cytotoxic sequalae of KA. For the DZP-related part of the study, the analysis of the contralateral hippocampus was not as important (but still carried out) since very few seizures were observed contralaterally in this group.

Interestingly, in our model, the treatment with DZP reduced both the number of seizures during focal ncSE and ncSE duration itself; these findings correlated with a much-reduced extension of brain damage in the hippocampus ipsilateral to KA injection, as demonstrated by the reduced density of NeuN, MAP2, GFAP, IgG and Fluoro-Jade (FJ) stainings. Even though a direct effect of DZP in reducing the time spent in seizures should also be considered, the less intense cell loss and gliosis spotted in DZP-treated guinea pigs strongly imply that the KA-induced damage is partially due to the direct excitotoxic action of KA at the injection site. Furthermore, the larger and more intense distribution of damage markers in the KA-injected hippocampus in the absence of DZP supports the notion that seizure discharges during focal ncSE are able to exacerbate the KA-induced hippocampal damage. Therefore, the damage inflicted upon the brain by KA injection has a twofold etiology: deterioration due to the direct toxicity of KA at the injection site and the exacerbated degeneration secondary to the KA elicited by

epileptiform activity. These findings are in line with other studies on focal secondarily generalized SE (FSGSE) induced by local intracerebral KA injections that reported reduced local brain damage at the site of injection when DZP was administrated after SE[48,55,96]. Our study is the first to our knowledge to demonstrate that DZP treatment dramatically reduces focal non-convulsive seizures during focal ncSE without secondary generalization and that these changes correlate with a reduced damage at the KA injection site.

When trying to establish if seizure activity is able to induce brain damage or not, the first line of evidence is obtained with the analysis of neuronal loss. In our study, we evaluated neuronal loss using neuronal markers NeuN and MAP2 and FJ (shown to label irreversibly damaged neurons[97]) and TUNEL (detects apoptotic DNA fragmentation[98]) apoptotic assays. Our results showed a consistent and recurrent neuronal cell loss in the ipsilateral hippocampus in 3 days acute KA and 1 month KA chronic animals, with no correspondent neuronal loss in the contralateral hippocampus. From which specifically molecular mechanism this neuronal loss was triggered requires further studies, but most likely there were several processes occurring simultaneously that contributed to this outcome. Glial cell loss was not evaluated, and additional studies are necessary to address this topic. Nevertheless, FJ^+ and $TUNEL^+$ cells were not observed in a remote brain region (contralateral hippocampus), where focal seizures during focal ncSE were also generated, as mentioned before. Moreover, observing the FJ and TUNEL results it was revealed that ipsilateral neuronal cell loss occurred in the 3 days KA animal cohort, with no positive cells observed in the KA chronic group. This seems to suggest that the bulk of apoptotic neurons were produced early after focal ncSE and that 1 month post-KA the neuronal loss observed in the NeuN and MAP2 stainings was very similar to the one observed early at 3-days post-KA with no major progression of neuronal cell loss in a time-dependent manner. These data are in line with findings showing that seizures after an initial epileptogenic insult may not lead to progressive cell loss[78]. Additionally, a lack of clear association between the number of lifetime seizures and the severity of neuronal loss was shown in a long follow-up study extended 8 months after SE[67,76]. Similar results were also described in post-surgical tissue obtained from patients with focal epilepsy submitted to surgery[99]. Also, in a post-mortem study, where 28 patients with poorly controlled seizures were examined, a subgroup was reported with no significant hippocampal neuronal loss despite decades of seizures, including SE[100]. However, there are also several

animal studies showing clear progressive neuronal loss produced by seizures not only in the local site of KA injection, but also in remote regions[48,49,101]. This discrepancy might be due to the use of protocols that induce a convulsive SE condition rather than a focal ncSE (as discussed in the Introduction section). In models of proper focal ncSE developed in different animal species, indeed, remote damage in the hippocampus contralateral to KA injection was never explicitly reported[46,47,50,52,61,72–74,102]. We cannot exclude that stronger and more intense seizure activity could induce secondary damage in remote regions and evolve into FSGSE, even though in our experiments no difference in the damage extent in both ipsi and contralateral hippocampi was found in those animals that experienced few secondary convulsive seizures during focal ncSE compared to those with focal seizure only. Nevertheless, a higher percentage of convulsive seizures might have produced different results.

In the present study, we did not examine the mossy fiber sprouting and granule cells dispersion into the dentate gyrus (DG) since it is a widely inconsistent feature of TLE-HS that, when present, is responsible for inducing synaptic reorganization and contribute to chronic hyperexcitability[28]. Additionally, a previous study from our group in the same animal model using Timm stainings showed no obvious cellular dispersion in DG, possibly due to the fact that small volumes of KA are injected focally in CA1 and these alterations could be more due to the KA toxicity than seizure activity *per se*, the authors concluded[72].

The possibility that immunohistochemical changes were not sensitive enough to detect minor changes in regions remote to focal ncSE was here considered and analyzed by evaluating gene expression levels (through mRNA) in acute and chronic post-ncSE guinea pigs. These experiments revealed that genes associated with inflammatory response (IL1-β and COX-2), brain activity (c-FOS) and oxidative stress (HO-1) were upregulated exclusively in the KA-ipsilateral hippocampus early during the acute phase, whereas only genes linked to glial function (AQP4 and Kir4.1) were upregulated 3 days post-KA (but not after 1 month) in the contralateral hippocampus (further discussed below).

For a thorough evaluation of brain damage in focal ncSE (or any other model), neuronal loss is just one of many aspects. Glial cells should be taken into account since their role is of the upmost importance for proper neuronal function. Specifically, they have a plethora of multitasking housekeeping functions such as sensing and responding

to alterations in energy supply, neuronal activity, extracellular ion concentrations, osmolarity, and many other signals. Their dysfunction has been associated to epilepsy for decades[80,103]. As observed in other focal ncSE studies[46,50,72–74,102], an intense gliosis in the injected hippocampus was detected in our model. Here, astro and microgliosis, BBB disruption (indirectly measured through the infiltration of blood-borne molecule IgG) and inflammatory genes IL1-β and COX-2 as well as activity dependent gene c-FOS and stress-related gene HO-1 mRNA levels were increased and, in the case of gliosis and BBB dysfunction, withstood 1 month after focal ncSE. In contrast, a mild astrocytic and microglial reactivity was detected in the contralateral hippocampus only at 3 days post-KA through GFAP densitometry analysis and Iba-1 morphological reconstructions, respectively. As mentioned above, astrogliosis was coupled with specific astrocytic genes AQP4 and $K_{ir}4.1$ upregulation, without overexpression of pro-inflammatory, activity or stress-related genes. A short-lived contralateral microgliosis was also reported, with a significant reduction of microglia complexity, number of processes and total length in CA1 and DG in the acute phase, but not in chronic animals. Interestingly, 1 month post-KA injection, all these alterations returned to basal levels and differences were no longer found with respect to control guinea pigs.

Overall, these results point towards a possible transient effect mediated by seizure activity on glial cells. Our data do not specifically show, however, if the same cells reverted to their inactivated state or if only the resting/inactivated glial cells remained 1 month after focal ncSE. Interestingly, these transient effects correlated with the absence of contralateral neuronal loss or BBB dysfunction. These findings suggest a possible early protective role promoted by glial cells in the hippocampus contralateral to KA injection: the astrocyte-specific expression of AQP4 and $K_{ir}4.1$ might enhance neuron potassium (K^+) clearing during seizure activity. Since both extracellular K^+ concentration and osmolarity have been shown to dramatically modulate neural excitability[81,104,105] it is plausible to speculate that astrocytes increase AQP4 and $K_{ir}4.1$ gene expression as a first line of defense to counter-balance the potential nefarious effect of seizure activity, hence reducing the hyperexcitability through the glial-network. It is unclear however if this compensatory gene upregulation is accompanied by a translation into functional proteins and further studies are required to address this issue. Nevertheless, studies have shown that a dysfunction of astroglial $K_{ir}4.1$ channels underlies impaired K^+ buffering and contributes to hyperexcitability in epileptic tissue[105]. Also, $AQP4^{-/-}$ mice have remarkably

slowed K^+ reuptake in models of seizure and were associated with increased seizure duration, supporting the hypothesis that AQP4 and Kir4.1 can act together in K^+ and H_2O regulation[106]. Additionally, in line with our findings, an acute reactive astro and microgliosis that decreased over time in the contralateral hippocampus, but remained altered in the KA-injected hippocampus was reported in an similar unilateral intrahippocampal KA mouse model[52]. This study reported a delayed upregulation in the contralateral hippocampus of SOCS3, which acts by limiting IL-6 mediated processes, possibly indicating an attempt to limit the intensity/duration of neuroinflammatory signals during the early phase of epileptogenesis. The authors hypothesized that the SOCS3 mRNA delayed increase could be involved in neuronal survival and/or induction of homeostatic mechanisms against neurodegeneration by limiting cytokine signaling in the contralateral hippocampus.

In summary, we were able to induce a focal ncSE in guinea pigs with clear damage being generated by seizure activity + KA in the ipsilateral hippocampus. In a remote region (contralateral hippocampus), even though seizure activity was still independently being generated, no inflammatory/stress-related gene upregulation, BBB dysfunction, neuronal loss or long-lasting astro/microgliosis were observed.

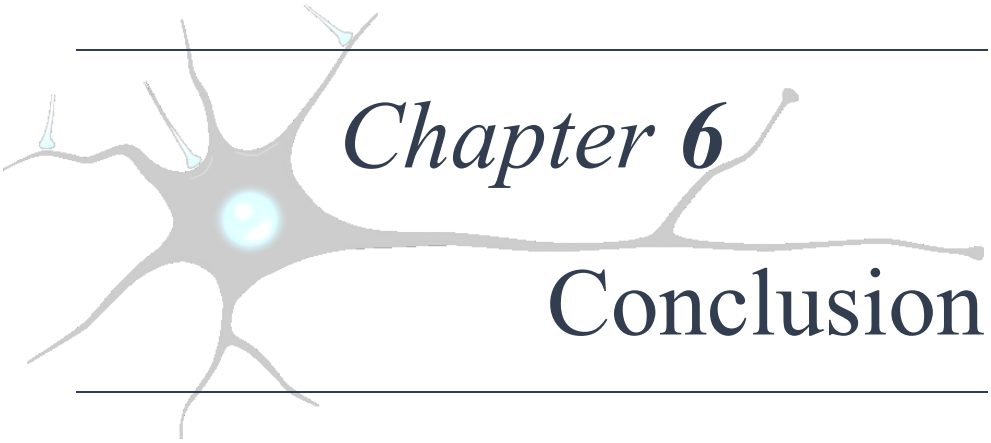

Chapter 6

Conclusion

6.1 Conclusion

As summarized below in Figure 1, in our focal ncSE animal model, brain tissue damage was aggravated by seizure activity when it occurred in combination with the excitotoxic effect of KA. The secondary spread of seizure activity to the contralateral hippocampus transiently activated glial cells, as a potential defense mechanism that prevented remote seizure-associated damage. Additionally, over time (1 month post-KA animal group data) the already established damage observed at 3 days post-KA injection was not augmented, contributing to the idea that after the initial acute SE phase further spontaneous chronic seizures do not lead to a progressive neuronal loss. Of note, these results might only hold true for this particular dosage of KA and/or for the specific seizure-ncSE pattern generated in this animal model. Even though the experimental findings here reported cannot directly be translated into clinical conclusions, our study recommends (examining the DZP findings) the use of anti-seizure treatment in patients suffering from focal ncSE to prevent localized seizure-mediated damage in addition to the injury determined by the primary *noxa*. When combined with a coexisting insult, seizures can work synergistically to further exacerbate the damage done by the underlying focal ncSE cause. However, if seizure activity spreads to regions away from the boundaries of the primary injury constraint, a detrimental action caused by seizure activity *per se* is not likely to occur in focal ncSE without secondary generalization.

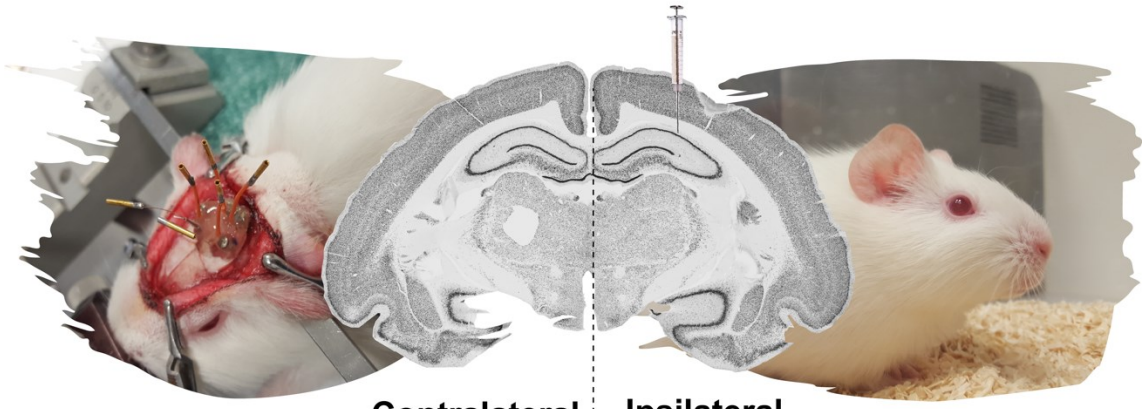

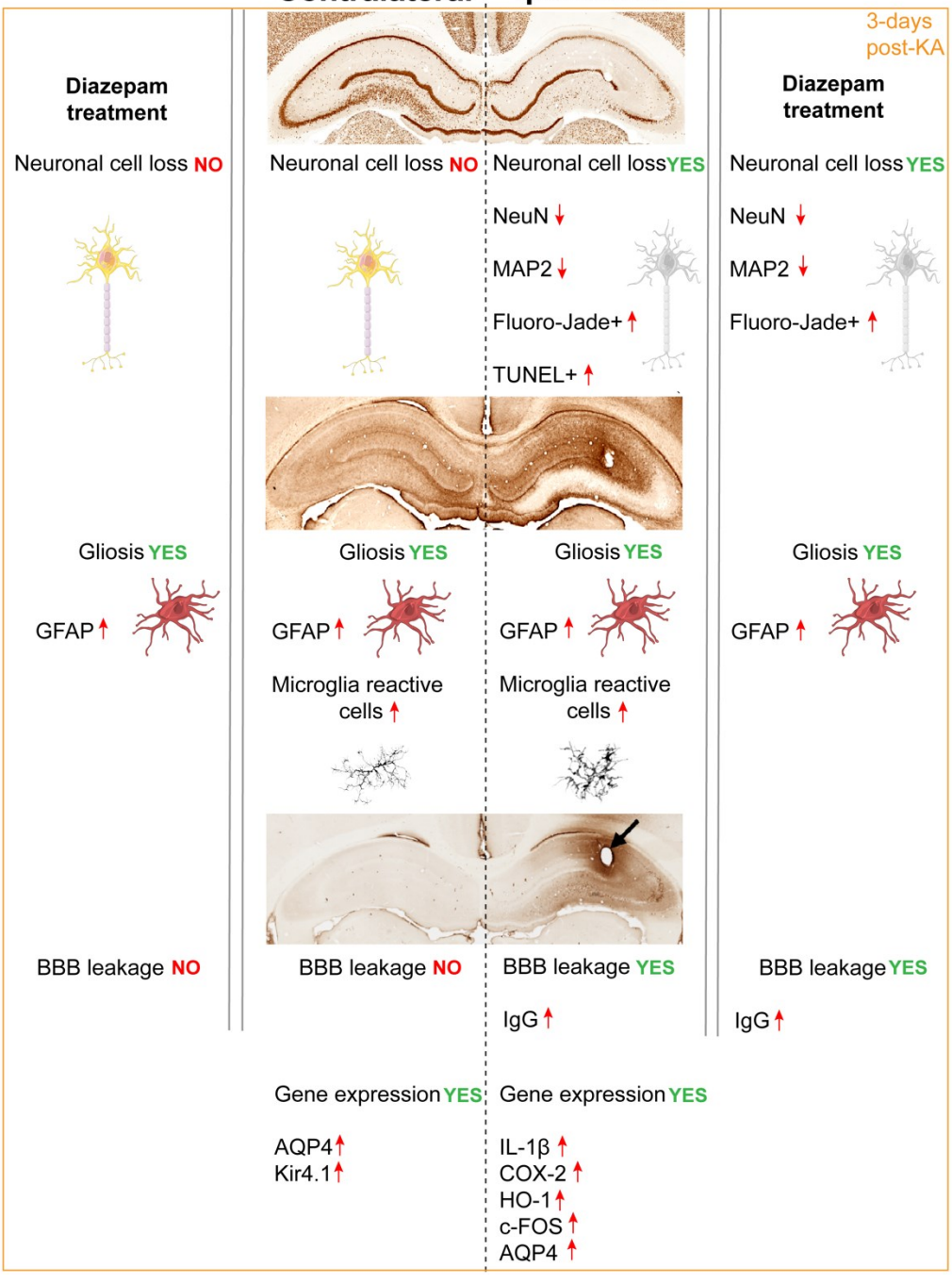
Contralateral
Ipsilateral
3-days post-KA
Diazepam treatment
Neuronal cell loss NO
Gliosis YES
GFAP ↑
BBB leakage NO
Neuronal cell loss NO
Gliosis YES
GFAP ↑
Microglia reactive cells ↑
BBB leakage NO
Gene expression YES
AQP4 ↑
Kir4.1 ↑
Neuronal cell loss YES
NeuN ↓
MAP2 ↓
Fluoro-Jade+ ↑
TUNEL+ ↑
Gliosis YES
GFAP ↑
Microglia reactive cells ↑
BBB leakage YES
IgG ↑
Gene expression YES
IL-1β ↑
COX-2 ↑
HO-1 ↑
c-FOS ↑
AQP4 ↑
Diazepam treatment
Neuronal cell loss YES
NeuN ↓
MAP2 ↓
Fluoro-Jade+ ↑
Gliosis YES
GFAP ↑
BBB leakage YES
IgG ↑

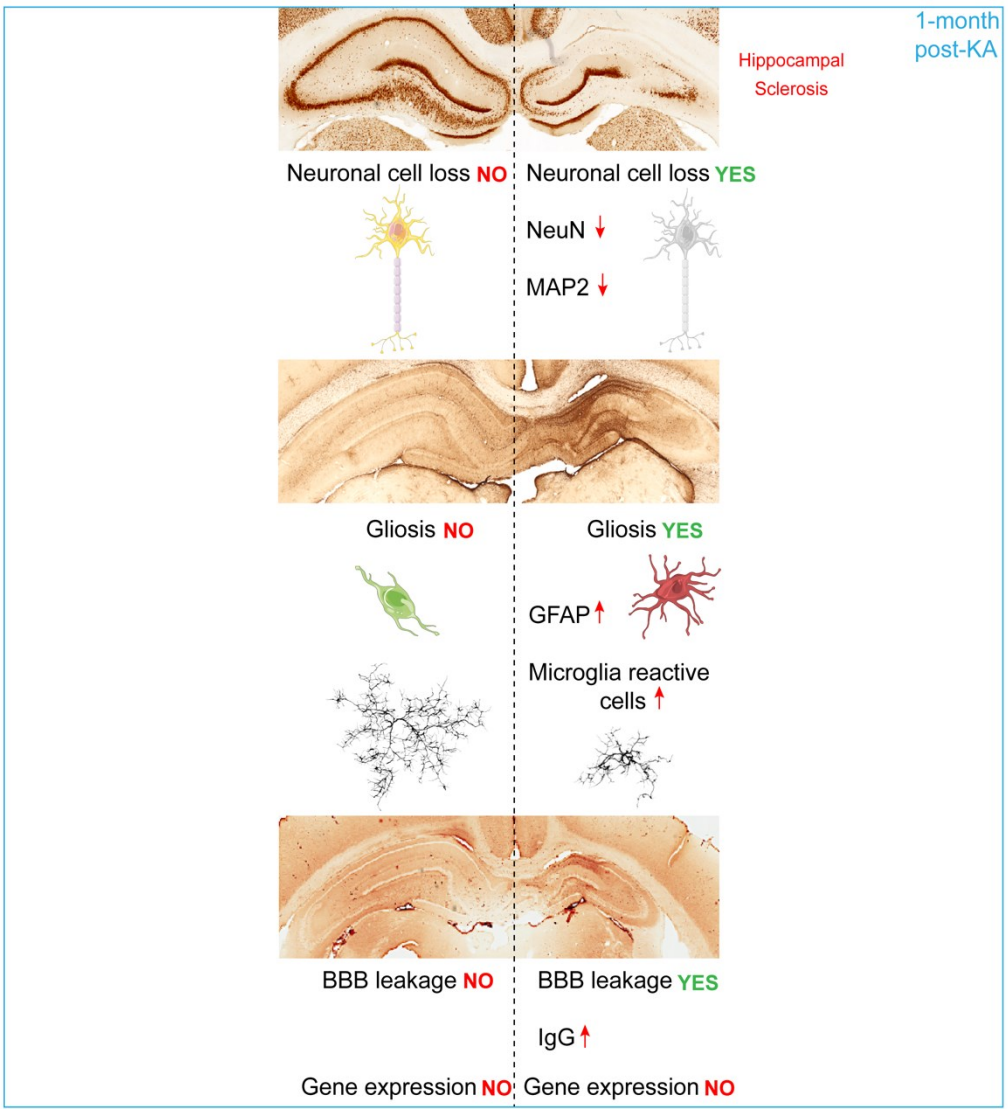

Figure 1 – Scheme with key findings of the study. **Orange rectangle:** Main conclusions in the 3 days post-KA group and DZP animal cohort as well, separated by a double grey line. The ipsilateral side in the 3 days post-KA animal group showed high levels of neuronal loss and gliosis as well as blood-brain barrier (BBB) leakage; the upregulation of genes Il-1β, COX-2, HO-1, c-FOS and AQP4 were also observed. Contralaterally, only gliosis and high mRNA levels of AQP4 and K_{ir}4.1 were found. No neuronal loss nor BBB dysfunction was observed. In the DZP guinea pigs, results were similar: while on the ipsilateral side neuronal loss, gliosis and BBB leakage was detected, on the contralateral side, only gliosis was found. **Blue rectangle:** Main findings in the 1-month post KA animal group. The ipsilateral side still had high levels of neuronal loss, gliosis and BBB dysfunction (with the development of hippocampal sclerosis) while the contralateral side maintained no neuronal loss or BBB dysfunction with the gliosis observed at 3 days post-KA being reverted to control levels. No gene upregulation was observed in any side at this time-point.

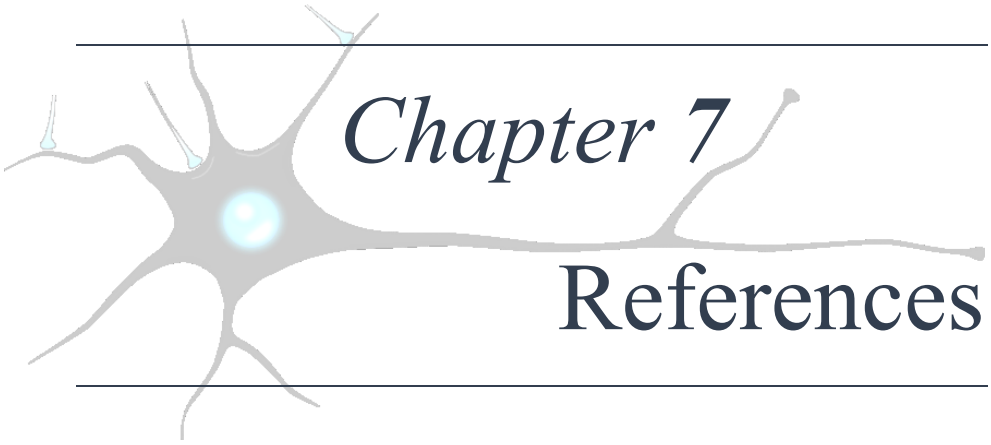

Chapter 7

References

7.1 References

1. Neligan A, Noyce AJ, Gosavi TD, et al. Change in Mortality of Generalized Convulsive Status Epilepticus in High-Income Countries over Time: A Systematic Review and Meta-analysis. JAMA Neurol. 2019;76(8):897–905.
2. Trinka E, Cock H, Hesdorffer D, et al. A definition and classification of status epilepticus - Report of the ILAE Task Force on Classification of Status Epilepticus. Epilepsia 2015;56(10):1515–1523.
3. Fernández-Torre JL. Status epilepticus in idiopathic generalized epilepsy. Epilepsia 2006;47(4):805–806.
4. Wasterlain CG, Fujikawa DG, Penix LR, Sankar R. Pathophysiological Mechanisms of Brain Damage from Status Epilepticus. Epilepsia 1993;34(1):37–53.
5. Shorvon S. Does convulsive status epilepticus (SE) result in cerebral damage or affect the course of epilepsy - The epidemiological and clinical evidence? Prog. Brain Res. 2002;135(1):85–93.
6. Young GB, Claassen J. Nonconvulsive status epilepticus and brain damage: Further evidence, more questions. Neurology 2010;75(9):760–770.
7. Genton P, Ferlazzo E, Thomas P. Absence status epilepsy: Delineation of a distinct idiopathic generalized epilepsy syndrome. Epilepsia 2008;49(4):642–649.
8. Leitinger M, Trinka E, Giovannini G, et al. Epidemiology of status epilepticus in adults: A population-based study on incidence, causes, and outcomes. Epilepsia 2019;60(1):53–62.
9. Rossetti AO, Trinka E, Stähli C, Novy J. New ILAE versus previous clinical status epilepticus semiologic classification: Analysis of a hospital-based cohort. Epilepsia 2016;57(7):1036–1041.
10. Sutter R, Kaplan PW, Rüegg S. Outcome predictors for status epilepticus - What really counts. Nat. Rev. Neurol. 2013;9(9):525–534.
11. Alvarez V, Januel JM, Burnand B, Rossetti AO. Role of comorbidities in outcome prediction after status epilepticus. Epilepsia 2012;53(5)
12. Helmstaedter C. Cognitive outcome of status epilepticus in adults. Epilepsia 2007;48(8):85–90.
13. DeGiorgio CM, Gott PS, Rabinowicz AL, et al. Neuron-specific enolase, a marker of acute neuronal injury, is increased in complex partial status epilepticus. Epilepsia 1996;37(7):606–609.
14. Rabinowicz AL, Correale JD, Bracht KA, et al. Neuron-Specific Enolase Is Increased After Nonconvulsive Status Epilepticus. Epilepsia 1995;36(5):475–479.
15. Rossetti AO, Logroscino G, Liaudet L, et al. Status epilepticus: An independent outcome predictor after cerebral anoxia. Neurology 2007;69(3):255–260.
16. Knake S, Rochon J, Fleischer S, et al. Status epilepticus after stroke is associated with increased long-term case fatality. Epilepsia 2006;47(12):2020–2026.
17. Logroscino G, Hesdorffer DC, Cascino G, Hauser WA. Status epilepticus without an underlying cause and risk of death: A population-based study. Arch. Neurol. 2008;65(2):221–224.

18. Szabo K, Poepel A, Pohlmann-Eden B, et al. Diffusion-weighted and perfusion MRI demonstrates parenchymal changes in complex partial status epilepticus. Brain 2005;128(6):1369–1376.

19. Verity CM, Ross EM, Golding J. Outcome of childhood status epilepticus and lengthy febrile convulsions: Finding of national cohort study. Br. Med. J. 1993;307(6898):225–228.

20. Cockerell OC, Walker MC, Sander JWAS, Shorvon SD. Complex partial status epilepticus: A recurrent problem. J. Neurol. Neurosurg. Psychiatry 1994;57(2):835–837.

21. Guberman A, Cantu-Reyna G, Stuss D, Broughton R. Nonconvulsive generalized status epilepticus: Clinical features, neuropsychological testing, and long-term follow-up. Neurology 1986;36(4):1284–1291.

22. Kaplan PW. No, some types of nonconvulsive status epilepticus cause little permanent neurolooic sequelae (or: « The cure may be worse than the disease »). Neurophysiol. Clin. 2000;30(1):377–382.

23. Gutierrez C, Chen M, Feng L, Tummala S. Non-convulsive seizures in the encephalopathic critically ill cancer patient does not necessarily portend a poor prognosis. J. Intensive Care 2019;7(62):1–9.

24. Adachi N, Kanemoto K, Muramatsu R, et al. Intellectual prognosis of status epilepticus in adult epilepsy patients: Analysis with Wechsler Adult Intelligence Scale-Revised. Epilepsia 2005;46(9):1502–1509.

25. Power KN, Gramstad A, Gilhus NE, et al. Cognitive function after status epilepticus versus after multiple generalized tonic-clonic seizures. Epilepsy Res. 2018;140:39–45.

26. Patterson KP, Baram TZ, Shinnar S. Origins of Temporal Lobe Epilepsy: Febrile Seizures and Febrile Status Epilepticus. Neurotherapeutics 2014;11(2):242–250.

27. Dalby NO, Mody I. The process of epileptogenesis: A pathophysiological approach. Curr. Opin. Neurol. 2001;14(3):187–192.

28. Sutula T, Cascino G, Cavazos J, et al. Mossy fiber synaptic reorganization in the epileptic human temporal lobe. Ann. Neurol. 1989;26(2):321–330.

29. Engel J. Introduction to temporal lobe epilepsy. Epilepsy Res. 1996;26(1):141–150.

30. Sutter R, Marsch S, Fuhr P, et al. Anesthetic drugs in status epilepticus: Risk or rescue? A 6-year cohort study. Neurology 2014;82(8):656–664.

31. Andrade P, Banuelos-Cabrera I, Lapinlampi N, et al. Acute Non-Convulsive Status Epilepticus after Experimental Traumatic Brain Injury in Rats. J. Neurotrauma 2019;36(11):1890–1907.

32. Martin JL, Sloviter RS. Focal inhibitory interneuron loss and principal cell hyperexcitability in the rat hippocampus after microinjection of a neurotoxic conjugate of saporin and a peptidase-resistant analog of substance P. J. Comp. Neurol. 2001;436(2):127–52.

33. Sperk G. Kainic acid seizures in the rat. Prog. Neurobiol. 1994;42(1):1–32.

34. Curia G, Longo D, Biagini G, et al. The pilocarpine model of temporal lobe epilepsy. J. Neurosci. Methods 2008;172(2):143–157.

35. Lévesque M, Avoli M. The kainic acid model of temporal lobe epilepsy. Neurosci. Biobehav. Rev. 2013;37(10):2887–2899.

36. Turski WA, Cavalheiro EA, Schwarz M, et al. Limbic seizures produced by pilocarpine in rats: Behavioural, electroencephalographic and neuropathological study. Behav. Brain Res. 1983;9(1):315–335.

37. Sloviter RS. Hippocampal epileptogenesis in animal models of mesial temporal lobe epilepsy with hippocampal sclerosis: The importance of the “latent period” and other concepts. Epilepsia 2008;49(1):85–92.

38. Kelly ME, Coulter DA. The Pilocarpine Model of Acquired Epilepsy. 2017.

39. Fujikawa DG. The temporal evolution of neuronal damage from pilocarpine-induced status epilepticus. Brain Res. 1996;725(1):11–22.

40. Aronica E, Mühlebner A, van Vliet EA, Gorter JA. Characterization of Pathology. 2017.

41. Engel J. J. Mesial temporal lobe epilepsy: What have we learned? Neuroscientist 2001;7(4):340–352.

42. Blümcke I, Coras R, Miyata H, Özkara C. Defining clinico-neuropathological subtypes of mesial temporal lobe epilepsy with hippocampal sclerosis. Brain Pathol. 2012;22(3):402–411.

43. Henshall DC. Poststatus Epilepticus Models: Focal Kainic Acid. In: Models of Seizures and Epilepsy: Second Edition. 2017 p. 611–624.

44. Riban V, Bouilleret V, Pham-Lê BT, et al. Evolution of hippocampal epileptic activity during the development of hippocampal sclerosis in a mouse model of temporal lobe epilepsy. Neuroscience 2002;112(1):101–111.

45. Arabadzisz D, Antal K, Parpan F, et al. Epileptogenesis and chronic seizures in a mouse model of temporal lobe epilepsy are associated with distinct EEG patterns and selective neurochemical alterations in the contralateral hippocampus. Exp. Neurol. 2005;194(6):76–90.

46. Bouilleret V, Ridoux V, Depaulis A, et al. Recurrent seizures and hippocampal sclerosis following intrahippocampal kainate injection in adult mice: Electroencephalography, histopathology and synaptic reorganization similar to mesial temporal lobe epilepsy. Neuroscience 1999;89(3):717–729.

47. Tanaka T, Tanaka S, Fujita T, et al. Experimental complex partial seizures induced by a microinjection of kainic acid into limbic structures. Prog. Neurobiol. 1992;38(3):317–334.

48. Ben-Ari Y, Tremblay E, Ottersen OP, Meldrum BS. The role of epileptic activity in hippocampal and “remote” cerebral lesions induced by kainic acid. Brain Res. 1980;5(1):515–518.

49. Schwob JE, Fuller T, Price JL, Olney JW. Widespread patterns of neuronal damage following systemic or intracerebral injections of kainic acid: A histological study. Neuroscience 1980;5(2):991–1014.

50. Mouri G, Jimenez-Mateos E, Engel T, et al. Unilateral hippocampal CA3-predominant damage and short latency epileptogenesis after intra-amygdala microinjection of kainic acid in mice. Brain Res. 2008;1213(6):140–151.

51. Bedner P, Dupper A, Hüttmann K, et al. Astrocyte uncoupling as a cause of human temporal lobe epilepsy. Brain 2015;138(5):1208–1222.

52. Pernot F, Heinrich C, Barbier L, et al. Inflammatory changes during epileptogenesis and spontaneous seizures in a mouse model of mesiotemporal lobe epilepsy. Epilepsia 2011;52(12):2315–2325.

53. Ben-Ari Y. Limbic seizure and brain damage produced by kainic acid: Mechanisms and relevance to human temporal lobe epilepsy. Neuroscience 1985;14(2):375–403.

54. Rattka M, Brandt C, Löscher W. The intrahippocampal kainate model of temporal lobe epilepsy revisited: Epileptogenesis, behavioral and cognitive alterations, pharmacological response, and hippoccampal damage in epileptic rats. Epilepsy Res. 2013;103(2):135–152.

55. Pitkänen A, Kharatishvili I, Narkilahti S, et al. Administration of diazepam during status epilepticus reduces development and severity of epilepsy in rat. Epilepsy Res. 2005;63(1):27–42.

56. Lothman EW, Bertram EH, Bekenstein JW, Perlin JB. Self-sustaining limbic status epilepticus induced by "continuous" hippocampal stimulation: electrographic and behavioral characteristics. Epilepsy Res. 1989;3(2):107–119.

57. Mazarati AM, Wasterlain CG, Sankar R, Shin D. Self-sustaining status epilepticus after brief electrical stimulation of the perforant path. Brain Res. 1998;801(2):251–253.

58. Gorter JA, Van Vliet EA. Post-Status Epilepticus Models: Electrical Stimulation. Model. Seizures Epilepsy Second Ed. 2017;

59. Racine RJ. Modification of seizure activity by electrical stimulation: II. Motor seizure. Electroencephalogr. Clin. Neurophysiol. 1972;32(3):281–294.

60. Pitkänen A, Sutula TP. Is epilepsy a progressive disorder? Prospects for new therapeutic approaches in temporal-lobe epilepsy. Lancet Neurol. 2002;1(7):173–181.

61. French ED, Aldinio C, Schwarcz R. Intrahippocampal kainic acid, seizures and local neuronal degeneration: Relationships assessed in unanesthetized rats. Neuroscience 1982;7(10):2525–2536.

62. Mathern GW, Cifuentes F, Leite JP, et al. Hippocampal EEG excitability and chronic spontaneous seizures are associated with aberrant synaptic reorganization in the rat intrahippocampal kainate model. Electroencephalogr. Clin. Neurophysiol. 1993;87(5):326–339.

63. Sloviter RS. "Epileptic" brain damage in rats induced by sustained electrical stimulation of the perforant path. I. Acute electrophysiological and light microscopic studies. Brain Res. Bull. 1983;10(2):675–697.

64. Gorter JA, Van Vliet EA, Lopes da Silva FH, et al. Sodium channel β1-subunit expression is increased in reactive astrocytes in a rat model for mesial temporal lobe epilepsy. Eur. J. Neurosci. 2002;16(2):360–364.

65. Avdic U, Ahl M, Chugh D, et al. Nonconvulsive status epilepticus in rats leads to brain pathology. Epilepsia 2018;59(5):945–958.

66. Nissinen J, Halonen T, Koivisto E, Pitkänen A. A new model of chronic temporal lobe epilepsy induced by electrical stimulation of the amygdala in rat. Epilepsy Res. 2000;38(2–3):177–205.

67. Pitkänen A, Nissinen J, Nairismägi J, et al. Progression of neuronal damage after status epilepticus and during spontaneous seizures in a rat model of temporal lobe epilepsy. Prog. Brain Res. 2002;135(4):67–83.

68. Bertmam EH, Lothman EW. Morphometric effects of intermittent kindled seizures and limbic status epilepticus in the dentate gyrus of the rat. Brain Res. 1993;603(1):25–31.

69. Brandt C, Glien M, Potschka H, et al. Epileptogenesis and neuropathology after different types of status epilepticus induced by prolonged electrical stimulation of the basolateral amygdala in rats. Epilepsy Res. 2003;55(1–2):83–103.

70. Mohapel P, Ekdahl CT, Lindvall O. Status epilepticus severity influences the long-term outcome of neurogenesis in the adult dentate gyrus. Neurobiol. Dis. 2004;15(2):196–205.

71. Gröticke I, Hoffmann K, Löscher W. Behavioral alterations in a mouse model of temporal lobe epilepsy induced by intrahippocampal injection of kainate. Exp. Neurol. 2008;213(1):71–83.

72. Carriero G, Arcieri S, Cattalini A, et al. A guinea pig model of mesial temporal lobe epilepsy following nonconvulsive status epilepticus induced by unilateral intrahippocampal injection of kainic acid. Epilepsia 2012;53(11):1917–1927.

73. Noè F, Cattalini A, Vila Verde D, et al. Epileptiform activity contralateral to unilateral hippocampal sclerosis does not cause the expression of brain damage markers. Epilepsia 2019;0(1):1–16.

74. Arcieri S, Velotti R, Noè F, et al. Variable electrobehavioral patterns during focal nonconvulsive status epilepticus induced by unilateral intrahippocampal injection of kainic acid. Epilepsia 2014;55(12):1978–1985.

75. Mathern GW, Pretorius JK, Babb TL. Influence of the type of initial precipitating injury and at what age it occurs on course and outcome in patients with temporal lobe seizures. J. Neurosurg. 1995;82(2):220–227.

76. Nairismägi J, Gröhn OHJ, Kettunen MI, et al. Progression of brain damage after status epilepticus and its association with epileptogenesis: A quantitative MRI study in a rat model of temporal lobe epilepsy. Epilepsia 2004;45(9):1024–1034.

77. Babb TL, Brown WJ, Pretorius J, et al. Temporal Lobe Volumetric Cell Densities in Temporal Lobe Epilepsy. Epilepsia 1984;25(7):729–740.

78. Bertram EH, Lothman EW, Lenn NJ. The hippocampus in experimental chronic epilepsy: A morphometric analysis. Ann. Neurol. 1990;27(1):43–48.

79. Mello LEAM, Cavalheiro EA, Tan AM, et al. Circuit Mechanisms of Seizures in the Pilocarpine Model of Chronic Epilepsy: Cell Loss and Mossy Fiber Sprouting. Epilepsia 1993;34(6):985–995.

80. Vezzani A, Granata T. Brain inflammation in epilepsy: Experimental and clinical evidence. Epilepsia 2005;46(11):1724–1743.

81. Binder DK, Steinhäuser C. Functional changes in astroglial cells in epilepsy. Glia 2006;54(5):358–368.

82. Gloor SM, Wachtel M, Bolliger MF, et al. Molecular and cellular permeability control at the blood-brain barrier. Brain Res. Rev. 2001;36(2–3):258–264.

83. Vezzani A, Balosso S, Ravizza T. The role of cytokines in the pathophysiology of epilepsy. Brain. Behav. Immun. 2008;22(6):797–803.

84. Vila Verde D, de Curtis M, Librizzi L. Seizure-Induced Acute Glial Activation in the in vitro Isolated Guinea Pig Brain. Front. Neurol. 2021;12(2):1–12.

85. Vila Verde D, Zimmer T, Cattalini A, et al. Seizure activity and brain damage in a model of focal non-convulsive status epilepticus. Neuropathol. Appl. Neurobiol. 2021;1(12):1–15.

86. Heinrich C, Nitta N, Flubacher A, et al. Reelin deficiency and displacement of mature neurons, but not neurogenesis, underlie the formation of granule cell dispersion in the epileptic hippocampus. J. Neurosci. 2006;26(17):4701–4713.

87. Heck N, Garwood J, Loeffler JP, et al. Differential upregulation of extracellular matrix

molecules associated with the appearance of granule cell dispersion and mossy fiber sprouting during epileptogenesis in a murine model of temporal lobe epilepsy. Neuroscience 2004;129(2):309–324.

88. Schwartz M, Shechter R. Systemic inflammatory cells fight off neurodegenerative disease. Nat. Rev. Neurol. 2010;6(7):405–410.

89. Liesz A, Suri-Payer E, Veltkamp C, et al. Regulatory T cells are key cerebroprotective immunomodulators in acute experimental stroke. Nat. Med. 2009;15(2):192–199.

90. Elenkov IJ, Webster EL, Torpy DJ, Chrousos GP. Stress, corticotropin-releasing hormone, glucocorticoids, and the immune/inflammatory response: Acute and chronic effects. Ann. N. Y. Acad. Sci. 1999;876(43):1–13.

91. Vezzani A, French J, Bartfai T, Baram TZ. The role of inflammation in epilepsy. Nat. Rev. Neurol. 2011;7(1):31–40.

92. Pitsch J, Becker AJ, Schoch S, et al. Circadian clustering of spontaneous epileptic seizures emerges after pilocarpine-induced status epilepticus. Epilepsia 2017;58(7):1159–1171.

93. Tavares G, Martins M, Correia JS, et al. Employing an open-source tool to assess astrocyte tridimensional structure. Brain Struct. Funct. 2017;222(4):1989–1999.

94. Ferreira TA, Blackman A V., Oyrer J, et al. Neuronal morphometry directly from bitmap images. Nat. Methods 2014;11(10):982–984.

95. Song Y, Gunnarson E. Potassium dependent regulation of astrocyte water permeability is mediated by camp signaling. PLoS One 2012;7(4):e34936.

96. Pollard H, Charriaut-Marlangue C, Cantagrel S, et al. Kainate-induced apoptotic cell death in hippocampal neurons. Neuroscience 1994;63(1):7–18.

97. Schmued LC, Albertson C, Slikker W. Fluoro-Jade: A novel fluorochrome for the sensitive and reliable histochemical localization of neuronal degeneration. Brain Res. 1997;751(1):37–46.

98. Loo DT. In situ detection of apoptosis by the TUNEL assay: An overview of techniques. Methods Mol. Biol. 2011;682(44):3–13.

99. Rossini L, Garbelli R, Gnatkovsky V, et al. Seizure activity per se does not induce tissue damage markers in human neocortical focal epilepsy. Ann. Neurol. 2017;82(3):331–341.

100. Thom M, Zhou J, Martinian L, Sisodiya S. Quantitative post-mortem study of the hippocampus in chronic epilepsy: Seizures do not inevitably cause neuronal loss. Brain 2005;128(3):1344–1357.

101. Cavazos JE, Das I, Sutula TP. Neuronal loss induced in limbic pathways by kindling: Evidence for induction of hippocampal sclerosis by repeated brief seizures. J. Neurosci. 1994;14(5):3106–3121.

102. Bedner P, Dupper A, Hüttmann K, et al. Astrocyte uncoupling as a cause of human temporal lobe epilepsy. Brain 2015;138(1):1208–1222.

103. Devinsky O, Vezzani A, O'Brien TJ, et al. Epilepsy. Nat. Rev. Dis. Prim. 2018;4(3):18–24.

104. Seifert G, Steinhäuser C. Neuron-astrocyte signaling and epilepsy. Exp. Neurol. 2013;244(9):4–10.

105. Steinhäuser C, Seifert G. Glial membrane channels and receptors in epilepsy: Impact for generation and spread of seizure activity. Eur. J. Pharmacol. 2002;447(2–3):227–237.

106. Binder DK, Yao X, Zador Z, et al. Increased seizure duration and slowed potassium kinetics in mice lacking aquaporin-4 water channels. Glia 2006;53(6):631–636.

Appendix

Publications

Received: 13 December 2018 | Revised: 24 April 2019 | Accepted: 24 April 2019

DOI: 10.1111/epi.15611

FULL-LENGTH ORIGINAL RESEARCH

Epilepsia®

Epileptiform activity contralateral to unilateral hippocampal sclerosis does not cause the expression of brain damage markers

Francesco Noè[1] | **Alessandro Cattalini**[1] | **Diogo Vila Verde**[1] | **Camilla Alessi**[1] | **Francesca Colciaghi**[1] | **Matteo Figini**[2] | **Ileana Zucca**[2] | **Marco de Curtis**[1]

[1]Epilepsy Unit, Fondazione IRCCS Istituto Neurologico Carlo Besta, Milan, Italy

[2]Scientific Direction, Fondazione IRCCS Istituto Neurologico Carlo Besta, Milan, Italy

Correspondence
Marco de Curtis, Epilepsy Unit, Fondazione IRCCS Istituto Neurologico Carlo Besta, via Celoria 11, 20133 Milano, Italy.
Email: marco.decurtis@istituto-besta.it

Funding information
Italian Health Ministry , Grant/Award Number: Ricerca Corrente; Fondazione Banca del Monte di Lombardia , Grant/Award Number: GR-2011-02348633; FP7 Ideas: European Research Council, Grant/Award Number: JTC2014-ERANET-Neuron 0004 (BrIE); European Commission

Abstract

Objective: Patients with epilepsy often ask if recurrent seizures harm their brain and aggravate their epileptic condition. This crucial question has not been specifically addressed by dedicated experiments. We analyze here if intense bilateral seizure activity induced by local injection of kainic acid (KA) in the right hippocampus produces brain damage in the left hippocampus.

Methods: Adult guinea pigs were bilaterally implanted with hippocampal electrodes for continuous video—electroencephalography (EEG) monitoring. Unilateral injection of 1 μg KA in the dorsal CA1 area induced nonconvulsive status epilepticus (ncSE) characterized by bilateral hippocampal seizure discharges. This treatment resulted in selective unilateral sclerosis of the KA-injected hippocampus. Three days after KA injection, the animals were killed, and the brains were submitted to ex vivo magnetic resonance imaging (MRI) and were processed for immunohistochemical analysis.

Results: During ncSE, epileptiform activity was recorded for 27.6 ± 19.1 hours in both the KA-injected and contralateral hippocampi. Enhanced T1-weighted MR signal due to gadolinium deposition, mean diffusivity reduction, neuronal loss, gliosis, and blood–brain barrier permeability changes was observed exclusively in the KA-injected hippocampus. Despite the presence of a clear unilateral hippocampal sclerosis at the site of KA injection, no structural alterations were detected by MR and immunostaining analysis performed in the hippocampus contralateral to KA injection 3 days and 2 months after ncSE induction. Fluoro-Jade and terminal deoxynucleotidyl transferase dUTP nick end labeling (TUNEL) staining at the same time points confirmed the absence of degenerating cells in the hippocampi contralateral to KA injection.

Significance: We demonstrate that intense epileptiform activity during ncSE does not cause obvious brain damage in the hippocampus contralateral to unilateral hippocampal KA injection. These findings argue against the hypothesis that epileptiform activity per se contributes to focal brain injury in previously undamaged cortical regions.

KEYWORDS
brain damage, epilepsy, focal seizures, nonconvulsive status epilepticus

Noè, Cattalini, and Vila Verde equally contributed to the realization of the manuscript.

1 | INTRODUCTION

Patients with epilepsy often ask if recurrent seizures harm their brain and aggravate epilepsy. Seizures and brain damage develop in parallel in many epilepsies and a definite answer to this question is missing.[1,2] In focal epilepsies due to structural and metabolic causes,[3] the progression of brain damage and the organization of an epileptogenic network could either be the consequence of the acute brain injury (as in posttraumatic epilepsy[4]) or may result from a persistent pathogenic condition, as in epileptic encephalopathies.[3,5] Because seizure frequency usually intensifies in parallel with brain injury worsening, it has been suggested that seizure activity by itself may have a direct pathogenic action on tissue reorganization and may possibly worsen brain damage.[6] Nevertheless, a *correlation* between seizure activity and brain damage does not necessarily demonstrate a cause-effect relationship, and experimental studies do not help to clarify if simple seizures by themselves damage the brain. Brain injury progression has been documented during the life span of animals that develop mesial temporal lobe epilepsy (mTLE) with hippocampal sclerosis as consequence of SE,[7–10] and after brain concussion.[7,11]

The core of the question here addressed is to understand if brain damage is produced by the seizure activity per se. To this end, we utilized a guinea pig model of unilateral mTLE[12,13] induced by local injection in one hippocampus of kainic acid (KA),[14–16] a neurotoxin known to induce within 24 hours an acute calcium-dependent neurodegeneration.[17] This procedure promotes a nonconvulsive status epilepticus (ncSE) characterized by bi-hippocampal epileptiform discharges. In a previous report, we observed that animals showed a clear damage in the KA-injected hippocampus, whereas the limbic regions contralateral to the KA-injected hemisphere were not apparently altered, despite their obvious epileptic activation during KA-induced ncSE.[12] We further investigated this aspect by quantifying brain changes in the hippocampi ipsilateral and contralateral to KA injection with neurophysiologic, neuropathologic, and imaging techniques. Because KA-induced brain damage is established within a few days after SE,[18–20] we focused the analysis of brain tissue at 3 days after ncSE, when gliosis, neuroinflammation,[21,22] and blood-brain barrier (BBB) permeability changes[23] are maximal, and other confounding factors (such as spontaneous seizures) are not yet established yet. We further validated the findings at a later time point, 2 months after ncSE, when the unilateral KA-induced hippocampal sclerosis is established.

Key Points

- Unilateral injection of kainic acid (KA) in one hippocampus induces nonconvulsive status epilepticus that results in unilateral hippocampal sclerosis
- Nonconvulsive status epilepticus is associated with bilateral epileptiform discharges in the KA-injected and in the contralateral hippocampi
- Epileptiform activity contralateral to the KA-injected hippocampus does not correlate with neuronal loss, cell degeneration/apoptosis, gliosis, and blood-brain barrier (BBB) alterations 3 days and 2 months after ncSE
- Our findings argue against the hypothesis that epileptiform activity per se contributes to focal brain injury

2 | METHODS

The study is based on a cohort of 32 adult male Hartley guinea pigs (200-250 g weight, 3 postnatal weeks of age; Charles River) housed in a 12-hour light-dark controlled cycle environment with ad libitum food and water supply. Four different experimental groups were utilized: nave guinea pigs (n = 10; 6 for the acute experiments and 4 for the chronic condition—see below); sham-operated and sham-treated animals (n = 5); and guinea pigs unilaterally injected with KA in the right dorsal hippocampus sacrificed 3 days (n = 11) and at 2 months (n = 6) after ncSE. The experimental protocol was reviewed and approved by the animal welfare office of the Italian Health Ministry (Authorization n. 36/2016-PR, January 18th, 2016), in accordance with the European Committee Council Directive (2010/63/EU) and with the 3Rs principle.[24]

2.1 | Implantation of electrodes and injection cannula

Twenty-two animals were surgically implanted with bilateral depth (intrahippocampal) and superficial (epidural) electroencephalography (EEG) recording electrodes. The procedures for electrode implantation and KA injection have been published previously[12] (see Appendix S1).

2.2 | Video-EEG recordings

Video-EEG monitoring started 1 week after surgery; implanted pedestals were connected to a cable mounted on a swivel coupled to the preamplifier stage of a Brain Quick EEG System (Micromed). After 24 hours of adaptation, video-EEG was continuously recorded for 5 days, including 48 hours before (baseline) and 3 days after either KA or NaCl hippocampal injection. EEG data were recorded wide-band (0.1-1.0 kHz at 2064 Hz sampling rate, with 16-bit precision) using the System Plus Evolution software (Micromed).

2.3 | Unilateral intrahippocampal KA and saline injection

Nine days after electrode implantation, 22 animals were injected in the CA1 area of the right hippocampus with either KA (n = 11 + 6) or 0.9% NaCl saline solution (sham-operated animals; n = 5), respectively, under continuous video-EEG recording. A 30-gauge needle, connected to a 5 μL Hamilton syringe via a polyethylene tube, was lowered through the guide cannula in the right hippocampus to slowly inject 1 μL of 1 μg KA (Sigma) diluted in 0.9% NaCl solution. Within 15 minutes after KA injection, epileptiform activity was recorded in all animals. Video-EEG was monitored for 3 days after KA (or NaCl) injection. None of the sham-operated/injected guinea pigs showed epileptiform activity on EEG. Six chronic mTLE animals were video-EEG recorded 7 days every other week for at least 2 months after ncSE to verify the presence of spontaneous epileptiform discharges and seizures.[12,13] Surgeries, animal shuffle in the different experimental groups, and intrahippocampal injections were performed by Fraqncesco Noè (acute ncSE) and Alessandro Cattalini (chronic mTLE animals).

2.4 | Video-EEG data analysis

Continuous 24-hour video-EEG recorded 2 days before and 3 days after KA (or saline) injection was analyzed off-line. Hippocampal EEG patterns during and after KA injection were identified and quantified for each animal. The EEG activity recorded in the frontal cortex was utilized to identify the presence of a diffuse EEG pattern and was not analyzed/quantified in the present study. KA-induced epileptiform activity was characterized by seizures combined with continuous rhythmic spiking activity at 1-3 Hz (Figure 1). Seizure events during KA-induced ncSE were defined by large-amplitude spiking activity with clear tonic and bursting phases longer than 20 seconds, followed by postictal depression (Figure 1B). The time spent in seizure during ncSE was quantified for both the right and left hippocampal recordings in the 11 animals killed 3 days after KA. Seizure discharges were identified as focal unilateral or bilateral, based on the EEG pattern distribution. Bilateral epileptiform discharges during ncSE have been characterized previously in the six chronic animals.[13] Extracellular population spike number and distribution (Figure 2) were quantified in both hippocampi by setting a threshold 2.5 standard deviations above the baseline amplitude, as calculated on the pre-KA injection EEG recording. Extracellular population spikes have been defined as sharp transient with a duration included between 70 and 200 milliseconds. Seizure activity and spike counts during ncSE were blindly analyzed by CA and FMN. In the six chronic animals, spontaneous seizures during the chronic phase were identified with 7 days of video-EEG recordings performed every other week for 2 months.[12,13] Details on the seizures and on the epileptic phenotype of the chronic epileptic animals are reported in previous articles.[12,13] In these animals, ncSE duration values were similar to those calculated for the animals killed at 3 days.

2.5 | Magnetic resonance imaging

After brain preparation for magnetic resonance imaging (MRI) (see Appendix S1), imaging was performed on isolated and fixed guinea pig brains using a 7T horizontal-bore scanner (BioSpec 70/30 USR; Bruker), equipped with actively shielded gradient/shim coil with a maximum gradient strength of 440 mT/m, and a 38 mm transmit/receive birdcage volume quadrature coil. The magnetic field homogeneity was optimized by a localized second-order shimming procedure featured on a volume of interest covering the whole field of view. Axial T1-weighted images and diffusion tensor imaging (DTI) were acquired by using a+ standard protocol (details in Appendix S1). On T1-weighted images, regions of Interest (ROIs) were manually delineated on the whole hippocampi using ITK-SNAP (www.itksnap.org) and their volume was computed. ROIs were also drawn on the dorsal part of the hippocampi and the ratio between their mean signal intensity and the mean signal in a reference ROI placed in the unaffected cortex was considered as an index of gadolinium enhancement. DTI images were corrected for motion and eddy current distortions with FMRIB's Linear Image Registration Tool in FSL (http://www.fmrib.ox.ac.uk/fsl/). The diffusion tensor in each voxel was estimated from the DTI raw data, and mean diffusivity (MD) and fractional anisotropy (FA) maps[25] were computed using Diffusion Toolkit (http://www.trackvis.org[26]). The mean MD and FA were calculated in ROIs manually delineated in the hippocampi and frontal cortices. Chronic mTLE animals were not submitted to MRI. MRI data were analyzed blindly by M.F. and I.Z.

2.6 | Immunohistochemical study

After completion of the MRI study, brains were cut into 50 μm coronal sections for immunohistochemical (IHC) processing. The following histologic parameters were investigated: (a) hippocampal neurodegeneration using neuronal nuclei (NeuN) and thionine staining; (b) reactive astrogliosis by glial fibrillary acid protein (GFAP) immunostaining; (c) acute neuronal injury by microtubule associated protein 2 (MAP2) staining, which concentrates in soma in the course of cytotoxic edema[27] and during reversible neuronal suffering[28,29]; (d) BBB permeability alteration by evaluating endogenous guinea pig immunoglobulin G (IgG), not present in the brain in normal conditions, (e) staining for DNA fragmentation (terminal deoxynucleotidyl transferase dUTP nick end labeling [TUNEL]) and neuronal degeneration (Fluoro-Jade). Serial coronal sections rostral and caudal to the KA injection local damage were selected and were analyzed blindly by A.C. and C.A.

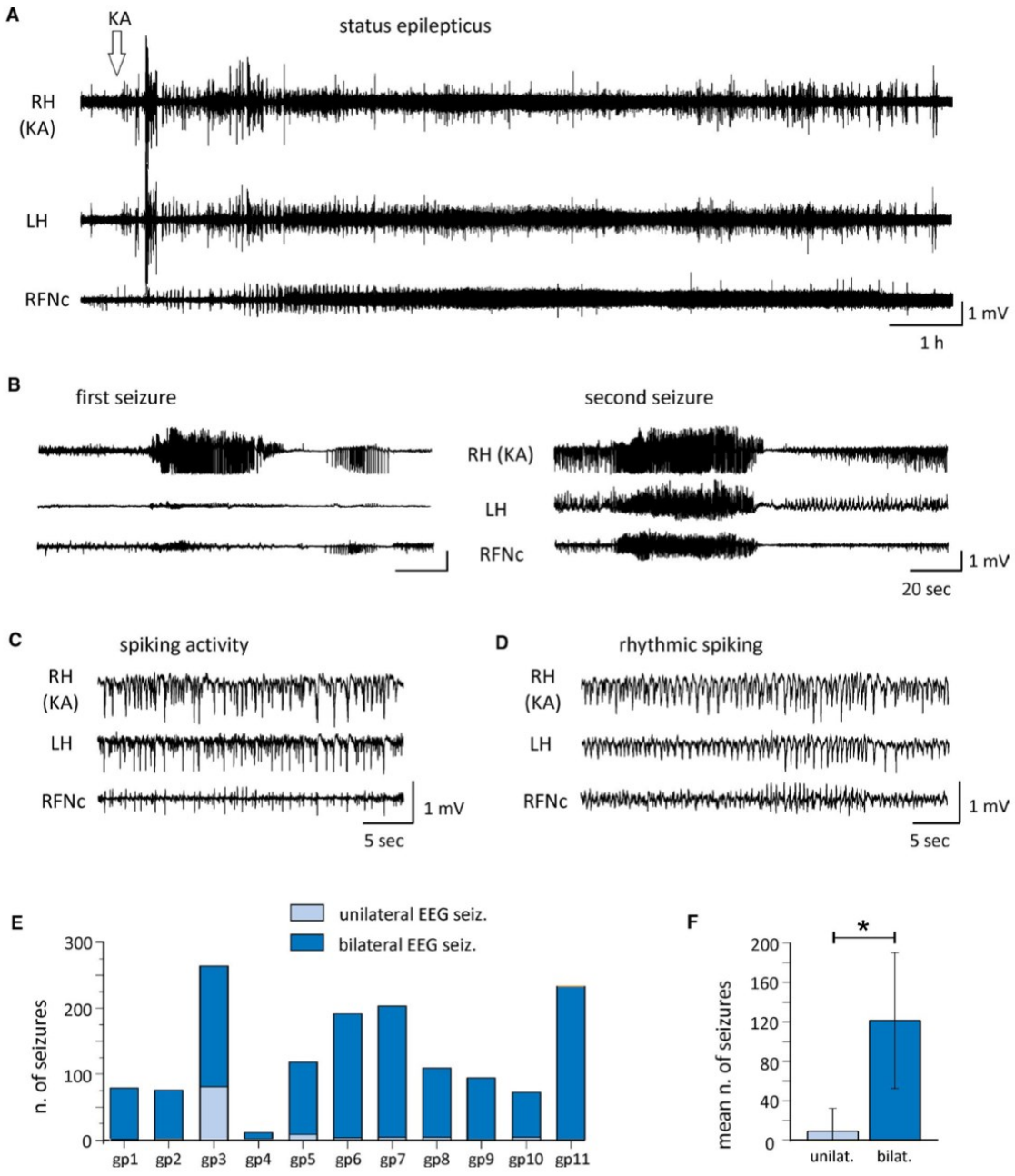

FIGURE 1 Status epilepticus activity induced by unilateral intrahippocampal kainic acid (KA) injection. A, Compressed electroencephalography (EEG) 12 h recording in the right (RH-KA) and left (LH) CA1 areas of the hippocampi and in the right frontal neocortex (RFNc). KA was injected in the right hippocampus (vertical arrow on RH(KA) trace). B, The first recorded focal EEG seizure (left panel) and the second bilateral EEG seizure (right panel), observed after KA injection illustrated in panel A are shown with expanded time scale. C, Irregular spiking involving both hippocampi. D, Regular, rhythmic spikes at 1-3 Hz in the two hippocampi, which inconstantly project to the RFNc. E, Number of seizures characterized by unilateral (light blue columns) and bilateral (blue columns) hippocampal EEG discharges, for each of the 11 KA-treated guinea pigs killed 3 days after KA treatment (gp1-11). F, Mean number of unilateral or bilateral EEG seizures observed in all animals. $*P < 0.05$ (by t test)

A standardized protocol has been used for NeuN, GFAP, MAP2, IgG, Fluoro-jade, and TUNEL histochemical staining (see Appendix S1). Thionine and GFAP staining was performed in the six chronic mTLE guinea pigs and in additional four naive guinea pigs. Immunostained sections were visualized using the Scanscope software (Aperio Technologies). Hippocampal and cortical staining for NeuN, GFAP, MAP2, and IgG was analyzed in the three

different experimental conditions (naive, sham-treated, and KA-injected animals). Quantitative field fraction estimates of NeuN, GFAP, MAP2, and IgG immunostaining were carried out in both hippocampi using Image-Pro Plus 7 software (Media Cybernetics, Inc). The percentage of neuronal occupancy (specific immunostaining density) had been estimated in previously determined ROIs positioned in CA1 and CA3 hippocampal subfields, in the granular layer of dentate gyrus (DG), and in the hilus (see upper left panel in Figure 4). The size of NeuN and thionine measurements of ROI was arbitrary established at 0.043 mm^2 for CA1, 0.086 mm^2 for CA3, 0.035 mm^2 for DG, and

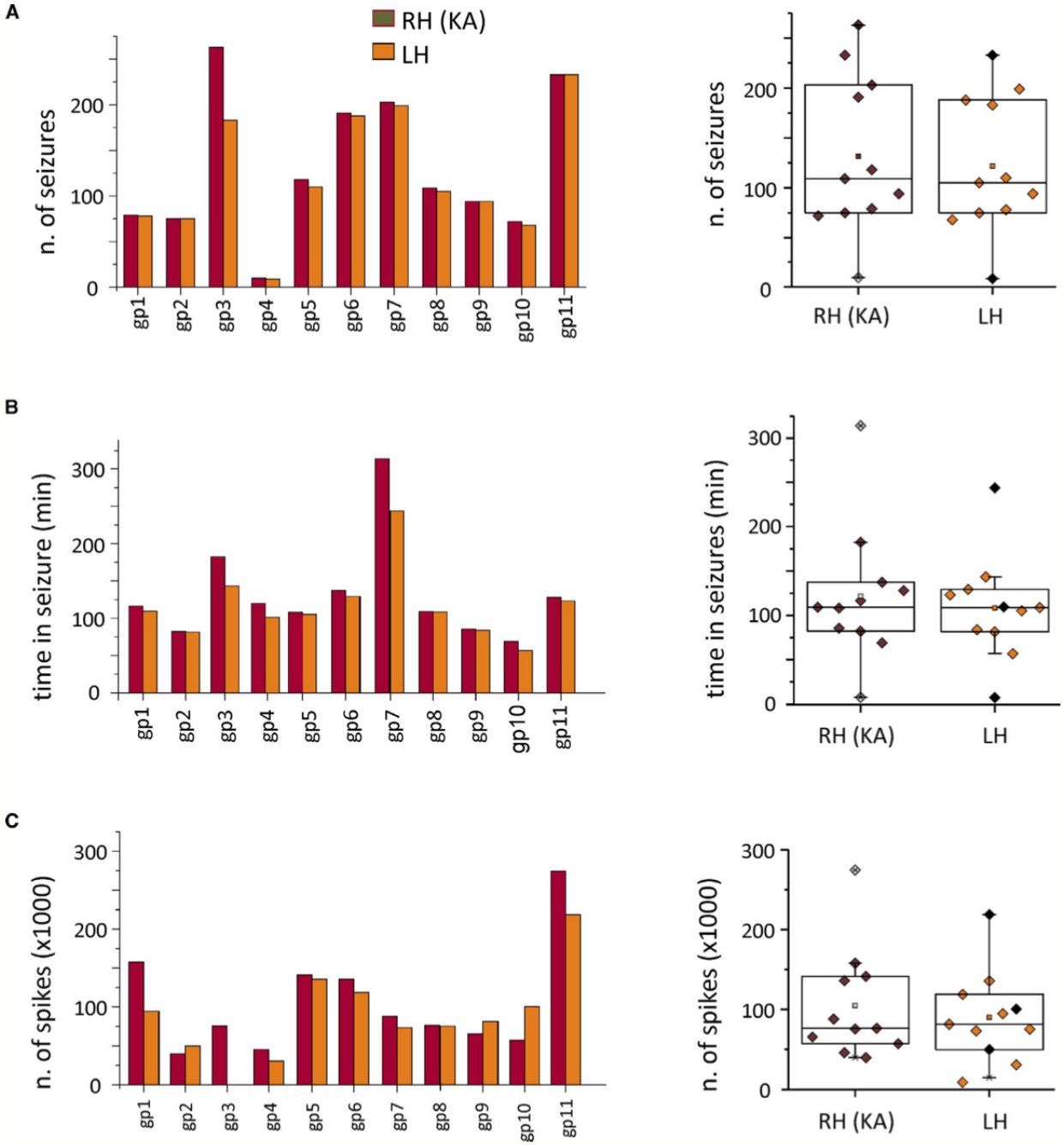

FIGURE 2 Quantification of hippocampal electroencephalography (EEG) epileptiform activity ipsi- and contralateral to kainic acid (KA) injection. Comparison of the number of seizures (A), the time spent in seizures (B), and the number of spikes (C) recorded in the KA-injected right hippocampal CA1 [RH(KA) in red] and in the contralateral left CA1 (LH in orange) in the 11 guinea pigs during the 3 days following ncSE induction. On the right column of each panel, box plots represent the distribution of the mean values for the same parameters, as analyzed in each KA-injected guinea pig sacrificed 3 days after KA treatment (n = 11)

0.35 mm^2 for the hilus region. For GFAP, MAP2, and IgG, measurements ROIs of 0.078 mm^2 were positioned on the different subfields in each analyzed section magnified at 5×; a threshold of staining intensity was defined with respect to background signal. Neuronal density in each ROI was automatically calculated by the software on two adjacent slices in each hippocampal subfield, after symmetry between right and left hippocampi was verified. For each slice in each experimental group, mean NeuN density was calculated on four ROIs in CA1, two in CA3, four in DG, and one in hilus for each slice. To avoid inclusion in the analyses of electrode-related tissue alterations, densitometric ROIs in KA-injected and sham-treated guinea pigs were positioned at least 0.5 mm away from the electrode tracks (arrows in the lower middle panel in Figure 4). C.A. and A.C. performed GFAP, MAP2-immunostaining analysis by blindly evaluating two ROIs on two different sections per animals in CA1, CA3, and hilus, using Image-Pro Plus 7 software. A single ROI in CA1 was analyzed on two sections from the same brain to evaluate IgG staining. Densitometric data from the above-mentioned ROIs were calculated in both the right and left hippocampi in naive and sham-operated animals and were pooled together (black columns in Figures 5 and 6).

To quantify Fluoro-Jade and TUNEL data, positive cells counting was performed in CA1, CA3, and hilar areas of both ipsilateral and contralateral hippocampus at 3-days in the KA-injected animals and in both hippocampi of the sham-experimental group (at least two section/each animal). For each section, at least two adjacent nonoverlapping fields per area were captured under identical conditions at 40× magnification (290 µm × 290 µm) by Leica TCS SP8 microscope. All TUNEL-positive nuclei and Fluoro-Jade$^-$positive cells were manually counted (independently by two investigators), and values were averaged to a single value per area in both the ipsilateral and contralateral side/each animal. Numbers of Fluoro-Jade cells and TUNEL-marked nuclei in the ipsilateral areas were compared to corresponding contralateral areas.

2.7 | Statistical analysis

Surgeries and KA injections were performed by FMN and CA; MF and AC analyzed raw EEG, MRI, and IHC data in a blinded manner. Data were tested for normality distribution and were statistically analyzed with Graph-Pad Prism 3.0 (GraphPad Software Inc.). Results are expressed as means ± standard deviation (SD). Differences in number of seizures, time spent in seizures, and number of spikes between the different experimental groups were evaluated using the unpaired Student's *t* test for unpaired data or the Tukey honestly significant difference test for multiple comparisons. For each MRI measure (hippocampal volume, dorsal hippocampus signal intensity, hippocampus MD, cortex MD, hippocampus FA, and cortex FA), the difference between the left and right (KA-injected) side and between RH (KA) from KA-injected animals and hippocampal values from control animals (sham-operated and naive) was evaluated using a nonparametric Wilcoxon signed-rank test; differences between experimental groups of animals were assessed using Wilcoxon rank-sum test.

For densitometric IHC, Fluoro-Jade, and TUNEL analysis, results are presented as means ± SD for the number of independent experiences (n) indicated in figure captions. After assessing the normal distribution of the data running the Kolmogorov-Smirnov normality test, unpaired Student's *t* test or paired Student's *t* test was employed in case of comparison between left and right hemispheres from the same animal. The confidence interval $(1 - \alpha)$ was set as 95% (0.95) so that the difference between means was considered statistically significant at *P* values of less than 5% (0.05), 1% (0.01), 0.1% (0.001), and 0.01% (0.0001) of significance level (α). The datasets generated and analyzed during the current study are available from the corresponding author on reasonable request.

3 | RESULTS

3.1 | Nonconvulsive SE activity after unilateral intrahippocampal KA injection

Seizure-like EEG discharges appeared in the injected hippocampus within 15 minutes of unilateral intrahippocampal KA injection, both in the 11 guinea pigs sacrificed 3 days after KA and in the 6 chronic epileptic animals (for the latter group, see references[12,13]). In the 11 acute animals, epileptiform activity propagated to both the ipsilateral neocortex and the contralateral left hippocampus (LH) either immediately (n = 9; Figure 1A,B, right panel) or within 10 minutes (n = 2). The recorded epileptiform activity correlated with recurrent nonconvulsive seizures[13] integrated in a continuous, irregular spiking activity (Figure 1C) that evolved rapidly into bilateral rhythmic spiking at 1-3 Hz (Figure 1D). Nonconvulsive seizures typically correlated with explorative behavior, tonic immobility, and lateralized facial and head myoclonias (for details, see reference [13]). KA-induced nonconvulsive SE (ncSE) lasted from a minimum of 6 to a maximum of 70 hours (average 27.63 ± 19.17 hours, mean ± SD), and remitted spontaneously. The number of seizures recorded during ncSE varied from a minimum of 10 to a maximum of 263 (Figure 1E), with an average of 5.45 ± 1.82 seizures per hour. As reported previously,[13] the large majority of nonconvulsive seizures engaged both hippocampi (Figure 1E,F). The unilateral EEG involvement at ncSE onset (left panel in Figure 1B) excludes the possibility that the bilateral activation observed later during the ncSE is due to a volume-conducted activity from the KA-injected hippocampus. None of

the five sham-operated animals injected with 0.9% NaCl solution showed EEG abnormalities during the 3 days of video-EEG monitoring.

To verify the involvement of the KA-injected right hippocampus [RH(KA)] and of the contralateral left hippocampus (LH) during ncSE, we quantified the number of EEG seizures (Figure 2A), the time spent in seizures (Figure 2B), and the number of spikes (Figure 2C). As illustrated in the box plots on the right of each panel in Figure 2, both RH(KA) and LH were equally involved in the generation of epileptiform activity. This is the precondition for the evaluation of the effects of epileptiform activity in the LH contralateral to KA injection. Six animals were video-EEG monitored for 2 months, when hippocampal sclerosis and chronic seizures develop, as described and characterized in two previous manuscripts.[12,13]

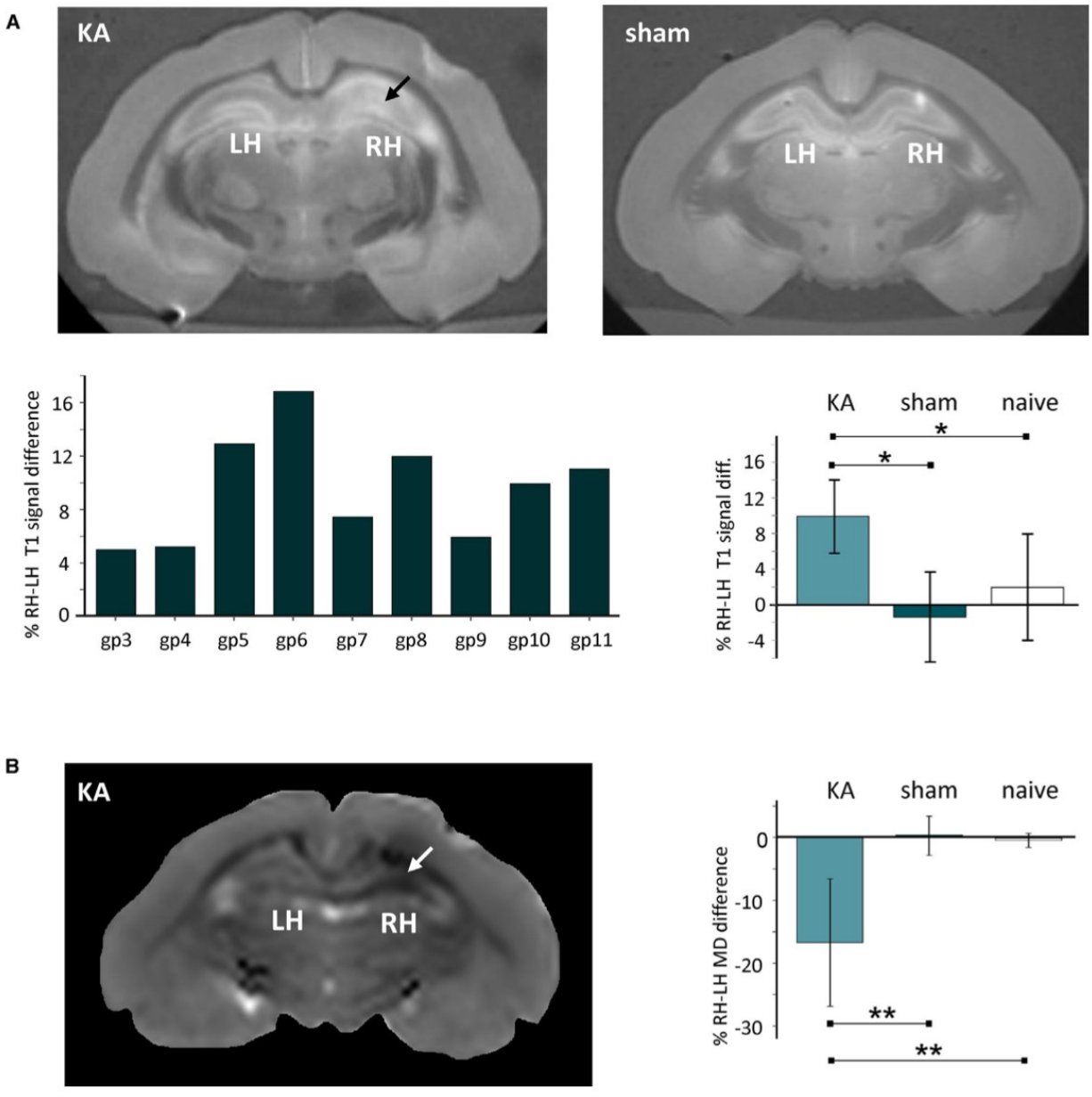

FIGURE 3 Magnetic resonance imaging (MRI) features 3 days after kainic acid (KA)–induced status epilepticus. A, On the top, representative T1-weighted images of a KA-treated (left) and sham-operated (right) guinea pig brains. Images were obtained with a 7T MR instrument in fixed brains from animals perfused with gadolinium during sacrifice (see Methods). On the bottom: percentage of T1-weighted signal differences between RH(KA) and LH for each KA-injected animal (left panel); average values obtained in KA-treated, sham, and naive animal groups are shown on the right panel. Positive values represent a higher T1-weighted signal in RH(KA) due to the presence of gadolinium. B, Representative MD map in a KA-treated brain (left) and difference between the MD in the RH(KA) and LH averaged in each group (right). *$P < 0.05$ by nonparametric Wilcoxon test

3.2 | Magnetic resonance imaging ipsi- and contralateral to KA injection

Three days after ncSE induction, animals were injected with a bolus of 4% gadolinium just before the transcardiac perfusion of paraformaldehyde (see Methods). MRI was performed on fixed brains (nine KA-treated, five sham-operated, and five naive) 1 week after animals were killed, to verify both brain damage and BBB permeability changes to gadolinium. MRI was not performed in two guinea pigs due to an error in the gadolinium administration protocol and was not implemented in the six chronic animals. The normalized T1-weighted signal measured on manually delineated ROIs of whole hippocampi in both RH and LH was 1.21 ± 0.14 and 1.31 ± 0.16 in KA-treated animals, 1.29 ± 0.21 and 1.27 ± 0.16 in naive animals, and 1.25 ± 0.13 and 1.26 ± 0.13 in sham-operated animals. It was significantly higher in RH(KA) than in the LH in all KA-treated animals ($P < 0.05$), whereas in the sham-operated and in the naive groups no significant differences were found between the left and the right hippocampi. The difference in T1-weighted signal between RH and LH was 7.95 ± 3.11% in the KA-injected group, as shown in Figure 3A. No significant difference in hippocampal volume was observed between experimental groups or between the LH and RH within each group. The mean diffusivity (MD) measures on whole hippocampal ROIs in RH and LH were $3.53 \pm 0.35 \times 10^{-4}$ and $4.09 \pm 0.26 \times 10^{-4}$ mm^2/s in KA-treated animals, $3.98 \pm 0.19 \times 10^{-4}$ and $3.99 \pm 0.21 \times 10^{-4}$ mm^2/s in naive animals, and $4.08 \pm 0.18 \times 10^{-4}$ and $4.07 \pm 0.22 \times 10^{-4}$ mm^2/s in sham-operated animals. The difference between RH and LH was significantly higher in KA-treated than in naive or sham-operated animals ($P < 0.0005$). MD values in the RH (KA) were significantly lower than in the contralateral LH of the same animals ($P = 0.001$) and also compared to the hippocampal measurements of naive and sham animals ($P < 0.005$; Figure 3B). No statistically significant difference

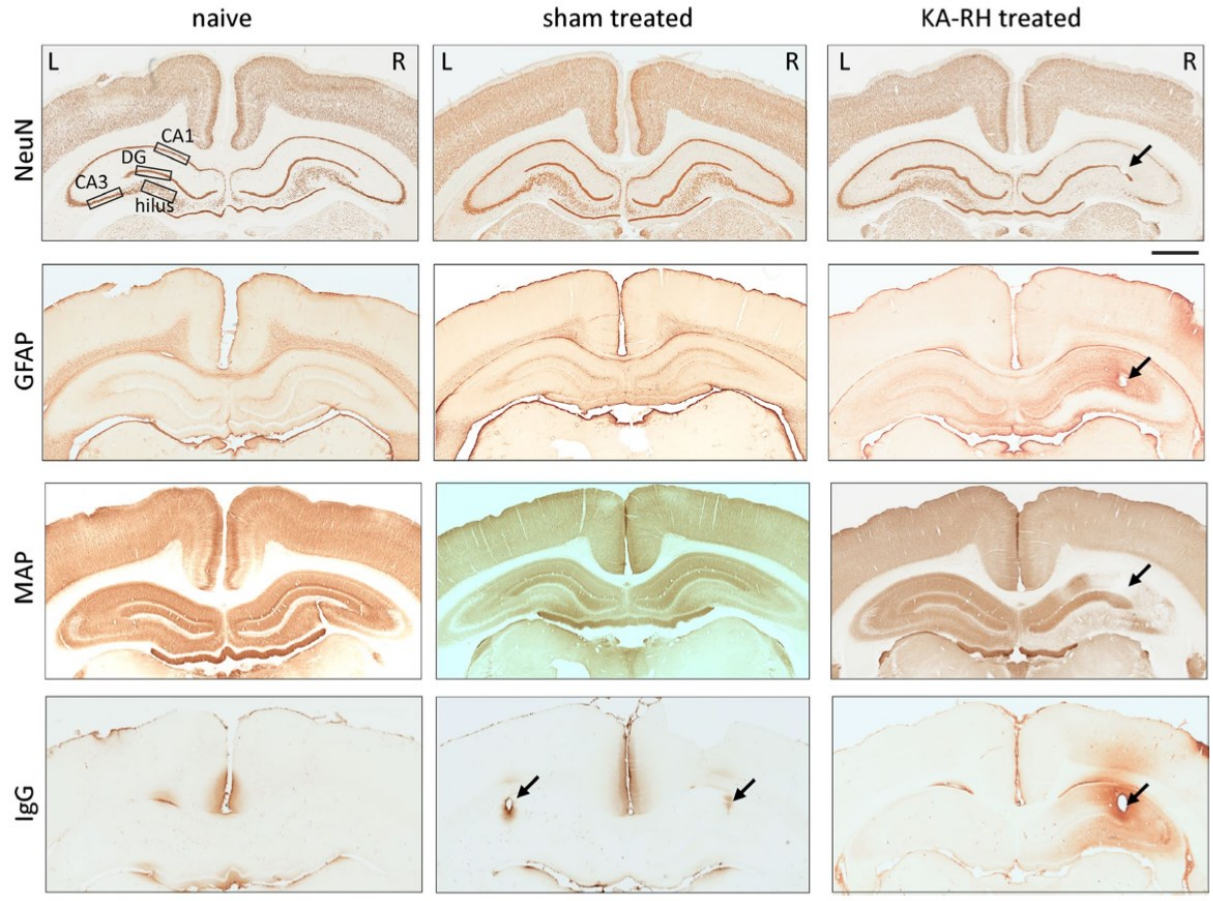

FIGURE 4 Immunohistochemical features of naive (left column), sham-operated (middle column), and KA-injected guinea pigs (right column), 3 days after KA-induced ncSE. KA was injected in the right hippocampal CA1 region. For each panel, neuronal density (neuronal nuclei immunostaining [NeuN]; first row), astrogliosis (glial fibrillary acidic protein staining [GFAP], second row), reversible neuronal sufferance (microtubule-associated protein 2 staining [MAP2], third row) and blood-brain barrier permeability changes (Ig, bottom row) are illustrated. Arrows mark the intrahippocampal recording electrode tracks. Calibration bar = 1 mm. Left and right (KA-injected) hemispheres are marked by L and R. Regions of interest (ROI) samples utilized for the densitometric quantification of immunostaining in CA1, CA3, DG, and hilus (Figure 5) are illustrated in the top left panel

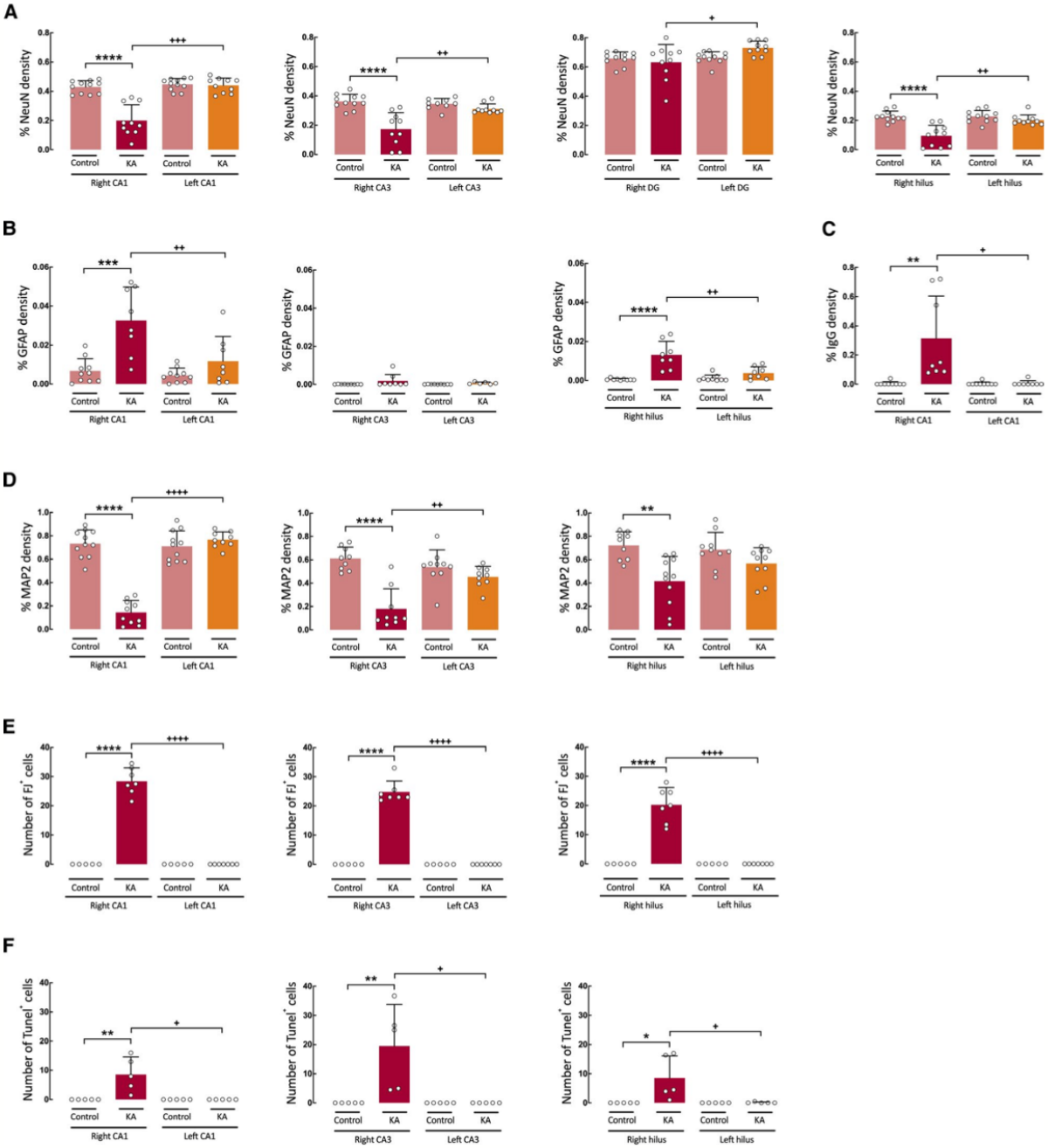

FIGURE 5 Semiquantitative analysis of NeuN, GFAP, MAP2, and IgG densitometry and Fluoro-Jade and TUNEL cell counts in the hippocampi ipsi- and contralateral to KA injection, 3 days after status epilepticus. A, Comparison between densitometric measurements of NeuN (A). The gray columns illustrate the average percentage of densitometric changes measured in CA1, CA3, DG, and hilus in the left and in the right hippocampi of KA-treated animals (n = 10); densitometric values obtained from the same areas in the right and left hippocampi of control animals (sham and naive) are illustrated by pink columns (n = 9-11). Comparison between densitometric GFAP (B), IgG (C), and MAP2 (D) measurements in KA-injected right and left hippocampi (fucsia and orange columns, respectively) and in control guinea pigs (pink columns; n = 9-11). For GFAP and MAP2 staining, ROIs were positioned in CA1, CA3, and hilus; for IgG staining, only CA1 ROIs were analyzed. Eight animals were utilized for GFAP measurements in CA1 and hilus and 6-8 in CA3; 9-11 animals were used for MAP2 counts in CA1, CA3, and hilus and 8 guinea pigs for IgG staining in CA1. E,F, Cell counts on sections of right and left CA1, CA3, and hilus regions of hippocampi stained for Fluoro-Jade (E) and TUNEL (F) 3 days after ncSE in KA-injected (fucsia and orange columns; Fluoro-Jade: n = 7; TUNEL: n = 5) and in control guinea pigs (n = 5 pink columns). Significance values: **** and $^{++++}$: $P < 0.0001$ to unpaired and paired *t* test, respectively; *** and $^{+++}$: $P = 0.0001$; ** and $^{++}$: $P < 0.01$; $^{+}$: $P < 0.05$. In C,E,F and middle panel of B, a one-tail unpaired/paired *t* test was performed, while the remaining statistical tests were two-tailed. For details on the statistical significance values, see Figure7

was found by comparing LH in KA-treated animals with naive/control MD measurements. MD reduction was also observed in the right frontal cortex in most KA-injected animals, and the difference between the right and the left cortex was significant in the KA group ($P < 0.05$) but not in the sham-operated and naive groups. The analysis of FA values in the same hippocampal ROIs did not show any statistically significant difference between hemispheres and between animal groups (not shown).

3.3 | Immunohistochemical analysis in the hippocampi ipsi- and contralateral to KA injection

One week after MRI scans, the brains were cut and sections including hippocampi were processed for NeuN, GFAP, MAP2, and IgG immunostaining (Figures 4 and 5) to retrospectively evaluate neuronal loss, astrogliosis, neuronal suffering (see below), and BBB permeability alterations. In both naive (left column in Figure 4) and sham-operated/treated controls (middle column in Figure 4), no sign of brain damage was observed, with the exception of GFAP and IgG staining in the tissue surrounding the hippocampal electrode tracks (arrows in the lower middle photo in Figure 4), likely due to a local inflammatory reaction. Of interest, MAP2 staining in control animals (both naive and sham-operated) showed a peculiar pattern, with no staining in the pyramidal cell/radiatum layers of CA2 and CA3/4 regions (Figure 4 and Figure S1B,C). In KA-treated animals (right column in Figure 4), neuronal cell loss and astrogliosis were observed in KA-injected hippocampi. A reduction of dendritic MAP2 signal in CA1-CA3 and hilus was observed, with an atypical staining of the neuronal soma at the boundaries of the lesional tissue (see Discussion). IgG staining was observed exclusively around the KA injection site (lower right photo in Figure 4).

The qualitative evaluation suggested that the hippocampus contralateral to KA injection did not show obvious expression of brain damage markers. To quantify this observation, we analyzed the density of immunostaining in different hippocampal areas (CA1, CA3, DG, and hilus) in the RH and in the contralateral (LH) hippocampi of KA-injected animals (Figure 5) and compared these values with densitometric measurements obtained from equivalent hippocampal subfields in both hemispheres of naive and sham-operated control animals. As illustrated in Figure 5A, the LH of KA-treated animals (n = 10) showed NeuN densitometric values in CA1 (44.04 ± 5.06% density), CA3 (31.14 ± 3.35%), DG (73.06 ± 4.59%), and hilus (20.23 ± 3.52%) similar to control animals (43.84 ± 4.21% in CA1; 36.12 ± 4.77% in CA3, 66.02 ± 4.24% in DG, and 22.79 ± 3.77% in the hilus; n = 9-11 for each subfield—measured in both right and left hippocampi), suggesting that NeuN immunostaining in non-KA-injected LH subfields was comparable to that in normal tissue. As expected, all right KA-injected hippocampal fields (left right columns in Figure 5A) showed cell loss (CA1: 19.94 ± 10.80% density, CA3: 17.30 ± 11.25%, DG: 63.23 ± 12.25%, and hilus: 9.46 ± 7.27%) compared to non-KA-injected left hippocampi and CA1, CA3, and hilus in respective controls. The statistical significance of NeuN findings is reported in Figure 7 and in the graph of Figure 5.

Densitometric measurements were also performed for GFAP, MAP2, and IgG immunostaining. Hippocampal subfields densities in KA-treated guinea pigs (gray columns in Figure 5A-D) were compared to control immunodensity values obtained by merging measurements of sham-operated and naive animals (black columns). The GFAP staining intensity measured on two ROIs on two slices per region in 6-8 KA-treated animals and in 9-10 controls (naive and shams) showed a statistically significant density increase in the CA1 and hilus of the right, KA-injected hippocampi (3.35 ± 2.43% and 1.36 ± 0.75%, respectively) compared to the corresponding areas of the controls (0.56 ± 0.53% and 0.08 ± 0.12%, respectively). No difference was observed between controls and the left hippocampi of KA-treated animals in CA1, CA3, and hilus (1.03 ± 0. 85% and 0.44 ± 0.52%, respectively; Figure 5B). MAP2 immune-signal was measured in 9-11 KA-injected animals and in 9-11 control guinea pigs (Figure 5D). MAP2 density was significantly lower in the right hippocampi of KA-treated animals (14.48 ± 10.16% in CA1, 20.18 ± 17.35% in CA3, and 41.58 ± 21.11% in the hilus) compared to controls (72.20 ± 12.21% in CA1,

FIGURE 6 Semiquantitative analysis of thionine and GFAP staining ipsi- and contralateral to KA injection in guinea pigs that developed mesial temporal lobe epilepsy (mTLE), sacrificed 2 months after the induction of ncSE. A, Representative microphotographs of thionine-stained coronal sections of the left (LH) and the KA-injected right RH(KA) hippocampi and of naive control animals. Higher magnification of the boxed area in the upper small photograph is illustrated in the lower panels. B, The average percentage of densitometric thionine-staining changes measured in CA1 (left panel) and CA3 (right panel) of five chronically epileptic guinea pigs; densitometric values obtained from the same areas in the right (fucsia columns) and left (orange columns) hippocampi of KA-injected guinea pigs and of control naive animals (pink columns) are illustrated (n = 4). C, Representative microphotographs of GFAP immunostained coronal sections of the left (LH) and the KA-injected right RH(KA) hippocampi. Higher magnification of the boxed area in the upper small photograph is illustrated in the lower panels. D, Densitometric GFAP measurements in right and left CA1 and CA3 of chronic epileptic KA-treated animals (gray columns; n = 4) and in control guinea pigs (black columns; n = 5). Statistical significance values: **** and $^{++++}$: $P < 0.0001$ to unpaired and paired *t* test, respectively; ** and $^{++}$: $P < 0.01$; $^{+}$: $P < 0.05$. One-tail unpaired/paired *t* test was performed for the right panel in B while the others were two-tailed. For details see Figure7

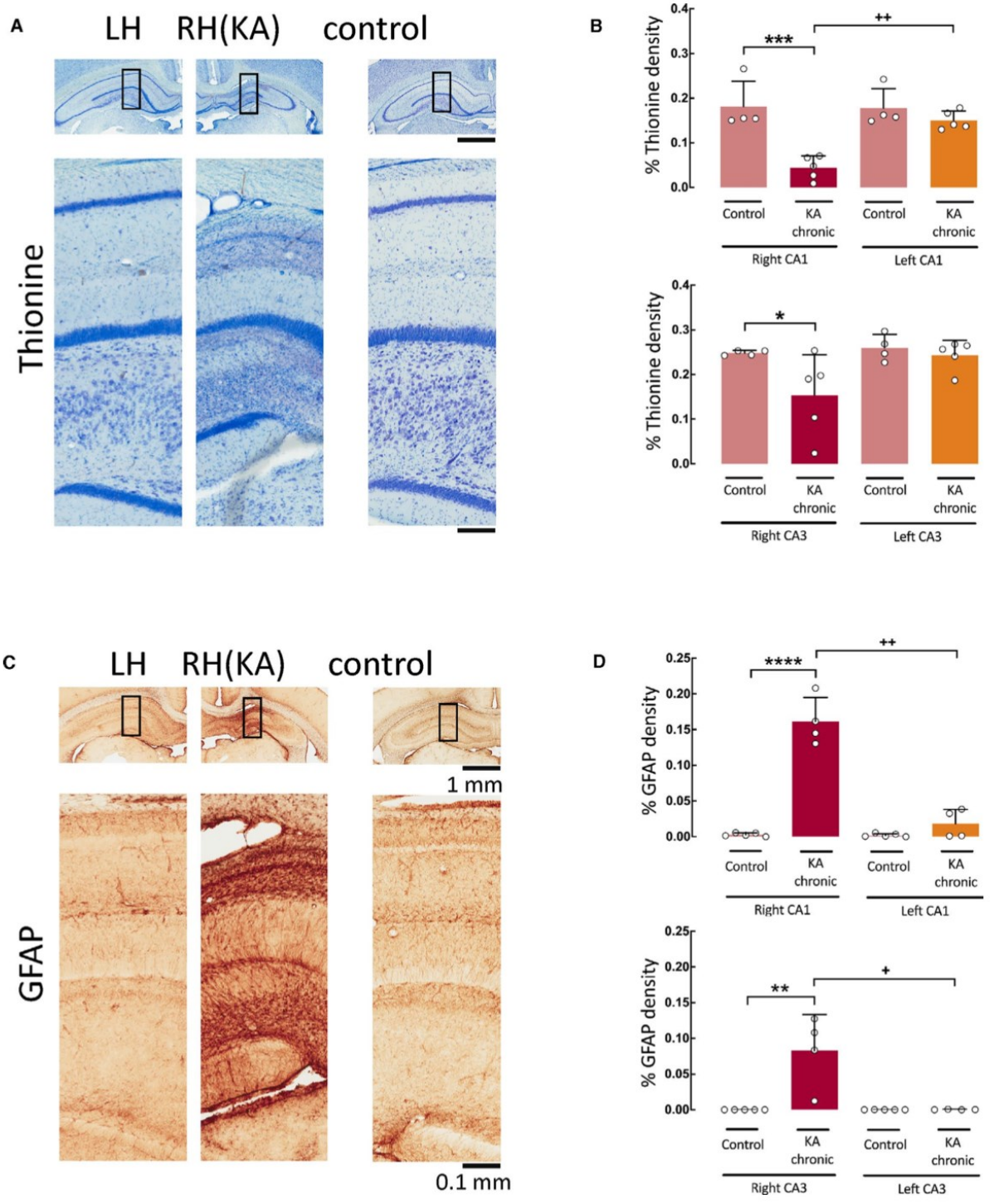

57.25 ± 12.77% in CA3, and 62.00 ± 25.12% in the hilus). The same observation was also true for the contralateral CA1 (70.65 ± 20.09%) and CA3 (44.69 ± 8.78%) areas; no significant difference was observed by comparing right and left measurements in the hilus of KA-treated guinea pigs (52.96 ± 17.99% in left hilus). IgG-immunostaining density was statistically increased in the right CA1 region (31.33 ± 29.08%) compared to left CA1 and control (n = 8; Figure 5C). No IgG staining was found in CA1 areas of naive animals (n = 9). The statistical significance of GFAP, MAP2, and IgG densitometric measurements is reported respectively in Figure 7 and in the graph of Figure 5. These findings demonstrated that BBB damage, cell loss, and gliosis are not detectable in the hippocampus contralateral to KA injection,

despite the occurrence of intense epileptiform activity during the ncSE.

Densitometric measurements were also performed on brain sections obtained from the 4-5 KA-injected animals recorded for 2 months after ncSE, when spontaneous seizures associated with unilateral hippocampal sclerosis in the KA-injected hippocampus developed.[12,13] Thionine density in CA1 and CA3 was 4.42 ± 3.95% and 15.37 ± 11.67% in the right KA-injected hippocampi and 15.05 ± 3.67% and 24.34 ± 4.49% in the left hippocampus of KA-treated guinea pigs; 15.40 ± 1.03% in CA1 and 25.48 ± 3.95% in CA3 of naive animals (n = 4; measured in two sections per animal). As illustrated in Figure 6B, mean densities were not significantly different when the values in the left hippocampus of KA-treated animals were compared to control animal (*P* values in Figure 7). GFAP intensity staining measured on two slices in four KA-treated animals (Figure 6C and D) showed a statistically significant increase in CA1 and CA3 density in the right KA-side (16.13 ± 6.01% and 8.29 ± 6.28%, respectively) compared to the contralateral side (1.83 ± 2.00% and 3.41 ± 3.52%, in CA1 and CA3) and to controls (2.12 ± 4.09% and 3.51 ± 4.54% in CA1 and CA3, respectively; two sections each in five animals). Statistical significance is reported in Figure 7 and in the graph of Figure 6.

To further evaluate the presence of cellular and neuronal damage in the KA-injected and in the contralateral hippocampus, we analyzed two additional markers for neuronal degeneration (Fluoro-Jade staining at 3 days and 1 month after KA-induced ncSE) and for apoptosis (TUNEL staining 3 days after ncSE). The average number of Fluoro-Jade positive cells were counted in CA1, CA3, and hilus of 3-day KA-treated animals (n = 7) and from the same areas in control animals (n = 5). Cell count was null in control hippocampi and in the left hippocampi contralateral to the KA injections (Figure S2A and Figure 5E). Three days post-ncSE we counted 28.43 ± 4.56 Fluoro-Jade-positive neurons in the right KA-injected CA1 area, 24.79 ± 3.78 in CA3 area, and

NeuN - 3 dd

CA1 (KA n=10; controls n=11)		
	LH	RH controls
RH (KA)	p=0.0001 (+++)	p<0.0001 (****)
LH controls	p=0.7186	
CA3 (KA n=10; controls n=9-10)		
	LH	RH controls
RH (KA)	p=0.0022 (++)	p<0.0001 (****)
LH controls	p=0.0520	
***hilus* (KA n=10; controls n=11)**		
	LH	RH controls
RH (KA)	p=0.0060 (++)	p<0.0001 (****)
LH controls	p=0.1479	
DG (KA n=10; controls n=11)		
	LH	RH controls
RH (KA)	p=0.0168 (+)	p=0.5373
LH controls	p=0.0520	

IgG - 3 dd

CA1 (KA n=8; controls n=9)		
	LH	RH controls
RH (KA)	p=0.0109 (+)	p=0.0030 (**)
LH controls	p=0.7176	

GFAP - 3 dd

CA1 (KA n=8; controls n=10)		
	LH	RH controls
RH (KA)	p=0.0070 (++)	p=0.0004 (***)
LH controls	p=0.0992	
CA3 (KA n=6-8; controls n=9)		
	LH	RH (Sham)
RH (KA)	p=0.2760	p=0.0671
LH controls	p=0.0554	
***hilus* (KA n=8; controls n=9)**		
	LH	RH controls
RH (KA)	p=0.0083 (++)	p<0.0001 (****)
LH controls	p=0.0699	

Fluoro-Jade - 3 dd

CA1 (KA n=7; controls n=5)		
	LH	RH controls
RH (KA)	p<0.0001 (++++)	p<0.0001 (****)
LH controls	p=0.2121	
CA3 (KA n=7; controls n=5)		
	LH	RH controls
RH (KA)	p<0.0001 (++++)	p<0.0001 (****)
LH controls	p=0.2121	
***hilus* (KA n=7; controls n=5)**		
	LH	RH controls
RH (KA)	p<0.0001 (++++)	p<0.0001 (****)
LH controls	p=0.2121	

Tionine - 1 month

CA1 (KA n=5; controls n=4)		
	LH	RH controls
RH (KA)	p=0.0012 (++)	p=0.0009 (***)
LH controls	p=0.1259	
CA3 (KA n=5; controls n=4)		
	LH	RH controls
RH (KA)	p=0.0624	p=0.0393 (*)
LH controls	p=0.2347	

GFAP - 1 month

CA1 (KA =4; controls = 5)		
	LH	RH controls
RH (KA)	p= 0.0057(++)	p<0.0001 (****)
LH controls	p=0.0552	
CA3 (KA =4; controls = 5)		
	LH	RH controls
RH (KA)	p=0.0232 (+)	p=0.0036 (**)
LH controls	p=0.0592	

MAP2 - 3 dd

CA1 (KA n=9-10; controls n=11)		
	LH	RH controls
RH (KA)	p<0.0001 (++++)	p<0.0001 (****)
LH controls	p=0.2657	
CA3 (KA n=9; controls n=9-10)		
	LH	RH controls
RH (KA)	p=0.0015 (++)	p<0.0001 (****)
LH controls	p=0.1543	
***hilus* (KA n=10-11; controls n=9-10)**		
	LH	RH controls
RH (KA)	p=0.1164	p=0.0011 (**)
LH controls	p=0.0805	

TUNEL - 3 dd

CA1 (KA n=5; controls n=5)		
	LH	RH controls
RH (KA)	p=0.0155 (+)	p=0.0058 (**)
LH controls	p=0.1733	
CA3 (KA n=5; controls n=5)		
	LH	RH controls
RH (KA)	p=0.0180 (+)	p=0.0077 (**)
LH controls	p=0.1733	
***hilus* (KA n=5; controls n=5)**		
	LH	RH controls
RH (KA)	p=0.0311 (+)	p=0.0171 (*)
LH controls	p=0.1471	

FIGURE 7 Statistical significance of densitometric values measured for NeuN (first row), GFAP (second row), MAP2 (third row), IgG (fourth row), and thionine (fifth row), and of Fluoro-Jade (sixth row) and TUNEL (seventh row) cell counts in hippocampal areas of both acutely sacrificed guinea pigs (3 days after KA treatment; rows 1-4 and 6-7) and of chronic animals evaluated 2 months after KA treatment (rows 2 and 5). Data are illustrated in Figures 4–6 and in Figure S2. The symbols (*) and (+) refer to significance values to paired and unpaired *t* test, respectively

20.21 ± 5.94 in the hilus. TUNEL staining was evaluated at 3 days post-ncSE (n = 5); no TUNEL$^-$positive cells were observed in both controls and in left hippocampi contralateral to KA injection. In the KA-injected side, we counted 8.63 ± 5.92 TUNEL$^-$positive cells in CA1, 19.53 ± 14.22 in CA3, and 8.57 ± 7.52 in the hilus (Figure S2B and Figure 5F). The statistical significance of Fluoro-Jade and TUNEL measurements is reported in Figure 7.

4 | DISCUSSION

We demonstrate that sustained recurrent seizure activity during ncSE does not induce the expression of brain damage markers associated with neuronal death, astrogliosis, and altered BBB permeability in the hippocampus contralateral to KA injection in a model of unilateral mTLE[14–16] applied to guinea pigs.[12,13] KA induces rapid excitotoxic neuronal death[22,30,31] in the CA1 region of the injected hippocampus and promotes epileptiform discharges that equally involve both the KA-injected and the contralateral hippocampi. The absence of gliosis and cell loss contralateral to KA injection is demonstrated 3 days after KA treatment and is confirmed 2 months after ncSE in chronic mTLE guinea pigs.

In the unilateral KA mTLE model, acute focal seizures are characterized by immobility, followed by facial clonus, masticatory movements, and head nodding, and could develop into bilateral forelimb clonus and rearing/falling.[12,13,32–34] Seizure activity in the unilateral KA model is characterized by acute bi-hippocampal discharges superimposed on a condition of continuous large-amplitude slow spikes at 1-3 Hz[12–14] that involve the injected hippocampus and propagate to the contralateral amygdala, hippocampus, and frontal cortex.[12–14,16] Of interest, periodic EEG slow spikes associated with focal seizures have been described during ncSE induced by acute brain injury in humans.[35]

Our study confirms that intracerebral KA establishes a focal unilateral hippocampal sclerosis[12] in the KA-injected hippocampus characterized by neuronal loss, astrogliosis, and altered BBB permeability. Enhanced GFAP, MAP2, and IgG immunostainings and the activation of markers for cell death and apoptosis are restricted to the ipsilateral CA1-CA3 region and to the DG. In line with our findings, a rapid increase in GFAP immunoreactivity was detected in the KA-injected hippocampus in the mouse.[22] MAP2 staining in large dendrites is abolished and/or transferred to neuron soma in acutely injured brain tissue during excitotoxic damage[27] and ischemia,[28] and relocated to the soma at the boundary of the damaged areas in the KA-injected CA1/DG areas in our experiments.

We utilize the unilateral KA injection model as an instrument to test whether epileptiform activity in regions remote from the KA injection area is sufficient to induce brain damage. The correlation between seizures and tissue damage is controversial and can be verified exclusively in animal models characterized by focal unilateral epileptogenic lesions, such as intracerebral KA injection and the local electrical stimulation models; it cannot be analyzed in epilepsy models that result from systemic pilocarpine or KA treatments, because these procedures induce diffuse bilateral alterations. In these systemic epileptogenic models, convulsive SE conditions are reliably induced that result in bilateral hippocampal damage and bilateral and diffuse hippocampal sclerosis. The study by Arabadzisz and colleagues[36] demonstrated that unilateral KA injection into one dorsal hippocampus induced ncSE followed by ipsilateral focal seizures and damage, whereas the contralateral hippocampus remained structurally unaffected and seizure-free. In two studies, contralateral hippocampal alterations were observed when a convulsive status epilepticus was promoted using either high doses of unilaterally injected KA[37] or repeated unilateral hippocampal stimulation.[38] In a recent report, unilateral hippocampal electrical stimulation in rats demonstrated cell loss and changes in the expression of N-cadherin in the hippocampus contralateral to stimulation[39] exclusively in a subgroup of animals that developed seizures 4 weeks after ncSE. Of interest, contralateral neuronal loss was not observed in rats submitted to ncSE that did not develop spontaneous seizures in the chronic phase. The study showed also a specific increase in Iba and GFAP (but not S100) protein levels in the hippocampi of animals with and without chronic spontaneous seizures; glial changes contralateral to the stimulated hippocampus are mentioned in the study but were not quantified. This report supports the evidence that ncSE activity does not induce obvious damage markers in rats that do not develop a chronic spontaneous seizures. The differences between these studies and our findings could be due to the very mild chronic epileptic phenotype observed in guinea pigs 2 months after ncSE,[12] characterized by an average of 1 behavioral seizure per week. Unilateral mTLE models data suggest that the contralateral hippocampus is not obligatorily altered after acute ncSE and support our findings that seizure and epileptiform activity during ncSE may not damage regions far away from the original epileptogenic focus. In the rat kindling model, apoptosis and neuronal loss were demonstrated in the DG, hilus, CA1, and CA3 areas and in the entorhinal cortex during kindling acquisition.[40,41] Nevertheless, spontaneous and stimulus-evoked seizures can reliably be induced without detectable cell loss in adult kindled rats,[42,43] suggesting that in this focal seizure model a consistent correlation between seizure activity and tissue damage is not demonstrated. Even though irreversible brain damage occurs in prolonged convulsive SE,[44] evidence of damage associated with ncSE is inconclusive in clinical studies (for review see [45]), because it is difficult to separate the possible effect of ncSE from the underlying cause of the

epilepsy; most ncSE, indeed, are generated by an underlying disease and the ensuing brain damage could be due to the primary comorbid neurologic insult (encephalitis, concussion, and so on).

Our MRI study on fixed brain tissue confirmed that brain damage is lateralized exclusively to the KA-injected hippocampus. These data confirmed the results of the above-mentioned study on the ncSE model induced by unilateral electrical stimulation of one hippocampus.[39] We utilized postfixed tissue because it allows longer MR scanning times that improve imaging definition without altering the significance of the recorded signals; apparent diffusion coefficient (ADC) measurements in fixed brains are characterized by lower values compared to in vivo condition.[46,47] T1-weighted MRI images showed signal changes suggesting BBB disruption only in KA-injected hippocampus, although we cannot exclude minor, undetectable BBB permeability changes on the contralateral side. DTI data showed a prominent MD decrease in all the KA-injected hippocampi and in the ipsilateral frontal cortex, probably caused by a reduction of the extracellular space due to cytotoxic edema, as suggested by DTI findings in the acute stage of KA lesions.[48,49] The IgG extravasation observed exclusively in the tissue surrounding the KA injection site confirmed the MRI findings. BBB permeability changes during KA-induced seizures are expected to promote IgG extravasation 3 days after intense epileptiform activity, when neurons and astrocytes incorporate BBB-leaked IgGs.[23] The absence of IgG extravasation in the hippocampus contralateral to KA injection contributes additional evidence on the absence of seizure-mediated damage in areas contralateral to KA injection. The lack of contralateral seizure-induced BBB alterations conflicts with the report that both permeability changes and inflammatory molecule expression are associated with seizure activity.[21,49] We hypothesize that if seizure-dependent BBB permeability changes occur in the hippocampus contralateral to KA injection, they are not sufficiently severe to induce extravasation of IgG and other factors that are required to initiate the epileptogenic process that produces tissue damage.

In conclusion, our study utilized an ncSE model as an instrument to evaluate the effect of epileptiform activity on brain tissue far from the primary epileptogenic lesion (the KA injection site). We provide experimental evidence that markers commonly utilized for the neuropathologic identification of neuronal cell loss, gliosis, BBB permeability changes, apoptosis, and cell degeneration are not stimulated by seizure activity per se in cortical areas there were not primarily altered by the direct application of KA. These findings are in line with those in recent report that recurrent seizures do not induce the expression of brain damage markers in perilesional epileptogenic cortex studied in postsurgical tissue obtained in patients with cryptogenic and focal cortical dysplasia (FCD).[51] The demonstration that seizures as such do not contribute to brain damage does not imply that seizures are not potentially dangerous events and that their control should not be pursued. It is obvious, and it has to be clearly stated here, that the need to treat seizures in the clinical setting is mandatory because of the cognitive and functional impairment that seizures produce and imply.

ACKNOWLEDGMENTS

The authors are grateful to Barbara Cipelletti, Gloria Milesi, and Patrizia Aracri for help with immunostaining analysis and statistics. The work was supported by grants JTC2014-ERANET-Neuron 0004 (BrIE) of the European Community, GR-2011-02348633 of Italian Health Ministry, and by a grant of the *Fondazione Banca del Monte di Lombardia*. The project has received funding from the European Union's Horizon 2020 research and innovation program under the Marie Sklodowska-Curie grant agreement N. 722053 (*EUGliaPhD*).

AUTHOR'S CONTRIBUTIONS

Md.C. and F.M.N. elaborated the conception and design of the study; F.M.N., C.A., D.V.V., F.C., A.C., M.F., and I.Z. contributed to the acquisition and analysis of data; Md.C., A.C., C.A., M.F., D.V.V., and F.M.N. drafted a significant portion of the manuscript and figures.

DISCLOSURE

The authors have no conflicts of interest or competing financial or nonfinancial interests to declare. We comply with the Data Availability rules of the Journal. The authors confirm that we have read the Journal's position on issues involved in ethical publication and affirm that this report is consistent with those guidelines.

ORCID

Francesco Noè https://orcid.org/0000-0002-0019-1615
Marco Curtis https://orcid.org/0000-0001-7443-6737

REFERENCES

1. Haut SR, Veliskova J, Moshe SL. Susceptibility of immature and adult brains to seizure effects. Lancet Neurol. 2004;3:608–17.
2. Avanzini G, Depaulis A, Tassinari A, de Curtis M. Do seizures and epileptic activity worsen epilepsy and deteriorate cognitive function? Epilepsia. 2013;54(suppl 8):14–21.
3. Berg AT, Cross JH. Towards a modern classification of the epilepsies? Lancet Neurol. 2001;9:459–61.

4. Annegers JF, Hauser WA, Coan SP, Rocca WA. A population-based study of seizures after traumatic brain injuries. N Engl J Med. 1998;338:20–4.
5. Korff CM, Brunklaus A, Zuberi SM. Epileptic activity is a surrogate for an underlying etiology and stopping the activity has a limited impact on developmental outcome. Epilepsia. 2015;56:1477–81.
6. Pitkanen A, Sutula TP. Is epilepsy a progressive disorder? Prospects for new therapeutic approaches in temporal-lobe epilepsy. Lancet Neurol. 2002;1:173–81.
7. Pitkanen A, Schwartzkroin PA, Moshe SL. Models of seizures and epilepsy. Burlington, MA: Elsevier Academic Press; 2006.
8. Bouilleret V, Boyet S, Marescaux C, Nehlig A. Mapping of the progressive metabolic changes occurring during the development of hippocampal sclerosis in a model of mesial temporal lobe epilepsy. Brain Res. 2000;852:255–62.
9. Roch C, Leroy C, Nehlig A, Namer IJ. Predictive value of cortical injury for the development of temporal lobe epilepsy in 21-day-old rats: an MRI approach using the lithium-pilocarpine model. Epilepsia. 2002;43:1129–36.
10. Sutula TP. Mechanisms of epilepsy progression: current theories and perspectives from neuroplasticity in adulthood and development. Epil Res. 2004;60:161–71.
11. Pitkänen A, Immonen RJ, Gröhn OHJ, Kharatishvili I. From traumatic brain injury to posttraumatic epilepsy: what animal models tell us about the process and treatment options. Epilepsia. 2009;50:21–9.
12. Carriero G, Arcieri S, Cattalini A, Corsi L, Gnatkovsky V, de Curtis M. A guinea pig model of mesial temporal lobe epilepsy following nonconvulsive status epilepticus induced by unilateral intrahippocampal injection of kainic acid. Epilepsia. 2012;53:1917–27.
13. Arcieri S, Velotti R, Noè F, Carriero G, Cattalini A, Galbardi B, et al. Variable electrobehavioral patterns during focal nonconvulsive status epilepticus induced by unilateral intrahippocampal injection of kainic acid. Epilepsia. 2014;55:1978–85.
14. Bouilleret V, Ridoux V, Depaulis A, Marescaux C, Nehlig A, Le Gal La Salle G. Recurrent seizures and hippocampal sclerosis following intrahippocampal kainate injection in adult mice: electroencephalography, histopathology and synaptic reorganization similar to mesial temporal lobe epilepsy. Neuroscience. 1999;89:717–29.
15. Bragin A, Engel J, Wilson CL, Vizentin E, Mathern GW. Electrophysiologic analysis of a chronic seizure model after unilateral hippocampal KA injection. Epilepsia. 1999;40:1210–21.
16. Riban V, Bouilleret V, Pham-Lê BT, Fritschy J-M, Marescaux C, Depaulis A. Evolution of hippocampal epileptic activity during the development of hippocampal sclerosis in a mouse model of temporal lobe epilepsy. Neuroscience. 2002;112:101–11.
17. Rao MS, Hattiangady B, Reddy DS, Shetty AK. Hippocampal neurodegeneration, spontaneous seizures, and mossy fiber sprouting in the F344 rat model of temporal lobe epilepsy. J Neurosci Res. 2006;83:1088–105.
18. Schwob JE, Fuller T, Price JL, Olney JW. Widespread patterns of neuronal damage following systemic or intracerebral injections of kainic acid: a histological study. Neuroscience. 1980;5:991–1014.
19. Fujikawa DG. The temporal evolution of neuronal damage from pilocarpine-induced status epilepticus. Brain Res. 1996;725:11–22.
20. Järvelä JT, Ruohonen S, Kukko-Lukjanov T-K, Plysjuk A, Lopez-Picon FR, Holopainen IE. Kainic acid-induced neurodegeneration and activation of inflammatory processes in organotypic hippocampal slice cultures: treatment with cyclooxygenase-2 inhibitor does not prevent neuronal death. Neuropharmacology. 2011;60:1116–25.
21. Ravizza T, Gagliardi B, Noé F, Boer K, Aronica E, Vezzani A. Innate and adaptive immunity during epileptogenesis and spontaneous seizures: evidence from experimental models and human temporal lobe epilepsy. Neurobiol Dis. 2008;29:142–60.
22. Pernot F, Heinrich C, Barbier L, Peinnequin A, Carpentier P, Dhote F, et al. Inflammatory changes during epileptogenesis and spontaneous seizures in a mouse model of mesiotemporal lobe epilepsy. Epilepsia. 2011;52:2315–25.
23. Van Vliet EA, da Costa Araujo S, Redeker S, van Schaik R, Aronica E, Gorter JA. Blood-brain barrier leakage may lead to progression of temporal lobe epilepsy. Brain. 2007;130:521–34.
24. Lidster K, Jefferys JG, Blümcke I, Crunelli V, Flecknell P, Frenguelli BG, et al. Opportunities for improving animal welfare in rodent models of epilepsy and seizures. J Neurosci Methods. 2016;260:2–25.
25. Basser PJ, Pierpaoli C. Microstructural and physiological features of tissues elucidated by quantitative-diffusion-tensor MRI. J Magn Reson. 1996;111:209–19.
26. Wang R, Benner T, Sorensen AG, Wedeen VJ. Diffusion toolkit: a software package for diffusion imaging data processing and tractography. Proc Intl Soc Mag Reson Med. 2007;15:3720.
27. Pierpaoli C, Righini A, Linfante I, Tao-Cheng JH, Alger JR, Di Chiro G. Histopathologic correlates of abnormal water diffusion in cerebral ischemia: diffusion-weighted MR imaging and light and electron microscopic study. Radiology. 1993;189:439–48.
28. Horvath E, Oradan A, Chiriac L, Dobreanu M, Nagy E-E, Hutanu A. Early excitability changes in a novel acute model of transient focal ischemia and reperfusion in the in vitro isolated guinea pig brain. Exp Neurol. 2007;204:95–105.
29. Breschi GL, Mastropietro A, Zucca I, Librizzi L, de Curtis M. Penumbra region excitability is not enhanced acutely after cerebral ischemia in the in vitro isolated guinea pig brain. Epilepsia. 2012;53:448–58.
30. Nadler JV, Perry BW, Cotman CW. Intraventricular kainic acid preferentially destroys hippocampal pyramidal cells. Nature. 1978;271:676–77.
31. Levesque M, Avoli M. The kainic acid model of temporal lobe epilepsy. Neurosci Biobehav Rev. 2013;37:2887–99.
32. Raedt R, Van Dycke A, Van Melkebeke D, De Smedt T, Claeys P, Wyckhuys T, et al. Seizures in the intrahippocampal kainic acid epilepsy model: characterization using long-term video-EEG monitoring in the rat. Acta Neurol Scand. 2009;119:293–303.
33. Leite JP, Babb TL, Pretorius JK, Kuhlman PA, Yeoman KM, Mathern GW. Neuron loss, mossy fiber sprouting, and interictal spikes after intrahippocampal kainate in developing rats. Epil Res. 1996;26:219–31.
34. Groticke I, Hoffmann K, Loscher W. Behavioral alterations in a mouse model of temporal lobe epilepsy induced by intrahippocampal injection of kainate. Exp Neurol. 2008;213:71–83.
35. Rodriguez Ruiz A, Vlachy J, Lee JW, Gilmore EJ, Ayer T, Haider HA, et al. Association of periodic and rhythmic electroencephalographic patterns with seizures in critically ill patients. JAMA Neurol. 2017;74:181–8.
36. Arabadzisz D, Antal K, Parpan F, Emri Z, Fritschy J-M. Epileptogenesis and chronic seizures in a mouse model of temporal

lobe epilepsy are associated with distinct EEG patterns and selective neurochemical alterations in the contralateral hippocampus. Exp Neurol. 2005;194:76–90.
37. Magloczky Z, Freund TF. Selective neuronal death in the contralateral hippocampus following unilateral kainate injections into the CA3 subfield. Neuroscience. 1993;56:317–35.
38. Gorter JA, Pereira PMG, Van Vliet EA, Aronica E, Da Silva FHL, Lucassen PJ. Neuronal cell death in a rat model for mesial temporal lobe epilepsy is induced by the initial status epilepticus and not by later repeated spontaneous seizures. Epilepsia. 2003;44:647–58.
39. Avdic U, Ahl M, Chugh D, Ali I, Chary K, Sierra A, et al. Nonconvulsive status epilepticus in rats leads to brain pathology. Epilepsia. 2018;59:945–58.
40. Bengzon J, Kokaia Z, Elmer E, Nanobashvili A, Kokaia M, Lindvall O. Apoptosis and proliferation of dentate gyrus neurons after single and intermittent limbic seizures. Proc Natl Acad Sci USA. 1997;94:10432–7.
41. Cavazos JE, Das I, Sutula TP. Neuronal loss induced in limbic pathways by kindling: evidence for induction of hippocampal sclerosis by repeated brief seizures. J Neurosci. 1994;14:3106–21.
42. Michael M, Holsinger D, Ikeda-Douglas C, Cammisuli S, Ferbinteanu J, DeSouza C, et al. Development of spontaneous seizures over extended electrical kindling. I. electrographic, behavioral, and transfer kindling correlates. Brain Res. 1998;793:197–211.
43. Brandt C, Ebert U, Loscher W. Epilepsy induced by extended amygdala-kindling in rats: lack of clear association between development of spontaneous seizures and neuronal damage. Epil Res. 2004;62:135–56.
44. Sloviter S, Walker M. Status epilepticus in idiopathic generalized epilepsy. Epilepsia. 2005;46(suppl 9):73–9.
45. Kaplan PW. Assessing the outcomes in patients with nonconvulsive status epilepticus: nonconvulsive status epilepticus is underdiagnosed, potentially overtreated, and confounded by comorbidity. J Clin Neurophysiol. 1999;16(4):341–52.
46. Zucca I, Milesi G, Medici V, Tassi L, Didato G, Cardinale F, et al. Type II focal cortical dysplasia: ex vivo 7T magnetic resonance imaging abnormalities and histopathological comparisons. Ann Neurol. 2016;79:42–58.
47. D'Arceuil HE, Westmoreland S, de Crespigny AJ. An approach to high resolution diffusion tensor imaging in fixed primate brain. NeuroImage. 2005;35:553–65.
48. Tokumitsu T, Mancuso A, Weinstein PR, Weiner MW, Naruse S, Maudsley AA. Metabolic and pathological effects of temporal lobe epilepsy in rat brain detected by proton spectroscopy and imaging. Brain Res. 1997;744:57–67.
49. Librizzi L, Noè F, Vezzani A, de Curtis M, Ravizza T. Seizure-induced brain-borne inflammation sustains seizure recurrence and blood-brain barrier damage. Ann Neurol. 2012;72:82–90.
50. Vezzani A, Friedman A. Brain inflammation as a biomarker in epilepsy. Biomark Med. 2011;5:607–14.
51. Rossini L, Garbelli R, Gnatkovsky V, Didato G, Villani F, Spreafico R, et al. Seizure activity per se does not induce tissue damage markers in human neocortical focal epilepsy. Ann Neurol. 2017;82:331–41.

SUPPORTING INFORMATION

Additional supporting information may be found online in the Supporting Information section at the end of the article.

How to cite this article: Noè F, Cattalini A, Vila Verde D, et al. Epileptiform activity contralateral to unilateral hippocampal sclerosis does not cause the expression of brain damage markers. *Epilepsia*. 2019;00:1–16. https://doi.org/10.1111/epi.15611

Received: 12 August 2020 | Revised: 29 December 2020 | Accepted: 30 December 2020

DOI: 10.1111/nan.12693

Neuropathology and Applied Neurobiology WILEY

ORIGINAL ARTICLE

Seizure activity and brain damage in a model of focal non-convulsive *status epilepticus*

Diogo Vila Verde[1] | Till Zimmer[2] | Alessandro Cattalini[1] | Marlene F. Pereira[3,4] | Erwin van Vliet[2,5] | Giuseppe Testa[3,4] | Vadym Gnatkovsky[1] | Eleonora Aronica[2,6] | Marco de Curtis[1]

[1]Epilepsy Unit, Fondazione Istituto Neurologico Carlo Besta, Milan, Italy

[2]Department of (Neuro) Pathology, Amsterdam UMC, University of Amsterdam, Amsterdam Neuroscience, Amsterdam, The Netherlands

[3]Department of Oncology and Hematooncology, University of Milan, Milan, Italy

[4]Laboratory of Stem Cell Epigenetics, IEO, European Institute of Oncology, IRCCS, Milan, Italy

[5]Swammerdam Institute for Life Sciences, Center for Neuroscience, University of Amsterdam, Amsterdam, The Netherlands

[6]Stichting Epilepsie Instellingen Nederland (SEIN), Heemstede, The Netherlands

Correspondence
Marco de Curtis, Epilepsy Unit, Fondazione Istituto Neurologico *Carlo Besta*, via Celoria 11, Milan, Italy.
Email: marco.decurtis@istituto-besta.it

Funding information
Italian Health Ministry; Associazione Paolo Zorzi pe le Neuroscienze; H2020 Marie Skłodowska-Curie Actions, Grant/Award Number: 722053 and 765966

Abstract

Aims: Focal non-convulsive *status epilepticus* (FncSE) is a common emergency condition that may present as the first epileptic manifestation. In recent years, it has become increasingly clear that *de novo* FncSE should be promptly treated to improve post-status outcome. Whether seizure activity occurring during the course of the FncSE contributes to ensuing brain damage has not been demonstrated unequivocally and is here addressed.

Methods: We used continuous video-EEG monitoring to characterise an acute experimental FncSE model induced by unilateral intrahippocampal injection of kainic acid (KA) in guinea pigs. Immunohistochemistry and mRNA expression analysis were utilised to detect and quantify brain injury, 3-days and 1-month after FncSE.

Results: Seizure activity occurring during the course of FncSE involved both hippocampi equally. Neuronal loss, blood-brain barrier permeability changes, gliosis and up-regulation of inflammation, activity-induced and astrocyte-specific genes were observed in the KA-injected hippocampus. Diazepam treatment reduced FncSE duration and KA-induced neuropathological damage. In the contralateral hippocampus, transient and possibly reversible gliosis with increase of aquaporin-4 and Kir4.1 genes were observed 3 days post-KA. No tissue injury and gene expression changes were found 1-month after FncSE.

Conclusions: In our model, focal seizures occurring during FncSE worsen ipsilateral KA-induced tissue damage. FncSE only transiently activated glia in regions remote from KA-injection, suggesting that seizure activity during FncSE without local pathogenic co-factors does not promote long-lasting detrimental changes in the brain. These findings demonstrate that in our experimental model, brain damage remains circumscribed to the area where the primary cause (KA) of the FncSE acts. Our study emphasises the need to use antiepileptic drugs to contain local damage induced by focal seizures that occur during FncSE.

KEYWORDS
seizures, brain damage, non-convulsive status epilepticus, epilepsy, hippocampus

INTRODUCTION

One of the recurrent questions in epilepsy research is whether seizures during *status epilepticus* (SE) can cause brain damage. While there is increasing experimental evidence that generalised convulsive SE produces long-lasting neuropathological changes in the brain of rodents and humans [1, 2], it has been questioned whether seizure events that commonly occur during focal non-convulsive *status epilepticus* (FncSE) results in long-term consequences and contributes to pathology [3]. The need to recognise if seizure activity during FncSE aggravates brain damage is critical, even more since seizures during FncSE are often overlooked and consequently not properly treated [4].

Human studies and clinical data have proven controversial, since it is not easy to distinguish seizure-induced brain damage from the underlying cause that triggers FncSE [5]. While one study has demonstrated that seizures during FncSE without an evident acute brain injury can trigger the production of blood biomarkers of neuronal damage [6], others have found that patients suffering from FncSE do not develop long-term cognitive, memory or behavioural deficits [7–10]. Also, animal data have not proven conclusive, since brain damage has been mainly evaluated in models that do not accurately represent a proper FncSE condition. Intraperitoneal injection with either pilocarpine or kainic acid (KA) induces an acute convulsive SE and widespread multifocal damage [11–13], and for these reasons cannot be considered pure models of focal SE [14]. Intracerebral KA injection offers a better approach to study focal ictogenesis and epileptogenesis [15]. Intra-hippocampal [16–19], intra-amygdala [20–22] or intracortical [23] microinjections of KA result in pathological alterations resembling hippocampal sclerosis. Some of these studies proposed that the acute SE promotes secondary epileptogenesis and alterations in brain regions remote to the KA injection site [17, 20, 21, 24, 25]. Nevertheless, intracerebral KA injection may promote either FncSE or secondarily convulsive SE, depending on the protocol (dose, site of injection, etc.) and animal species [16, 18–20, 26]. Moreover focal electrical stimulation of the perforant path or other limbic structures can also induce either focal or secondary convulsive SE, with or without damage beyond the area of stimulation [27–31]. In conclusion, the aforementioned experimental models do not unequivocally resolve whether focal seizures occurring during FncSE have an impact on the extent, severity or distribution of brain damage.

Here, we investigated how much acute seizure activity *per se* affects the development of both localised and remote brain damage in a model of FncSE, defined as a model in which focal seizures predominantly occur during the acute SE [5]. The present report extends preliminary observations [32] by focusing on RNA expression changes and glial activation patterns that transiently occur outside the KA-injected region.

MATERIAL AND METHODS

The study is based on a population of 49 adult female Hartley guinea pigs (250–300 g, 3 postnatal weeks of age; Charles River, Calco, Italy), housed in a 12-h light-dark controlled cycle environment with *ad libitum* food and water supply. The experimental protocol was reviewed and approved by the Animal Welfare Office of the Italian Health Ministry (Authorization n. 36/2016-PR), in accordance with the European Committee Council Directive (2010/63/EU) and with the 3Rs principle. Efforts were made to minimise the number of animals and their suffering. Thirty-four animals were processed for molecular analysis and 15 were submitted to gene expression analysis (see below).

Electrode implantation and unilateral intrahippocampal injection

Forty-four guinea pigs were surgically implanted with bilateral intrahippocampal (AP −3 mm, ML ±3 mm, DV −3.25 mm relatively to Bregma) and epidural EEG recording electrodes, as described previously [33]. Seven days after electrode implantation, animals were injected in the dorsal *cornu ammonis* (CA1) of the right hippocampus with either a solution containing kainic acid (KA; n = 34) or 0.9% NaCl saline (sham operated animals; n = 10) under continuous video-EEG recording. A 30-gauge needle, connected to a 5 µl Hamilton syringe, was lowered through the guide cannula in the right hippocampus to inject a volume of 1 µl 0.9% NaCl solution with 1 µg KA (Sigma, St. Louis, MO, USA) over a period of 2 min. The needle was kept in place for 2 min to prevent backflow of the injected solution. Within 10 min after KA injection, epileptiform activity typical of a focal non-convulsive *status epilepticus* (FncSE) was recorded in all animals. Six animals were twice injected *i.p.* with diazepam (DZP; 25 µl/kg dissolved in NaCl) 30 min before and 30 min after KA injection (12.5 µl/kg). Sham animals were injected in the right hippocampus with 1 µl 0.9% NaCl following the same procedure. None of the sham operated/injected guinea pigs showed epileptiform activity. Acute animals were recorded for 3 days post-KA injection; chronic animals were video-EEG recorded for no less than 4 weeks after FncSE, to verify the presence of spontaneous seizures [33, 34]. Video-EEG monitoring was performed in 10 sham-operated/treated animals, 28 KA-injected guinea pigs and in 6 KA-injected animals treated with DZP (DZP+KA). A fifth group of naïve animals was used but not video-EEG monitored (n = 5).

Video-EEG recordings

Continuous 24/24-hour video-EEG monitoring started 1 week after surgery; implanted pedestals were connected to a cable mounted on a swivel coupled to the preamplifier of a BrainQuick EEG System (Micromed, Mogliano Veneto, Italy). Synchronised video-EEG was continuously recorded 48 h before injection, during the induction of FncSE and for the following 3 days in the acute animals (KA and DZP+KA) and for 4 weeks in the chronic KA group. EEG data were recorded at 0.1–1.0 kHz, 2064 Hz sampling rate, with 16-bit precision and high-pass filter at 0.1 Hz,

using the System Plus Evolution (Micromed). Video signals were simultaneously acquired with digital cameras to detect motor events. Video-EEG was analysed offline and hippocampal EEG patterns were identified and quantified for each animal. The EEG activity recorded with epidural electrodes was used to identify diffuse seizure patterns. KA-induced epileptiform activity was characterised by seizures combined with continuous 1–3 Hz spiking [32–34]. Seizure events during KA-induced FncSE were defined by researchers that were blinded to the treatment group. Seizures were also automatically counted with a software developed by Vadym Gnatkovsky to analyse long EEG recording periods with a compressed time scale. Seizure discharges were identified as focal unilateral, bilateral, convulsive or non-convulsive based on the EEG pattern distribution and on video analysis. In the chronic animals, spontaneous focal seizures were identified with 24/24-hour video-EEG monitoring recorded every other week for 4 weeks; the features of chronic spontaneous seizures were comparable to those described in previous studies [33, 34]. In these animals, FncSE profile was similar to the animals sacrificed at 3 days.

Immunohistochemical analysis

Following video-EEG recordings, animals were anaesthetised with sodium thiopental (125 mg/kg i.p., Farmotal; Pharmacia, Milan, Italy) and were trans-cardially perfused with 0.9% NaCl, followed by 4% paraformaldehyde in phosphate buffer 0.1 M for 5 min. Brains were explanted, immersed in 4% paraformaldehyde for 24 h and cut into 50 µm coronal sections. For immunohistochemical processing, the following antibodies were used: (a) monoclonal mouse anti-neuronal nuclei (NeuN 1:1000 – Merck-Millipore, Darmstadt, Germany); (b) mouse anti-microtubule associated protein 2 (MAP2 1:1000 – Neomarker-Invitrogen, Fremont, CA, USA); (c) polyclonal rabbit anti-glial fibrillary acid protein (GFAP 1:500 - DAKO, Glostrup, Denmark); (d) ionised calcium-binding adapter molecule 1 (Iba-1 1:200 – Merck-Millipore, Darmstadt, Germany) and (e) Immunoglobulin G (IgG 1:200 – Vector Laboratories, Burlingame, CA USA). Two serial coronal sections *per* animal were selected and analysed by researchers that were blinded to the treatment group. A standardised protocol was used for histochemical staining [32,33]. Immuno-stained sections were digitised using Scanscope software (Aperio Technologies, Sausalito, CA, USA). Staining for NeuN, MAP2, GFAP and IgG were analysed in naïve, sham-treated, acute KA, acute DZP+KA and chronic KA animals. Quantitative field fraction estimates of these immunostains were carried out in both hippocampi using Image-Pro Plus 7 software (Media Cybernetics, Inc. Rockville, MD, USA). Specific immunostaining density was estimated at 5x magnification in 2 regions of interest (ROIs) positioned in CA1, CA3 and dentate gyrus (DG) with respect to background signal. For each ROI densitometry was automatically calculated by the software on 2 adjacent slices in each hippocampal subfield (18 ROIs *per* brain slice; 3 ROIs *per* subfield) ipsilateral (right) and contralateral (left) to KA injection. Densitometric ROIs were positioned at least 0.5 mm away from the electrode tracks. For three dimensional reconstruction of microglial cells, immunofluorescence for Iba-1 and DAPI (1:5000) conjugated to Cy3 was performed on 50 µm thick coronal sections.

Fluoro-jade staining

Sections were mounted and then treated with 0.06% potassium permanganate for 15 min, washed 3 times, immersed in 0.001% FJ (Histo-Chem, Inc., Jefferson, Arkansas, USA) in 0.1% acetic acid for 30 min and rinsed in distilled water. After drying, slides were clarified in xylene and cover slipped with distyrene plasticizer xylene (DPX; BDH Lab Supplies, Leicestershire, UK) [32]. All fluoro-jade positive (FJ^+) cells were counted using FIJI-ImageJ (v2.0.0). Non-overlapping fields in CA1, CA3 and DG areas of both ipsi- and contralateral hippocampi were captured under identical conditions at 20x and 40x magnification with a Leica TCS SP8 microscope (Leica Microsystems, Germany). Cell counting was independently performed by 2 investigators in each experimental group (2 sections *per* animal, 0.5 mm away from the electrode tracks).

Morphometric analysis of microglia

Sections were visualised using a Leica SP8 confocal microscope (Leica Microsystems, Germany), applying the LASX software with navigator (version 3.1.5.16). Regions in dorsal CA1 *stratum radiatum* and the *hilus* of DG were acquired at high resolution (2 sections *per* animal, 0.5 mm away from the electrode tracks) using a 63X/1.4 oil objective with a x-y sampling of 72 nm. Cells were eligible for reconstruction if the following criteria were met: i) an Iba-1 positive cell was surrounding a single DAPI-stained nucleus; ii) the cell did not have truncated processes; iii) the cell was sufficiently separated from neighbouring cells to ensure correct reconstruction. A total of 240 cells, 120 for CA1 and 120 for DG, were selected for reconstruction performed using simple neurite tracer available in FIJI-ImageJ software (v2.0.0) [35]. Microglial morphometric properties were evaluated by quantifying the number of processes, total length, average number of intersections and Sholl analysis (number of intersections at radial intervals of 2 µm starting from the soma central point).

RNA isolation and quantitative real-time PCR measurements

Fresh hippocampal brain tissue for gene expression analysis was obtained from a group of 5 sham-operated and KA-injected guinea pigs either 3 days (n = 5) or 4 weeks (n = 5) post-injection. After saline intra-cardiac perfusion, brains were removed and the

whole hippocampus dissected out on a cold Petri dish. Dorsal CA1 and DG ipsilateral and contralateral to KA injection were further dissected and separately stored at −80°C. Samples were shipped to Amsterdam UMC where gene expression analysis was performed. Frozen brain tissue was homogenised in 700 μL Qiazol Lysis Reagent (Qiagen Benelux, Venlo, the Netherlands). Total RNA was isolated using the miRNeasy Mini kit (Qiagen Benelux, Venlo, the Netherlands) according to the manufacturer's instructions. RNA concentration and purity were determined at 260/280 nm using a Nanodrop 2000 spectrophotometer (Thermo Fisher Scientific, Waltham, MA, USA). To evaluate mRNA expression, 1 μg tissue-derived total RNA was reverse-transcribed into cDNA using oligo-dT primers. PCRs were run on a thermocycler (Lightcycler 480, Roche Applied Science, Basel, Switzerland) using housekeeping reference genes actin and glyceraldehyde 3-phosphate dehydrogenase (GAPDH). PCR mix contained 1 μL cDNA, 2.5 μL SensiFAST SYBR Green NoROX kit (Bioline Reagents Limited, London, UK), 0.4 μM of forward/reverse primers plus water to a final volume of 5 μL/well. PCR reactions were run in duplicates and a negative control containing water instead of cDNA was included for each gene in each run. Cycling conditions were as follows: initial denaturation at 95 °C for 5 min, followed by 45 cycles of denaturation at 95 °C for 15 s, annealing at 65 °C for 5 s and extension at 72 °C for 10 s. Sample fluorescence was measured via single acquisition mode at 72 °C after each cycle. Primer specificity was assessed using melt curve analysis after each run. To analyse potentially relevant pathogenic elements (inflammation, glial function, activity-dependent changes) associated with brain damage, the following genes were analysed: (a) interleukin 1 beta (IL-1 β); (b) cyclo-oxygenase-2 (COX-2); (c) haem oxygenase 1 (HO-1); (d) c-FOS; (e) aquaporin-4 (AQP4) and (f) inwardly rectifying potassium channel 4.1 (Kir4.1). Quantification of data was performed using LinRegPCR as described elsewhere [36].

Statistical analysis

Statistical analysis was performed using Prism 8.2 (GraphPad Software Inc., San Francisco, CA, USA). After identification of outliers (ROUT method), the Shapiro–Wilk normality test was performed to assess normality of the distribution. Where a normal distribution was found, one-way analysis of variance (ANOVA) was used to compare four independent groups and a paired or unpaired Student *t*-test to match 2 groups directly, for dependent or independent data respectively. When the data was not normally distributed, the non-parametric Kruskal-Wallis test followed by a Mann-Whitney U post-hoc test was employed to compare four independent groups and a paired Wilcoxon signed-rank test to relate two groups against each other. In the morphology data, results are expressed as means ±standard deviation (SD) for the number of independent experiments (*n*). The remaining graphical data is illustrated with boxplots with min., max., median and quartiles shown. The confidence interval (1- α) was set as 95% (0.95) so that the difference between means was considered statistically significant at p values of less than 5% (0.05), 1% (0.01), 0.1% (0.001) and 0.01% (0.0001) of significance level (α).

RESULTS

Focal non-convulsive *status epilepticus* (FncSE) was induced in 34 guinea pigs. Of these, 14 were sacrificed 3 days post-KA injection (acute post-FncSE phase) to evaluate the peak phase of brain damage [32, 34]. A different group of animals (n = 14; KA chronic group) was sacrificed 4 weeks post-KA injection [33, 34]. We treated another group of animals with intraperitoneal diazepam (DZP) before KA injection (DZP+KA group; n = 6). Sham-operated animals (n = 10) were injected in one hippocampus with saline solution. Video-EEG, immunohistochemical and morphological evaluations were performed in a total of 5 naïve, 5 sham, 9 acute post-KA, 9 KA chronic and 6 DZP+KA animals. Gene expression analysis was performed in 5 sham, 5 acute post-KA and 5 KA chronic guinea pigs.

Within 10 min of KA injection, FncSE started in the injected right hippocampus (ipsilateral KA in Figure 1A) and subsequently propagated within 1 min to the contralateral hippocampus. Seizures occurring during FncSE were classified by video-EEG monitoring as non-convulsive or secondarily convulsive according to the Racine scale [37] (stages 1–3 correspond to non-convulsive phenotype and 4/5 to convulsive phenotype with bilateral and diffuse EEG discharges). In the KA groups, seizures during FncSE were 89.1 ± 12.9% non-convulsive (Figure 1G), with the most common phenotype observed being mouth and head myoclonus with the occasional unilateral front limb myoclonus [34]. A total of 115 focal secondarily convulsive seizures lasting less than 30 s were counted among 1071 seizures occurring during the FncSE in all 18 animals. The time spent in secondarily convulsive seizures was minimal compared to the duration of the SE. In only 4 animals 10 to 15 convulsive seizures were observed (out of 353; Figure 1F), while the remaining 14 animals had from 1 to 3 convulsions (Figure 1F). The inclusion of the four animals with >10 convulsive seizures did not modify the overall immunostaining densitometric results (see below). None of the animals processed for the RNA expression analysis showed convulsive seizures during FncSE. The large majority of focal seizures recorded during the FncSE (79.7 ± 11.9%) involved both the KA injected and the contralateral hippocampi (Figure 1H) with no cortical EEG involvement. Epileptiform activity was not detected in sham animals recorded for 6 h after intrahippocampal saline injection (data not shown). As illustrated in Figure 1B, C and E, FncSE duration was 8.3 ± 2.0 h in KA-injected animals (n = 18) and was significantly shorter in the DZP+KA group (3.5 ± 1.5 h; n = 6). Moreover the number of seizures *per* animal was higher in the KA group (63.5 ± 14.3 seizures *per* animal; n = 18) in comparison to the DZP+KA group (11 ± 6.3 seizures *per* animal; n = 6; Figure 1D).

Animals were sacrificed and brains were processed for morphological analysis either 3 days or 4 weeks post FncSE. First, we

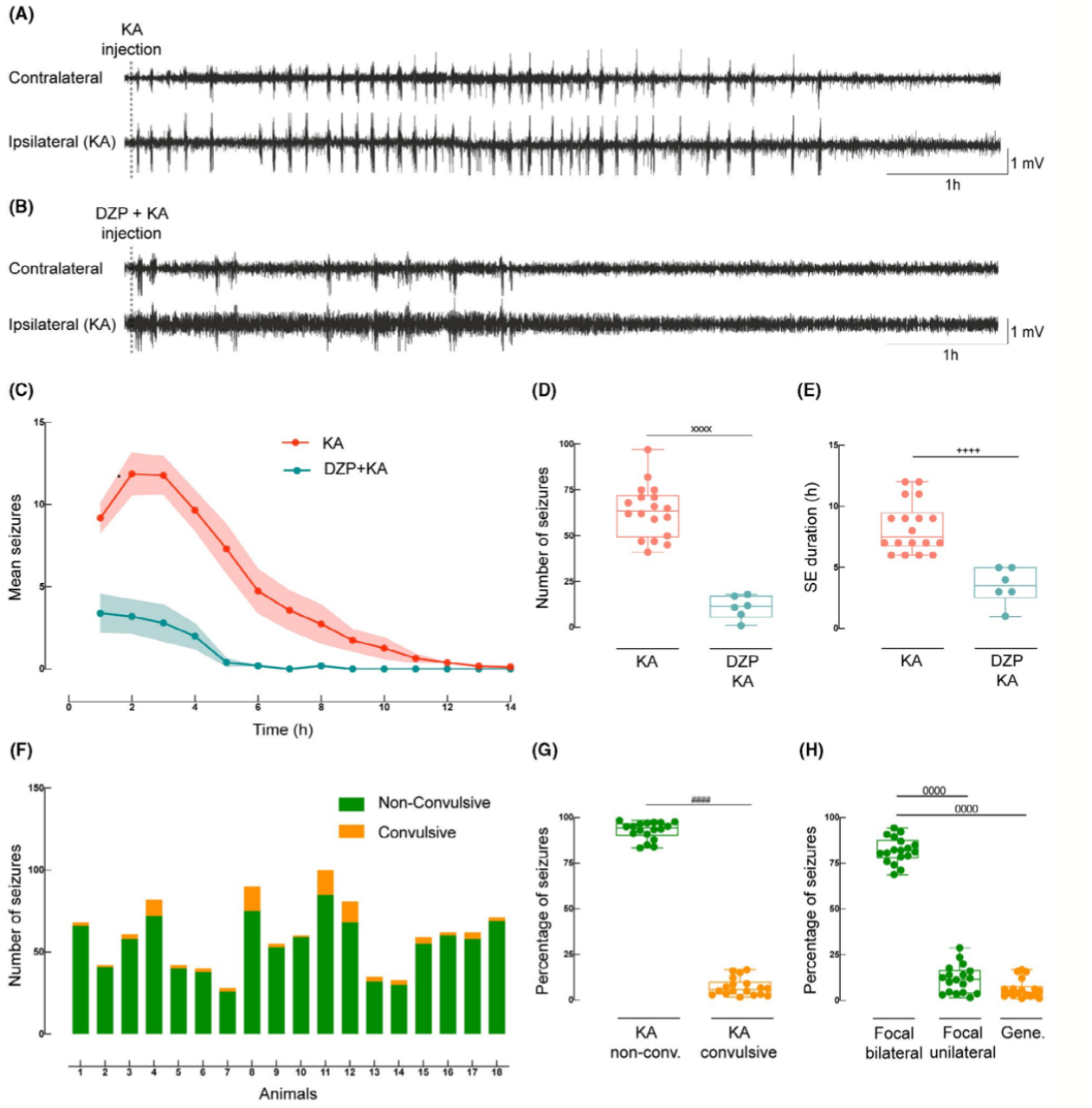

FIGURE 1 EEG and seizure features during the focal non convulsive *status epilepticus* induced by unilateral intrahippocampal KA injection in KA and diazepam +KA animals. EEG analysis was performed in 18 KA animals (9 processed 3 days after SE onset, and 9 chronic KA animals recorded/analysed in acute phase - n = 18) and in 6 DZP+KA animals (n = 6). (A) Compressed 7 h EEG recording from left (contralateral) and right [ipsilateral (KA)]) hippocampus after KA injection in the dorsal CA1 area of right hippocampus (vertical dotted line on both traces). (B) Compressed 7 h EEG recording from left (contralateral) and right [ipsilateral (KA)] hippocampus after intraperitoneal administration of diazepam (DZP) followed by intrahippocampal KA injection. (C) Mean seizures *per* hour after KA injection (red trace) and KA preceded by DZP (blue trace). (D) Number of seizures *per* animal treated with KA injection (red) *vs* DZP+KA (blue). (^{xxxx}): $p < 0.0001$ (unpaired *t*-test). (E) *Status epilepticus* duration in hours *per* animal after KA injection (red) *vs* DZP+KA (blue). ($^{++++}$): $p < 0.0001$ (Mann-Whitney U test). (F) Number of convulsive (yellow) and non-convulsive (green) seizures for each animal individually. (G) Percentage of seizures characterised by a convulsive (yellow) *vs* non-convulsive phenotype (green); one dot *per* column represents the same animal. ($^{\#\#\#\#}$): $p < 0.0001$ (Wilcoxon signed-rank test). (H) Percentage of seizures *per* animal defined as focal bilateral (green) *vs* focal unilateral (green) *vs* generalised (yellow). (^{0000}): $p < 0.0001$ (paired *t*-test)

assessed two weeks after implantation if the surgery procedure provoked any type of damage with densitometric analysis of NeuN, MAP2, GFAP and IgG in CA1, CA3 and DG of naïve animals (n = 5) *vs* sham-operated animals (n = 5). No statistical difference was found by comparing these two groups (Figure S1A–D); therefore, the sham group was used as our control condition throughout the study.

Densitometric measurements separately performed in the hippocampus ipsilateral (KA+seizures) and contralateral (seizures only) to the KA-injection were compared to their respective regions in sham-operated animals and DZP+KA (Figures 2B–C and 4B–C). As previously shown in a different group of animals [32], the densitometric values of NeuN and MAP2, 3 days post-KA, in the ipsilateral CA1, CA3 and DG (only NeuN) were lower with respect to the homologous subfields of sham-operated animals (Figure 2B–C, representative

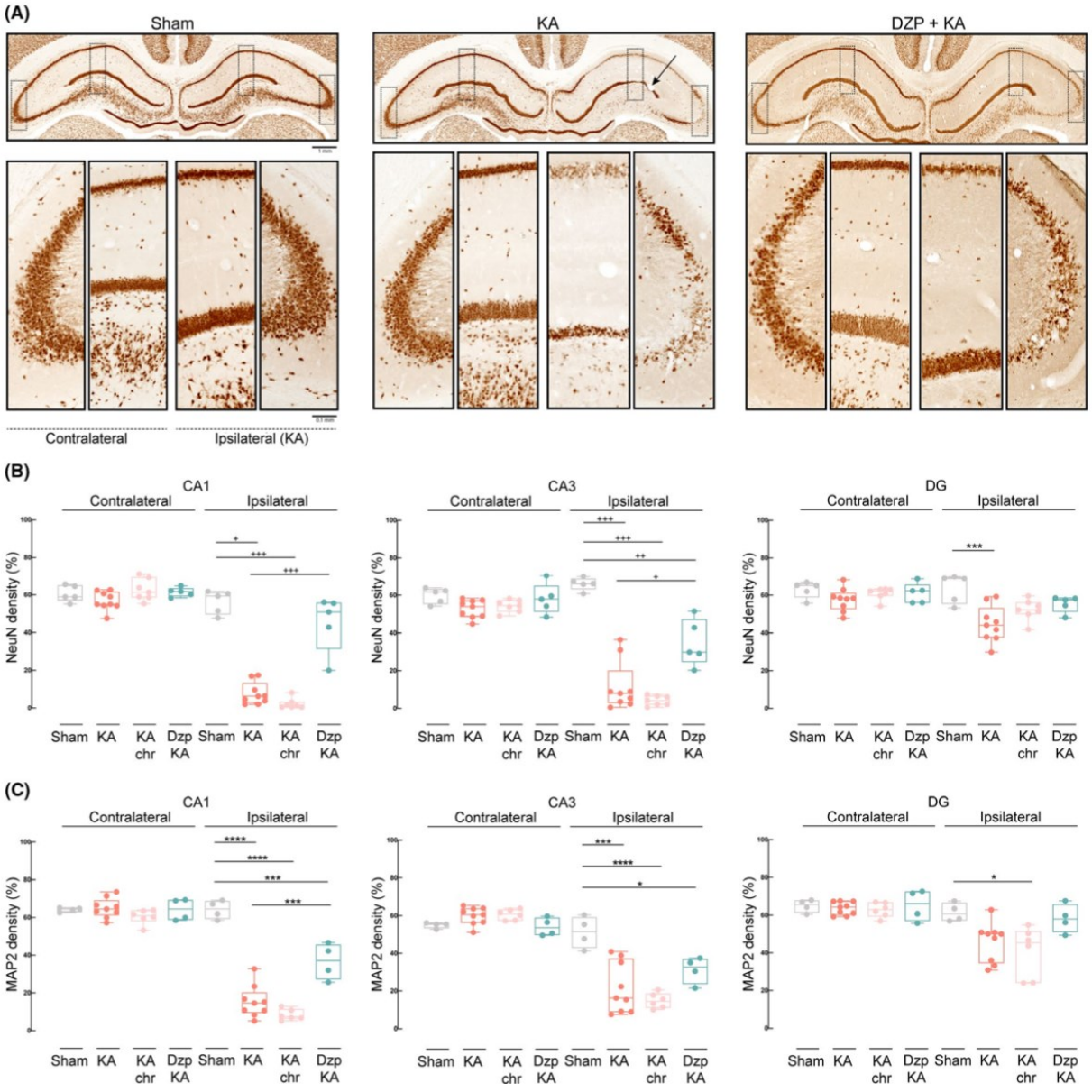

FIGURE 2 NeuN and MAP2 semi-quantitative densitometry analysis. (A) NeuN immunostained coronal sections represented at low (upper pictures) and high magnification (lower pictures; dotted area outlined in the upper photographs) for sham (left), KA (middle) and DZP+KA (right) animals 3 days post-KA. KA was injected in the right dorsal CA1 region (injection cannula artifact marked by arrowhead in the middle panel). Left and right hemispheres contralateral and ipsilateral to hippocampal KA injection, respectively, are illustrated. Calibration bars in higher magnification =0.1 mm and in lower magnification =1 mm. For B and C: Grey plots: sham-operated animals. Red plots: 3 days post-KA injection (KA). Pink plots: 1 month post-KA injection animals (KA chronic). Green plots: animals treated with DZP and KA injected (DZP+KA). Average percentage of densitometric changes in the KA-injected (ipsilateral) and contralateral hippocampal CA1 (left panels), CA3 (middle panels) and DG (right panels) subregions are illustrated. (B) NeuN densitometric values obtained from sham (n = 5), KA (n = 9), KA chronic (n = 7) and DZP+KA (n = 5) guinea pigs. ($^{+}$): $p < 0.05$; ($^{++}$): $p < 0.01$; ($^{+++}$): $p < 0.001$ (Mann-Whitney U test); (***): $p < 0.001$ [one-way analysis of variance (ANOVA)]. (C) MAP2 densitometric changes from the same areas of sham (n = 4), KA (n = 9), KA chronic (n = 6) and DZP+KA injection (n = 4) guinea pigs. (*): $p < 0.05$; (***): $p < 0.001$; (****): $p < 0.0001$ (ANOVA)

panels in Figure 2A). The neuronal loss in the KA-injected CA1, CA3 and DG observed in the acute phase remained in the KA chronic group, except for the DG when compared to the 3-days KA group (Figure 2B,C; Figure S1 E). Interestingly, densitometric NeuN and MAP2 values in the DZP+KA animal group (Figure 2B,C; also, right panel in Figure 2A) were higher than the 3 days KA group for all subfields and were similar to the sham-group for NeuN in CA1 and DG and for MAP2 in DG. Of note, in the DZP+KA groups the values in CA3 for NeuN and in CA1, CA3 for MAP2 were lower compared to the sham groups (Figure 2B,C). NeuN and MAP2 densitometric values did not differ in the contralateral hippocampi of both KA (at 3 days and 4 weeks) and DZP+KA animals when compared to their respective sham-controls (Figure 2B,C). In line with these findings, fluoro-jade positive cells (FJ^+) in the ipsilateral CA1, CA3 and DG were observed exclusively and consistently in the 3 days post-KA injection and DZP+KA groups (Figure 3B, also representative panel 3A). FJ^+ cells were never detected either 4 weeks post-KA or the hippocampus contralateral to KA injection in any group (Figure 3B). NeuN, MAP2, GFAP and IgG staining patterns were identical when the four animals that featured >10 convulsive seizures were excluded from the densitometric analysis and also when data from those four animals were compared against the remaining five animals from the same group that experienced only focal seizures (Figure S2).

Next, we investigated astrocytic activation in the same animal groups. As illustrated in Figure 4A astrogliosis was induced by KA injection. The densitometric values were higher in all subfields ipsilateral to KA injection at 3 days post-FncSE when compared to the sham-group (Figure 4B; also, middle column in Figure 4A). High GFAP immuno-density was maintained in CA1 and DG of the KA chronic group (Figure 4B; also, right column in Figure S1E). DZP+KA

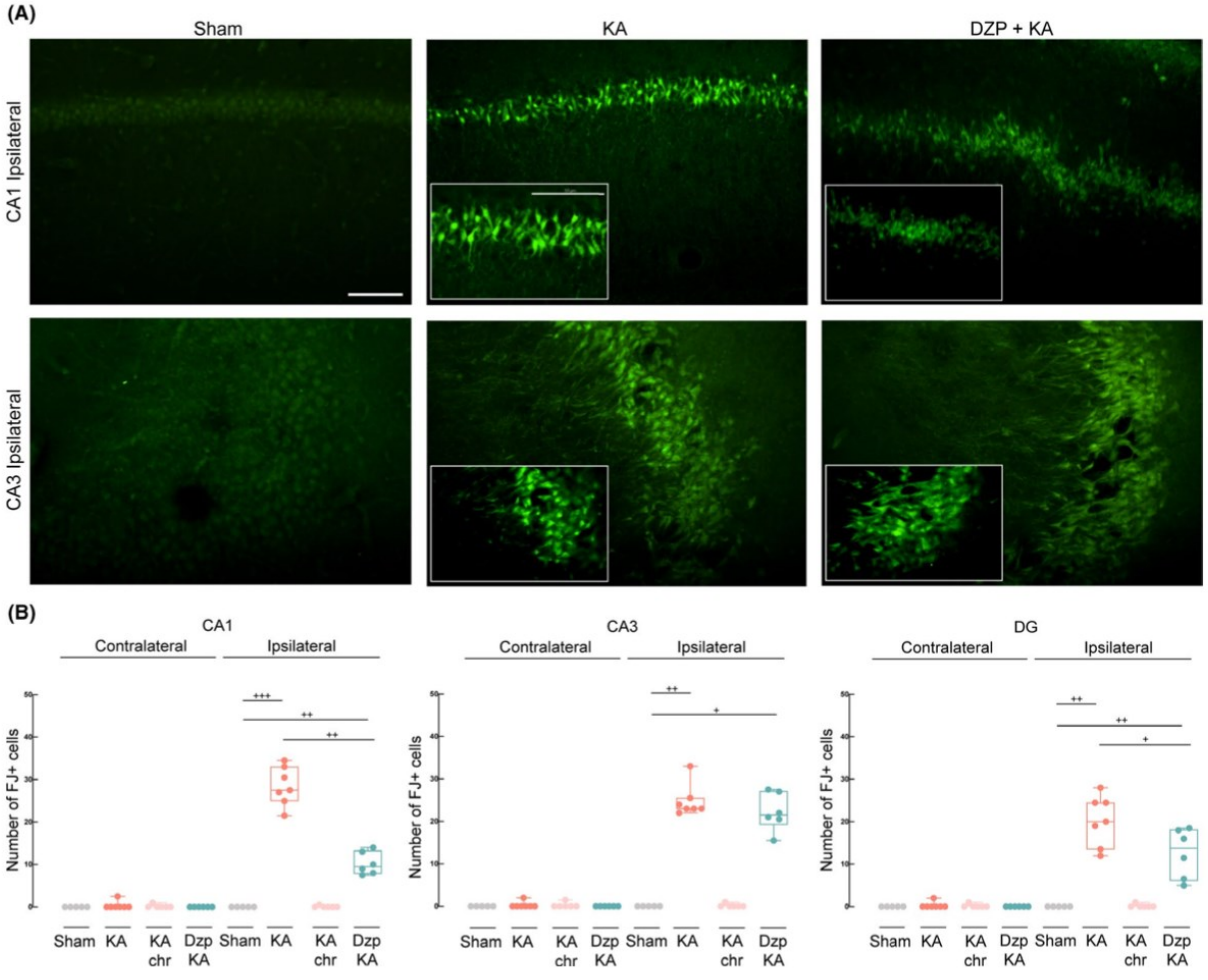

FIGURE 3 Fluoro-jade immunostaining and quantification in CA1, CA3 and DG subregions. (A) Representative micrographs of CA1 (upper part) and CA3 (lower part) subregions in the right hippocampi ipsilateral to the injection of sham-operated (left column), 3 day post-KA injection (middle column) and DZP+KA injection (right column) guinea pigs. Higher magnification photos are illustrated in the inserts. Calibration bars at higher magnification =50 μm and at lower magnification =100 μm. (B) Comparison between number of fluoro-jade$^+$ cells in the KA injected (ipsilateral) and contralateral hippocampal subregions. In all graphics, grey, red, pink and green plots show counts from sham (n = 5), KA 3 days after FncSE (n = 7), chronic KA (n = 6) and DZP+KA (n = 6) guinea pigs, respectively. ($^+$): $p < 0.05$; ($^{++}$): $p < 0.01$; ($^{+++}$): $p < 0.001$ (Mann-Whitney U test)

treated animals had the same high densitometric profile of the 3 days post-KA injected guinea pigs (Figure 4B, also right column in Figure 4A). Unlike previously noted [32], higher GFAP densitometry values were also observed in the contralateral hippocampus of both KA (CA1, CA3 and DG; Figure 4B) and DZP+KA animals (CA3 and DG; Figure 4B) in comparison to sham-operated animals. Control

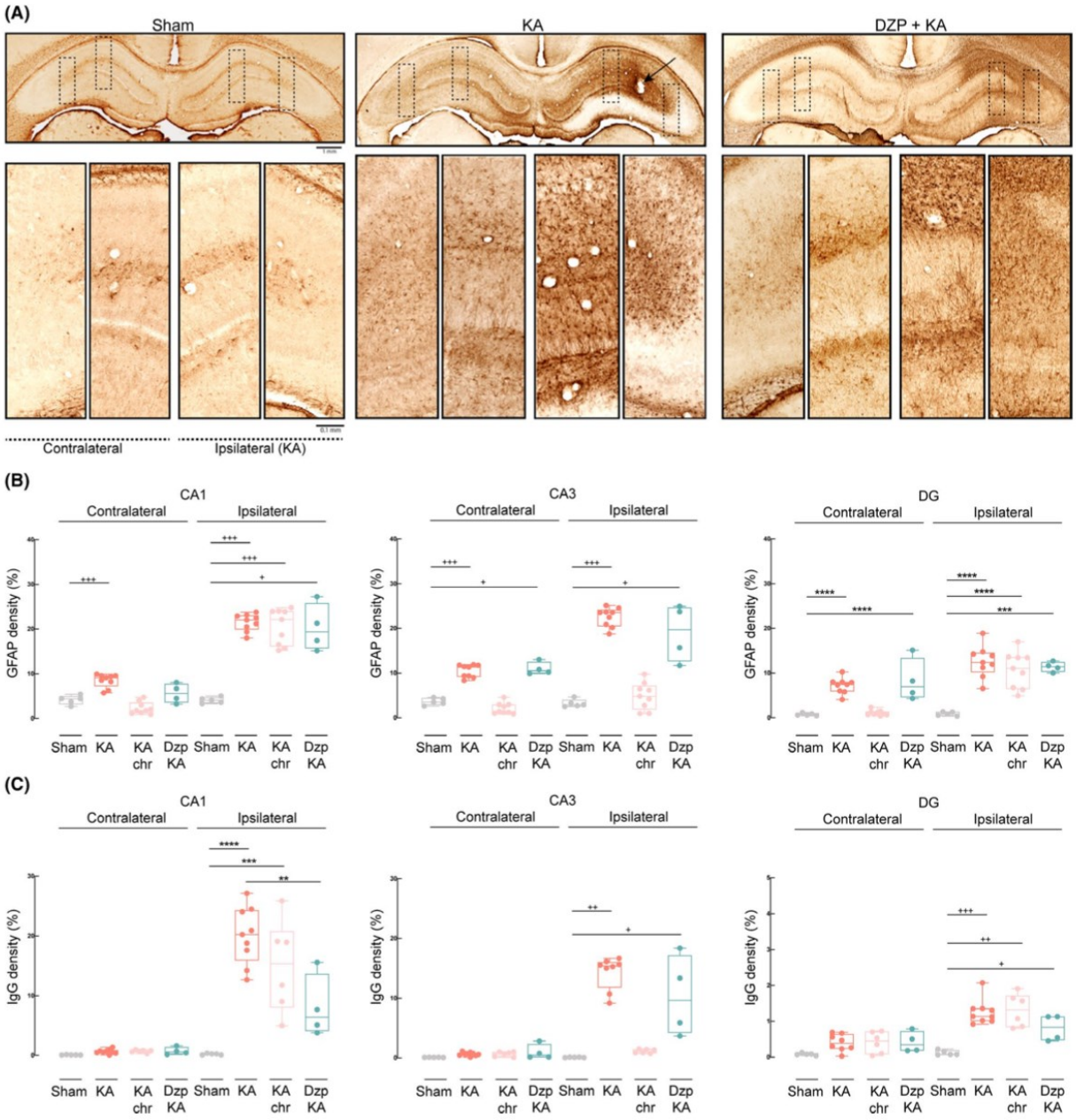

FIGURE 4 GFAP and IgG semi-quantitative densitometry analysis. (A) GFAP immunostained coronal sections are represented at low (upper pictures) and high magnification (lower pictures; dotted area outlined in the upper photographs) for sham (left panel), KA (middle panel) and DZP+KA (right panel) animals 3 days post-KA. Left and right hemispheres are marked as contralateral and ipsilateral (KA) respectively. Arrows mark in the upper middle panel points to the track of the intrahippocampal injection needle. Calibration bars in higher magnification =0.1 mm and in lower magnification =1 mm. (B and C): Average percentage of densitometric changes in the KA injected (ipsilateral) and contralateral hippocampal CA1, CA3 and DG subregions. Grey plots: sham-operated animals. Red plots: 3 days post-KA injection guinea pigs (KA). Pink plots: 1 month post-KA injection animals (KA chronic). Green plots: animals treated with DZP and KA injected (DZP+KA). (B) GFAP densitometric changes from sham (n = 5), KA (n = 9), KA chronic (n = 9) and DZP+KA (n = 4) guinea pigs. ($^{+}$): $p < 0.05$; ($^{+++}$): $p < 0.001$ (Mann-Whitney U test); (***): $p < 0.001$; (****): $p < 0.0001$ (ANOVA). (C) Average percentage of densitometric IgG staining in sham (n = 5), KA (n = 9), KA chronic (n = 6) and DZP+KA (n = 4) guinea pigs. ($^{+}$): $p < 0.05$; ($^{++}$): $p < 0.01$; ($^{+++}$): $p < 0.001$ (Mann-Whitney U test); (**): $p < 0.01$; (***): $p < 0.001$; (****): $p < 0.0001$ (ANOVA)

values were observed in contralateral hippocampi 4 weeks after KA (Figure 4B; see also right panel in Figure S1E).

Finally, we observed higher IgG densitometry values in the ipsilateral hippocampus 3 days post-KA injection in all regions compared to the sham group (Figure 4C); these values were similar in CA1 and DG 4 weeks post-KA injection (Figure 4C). Furthermore, in the DZP+KA group, CA3 and DG values were higher than the sham guinea pigs (Figure 4C). IgG staining was never observed in the contralateral hippocampus (Figure 4C). Overall, these data suggest that KA induced a local increase in BBB permeability [38] exclusively in the KA-injected hippocampus.

To further evaluate glial involvement in KA-induced FncSE, we also investigated with Iba-1 immunofluorescence, the morphological changes of microglia cells in the hippocampi ipsilateral and contralateral to KA injection (Figure 5A and F). Sholl analysis employed to quantify the number of intersections at radial intervals of 2 μm starting from the soma (Figure 5B–E) showed smaller values in the ipsi- (CA1 and DG) and contralateral (CA1) hippocampi of KA

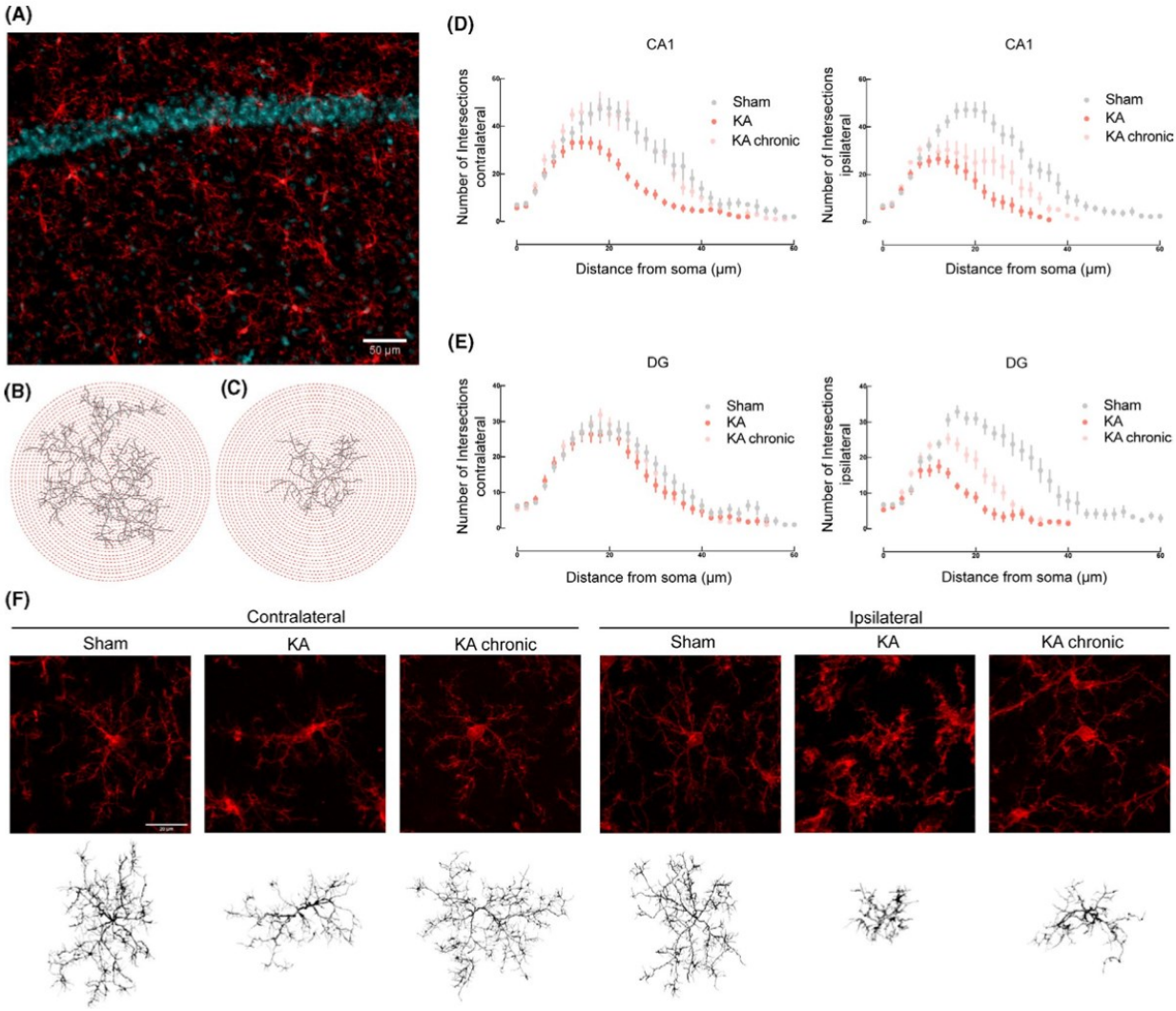

FIGURE 5 Morphological analysis and reconstruction of microglial cells in hippocampal CA1 and DG. (A) Representative immunofluorescence of a hippocampal coronal section of CA1 pyramidal layer: neurons marked by DAPI in blue, microglia stained by Iba-1 in red. Calibration bar =50 μm. (B) Representative Sholl analysis setting of a manually reconstructed microglia cell from a KA animal (contralateral hippocampus) and (C) from the ipsilateral hippocampus of the same animal. The circles centred around the soma are separated by radial intervals of 2 μm. (D) Number of intersections *per* 2 μm radius plotted against the distance from the cell soma in the contralateral (left) and ipsilateral (right) CA1 hippocampal region. Grey line: sham-operated animals. Red line: 3 days post-KA injection (KA). Pink line: 1 month post-KA injection (KA chronic). (E) Number of intersections *per* 2 μm radial steps in the contralateral (left) and ipsilateral (right) DG region. (F) Representative morphologies of microglial cells in Iba-1 immunofluorescence coronal sections in the CA1 hippocampal regions are shown for sham, KA and KA chronic animals.; the correspondent reconstruction of the microglial cell is illustrated in the lower part of the panel. Left and right (KA-injected) hippocampus are marked by contralateral and ipsilateral, respectively. Calibration bar = 20 μm

animals compared to sham animals (Figure 5D–E). In chronic KA animals, Sholl analysis confirmed microglia morphological changes in the KA-injected ipsilateral hippocampi, whereas values similar to sham condition were found in the contralateral hippocampus (Figure 5D–E). As expected, microglial cells had a lower number of processes (Figure 6A I and B I), total length (Figure 6 A II and B II) and average intersections (Figure 6 A III and B III) at 3 days post-KA in the ipsilateral CA1 and DG in comparison to sham-animals (see also Figure 5F). A similar profile was obtained in the contralateral hippocampi 3-days post KA (Figure 6AI–III and B I–II), except for the DG number of intersections (Figure 6 B III). Interestingly, while in the ipsilateral hippocampus these changes were maintained over time (except average intersections in CA1 - compare the KA chronic groups with the matched sham-groups; in Figure 6A I and II and B I-III), in the contralateral hippocampus of KA chronic animals, all parameters were similar to the respective sham-animals (Figure 6A I–III and B I-III). These experiments show a transient and possibly reversible glial activation pattern, coupled with no apparent cell loss in the hippocampi, contralateral to the KA injection.

We complemented the morphological analysis with the study of gene expression (through mRNA relative expression) in CA1 and DG using quantitative real-time PCR (Figure 7). First, we measured mRNA expression of pro-inflammatory genes, IL1-β and COX-2 (Figure 7A,B, respectively). In line with the densitometry analysis, we observed a higher expression of both genes in the ipsilateral CA1, 3 days post-FncSE with respect to their sham-operated animals; expression was also higher in DG, with statistical significance only for COX-2 (Figure 7B). At one-month post-KA injection, these genes were no longer upregulated. In the contralateral hippocampus, the expression of the aforementioned genes was similar in all groups (Figure 7A,B). Stress-induced gene HO-1 and activity-dependent c-Fos expression were upregulated in the ipsilateral side 3 days post-KA injection compared to sham in CA1 and DG (Figure 7C,D). mRNA expression did not change in the KA chronic group in the ipsilateral side and in all contralateral side groups compared to the respective sham-operated groups (Figure 7C,D). AQP4 expression was higher than in sham animals in the ipsilateral DG at 3 days post-KA injection, but not in KA chronic animals (Figure 7E). Interestingly, higher expression of AQP4 in CA1 and

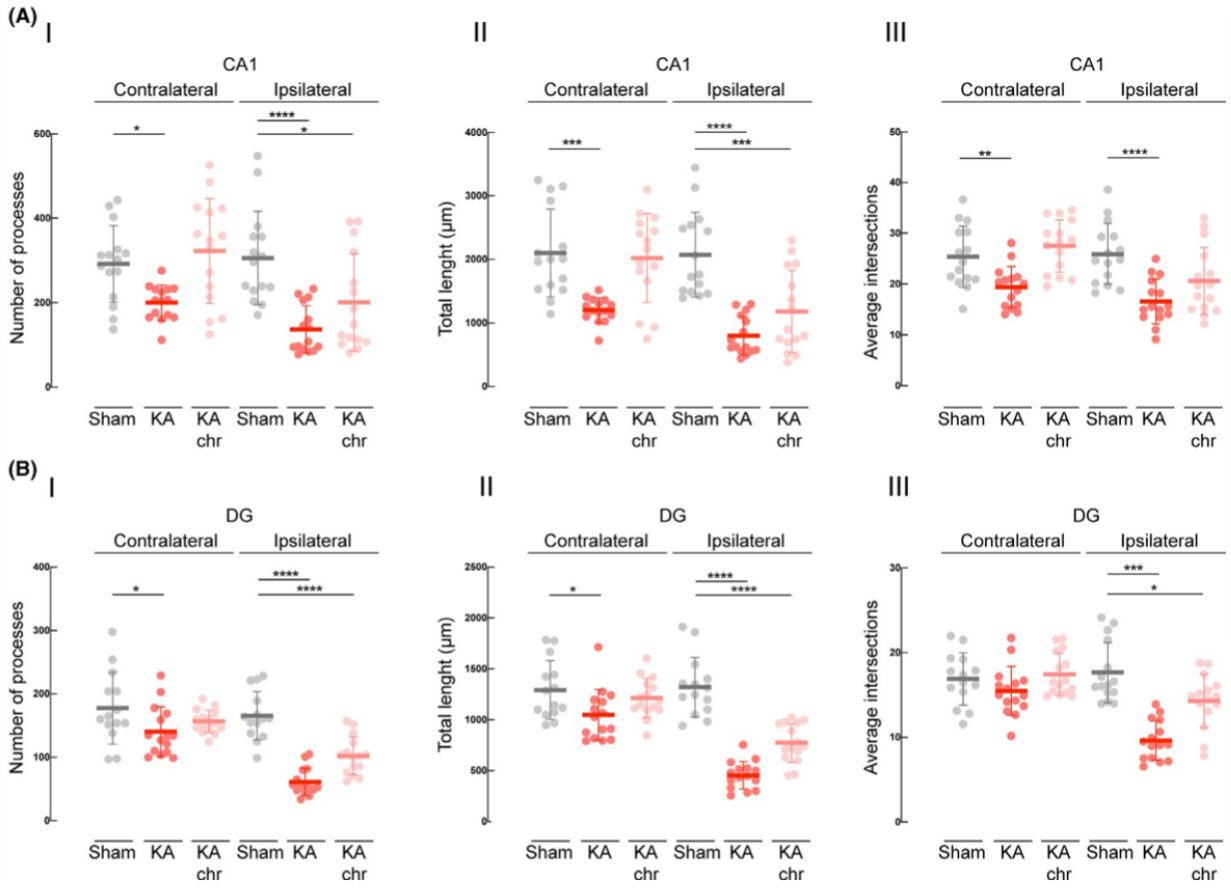

FIGURE 6 Comparative analysis of microglial three dimensional morphology based on Sholl analysis. Grey plots: sham-operated animals. Red plots: 3 days post-KA injection guinea pigs (KA). Pink plots: 1 month post-KA injection animals (KA chronic). (A) Number of processes *per* 2 μm radius (A I), total length (A II) and average number of intersections (A III) of microglia cells in CA1 hippocampal formation from sham (n = 15 cells), KA (n = 15 cells) and KA chronic (n = 15 cells) guinea pigs (3 cells *per* animal). (*): $p < 0.05$; (**): $p < 0.01$; (***): $p < 0.001$; (****): $p < 0.0001$ (ANOVA). (B) Number of processes *per* 2 μm radius (B I), total length (B II) and average number of intersections (B III) of microglia cells in DG from sham (n = 15 cells), KA (n = 15 cells) and KA chronic (n = 15 cells) animals (3 cells *per* animal). (*): $p < 0.05$; (***): $p < 0.001$; (****): $p < 0.0001$ (ANOVA)

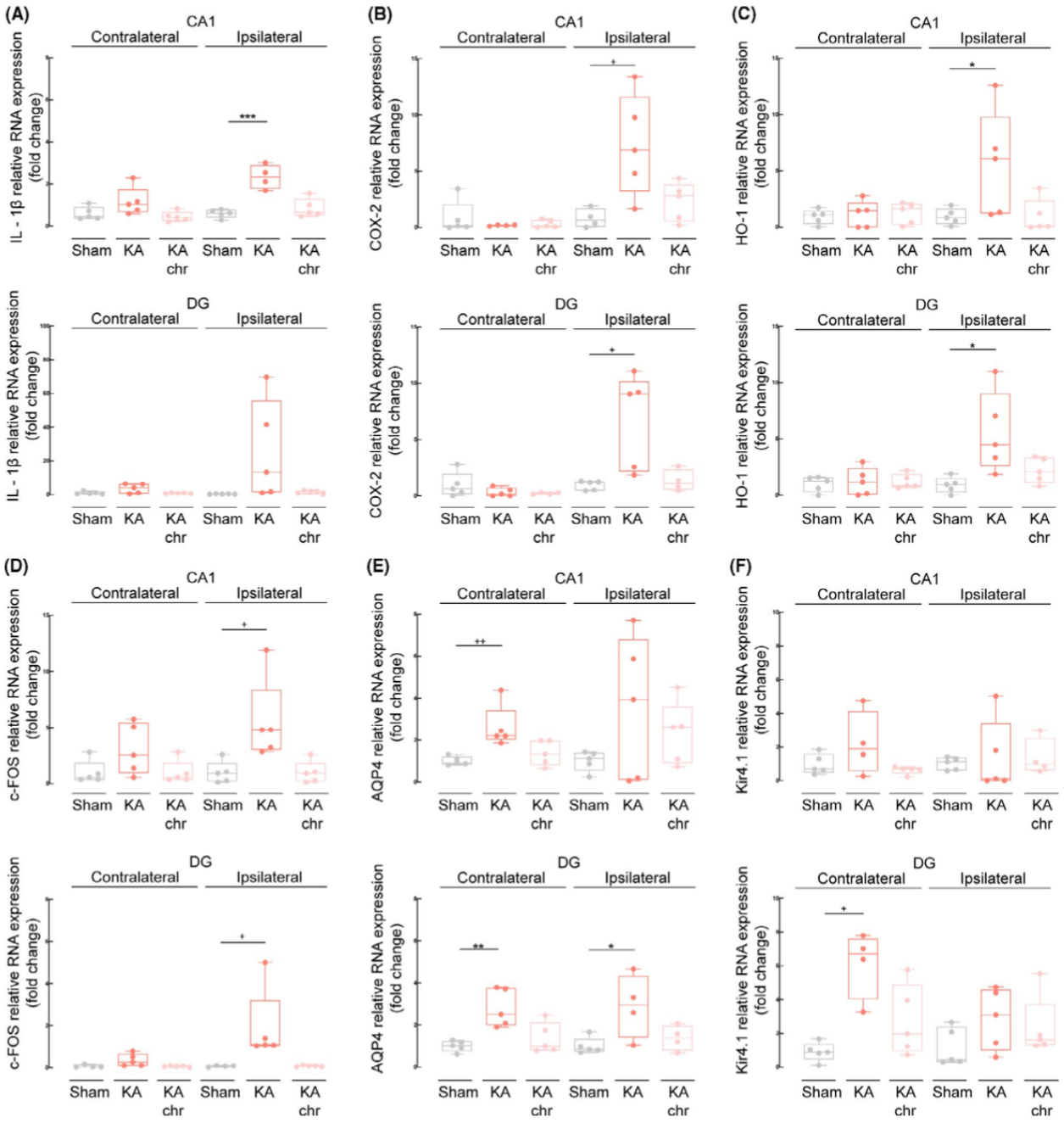

FIGURE 7 Quantitative real-time PCR gene expression analysis of IL-1β, COX-2, HO-1, c-Fos, AQP4 and Kir4.1 genes. Grey plots: sham-operated animals. Red plots: 3 days post-KA injection guinea pigs (KA). Pink plots: 1 month post-KA injection animals (KA chronic). Average relative mRNA expression (fold change) in the hippocampal CA1 and DG subregions ipsi- and contralateral to KA injection are represented. The mean value of five animals for each of the three groups is reported, unless indicated. All values were normalised to housekeeping genes (Actin and GADPH) as well as to their respective sham-operated animal groups. (A) IL-1β RNA expression obtained from sham, KA and KA chronic guinea pigs in CA1 (upper graphic) and DG (lower graphic). (***): $p < 0.001$ (ANOVA). (B) COX-2 mRNA expression levels obtained from the same areas of sham ($n = 4–5$), KA and KA chronic ($n = 4–5$) guinea pigs in CA1 (upper graphic) and DG (lower graphic). ($^{+}$): $p < 0.05$ (Mann-Whitney U test). (C) HO-1 RNA expression levels obtained from the same areas of sham, KA and KA chronic guinea pigs in CA1 (upper graphic) and DG (lower graphic). (*): $p < 0.05$ (ANOVA). (D) c-FOS mRNA expression levels obtained from the same areas of sham, KA and KA chronic guinea pigs in CA1 (upper graphic) and DG (lower graphic). ($^{+}$): $p < 0.05$ (Mann-Whitney U test). (E) AQP4 mRNA expression levels obtained from the same areas of sham, KA and KA chronic($n = 4–5$) guinea pigs in CA1 (upper graphic) and DG (lower graphic). ($^{++}$): $p < 0.01$ (Mann-Whitney U test); (*): $p < 0.05$; (**): $p < 0.01$ (ANOVA). (F) Kir4.1 mRNA expression levels obtained from the same areas of sham, KA and KA chronic ($n = 4–5$) guinea pigs in CA1 (upper graphic) and DG (lower graphic). ($^{+}$): $p < 0.05$ (Mann-Whitney U test)

DG and Kir4.1 in DG was observed in the contralateral hippocampus as compared to the sham animals (Figure 7E,F), suggesting a seizure activity-mediated upregulation of both genes selectively expressed in astrocytes [39]. These acute changes reverted to sham values in KA chronic animals (Figure 7E,F).

DISCUSSION

The present study analyses a model of FncSE that mimics one of the most frequent and often unrecognised types of human SE. Our results uphold the concept that focal seizures recorded during the course of FncSE have no detrimental effect on the brain unless they are paired with the local excitotoxic effect of KA. Most animal studies that use localised intracerebral KA injection report focal secondarily generalised seizures [20, 21, 40]. The presence of prominent convulsive generalised seizures in these studies is a major confounder for the evaluation of tissue pathology, since convulsive seizures have been demonstrated to promote brain damage via complex generalised and systemic pathogenic mechanisms (for reviews, see [1, 2]).

Our protocol induced a primary epileptogenic area in the hippocampus injected with the KA; within a minute epileptiform activity propagated to the contralateral hippocampus. In this remote secondary region, seizure activity during FncSE was not associated with any underlying damaging event. For the data to be as coherent as possible, all animals included in this study developed a FncSE with focal non-convulsive seizures entraining both hippocampi; focal seizures could secondarily evolve in diffusely propagated epileptiform discharges that correlated with a generated convulsive behaviour (see also [32, 34]). With the exception of 4 animals that presented 10 to 15 secondarily seizures during FncSE, the number of brief (<30 s) convulsive seizures in our experimental group was minimal (1–3 *per* animal, as illustrated in Figure 1F).

In our model the treatment with DZP reduced both the number of seizures during FncSE and FncSE duration itself; these findings correlated with a much-reduced extension of brain damage in the hippocampus ipsilateral to KA injection, as demonstrated by the density of NeuN, MAP2, GFAP, IgG and FJ staining. Even though a direct effect of DZP in reducing the time spent in seizures should also be considered, the less intense cell loss and gliosis observed in DZP-treated animals strongly suggest that the KA-induced damage is partially due to the direct excitotoxic action of KA at the injection site. The larger and more intense distribution of damage markers in the KA-injected hippocampus in the absence of DZP supports the concept that seizure discharges during FncSE are able to exacerbate the KA-induced hippocampal damage. These findings are in line with other studies on focal secondarily generalised seizures induced by local intracerebral KA injections that reported reduced local brain damage at the site of injection when DZP was administrated after SE [20, 41, 42]. Our study is the first, to our knowledge, to demonstrate that DZP treatment dramatically reduces focal non-convulsive seizures during FncSE; these changes correlate with reduced damage at the KA injection site.

We analysed neuronal loss by both NeuN and FJ staining that label irreversibly damaged neurons [43] and by MAP2 immunostaining that has been shown to concentrate in neuronal somata during reversible neuronal suffering [44]. Our results showed a consistent and recurrent cell loss and neuronal stress in the ipsilateral hippocampus in KA acute and chronic animals, with no correspondent neuronal loss in the contralateral hippocampus. The FJ results revealed ipsilateral cell loss in the 3 days KA group, with no positive cells observed in the KA chronic group, suggesting that the bulk of apoptotic neurons were produced early after FncSE. Similar findings were published by our group in the same animal model using TUNEL assay that specifically targets DNA-fragmented neurons [32]. Notably, FJ^+ were not observed in remote brain regions (contralateral hippocampus), where focal seizures during FncSE were also generated. These data are in line with the finding that seizures, after an initial epileptogenic insult, do not lead to progressive cell loss [45]. Moreover, a lack of clear association between the number of lifetime seizures and the severity of neuronal loss in the hilus was shown in a long follow-up study extended 8 months after SE [46, 47]. Similar conclusions were also reported in post-surgical tissue obtained from patients with focal epilepsy submitted to surgery [48]. Nevertheless, there are also several animal studies showing clear progressive neuronal loss produced by seizures not only in the local site of KA injection, but also in remote regions [20, 21, 49]. This discrepancy might be due to the use of protocols that induce a convulsive SE condition rather than a FncSE. In models of proper FncSE developed in different animal species, indeed, remote damage in the hippocampus contralateral to KA injection was never explicitly reported [18, 19, 22–24,50]. We cannot exclude that stronger and more intense seizure activity could induce secondary damage in remote regions, even though in our experiments, no difference in the extent of damage in both ipsi- and contralateral hippocampi was found in those animals that experienced secondary convulsive seizures during FncSE compared to those with focal seizure only.

The possibility that immunohistochemical changes were not sensitive enough to detect minor changes in regions remote to FncSE was considered and analysed by evaluating gene expression levels in acute and chronic post-SE animals. These experiments revealed that genes associated with inflammatory response (IL1-β and COX-2), brain activity (c-FOS) and oxidative stress (HO-1) were upregulated exclusively in the KA-ipsilateral hippocampus early during the acute phase, whereas only genes linked to glial function (AQP4 and Kir4.1) were upregulated 3 days post-KA (but not after 1 month) in the contralateral hippocampus. Glial cells have a plethora of multitasking housekeeping functions such as sensing and responding to alterations in energy supply, neuronal activity, extracellular ion concentrations, osmolarity and many other signals. Their dysfunction has been associated with epilepsy mainly through hyperexcitability and inflammatory-related processes (for extensive reviews see [51, 52]). As observed in other FncSE studies [18,22,23,32], astro- and micro-gliosis in the injected hippocampus was also confirmed in our model. Here, astro- and microgliosis, BBB disruption and

upregulation of inflammatory genes IL1-β and COX-2, as well as stress-related genes c-FOS and HO-1 were evident and persisted 1 month after FncSE in some areas. In contrast, a mild astrocytic and microglial activation was detected in the contralateral hippocampus only at 3 days post-KA with GFAP densitometry analysis and Iba-1 morphological reconstructions. As mentioned above, gliosis was coupled with upregulation of specific astrocytic genes AQP4 and Kir4.1 without overexpression of pro-inflammatory, activity-related or oxidative stress-related genes. Furthermore, 1 month post-KA injection, these alterations returned to basal expression levels comparable to sham-operated animals. A short-lived contralateral microgliosis was also reported, with a significant reduction of microglia complexity, number of processes and total length in CA1 and DG in the acute phase, but not in chronic animals. Overall, these results point towards a possible transient effect mediated by seizure activity on glial cells. Our data do not specifically show, however, if the same cells reverted to their inactivated state or if only the resting/inactivated glial cells remained 1 month after FncSE. Interestingly, these transient effects correlated with the absence of contralateral neuronal loss or BBB leakage. These findings suggest a possible early protective role promoted by glial cells in the hippocampus contralateral to KA injection; the astrocyte-specific expression of AQP4 and Kir4.1 might enhance neuronal potassium clearing during seizure activity. Since both extracellular K^+ concentration and osmolarity have been shown to dramatically modulate neural excitability [53–56], it is plausible to speculate that astrocytes increase AQP4 and Kir4.1 gene expression as a first line of defence to counter-balance the potential nefarious effect of seizure activity, hence reducing the hyperexcitability through the glial-network. It is unclear however if this compensatory gene upregulation is accompanied by a translation into functional proteins, and further studies are required to address this issue. Nevertheless, studies have shown that a dysfunction of astroglial Kir4.1 channels underlies impaired K^+ buffering and contributes to hyperexcitability in epileptic tissue [56]. Moreover AQP4$^{-/-}$ mice have remarkably slowed K^+ reuptake in seizure models and were associated with increased seizure duration, supporting the hypothesis that AQP4 and Kir4.1 can act together in K^+ and H_2O regulation [54]. In line with our findings, an acute reactive astrogliosis and microgliosis that decreased over time in the contralateral hippocampus but remained altered in the KA-injected hippocampus was reported in an unilateral intrahippocampal KA mouse model [24]. This study reported a delayed upregulation in the contralateral hippocampus of SOCS3, which acts by limiting IL-6 mediated processes, possibly indicating an attempt to limit the intensity/duration of neuroinflammatory signals during the early phase of epileptogenesis. The authors hypothesised that the SOCS3 mRNA increase could be involved in neuronal survival and/or induction of homeostatic mechanisms against neurodegeneration by limiting cytokine signalling in the contralateral hippocampus.

In conclusion, in our FncSE model brain tissue damage is aggravated by seizure activity when it occurs in combination with the excitotoxic effect of KA. The secondary spread of seizure activity to the contralateral hippocampus transiently activated glial cells, as a potential defence mechanism that prevented remote seizure-associated damage. These results might only hold true for this particular dosage of KA and/or for the specific seizure-FncSE pattern generated in this animal model. Even though the experimental findings here reported cannot directly be translated into clinical conclusions, our study recommends the use of anti-seizure treatment in patients suffering from FncSE to prevent further localised seizure-mediated damage in addition to the injury determined by the primary *noxa*. When combined with a coexisting insult, seizures can work synergistically to further exacerbate the damage done by the underlying FncSE cause. However, if seizure activity spreads to regions away from the boundaries of the primary injury constraint, a detrimental action caused by seizures *per se* is not likely to occur.

ACKNOWLEDGMENTS

None of the authors has any conflict of interest to disclose. We confirm that we have read the Journal's position on issues involved in ethical publication and affirm that this report is consistent with those guidelines. This work was supported by: the European Union's Horizon 2020 Research and Innovation Programme under the Marie Sklodowska-Curie grant agreement no. 722053 (EU-GliaPhD; DVV, TSZ, EA, MC) and agreement no. 765966 (EpiSyStem; MFP, GT), the Italian Health Ministry (Ricerca Corrente 2018-2020) and the EPICARE project of the Associazione Paolo Zorzi per le Neuroscienze.

AUTHOR CONTRIBUTIONS

DVV, MdC, EA and EV contributed to conception and design of the study. DVV, TZ, AC, MFP, GT and VG contributed to acquisition and analysis of data.. DVV and MdC contributed to drafting a significant portion of the manuscript or figures.

Our experimental protocol has been ethically reviewed and approved by the Animal Welfare Office of the Italian Health Ministry (Authorization n. 36/2016-PR), in accordance with the European Committee Council Directive (2010/63/EU) and with the 3Rs principle.

PEER REVIEW

The peer review history for this article is available at https://publons.com/publon/10.1111/nan.12693.

DATA AVAILABILITY STATEMENT

The data that support the findings of this study are available from the corresponding author upon reasonable request.

ORCID

Diogo Vila Verde https://orcid.org/0000-0003-3084-6552
Marlene F. Pereira https://orcid.org/0000-0002-8890-2994
Erwin van Vliet https://orcid.org/0000-0001-5747-3202
Marco de Curtis https://orcid.org/0000-0001-7443-6737

REFERENCES

1. Wasterlain CG, Fujikawa DG, Penix LR, Sankar R. Pathophysiological mechanisms of brain damage from status epilepticus. *Epilepsia*. 1993;34:37-53.
2. Shorvon S. Does convulsive status epilepticus (SE) result in cerebral damage or affect the course of epilepsy - the epidemiological and clinical evidence? *Prog Brain Res*. 2002;135:85-93.
3. Young GB, Claassen J. Nonconvulsive status epilepticus and brain damage: Further evidence, more questions. *Neurology*. 2010;75:760-770.
4. Claassen J, Mayer SA, Kowalski RG, Emerson RG, Hirsch LJ. Detection of electrographic seizures with continuous EEG monitoring in critically ill patients. *Neurology*. 2004;62:1743-1748.
5. Trinka E, Cock H, Hesdorffer D, et al. A definition and classification of status epilepticus - report of the ILAE Task Force on Classification of Status Epilepticus. *Epilepsia*. 2015;56:1515-1523.
6. Rabinowicz AL, Correale JD, Bracht KA, Smith TD, DeGiorgio CM. Neuron-specific enolase is increased after nonconvulsive status epilepticus. *Epilepsia*. 1995;36:475-479.
7. Cockerell OC, Walker MC, Sander JWAS, Shorvon SD. Complex partial status epilepticus: a recurrent problem. *J Neurol Neurosurg Psychiatry*. 1994;57:835-837.
8. Guberman A, Cantu-Reyna G, Stuss D, Broughton R. Nonconvulsive generalized status epilepticus: clinical features, neuropsychological testing, and long-term follow-up. *Neurology*. 1986;36:1284-1291.
9. Kaplan PW. No, some types of nonconvulsive status epilepticus cause little permanent neurolooic sequelae (or: « The cure may be worse than the disease »). *Neurophysiol Clin*. 2000;30:377-382.
10. Gutierrez C, Chen M, Feng L, Tummala S. Non-convulsive seizures in the encephalopathic critically ill cancer patient does not necessarily portend a poor prognosis. *J Intensive Care*. 2019;7:1-9.
11. Sperk G. Kainic acid seizures in the rat. *Prog Neurogibol*. 1994;42:1-32.
12. Curia G, Longo D, Biagini G, Jones RSG, Avoli M. The pilocarpine model of temporal lobe epilepsy. *J Neurosci Methods*. 2008;172:143-157.
13. Lévesque M, Avoli M. The kainic acid model of temporal lobe epilepsy. *Neurosci Biobehav Rev*. 2013;37:2887-2899.
14. Sloviter RS. Hippocampal epileptogenesis in animal models of mesial temporal lobe epilepsy with hippocampal sclerosis: the importance of the "latent period" and other concepts. *Epilepsia*. 2008;49:85-92.
15. Henshall DC. Poststatus epilepticus models: focal kainic acid. In: Pitkänen A, Galanopoulou AS, Buckmaster PS, Moshé SL, eds. *Models of Seizures and Epilepsy*. 2nd ed. Cambridge, MA, USA: Academic Press. 2017:611-624.
16. Riban V, Bouilleret V, Pham-Lê BT, Fritschy JM, Marescaux C, Depaulis A. Evolution of hippocampal epileptic activity during the development of hippocampal sclerosis in a mouse model of temporal lobe epilepsy. *Neuroscience*. 2002;112:101-111.
17. Arabadzisz D, Antal K, Parpan F, Emri Z, Fritschy JM. Epileptogenesis and chronic seizures in a mouse model of temporal lobe epilepsy are associated with distinct EEG patterns and selective neurochemical alterations in the contralateral hippocampus. *Exp Neurol*. 2005;194:76-90.
18. Bouilleret V, Ridoux V, Depaulis A, et al. Recurrent seizures and hippocampal sclerosis following intrahippocampal kainate injection in adult mice: electroencephalography, histopathology and synaptic reorganization similar to mesial temporal lobe epilepsy. *Neuroscience*. 1999;89:717-729.
19. Tanaka T, Tanaka S, Fujita T, et al. Experimental complex partial seizures induced by a microinjection of kainic acid into limbic structures. *Prog Neurogibol*. 1992;38:317-334.
20. Ben-Ari Y, Tremblay E, Ottersen OP, Meldrum BS. The role of epileptic activity in hippocampal and "remote" cerebral lesions induced by kainic acid. *Brain Res*. 1980;5:515-518.
21. Schwob JE, Fuller T, Price JL, Olney JW. Widespread patterns of neuronal damage following systemic or intracerebral injections of kainic acid: a histological study. *Neuroscience*. 1980;5:991-1014.
22. Mouri G, Jimenez-Mateos E, Engel T, et al. Unilateral hippocampal CA3-predominant damage and short latency epileptogenesis after intra-amygdala microinjection of kainic acid in mice. *Brain Res*. 2008;1213:140-151.
23. Bedner P, Dupper A, Hüttmann K, et al. Astrocyte uncoupling as a cause of human temporal lobe epilepsy. *Brain*. 2015;138:1208-1222.
24. Pernot F, Heinrich C, Barbier L, et al. Inflammatory changes during epileptogenesis and spontaneous seizures in a mouse model of mesiotemporal lobe epilepsy. *Epilepsia*. 2011;52:2315-2325.
25. Ben-Ari Y. Limbic seizure and brain damage produced by kainic acid: mechanisms and relevance to human temporal lobe epilepsy. *Neuroscience*. 1985;14:375-403.
26. Rattka M, Brandt C, Löscher W. The intrahippocampal kainate model of temporal lobe epilepsy revisited: epileptogenesis, behavioral and cognitive alterations, pharmacological response, and hippoccampal damage in epileptic rats. *Epilepsy Res*. 2013;103:135-152.
27. Sloviter RS. "Epileptic" brain damage in rats induced by sustained electrical stimulation of the perforant path. I. Acute electrophysiological and light microscopic studies. *Brain Res Bull*. 1983;10:675-697.
28. Lothman EW, Bertram EH, Bekenstein JW, Perlin JB. Self-sustaining limbic status epilepticus induced by "continuous" hippocampal stimulation: electrographic and behavioral characteristics. *Epilepsy Res*. 1989;3:107-119.
29. Mazarati AM, Wasterlain CG, Sankar R, Shin D. Self-sustaining status epilepticus after brief electrical stimulation of the perforant path. *Brain Res*. 1998;801:251-253.
30. Gorter JA, Van Vliet EA, Lopes da Silva FH, Isom LL, Aronica E. Sodium channel β1-subunit expression is increased in reactive astrocytes in a rat model for mesial temporal lobe epilepsy. *Eur J Neurosci*. 2002;16:360-364.
31. Avdic U, Ahl M, Chugh D, et al. Nonconvulsive status epilepticus in rats leads to brain pathology. *Epilepsia*. 2018;59:945-958.
32. Noè F, Cattalini A, Vila Verde D, et al. Epileptiform activity contralateral to unilateral hippocampal sclerosis does not cause the expression of brain damage markers. *Epilepsia*. 2019;1-16.
33. Carriero G, Arcieri S, Cattalini A, Corsi L, Gnatkovsky V, De Curtis M. A guinea pig model of mesial temporal lobe epilepsy following nonconvulsive status epilepticus induced by unilateral intrahippocampal injection of kainic acid. *Epilepsia*. 2012;53:1917-1927.
34. Arcieri S, Velotti R, Noè F, et al. Variable electrobehavioral patterns during focal nonconvulsive status epilepticus induced by unilateral intrahippocampal injection of kainic acid. *Epilepsia*. 2014;55:1978-1985.
35. Tavares G, Martins M, Correia JS, et al. Employing an open-source tool to assess astrocyte tridimensional structure. *Brain Struct Funct*. 2017;222:1989-1999.
36. van Scheppingen J, Iyer AM, Prabowo AS, et al. Expression of microRNAs miR21, miR146a, and miR155 in tuberous sclerosis complex cortical tubers and their regulation in human astrocytes and SEGA-derived cell cultures. *Glia*. 2016;64:1066-1082.
37. Racine RJ. Modification of seizure activity by electrical stimulation: II. Motor seizure. *Electroencephalogr Clin Neurophysiol*. 1972;32:281-294.
38. Noé FM, Bellistri E, Colciaghi F, et al. Kainic acid-induced albumin leak across the blood-brain barrier facilitates epileptiform hyperexcitability in limbic regions. *Epilepsia*. 2016;57:967-976.

39. Song Y, Gunnarson E. Potassium dependent regulation of astrocyte water permeability is mediated by camp signaling. *PLoS One*. 2012;7:e34936.
40. Mathern GW, Cifuentes F, Leite JP, Pretorius JK, Babb TL. Hippocampal EEG excitability and chronic spontaneous seizures are associated with aberrant synaptic reorganization in the rat intrahippocampal kainate model. *Electroencephalogr Clin Neurophysiol*. 1993;87:326-339.
41. Pollard H, Charriaut-Marlangue C, Cantagrel S, et al. Kainate-induced apoptotic cell death in hippocampal neurons. *Neuroscience*. 1994;63:7-18.
42. Pitkänen A, Kharatishvili I, Narkilahti S, Lukasiuk K, Nissinen J. Administration of diazepam during status epilepticus reduces development and severity of epilepsy in rat. *Epilepsy Res*. 2005;63:27-42.
43. Schmued LC, Albertson C, Slikker W. Fluoro-Jade: a novel fluorochrome for the sensitive and reliable histochemical localization of neuronal degeneration. *Brain Res*. 1997;751:37-46.
44. Johnson GVW, Jope RS. The role of microtubule-associated protein 2 (MAP-2) in neuronal growth, plasticity, and degeneration. *J Neurosci Res*. 1992;33:505-512.
45. Bertram EH, Lothman EW, Lenn NJ. The hippocampus in experimental chronic epilepsy: a morphometric analysis. *Ann Neurol*. 1990;27:43-48.
46. Nairismägi J, Gröhn OHJ, Kettunen MI, Nissinen J, Kauppinen RA, Pitkänen A. Progression of brain damage after status epilepticus and its association with epileptogenesis: a quantitative MRI study in a rat model of temporal lobe epilepsy. *Epilepsia*. 2004;45:1024-1034.
47. Pitkänen A, Nissinen J, Nairismägi J, et al. Progression of neuronal damage after status epilepticus and during spontaneous seizures in a rat model of temporal lobe epilepsy. *Prog Brain Res*. 2002;135:67-83.
48. Rossini L, Garbelli R, Gnatkovsky V, et al. Seizure activity *per se* does not induce tissue damage markers in human neocortical focal epilepsy. *Ann Neurol*. 2017;82:331-341.
49. Cavazos JE, Das I, Sutula TP. Neuronal loss induced in limbic pathways by kindling: evidence for induction of hippocampal sclerosis by repeated brief seizures. *J Neurosci*. 1994;14:3106-3121.
50. French ED, Aldinio C, Schwarcz R. Intrahippocampal kainic acid, seizures and local neuronal degeneration: relationships assessed in unanesthetized rats. *Neuroscience*. 1982;7:2525-2536.
51. Vezzani A, Granata T. Brain inflammation in epilepsy: experimental and clinical evidence. *Epilepsia*. 2005;46:1724-1743.
52. Devinsky O, Vezzani A, O'Brien TJ, et al. Epilepsy. *Nat Rev Dis Prim*. 2018;4:18-24.
53. Binder DK, Steinhäuser C. Functional changes in astroglial cells in epilepsy. *Glia*. 2006;54:358-368.
54. Binder DK, Yao X, Zador Z, Sick TJ, Verkman AS, Manley GT. Increased seizure duration and slowed potassium kinetics in mice lacking aquaporin-4 water channels. *Glia*. 2006;53:631-636.
55. Seifert G, Steinhäuser C. Neuron-astrocyte signaling and epilepsy. *Exp Neurol*. 2013;244:4-10.
56. Steinhäuser C, Seifert G. Glial membrane channels and receptors in epilepsy: Impact for generation and spread of seizure activity. *Eur J Pharmacol*. 2002;447:227-237.

SUPPORTING INFORMATION

Additional supporting information may be found online in the Supporting Information section.

How to cite this article: Vila Verde D, Zimmer T, Cattalini A, et al. Seizure activity and brain damage in a model of focal non-convulsive *status epilepticus*. *Neuropathol Appl Neurobiol*. 2021;00:1–15. https://doi.org/10.1111/nan.12693

frontiers in Neurology

ORIGINAL RESEARCH
published: 26 January 2021
doi: 10.3389/fneur.2021.607603

Seizure-Induced Acute Glial Activation in the *in vitro* Isolated Guinea Pig Brain

*Diogo Vila Verde, Marco de Curtis and Laura Librizzi**

Epilepsy Unit, Fondazione IRCCS Istituto Neurologico Carlo Besta, Milano, Italy

Introduction: It has been proposed that seizures induce IL-1β biosynthesis in astrocytes and increase blood brain barrier (BBB) permeability, even without the presence of blood borne inflammatory molecules and leukocytes. In the present study we investigate if seizures induce morphological changes typically observed in activated glial cells. Moreover, we will test if serum albumin extravasation into the brain parenchyma exacerbates neuronal hyperexcitability by inducing astrocytic and microglial activation.

Methods: Epileptiform seizure-like events (SLEs) were induced in limbic regions by arterial perfusion of bicuculline methiodide (BMI; 50 μM) in the *in vitro* isolated guinea pig brain preparation. Field potentials were recorded in both the hippocampal CA1 region and the medial entorhinal cortex. BBB permeability changes were assessed by analyzing extravasation of arterially perfused fluorescein isothiocyanate (FITC)–albumin. Morphological changes in astrocytes and microglia were evaluated with tridimensional reconstruction and Sholl analysis in the ventral CA1 area of the hippocampus following application of BMI with or without co-perfusion of human serum albumin.

Results: BMI-induced SLE promoted morphological changes of both astrocytes and microglia cells into an activated phenotype, confirmed by the quantification of the number and length of their processes. Human-recombinant albumin extravasation, due to SLE-induced BBB impairment, worsened both SLE duration and the activated glia phenotype.

Discussion: Our study provides the first direct evidence that SLE activity *per se* is able to promote the activation of astro- and microglial cells, as observed by their changes in phenotype, in brain regions involved in seizure generation; we also hypothesize that gliosis, significantly intensified by h-recombinant albumin extravasation from the bloodstream to the brain parenchyma due to SLE-induced BBB disruption, is responsible for seizure activity reinforcement.

Keywords: blood brain barrier, inflammation, albumin, microglia, astrocytes

OPEN ACCESS

Edited by:
Kjell Heuser,
Oslo University Hospital, Norway

Reviewed by:
Luiz E. Mello,
Federal University of São Paulo, Brazil
Damir Janigro,
Case Western Reserve University, United States

****Correspondence:***
Laura Librizzi
laura.librizzi@istituto-besta.it

Specialty section:
This article was submitted to Epilepsy, a section of the journal Frontiers in Neurology

Received: *17 September 2020*
Accepted: *04 January 2021*
Published: *26 January 2021*

Citation:
Vila Verde D, de Curtis M and Librizzi L (2021) Seizure-Induced Acute Glial Activation in the in vitro Isolated Guinea Pig Brain. Front. Neurol. 12:607603. doi: 10.3389/fneur.2021.607603

INTRODUCTION

Blood brain barrier (BBB) dysfunction has been associated with disturbances of neural function in the central nervous system (CNS). A compromised BBB is often found in epileptic brain tissue obtained from epilepsy surgery (1, 2) and in patients with post-traumatic epilepsy (3) as well as in pharmacological models of status epilepticus (4). Experimental BBB leakage during intense seizures and the associated extravasation of serum albumin have been recognized as important contributors to glial dysfunction and epileptogenesis (5–7). Serum albumin binds the transforming growth factor ß (TGF-ß) receptor II in astrocytes and activates a transcriptional response resulting in a cascade of events culminating in the generation of epileptiform discharges (8, 9). Accumulating data from human and animal studies support the notion that glial cells make an important contribution to the pathogenesis of neurological diseases (10–12). Astrocytes are indispensable for proper brain development, playing fundamental roles in promoting formation and function of synapses, maintaining ion, neurotransmitter, water and ATP homeostasis and modulating neuronal signaling (13–16). Astrocytes can become reactive and develop a gliosis-like state where inflammation processes are triggered and up-regulated in a positively-feedback loop after brain injury and disease (17, 18), having a key role in in the generation and spread of seizure activity (11, 19–21).

Through dedicated molecular cascades, astrocytes (i) protect neurons against glutamate excitotoxicity by removing and recycling this neurotransmitter released during neuronal activity from the extracellular space; (ii) remove extracellular activity-dependent potassium accumulation; (iii) reduce the subsequent neuronal depolarization and hyperactivity (22, 23). Astrocytes also represent an important source of pro-inflammatory mediators and have been shown to initiate and regulate many immune-mediated mechanisms in the CNS (24–26). Changes of astrocytic receptors, transporters, ion channels and intracellular proteins are present in almost all forms of epilepsy (27). Accordingly, modified astroglial functioning is a key element leading to a reduction in: (i) expression of potassium inward-rectifying channels (Kir4.1) and water channels (aquaporin 4, AQP4) resulting in impaired potassium $[K^+]_o$ buffering, $[K^+]_o$ accumulation and consequent neuronal depolarization and seizures (28, 29); (ii) gap junction expression, with consequent alteration of spatial buffering of small molecules (e.g., K^+) (30, 31); (iii) glutamate uptake, favoring brain excitability increase (11).

Microglial cells are brain-resident macrophage-like cells that contribute to innate immune system mechanisms and respond early to CNS injuries (32). Accordingly, their reaction to damage can be either detrimental or protective (33). In a resting state, microglial cells feature a small cell body with vastly ramified processes (surveilling microglia). After a pathological challenge, microglial cells acquire amoeboid-like shape somata with almost no processes and achieve phagocytic properties (32). Recently, resident microglial cells have been implicated in driving astrocytes reactivity (34, 35) contributing to neuronal hyperexcitability and neurodegeneration (36, 37) and to the process of epileptogenesis in human and animal models of epilepsy (38, 39). Serum albumin-activated microglia releases pro-inflammatory cytokines [TNF-α; (40, 41)] and interacts with the damage-associated molecular patterns [DAMPs; (42)], contributing to astrocytes activation, brain inflammation and seizure recurrence (24, 40, 43). Seizures by themselves can induce brain inflammation and gliosis independent from blood-borne molecules, mediated by the synthesis and release of IL-1β that promotes BBB disruption (44).

In this study, we aim to investigate more in detail the effects of seizure activity on glial response, focusing on the morphological changes characterizing reactive glial cells. We also investigate if brain parenchyma exposure to serum albumin worsens glial cells reactivity and, as consequence, favors brain excitability and seizure recurrence. To verify these hypotheses, we induced pharmacological seizures in the *in vitro* isolated guinea pig brain (44, 45), a preparation that retains the physiological interactions between neurons, glia and vascular compartments (BBB included) in a condition close to *in vivo* (46, 47). In this isolated preparation, seizure-induced inflammatory responses can be analyzed in the absence of peripheral immune cells or blood-derived molecules.

MATERIALS AND METHODS

Procedures involving animals and their care were conducted in accordance with the ethically approved institutional guidelines that are in compliance with national and international laws and policies (European Economic Community Council Directive 86/609, Official Journal L 358, 1, December 12, 1987; Guide for the Care and Use of Laboratory Animals, U.S. National Research Council, 1996). All efforts were made to minimize the number of animals used and their suffering. Brains were isolated from young adult Hartley guinea pigs (150–200 g; Charles River Laboratories, Comerio, Italy) according to the standard technique described in detail elsewhere (46, 48). After barbiturate anesthesia the brain was carefully isolated and transferred to the incubation chamber. The basilar artery was cannulated with a polyethylene cannula to ensure arterial perfusion with a saline solution (composition: NaCl, 126 mM, KCl, 3 mM, KH_2PO_4, 1.2 mM, $MgSO_4$, 1.3 mM, $CaCl_2$, 2.4 mM, $NaHCO_3$, 26 mM, glucose, 15 mM, 3% dextran M.W. 70,000) oxygenated with a 95% O_2-5% CO_2 gas mixture (pH 7.3). This solution was arterially perfused at a rate of 6.5 ml/min via a peristaltic pump (Gilson Minipulse, Villiers Le Bel, France). Brain isolation was performed at low temperature (15°C) and experiments were carried out at 32°C, to maintain the isolated brain under hypothermic anesthesia. Human recombinant albumin (h-ALB; Sigma-Aldrich, Italy; 1 gr/250 ml) and bicuculline methiodide (Sigma-Aldrich, Italy) were applied by arterial perfusion (49, 50).

Induction of Epileptiform Activity

In a first set of experiments, epileptiform seizure-like events (SLEs) were induced by arterial perfusion of the $GABA_A$ antagonist BMI (50 μM; $n = 4$) and a second BMI perfusion was applied 90 min after the first one (**Figure 1**, protocol B). In

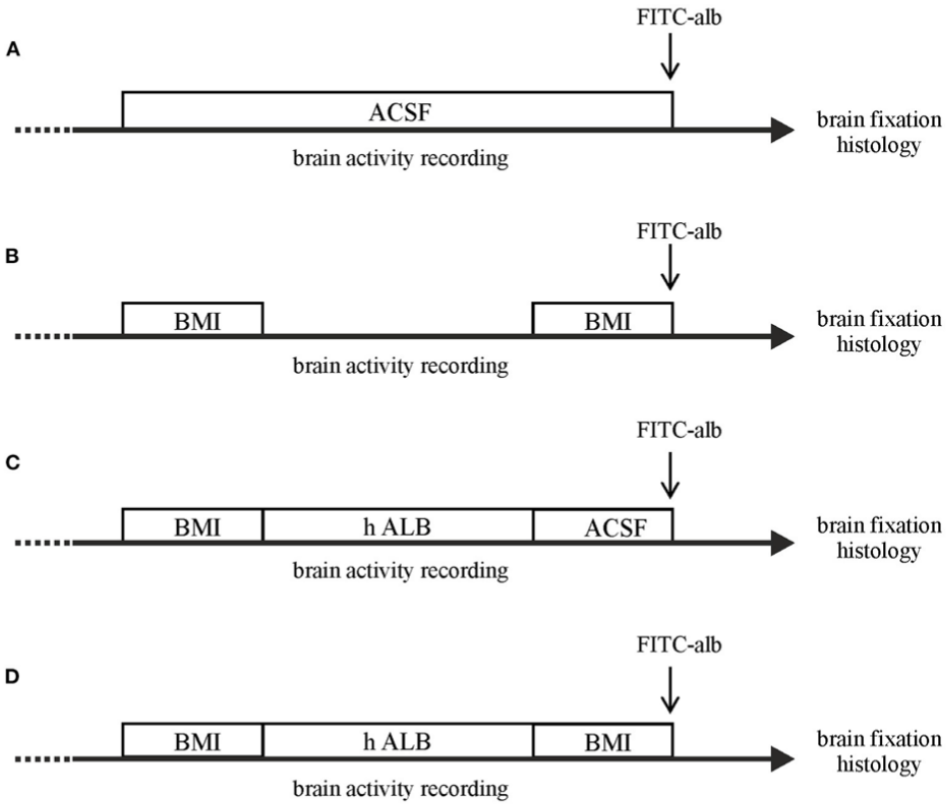

FIGURE 1 | Schematic drawing of the different experimental protocols utilized in the study. The *in vitro* brains were arterially perfused with: **(A)** control saline solution; **(B)** a double 3-min bolus of BMI; **(C)** 30-min perfusion with h-recombinant albumin (h-ALB) after the birst bolus of BMI; **(D)** 30-min perfusion with h-recombinant albumin (h-ALB) interposed between two boli of BMI. At the end of each experiment the brain was perfused with FITC-albumin for 4 min to evaluate BBB leakage. Each experimental protocol lasted 4 h.

a second set of the experiments, h-ALB (4 g/L, 329 mOsm; $n = 3$) added to control solution was arterially perfused for 30 min after the first bolus of BMI (**Figure 1**, protocol C). In a third set of the experiments, h-ALB ($n = 4$) added to control solution was arterially perfused for 30 min, between the two BMI applications (**Figure 1**, protocol D), just after the recovery of the first SLE. Brains were maintained *in vitro* for 4 h. In control experiments, brains were perfused only with control saline solution (**Figure 1**, protocol A; $n = 4$). Two control brains were perfused with FITC-albumin at the end of the experiment.

Electrophysiology

To test brain viability during the experiments, simultaneous extracellular recordings were performed in the piriform cortex (PC), medial entorhinal cortex (mEC), and the CA1 hippocampal region with glass micropipettes filled with a 0.9% NaCl solution (2–5 MOhm input resistance) during stimulation of the lateral olfactory tract with bipolar twisted-wire silver electrodes (51, 52).

Evaluation of BBB Permeability

The morphological and functional integrity of the BBB in the *in vitro* isolated guinea pig brain preparation has been previously demonstrated (47). We assessed the presence of BBB breakdown in isolated brains by perfusing fluorescein-isothiocyanate (FITC)–albumin (50 mg/10 ml, Sigma-Aldrich, Italy; $n = 9$) for 4 min immediately before the brains were fixed for histologic analysis. Control brains ($n = 4$) were maintained *in vitro* for a comparable time as experimental brains. The brief FITC-alb perfusion at the end of the experiment was utilized as a fluorescent marker of protein extravasation; the prolonged non-fluorescent h-ALB perfusion was used to enhance tissue excitability.

Immunohistochemistry

At the end of the electrophysiological experiments, brains were removed from the recording chamber and were fixed by immersion into 4% paraformaldehyde in phosphate-buffered saline (PBS; 0.1M, pH 7.4) for at least 24 h; 50 μm thick coronal sections were cut by vibratome (VT 1000S Leica, Heidelberg, Germany) throughout the extension of the hippocampus (plates A5.4–A7.4 of guinea pig brain atlas by Luparello). Sections collected on gelatin-coated slides were mounted in Fluorosave (Calbiochem, San Diego, CA, U.S.A.), and were cover-slipped. Two sections corresponding to plates A5.40

and A5.76 were collected for each brain to assess the intraluminal vs. extravascular FITC–albumin fluorescein signal. Slide-mounted sections were examined with a laser scanning confocal microscope using excitation of 488 nm (Laser Ar). Quantification of parenchymal FITC–albumin was performed in the hippocampal formation. In each brain, three high -power non-overlapping fields per section were acquired bilaterally at 10x magnification. Laser intensity was set at 30–35% power. Gain and photomultiplier were kept constant during acquisition of all images. As index of BBB damage, the area (number of pixels) occupied by the extravascular parenchymal FITC signal was quantified. Data obtained were used for statistical analysis. Values for experimental groups were expressed as percentage of the mean leakage area in the control group (defined as 100%). A standardized protocol was used for histochemical staining: in short, after endogenous peroxidase inactivation (3% H_2O_2 in PBS) and non-specific antigen binding sites blocking (1% BSA/0.2% Triton-X 100 in PBS), free-floating sections were incubated overnight at 4°C with the desired primary antibody in 0.1% BSA/0.2% Triton-X 100 at 4°C. On the subsequent day, sections were incubated for 75 min in the correspondent secondary antibody diluted in 0.1% BSA. Tissue was washed in PBS 3 times and then rinsed, mounted, dehydrated, and cover-slipped with fluorsave (Calbiochem, San Diego, CA, USA). For tridimensional reconstruction of microglial cells, immunofluorescence for ionized calcium-binding adapter molecule 1 (Iba-1 1:200 – Merck- Millipore, Darmstadt, Germany) and DAPI (1:5,000) conjugated with cy3 (1:600 – Neomarker-Invitrogen, Fremont, CA, USA) was performed. Regarding astrocytes, polyclonal rabbit anti-glial fibrillary acid protein (GFAP 1:500 - DAKO, Glostrup, Denmark) counterstained with DAPI (1:5,000) and coupled with alexa 594 (1:500 – Neomarker-Invitrogen, Fremont, CA, USA) was used.

Morphometric Analysis of Glial Cells

For tridimensional reconstruction of glia, two coronal sections *per* animal were stained for Iba-1 and DAPI (cell nuclei) for microglial cells or GFAP and DAPI for astrocytes, as described before. Sections were visualized using a Leica SP8 Confocal (Leica Microsystems, Germany), applying LASX software (version 3.1.5.1). Previews of the whole section in widefield (10X/0.3 dry) using the DAPI channel were taken to choose areas of interest in the ventral CA1 *stratum radiatum,* that was further acquired at a higher resolution with the confocal mode. Two channel (Iba-1/GFAP and DAPI) Z-stack images (Z-step intervals of 0.3 μm) were acquired using a 63X/1.4 oil objective and a DFC365 FX CCD Camera (Leica) with a x-y sampling of 72 nm. Cells were eligible for reconstruction if the following criteria were met: (i) the Iba-1/GFAP positive cell coincided with a single DAPI-stained nucleus; (ii) the cell did not present truncated processes; (iii) the cell could be singled out from neighboring cells to ensure correct reconstruction. A total of 75 cells (5 ROIs *per* animal) were selected for reconstruction performed using simple neurite tracer plugin available in FIJI-ImageJ software (v2.0.0), an open-source tool previously described to effectively assess tridimensional morphology of neurons and glial cells (53). Glia morphometric properties were evaluated by quantifying the number of processes, total length (in μm), sum of intersections; Sholl analysis was also performed to identify the number of intersections at radial intervals of 2 μm starting from the central point of the soma, as a measure of the complexity of glial cells ramifications and branches.

Statistical Analysis

Quantitative results were analyzed using Student *t* and Mann–Whitney tests and ANOVA. The normal distribution of samples was checked with Shapiro–Wilks test and the homogeneity of variances was evaluated with *F* test. When the equal variance criterion was violated, the Welch correction was used. The Mann–Whitney non-parametric test was chosen when data were not normally distributed. Otherwise, Student *t*-test was used. All statistical tests were performed in Origin 9.0 (OriginLab Corporation, Northampton, MA, USA), except the morphology experiments for which statistical analysis was performed using Prism 8.2 (GraphPad Software Inc., San Francisco, CA, USA). The format of Student *t*-test results is: $t(\mathrm{df}) = t$ statistic, p significance value. The format of Mann–Whitney test results is: $U(\mathrm{n1}, \mathrm{n2}) = \mathrm{x}$, $p \leq$ significance value. The format for ANOVA test was $F(\mathrm{df}) = F$, p significance value. The tests are two-sided and confidence interval was set at 95% (0.95) so that the difference between means was considered statistically significant at p-values of <5% (0.05), 1% (0.01), and 0.1% (0.001). Data are shown as mean ± standard deviation (SD).

RESULTS

Experiments were performed in 15 isolated guinea pig brains. Control condition brains were maintained *in vitro* with control solution for 4 h before perfusing FITC-alb (**Figure 1A**). The reasoning behind the 4 h timeline was due to technical issues. The isolated *in vitro* brain takes 90 min (0.2°C/ min) to reach 32°C, which is the optimal temperature for the experiments to be carried on. Subsequently, LOT-evoked potentials were induced to verify the viability of the preparation throughout the experiment and assess the position of depth electrodes. The infusion of the first bolus of bicucculline followed. A second perfusion of bicuculline was applied 90 min after the first and the recording were carried on for 30 min. In the end, the brain was perfused for 4 min with FITC albumin. As expected, no SLEs were observed in control experiments ($n = 4$). SLEs were induced by arterial perfusion of BMI (50 μM) for 3 min. The first BMI application evoked a 13.5 ± 2.6 min SLEs in the limbic region, recorded in the hippocampus (area CA1; left trace in **Figure 2A**) and in the mEC. A second BMI perfusion applied 90 min after the first one (**Figure 1B**) induced SLEs lasting 12.1 ± 3.4 min ($n = 4$; see **Figure 2C**). This protocol induced significant brain extravasation of FITC-albumin compared to control animals (**Figures 3A,B**; $t(18) = -5, 5$; $p < 0.001$ with two samples Student *t*-test). The increase in BBB permeability induced by a first SLE allowed extravasation of later perfused FITC-alb (49). Therefore, we perfused 4 g/L h-ALB via the basilar artery for 30 min immediately after the occurrence of the first BMI-induced SLE ($n = 4$; **Figure 1C**) and 60 min before the second BMI bolus ($n = 4$; **Figure 1D**). The perfusion of h-ALB increased both SLE

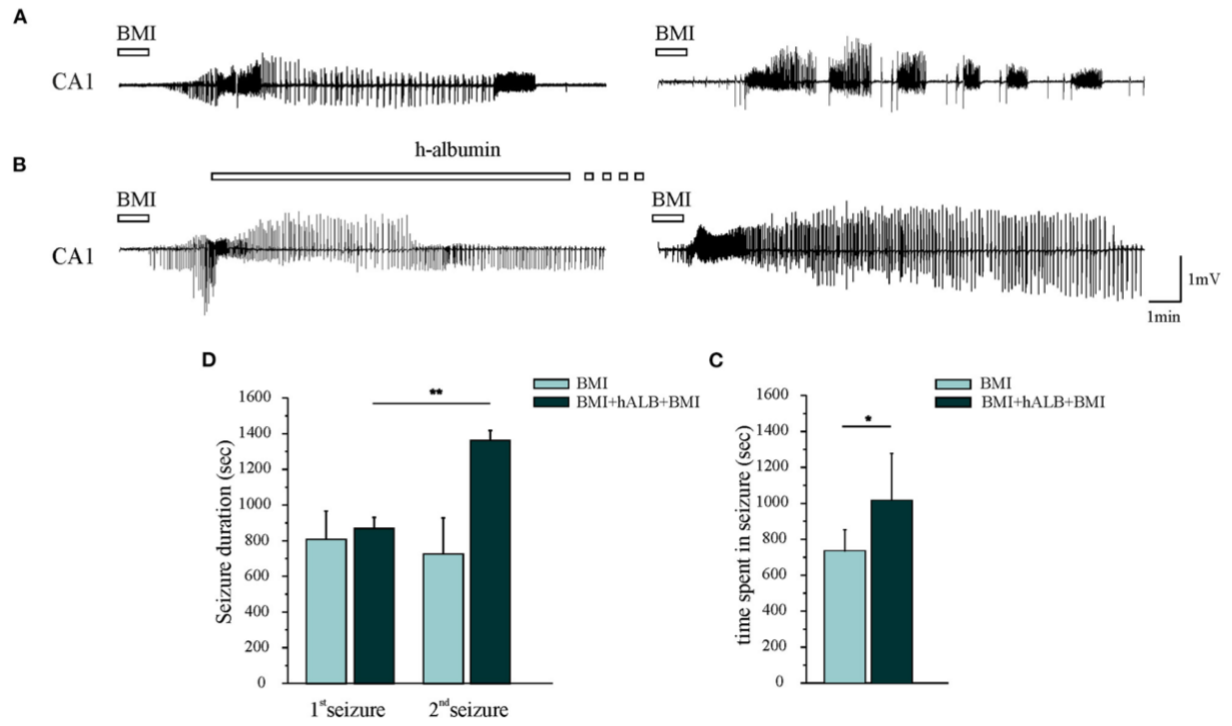

FIGURE 2 | Epileptiform discharges recorded in CA1. **(A)** The first and the second 3-min application of BMI induced one seizure-like event (SLE). **(B)** 30-min h-recombinant albumin (h-ALB) perfusion after the first BMI-induced SLE (left trace) significantly increased the duration of the second BMI-induced SLE (right trace). **(C)** Mean SLE durations induced by the first (1st SLE) and the second application of BMI with and without h-recombinant albumin application (2nd SLE). **(D)** Total time spent in seizure after the application of the experimental protocols B and C, respectively. *$p < 0.05$; **$p < 0.01$ with Student *t*-test.

duration induced by the second BMI perfusion (**Figures 2B,C**; 22.7 ± 0.9 min; t(5) = −4, 2; $p < 0.01$ with two sample student *t*-test) and the total time spent in SLE (**Figure 2D**; $t(12) = -2, 4$; $p < 0.05$ with two sample student *t*-test) compared to the experiments without h-ALB perfusion between the two BMI tests. As expected, the extent of BBB leakage, assessed by measuring the area of FITC-alb extravasation, was up to 3-fold larger after BMI + hALB + BMI perfusion compared to BMI only (**Figures 3A,B**; $F(2) = 60$; $p < 0.001$ with ANOVA). Also, the extent of BBB leakage induced by application of BMI +hALB was lower compared to BMI+hALB+BMI (**Figures 3A,C**; $t(23) = 2, 3$; $p < 0.05$ with two samples Student *t*-test).

To exclude unspecific effects, in 2 experiments h-ALB was perfused via the basilar artery for 30 min without BMI. H-ALB perfusion alone was unable to spontaneously evoke ictal discharge (data not shown). Afterwards, we evaluated the influence of SLE activity either alone (BMI) or in combination with h-ALB (BMI + hALB) on the reactive state of GFAP immunostained astrocytes (**Figure 4**) and IBA-1 stained microglial cells (**Figure 5**) analyzed in the CA1 hippocampal field, where epileptiform activity was recorded. In order to better investigate the role of serum albumin on glial dysfunction and BBB damage, in a separate set of experiments we also studied the effect of h-ALB after the first BMI-induced SLE. In this case, at the end of the h-ALB treatment, the isolated brain was perfused with perfusion solution until the end of the experiment ($n = 3$). Sholl analysis was used to quantify the number of intersections at radial intervals of 2 μm starting from the soma of glial cells (**Figures 4B,C**, **5B,C**). As summarized in **Figure 4C**, the number of intersections counted in CA1 astrocytes from guinea pig brains submitted to BMI, BMI + hALB and BMI + hALB +BMI was higher than control brains ($F(3) = 115.9$; $p < 0.001$ with ANOVA). Representative astroglia typical of the four experimental conditions are illustrated in **Figure 4A**. Furthermore, astrocytes had a higher number of processes (**Figure 4D**), total length of their processes (**Figure 4E**), and sum of intersections in Sholl analysis (**Figure 4F**) in BMI, BMI + hALB, and BMI + hALB + BMI in comparison to CT animals ($F(3) = 65.18$, $F(3) = 119.3$, and $F(3) = 115.9$, respectively; $p < 0.001$ with ANOVA). Interestingly, there was a consistent increase in all three parameters when comparing BMI against BMI + hALB + BMI (**Figures 4D–F**), indicating that the astrocitic morphological changes that occured in the presence of SLEs only (BMI) worsened in the BMI + hALB + BMI protocol.

Lastly, microglial morphology was also assessed (**Figure 5**) using the same methodology employed for astrocyte reconstruction. Sholl analysis revealed that microglia in BMI, BMI + hALB, BMI + hALB + BMI animals had a lower number of intersections when compared to control animals ($F(3) = 99.2$; $p < 0.001$ with ANOVA; **Figures 5B,C** – representative

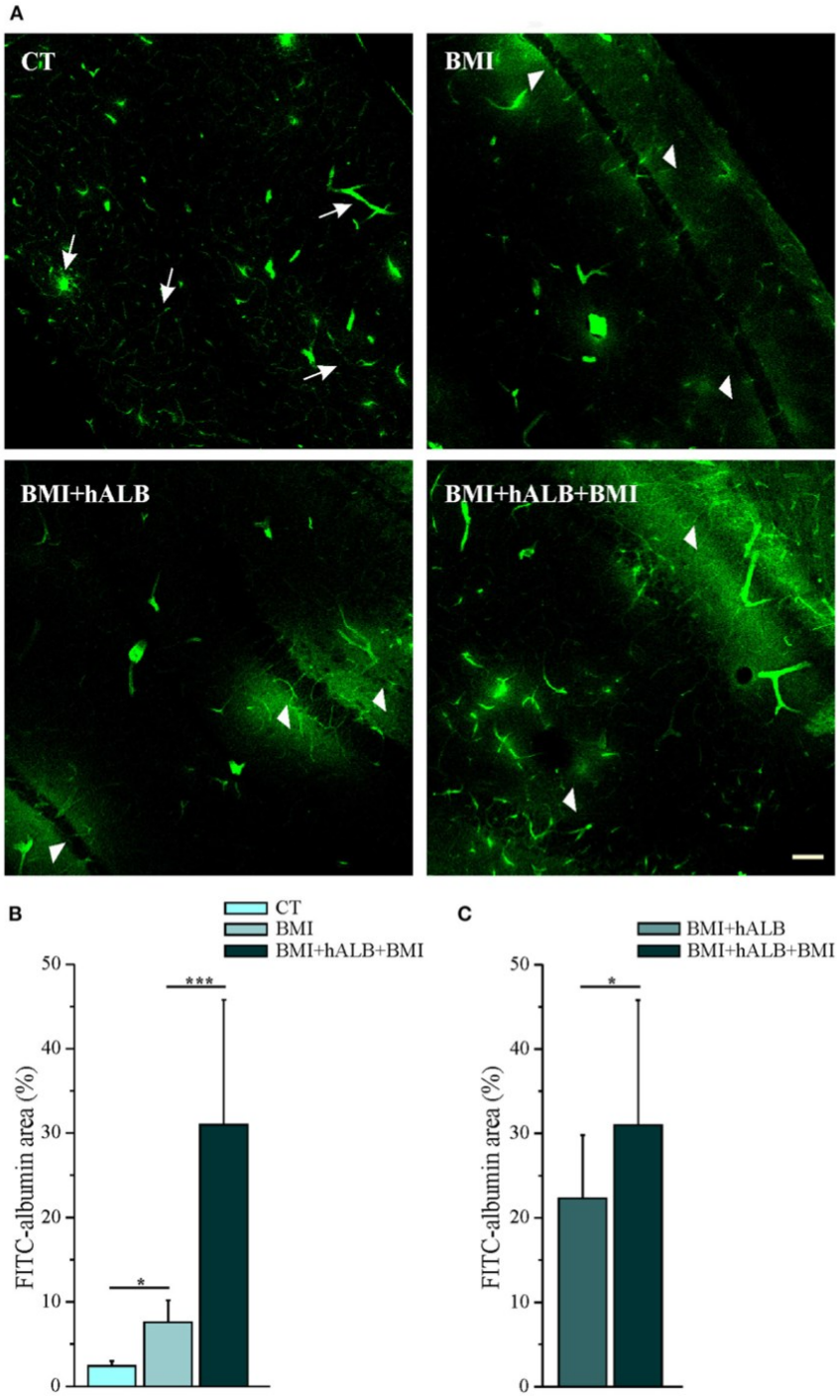

FIGURE 3 | Quantification of parenchymal Fluorescein isothiocyanate (FITC)–albumin leakage. **(A)** Representative photomicrographs of intraparenchymal FITC–albumin signal in the limbic area in control solution (top, left), BMI (top, right), BMI + h-ALB (bottom, left), and BMI + h-ALB + BMI (bottom, right) treated brains. Control sections show intraluminal signal with scattered perivascular spots (white arrow). Areas of FITC–albumin parenchymal extravasation around vessels (white arrowheads) after the second pulse of BMI alone or co-perfused with h-recombinant albumin, showed as FITC–albumin parenchymal leakage is broader after the application of protocol C and D (see **Figure 1**). **(B,C)** Quantification of parenchymal FITC–albumin leakage in the experimental conditions. FITC-albumin leakage has been evaluated as spot area (number of pixels) and it is expressed as percentage of values vs. control experiments $^{*}p < 0.05$; $^{***}p < 0.001$ with ANOVA and Student *t*-test. Calibration bar = 100 μm.

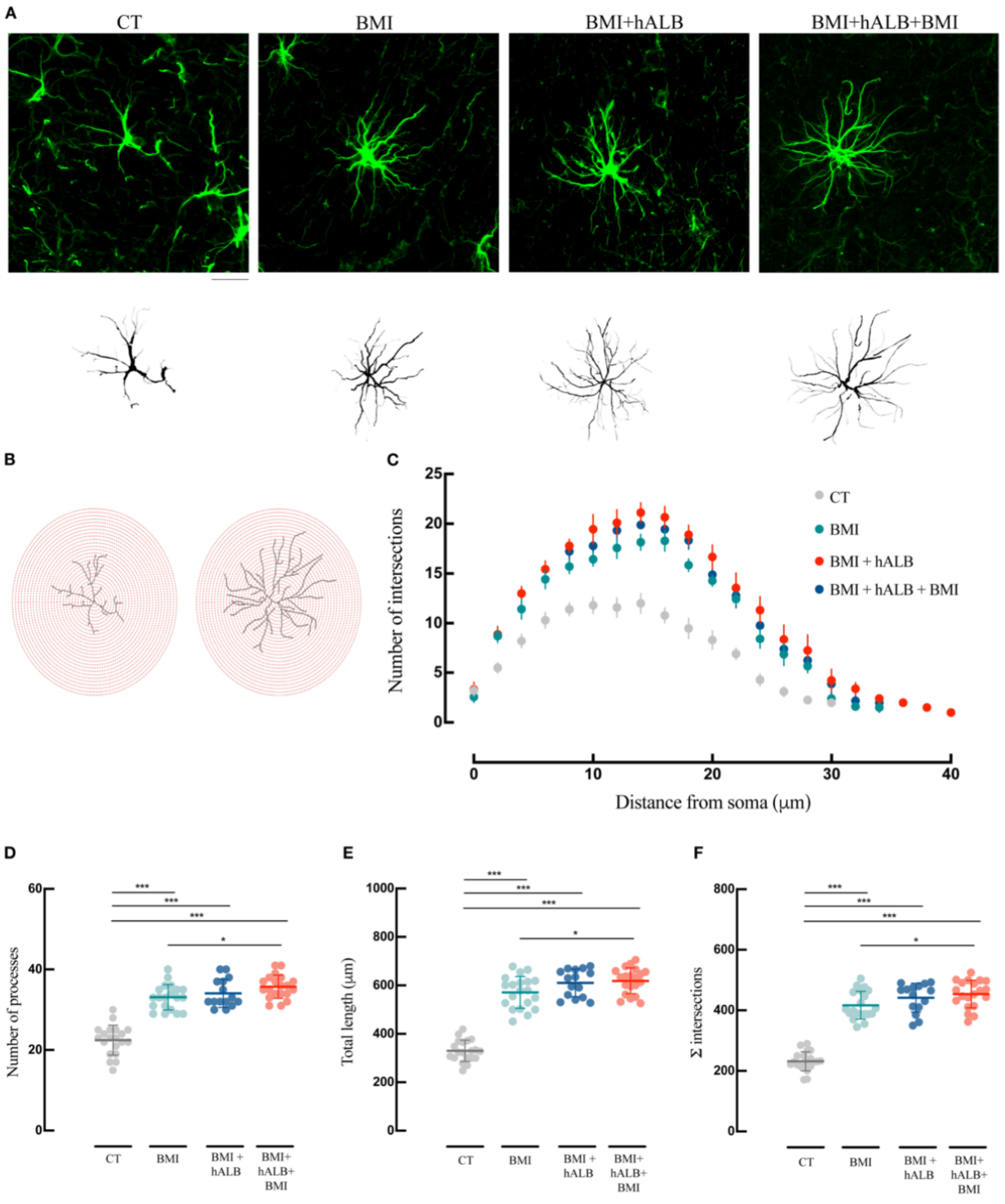

FIGURE 4 | Morphological analysis and reconstruction of astrocytes in ventral hippocampal CA1. **(A)** Representative morphologies of astrocytes in GFAP immunofluorescence coronal sections of the ventral CA1 hippocampal region are shown for CT, BMI, BMI+hALB, and BMI+hALB+BMI; the correspondent reconstruction of the astrocyte is illustrated in the lower part of the panel. Calibration bar = 20 μm. **(B)** Representative Sholl analysis setting of a manually reconstructed astrocyte from CT (left) and BMI+hALB+BMI (right). The circles centered around the soma are separated by radial intervals of 2 μm. **(C)** Number of intersections *per* 2 μm radius plotted against the distance from the cell soma in CT, BMI, BMI+hALB, and BMI+hALB+BMI animals. **(D)** Number of processes *per* 2 μm radius of astrocytes in CT ($n = 20$ cells), BMI ($n = 20$ cells), BMI+hALB ($n = 15$ cells), and BMI+hALB+BMI ($n = 20$ cells) animals. **(E)** Total length in μm of

(Continued)

FIGURE 4 | astrocytes in CT ($n = 20$ cells), BMI ($n = 20$ cells), BMI+hALB ($n = 15$ cells), and BMI+hALB+BMI ($n = 20$ cells) guinea pigs. **(F)** Sum of intersections of astrocytic cells CT ($n = 20$ cells), BMI ($n = 20$ cells), BMI+hALB ($n = 15$ cells), and BMI+hALB+BMI ($n = 20$ cells) animal groups. *$p < 0.05$; ***$p < 0.001$ with ANOVA test. All experiments were done in 5 cells *per* animal.

panel in **Figure 5A**). Moreover, microglia consistently had lower number of processes (**Figure 5D**), total length of their processes (**Figure 5E**) and sum of Sholl-analysis intersections (**Figure 5F**) in BMI, BMI + hALB, and BMI + hALB + BMI animal cohorts, in comparison to control brains ($F(3) = 71.18$, $F(3) = 225.9$ and $F(3) = 99.2$, respectively; $p < 0.001$ with ANOVA). Similar to astrocytes, when BMI was coupled with h-ALB + BMI, the morphology of microglia had a more activated phenotype when compared to BMI alone (**Figures 5D–F**). Additionally, comparing microglia cells that had the same seizure profile (single seizure induced by BMI), cells that were perfused with hALB as well had a higher gliosis-like phenotype when compared to BMI only protocol (BMI vs. BMI + hALB in **Figures 5D–F**). In sum, our data demonstrate a worsening of the astro and microgliosis state when major seizure activity is in coallition with h-ALB extravasation into the brain. However, h-ALB by itself is also able to induce major gliosios (to a less extent than the previous mentioned protocol).

DISCUSSION

A growing body of evidence supports gliosis as a primary factor in the pathogenesis of neurological diseases (54, 55). Data from human and animal studies support the notion that glial cells contribute to the control of neuronal function under both physiological and pathological conditions (11, 12, 56) and respond to changes in normal physiology of the CNS by establishing and coordinating response to disease resulting in gliosis (57). Recent evidences from experimental models of epilepsy and drug-resistant forms of human epilepsy suggest that epilepsy is often accompanied by astrocytes and microglia phenotypic and functional alterations (12, 21, 58).

We previously demonstrated that pharmacologically-evoked SLEs in the *in vitro* guinea pig brain induce IL-1β expression in perivascular astrocytes and compromise BBB permeability (44, 49). Our data confirmed that serum albumin entering into the brain through an impaired BBB contributed to the generation of sustained epileptiform activity (49). In the present study we investigated the role of serum albumin extravasation into brain parenchyma following seizure-induced BBB damage in enhancing reactive gliosis without the contribution of any blood-borne molecules/cells, since our guinea pig brain preparation is maintained in isolation. The BBB is involved in almost all pathologies of the CNS (59–61). Its alterations can compromise the fundamental processes which govern brain functions. Serum albumin extravasation into brain parenchyma following BBB integrity loss is reported to lead to glial activation and alterations in the extracellular milieu around neurons (8, 62). Normal brain albumin concentration is much lower (35–50 microg/mL) than blood albumin concentration, that ranges from 35 to 50 mg/mL (63, 64). Thus, BBB opening has the potential to expose brain cells to high levels of albumin (65). The contribution of serum albumin in astrocytes activation is supported by several studies showing induction of calcium signaling and DNA synthesis in astrocytes (66, 67). One pivotal mechanism involved in these effects is the albumin-mediated activation of the *transforming growth factor beta receptor II* (TGF-βR); recent studies demonstrated that serum albumin leaks into brain parenchyma through a dysfunctional BBB to bind astrocytic TGF-βR activating TGF-β signaling (8, 9, 68, 69). This cascade of events leads to astrocytes Kir4.1 downregulation and to their consequent failure to buffer extracellular K^+ and glutamate, that culminates in the synthesis of inflammatory molecules and increase brain excitability (9, 56). Accordingly, blockade of Kir4.1 in glia with cesium has been demonstrated to promote seizure like activity (70). Furthermore, activation of TGF-β signaling by albumin induced rapid and persistent up-regulation of genes related to inflammation (9). BBB impairment also easily allows microglia to be exposed to high concentrations of albumin. Even though the effects of albumin on cells in the brain have mainly been investigated in astrocytes, several studies support the pathological role of microglial activation by albumin (63, 69, 71). Since albumin can activate microglia, which in turn can activate astrocytes and exacerbate reactive pathways (40, 41), it is of the upmost interest to understand which signaling cascades are activated in microglia exposed to serum albumin after BBB damage. Hooper and colleagues demonstrated that microglia respond to serum albumin by increasing intracellular calcium *via* Src tyrosine kinases, which successively leads to glutamate and TNF-α release (63, 65).

In our experiments, the concentration of albumin perfused in the arterial system of the *in vitro* guinea pig brain (4 mg/ml) falls within the range associated with BBB damage occurring in a pathology associated condition (65). The changes observed in our acute ictogenic model confirmed that astro- and microglial cells promptly respond to seizure activity. BMI-evoked SLE determined changes in astrocytic and microglial morphological phenotype toward a more activated state. SLEs-induced microglia adopts an amoeboid shape, starting from a ramified structure in the control brains (72, 73), while astrocytes express a hypertrophic phenotype with longer processes compared to control condition (74). Interestingly, seizure pattern, duration and astro- and microgliosis were exacerbated when SLE activity was combined with the perfusion of h-albumin. Our data support the hypothesis that albumin increases SLE activity in limbic areas by directly inducing a reactive state in both astrocytes and microglia. Whether acute gliosis represents an early possible defensive mechanism triggered by seizure activity or their activation is actively involved in the epileptogenic process cannot be answered in our acute experimental conditions. However, *in vivo* studies performed in our laboratory in the intrahippocampal

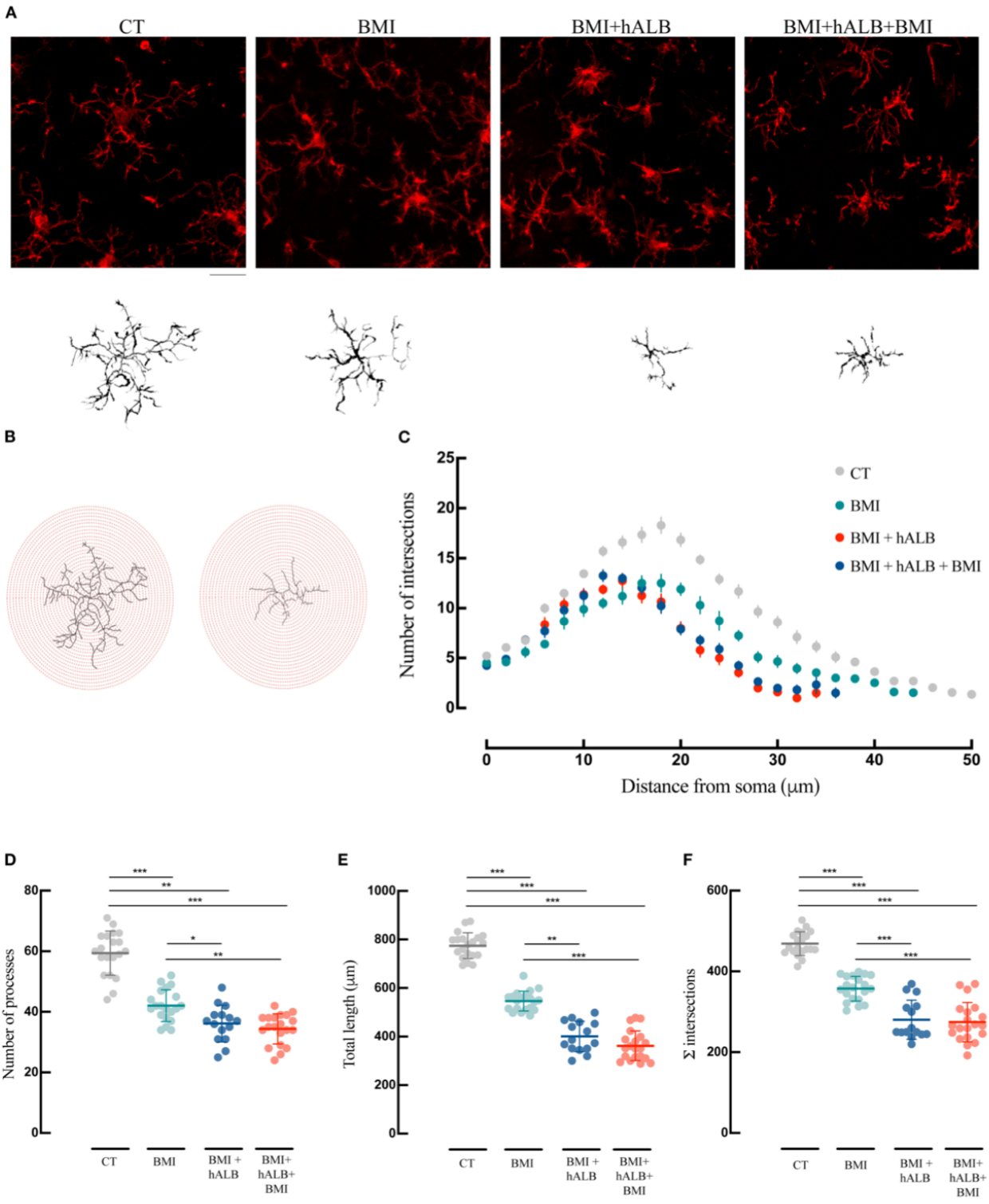

FIGURE 5 | Morphological analysis and reconstruction of microglia in ventral hippocampal CA1. **(A)** Representative morphologies of microglial cells in Iba-1 immunofluorescence coronal sections of the ventral CA1 hippocampal region are represented for CT, BMI, BMI+hALB, and BMI+hALB+BMI; the correspondent reconstruction of the microglial cell is illustrated in the bottom part of the panel. Calibration bar = 20 μm. **(B)** Representative Sholl analysis setting of a manually reconstructed microglia cell from CT (left) and BMI+hALB+BMI (right). The circles centered around the soma are separated by radial intervals of 2 μm. **(C)** Number of

(Continued)

FIGURE 5 | intersections *per* 2 μm radius plotted against the distance from the cell soma in CT, BMI, BMI+hALB, and BMI+hALB+BMI animals. **(D)** Number of processes *per* 2 μm radius of microglia cells in CT ($n = 20$ cells), BMI ($n = 20$ cells), BMI+hALB ($n = 15$ cells), and BMI+hALB+BMI ($n = 20$ cells) guinea pigs. **(E)** Total length in μm of microglia cells in CT ($n = 20$ cells), BMI ($n = 20$ cells), BMI+hALB ($n = 15$ cells), and BMI+hALB+BMI ($n = 20$ cells) animal groups. **(F)** Sum of intersections of microglia cells in CT ($n = 20$ cells), BMI ($n = 20$ cells), BMI+hALB ($n = 15$ cells) and BMI+hALB+BMI ($n = 20$ cells) animals. $^{*}p < 0.05$; $^{**}p < 0.01$; $^{***}p < 0.001$ with ANOVA test. All experiments were done in 5 cells *per* animal.

kainic acid (KA) model suggest that seizures, gliosis and BBB damage contribute to epileptogenesis at the site of kainic acid injection, but not in regions remote from the injection site. Even though gliosis was still present at an early phase and seizure activity was present in both regions, no detrimental markers of brain damage were detected (75). In the same animal model, genes associated with inflammatory response (IL1-β and COX-2), brain activity (c-FOS) and oxidative stress (HO-1) were early upregulated exclusively in the KA-injected hippocampus during the acute phase and remained upregulated 1 month post-KA injection. Interestingly, only genes linked to glial function (AQP4 and Kir4.1) were upregulated 3 days post-KA (but not after 1 month) in regions remote from the kainic acid injection site that also generated epileptiform discharges. In these regions late damage did not develop (Vila Verde in press on Neurophatolo Appl Neurobiol). It can be hypothesized that early after seizure occurrence transient gliosis could helping neurons to cope seizure activity preventing neuronal damage, whereas in regions in which seizures are coupled with the excitotoxic effects of kainic acid, persistent gliosis may have nefarious effects to the brain. It can therefore be expeculated that, early after seizure occurrence, transient gliosis may help neurons cope with seizure activity preventing neuronal damage development, whereas in regions in which seizures are coupled with the excitotoxic effects of kainic acid, persistent gliosis induces permanent nefarious effects in the brain.

In conclusion, the present study reinforces our previous observation that in an *in vitro* acute model of ictogenesis seizure activity *per se* enhances BBB permeability in brain regions involved in seizure generation and that extravasation of albumin into brain parenchyma increases seizure activity in those regions affected by BBB impairment (44, 49). We demonstrate for the first time simultaneous morphological phenotype changes in both astrocytes and microglia due to seizure activity. Our data strongly suggest seizure-induced BBB breakdown and the consequent albumin extravasation leads to astrocytes and microglia reactivity and eventually to reinforce seizure activity by increasing its duration. Further studies are required to recognize when astro- and microgliosis might help or harm the brain in our experimental conditions.

DATA AVAILABILITY STATEMENT

The original contributions presented in the study are included in the article/supplementary materials, further inquiries can be directed to the corresponding author.

ETHICS STATEMENT

The animal study was reviewed and approved by Organismo Preposto al Benessere Animale - OPBA Fondazione Istituto Neurologico C. Besta Via Celoria 11 20133 Milano.

AUTHOR CONTRIBUTIONS

DV and LL: conception, design of the study, acquisition, and analysis of data. DV, LL, and MC: drafting a significant portion of the manuscript or figures. All authors contributed to the article and approved the submitted version.

FUNDING

This work was supported by the European Union's Horizon 2020 Research and Innovation Programme under the Marie Sklodowska-Curie grant agreement no. 722053 (EU-GliaPhD).

ACKNOWLEDGMENTS

The authors thank Maria Cristina Regondi and Barbara Cipelletti for technical support.

REFERENCES

1. Oby E, Janigro D. The blood-brain barrier and epilepsy. *Epilepsia*. (2006) 47:1761–74. doi: 10.1111/j.1528-1167.2006.00817.x
2. Van Vliet EA, Araújo SDC, Redeker S, Van Schaik R, Aronica E, Gorter JA. Blood-brain barrier leakage may lead to progression of temporal lobe epilepsy. *Brain*. (2007) 130:521–34. doi: 10.1093/brain/awl318
3. Tomkins O, Shelef I, Kaizerman I, Eliushin A, Afawi Z, Misk A, Gidon M, et al. Blood-brain barrier disruption in post-traumatic epilepsy. *J Neurol Neurosurg Psychiatry*. (2008) 79:774–77. doi: 10.1136/jnnp.2007.126425
4. van Vliet EA, Aronica E, Gorter JA. Role of blood-brain barrier in temporal lobe epilepsy and pharmacoresistance. *Neuroscience*. (2014) 277:455–73. doi: 10.1016/j.neuroscience.2014.07.030
5. Friedman A, Kaufer D, Heinemann U. Blood-brain barrier breakdown-inducing astrocytic transformation: novel targets for the prevention of epilepsy. *Epilepsy Res*. (2009) 85:142–9. doi: 10.1016/j.eplepsyres.2009.03.005
6. Bar-Klein G, Cacheaux LP, Kamintsky L, Prager O, Weissberg I, Schoknecht K, et al. Losartan prevents acquired epilepsy via TGF-β signaling suppression. *Ann Neurol*. (2014) 75:864–75. doi: 10.1002/ana.24147
7. Van Vliet EA, Otte WM, Wadman WJ, Aronica E, Kooij G, De Vries HE, et al. Blood-brain barrier leakage after status epilepticus in rapamycin-treated rats I: magnetic resonance imaging. *Epilepsia*. (2016) 57:59–69. doi: 10.1111/epi.13246
8. Ivens S, Kaufer D, Flores LP, Bechmann I, Zumsteg D, Tomkins O, et al. TGF-β receptor-mediated albumin uptake into astrocytes is involved in neocortical epileptogenesis. *Brain*. (2007) 130:535–47. doi: 10.1093/brain/awl317

9. Cacheaux LP, Ivens S, David Y, Lakhter AJ, Bar-Klein G, Shapira M, et al. Transcriptome profiling reveals TGF-β signaling involvement in epileptogenesis. *J Neurosci.* (2009) 29:8927–35. doi: 10.1523/JNEUROSCI.0430-09.2009
10. Araque A, Carmignoto G, Haydon PG. Dynamic signaling between astrocytes and neurons. *Annu Rev Physiol.* (2001) 63:795–813. doi: 10.1146/annurev.physiol.63.1.795
11. Seifert G, Schilling K, Steinhäuser C. Astrocyte dysfunction in neurological disorders: a molecular perspective. *Nat Rev Neurosci.* (2006) 7:194–206. doi: 10.1038/nrn1870
12. Wetherington J, Serrano G, Dingledine R. Astrocytes in the epileptic brain. *Neuron.* (2008) 58:168–78. doi: 10.1016/j.neuron.2008.04.002
13. Parpura V, Verkhratsky A. Astrocytes revisited: concise historic outlook on glutamate homeostasis and signaling. *Croat Med J.* (2012) 53:518–28. doi: 10.3325/cmj.2012.53.518
14. Pekny M, Pekna M, Messing A, Steinhäuser C, Lee JM, Parpura V, et al. Astrocytes: a central element in neurological diseases. *Acta Neuropathol.* (2016) 131:323–45. doi: 10.1007/s00401-015-1513-1
15. Haydon PG, Carmignoto G. Astrocyte control of synaptic transmission and neurovascular coupling. *Physiol Rev.* (2006) 86:1009–31. doi: 10.1152/physrev.00049.2005
16. Wolf F, Kirchhoff F. Imaging astrocyte activity. *Science.* (2008) 320:1597–99. doi: 10.1126/science.1160122
17. Zamanian JL, Xu L, Foo LC, Nouri N, Zhou L, Giffard RG, Barres BA. Genomic analysis of reactive astrogliosis. *J Neurosci.* (2012) 32:6391–410. doi: 10.1523/JNEUROSCI.6221-11.2012
18. Anderson MA, Burda JE, Ren Y, Ao Y, O'Shea TM, Kawaguchi R, et al. Astrocyte scar formation AIDS central nervous system axon regeneration. *Nature.* (2016) 532:195–200. doi: 10.1038/nature17623
19. Rogawski MA. Update on the neurobiology of alcohol withdrawal seizures. *Epilepsy Curr.* (2005) 5:225–30. doi: 10.1111/j.1535-7511.2005.00071.x
20. Araque A, Perea G. Glial modulation of synaptic transmission in culture. *Glia.* (2004) 47:241–8. doi: 10.1002/glia.20026
21. Dossi E, Vasile F, Rouach N. Human astrocytes in the diseased brain. *Brain Res Bull.* (2018) 136:139–56. doi: 10.1016/j.brainresbull.2017.02.001
22. Vezzani A, Granata T. Brain inflammation in epilepsy: experimental and clinical evidence. *Epilepsia.* (2005) 46:1724–43. doi: 10.1111/j.1528-1167.2005.00298.x
23. Devinsky O, Vezzani A, O'Brien TJ, Jette N, Scheffer IE, De Curtis M, et al. Epilepsy. *Nat Rev Dis Prim.* (2018) 4:18–24. doi: 10.1038/nrdp.2018.24
24. Aronica E, Ravizza T, Zurolo E, Vezzani A. Astrocyte immune responses in epilepsy. *Glia.* (2012) 60:1258–68. doi: 10.1002/glia.22312
25. Allaman I, Bélanger M, Magistretti PJ. Astrocyte-neuron metabolic relationships: for better and for worse. *Trends Neurosci.* (2011) 34:76–87. doi: 10.1016/j.tins.2010.12.001
26. Ransohoff RM, Engelhardt B. The anatomical and cellular basis of immune surveillance in the central nervous system. *Nat Rev Immunol.* (2012) 12:623–35. doi: 10.1038/nri3265
27. Thom M. Review: hippocampal sclerosis in epilepsy: a neuropathology review. *Neuropathol Appl Neurobiol.* (2014) 40:520–43. doi: 10.1111/nan.12150
28. Binder DK, Yao X, Zador Z, Sick TJ, Verkman AS, Manley GT. Increased seizure duration and slowed potassium kinetics in mice lacking aquaporin-4 water channels. *Glia.* (2006) 53:631–6. doi: 10.1002/glia.20318
29. Djukic B, Casper KB, Philpot BD, Chin LS, McCarthy KD. Conditional knock-out of Kir4.1 leads to glial membrane depolarization, inhibition of potassium and glutamate uptake, and enhanced short-term synaptic potentiation. *J Neurosci.* (2007) 27:11354–65. doi: 10.1523/JNEUROSCI.0723-07.2007
30. Simard M, Nedergaard M. The neurobiology of glia in the context of water and ion homeostasis. *Neuroscience.* (2004) 129:877–96. doi: 10.1016/j.neuroscience.2004.09.053
31. Bedner P, Dupper A, Hüttmann K, Müller J, Herde MK, Dublin P, et al. Astrocyte uncoupling as a cause of human temporal lobe epilepsy. *Brain.* (2015) 138:1208–22. doi: 10.1093/brain/awv067
32. Wyatt-Johnson SK, Herr SA, Brewster AL. Status epilepticus triggers time-dependent alterations in microglia abundance and morphological phenotypes in the hippocampus. *Front Neurol.* (2017) 8:700. doi: 10.3389/fneur.2017.00700
33. Miron VE, Boyd A, Zhao JW, Yuen TJ, Ruckh JM, Shadrach JL, et al. M2 microglia and macrophages drive oligodendrocyte differentiation during CNS remyelination. *Nat Neurosci.* (2013) 16:1211–8. doi: 10.1038/nn.3469
34. Buffo A, Rolando C, Ceruti S. Astrocytes in the damaged brain: molecular and cellular insights into their reactive response and healing potential. *Biochem Pharmacol.* (2010) 79:77–89. doi: 10.1016/j.bcp.2009.09.014
35. Liddelow SA, Guttenplan KA, Clarke LE, Bennett FC, Bohlen CJ, Schirmer L, et al. Neurotoxic reactive astrocytes are induced by activated microglia. *Nature.* (2017) 541:481–7. doi: 10.1038/nature21029
36. Eyo UB, Murugan M, Wu LJ. Microglia–neuron communication in epilepsy. *Glia.* (2017) 65:5–18. doi: 10.1002/glia.23006
37. Hiragi T, Ikegaya Y, Koyama R. Microglia after seizures and in epilepsy. *Cells.* (2018) 7:26. doi: 10.3390/cells7040026
38. Benson MJ, Manzanero S, Borges K. Complex alterations in microglial M1/M2 markers during the development of epilepsy in two mouse models. *Epilepsia.* (2015) 56:895–905. doi: 10.1111/epi.12960
39. Binder DK, Steinhäuser C. Functional changes in astroglial cells in epilepsy. *Glia.* (2006) 54:358–68. doi: 10.1002/glia.20394
40. Santello M, Bezzi P, Volterra A. TNFα controls glutamatergic gliotransmission in the hippocampal dentate gyrus. *Neuron.* (2011) 69:988–1001. doi: 10.1016/j.neuron.2011.02.003
41. Bedner P, Steinhäuser C. TNFα-driven astrocyte purinergic signaling during epileptogenesis. *Trends Mol Med.* (2019) 25:70–2. doi: 10.1016/j.molmed.2018.12.001
42. Presta I, Vismara M, Novellino F, Donato A, Zaffino P, Scali E, et al. Innate immunity cells and the neurovascular unit. *Int J Mol Sci.* (2018) 19:3856. doi: 10.3390/ijms19123856
43. Ravizza T, Noé F, Zardoni D, Vaghi V, Sifringer M, Vezzani A. Interleukin converting enzyme inhibition impairs kindling epileptogenesis in rats by blocking astrocytic IL-1β production. *Neurobiol Dis.* (2008) 31:327–33. doi: 10.1016/j.nbd.2008.05.007
44. Librizzi L, Noè F, Vezzani A, De Curtis M, Ravizza T. Seizure-induced brain-borne inflammation sustains seizure recurrence and blood-brain barrier damage. *Ann Neurol.* (2012) 72:82–90. doi: 10.1002/ana.23567
45. Uva L, Librizzi L, Wendling F, De Curtis M. Propagation dynamics of epileptiform activity acutely induced by bicuculline in the hippocampal-parahippocampal region of the isolated guinea pig brain. *Epilepsia.* (2005) 46:1914–25. doi: 10.1111/j.1528-1167.2005.00342.x
46. De Curtis M, Biella G, Buccellati C, Folco G. Simultaneous investigation of the neuronal and vascular compartments in the guinea pig brain isolated *in vitro*. *Brain Res Protoc.* (1998) 3:221–8. doi: 10.1016/S1385-299X(98)00044-0
47. Librizzi L, Janigro D, De Biasi S, De Curtis M. Blood-brain barrier preservation in the *in vitro* isolated guinea pig brain preparation. *J Neurosci Res.* (2001) 66:289–97. doi: 10.1002/jnr.1223
48. Mühlethaler M, de Curtis M, Walton K, Llinás R. The isolated and perfused brain of the guinea-pig *in vitro*. *Eur J Neurosci.* (1993) 5:915–26. doi: 10.1111/j.1460-9568.1993.tb00942.x
49. Noé FM, Bellistri E, Colciaghi F, Cipelletti B, Battaglia G, De Curtis M, et al. Kainic acid-induced albumin leak across the blood-brain barrier facilitates epileptiform hyperexcitability in limbic regions. *Epilepsia.* (2016) 57:967–76. doi: 10.1111/epi.13394
50. Uva L, Strowbridge BW, de Curtis M. Olfactory bulb networks revealed by lateral olfactory tract stimulation in the *in vitro* isolated guinea-pig brain. *Neuroscience.* (2006) 142:567–77. doi: 10.1016/j.neuroscience.2006.06.047
51. Uva L, De Curtis M. Propagation pattern of entorhinal cortex subfields to the dentate gyrus in the guinea-pig: an electrophysiological study. *Neuroscience.* (2003) 122:843–51. doi: 10.1016/S0306-4522(03)00551-7
52. Biella G, De Curtis M. Olfactory inputs activate the medial entorhinal cortex via the hippocampus. *J Neurophysiol.* (2000) 83:1924–31. doi: 10.1152/jn.2000.83.4.1924
53. Tavares G, Martins M, Correia JS, Sardinha VM, Guerra-Gomes S, das Neves SP, et al. Employing an open-source tool to assess astrocyte tridimensional structure. *Brain Struct Funct.* (2017) 222:1989–99. doi: 10.1007/s00429-016-1316-8
54. Vezzani A, Balosso S, Ravizza T. The role of cytokines in the pathophysiology of epilepsy. *Brain Behav Immun.* (2008) 22:797–803. doi: 10.1016/j.bbi.2008.03.009

55. Aronica E, Crino PB. Inflammation in epilepsy: clinical observations. *Epilepsia*. (2011) 52:26–32. doi: 10.1111/j.1528-1167.2011.03033.x
56. David Y, Cacheaux LP, Ivens S, Lapilover E, Heinemann U, Kaufer D, et al. Astrocytic dysfunction in epileptogenesis: consequence of altered potassium and glutamate homeostasis? *J Neurosci*. (2009) 29:10588–99. doi: 10.1523/JNEUROSCI.2323-09.2009
57. Stevens B, Fields RD. Regulation of the cell cycle in normal and pathological glia. *Neuroscientist*. (2002) 8:93–7. doi: 10.1177/107385840200800205
58. Bedner P, Jabs R, Steinhäuser C. Properties of human astrocytes and NG2 glia. *Glia*. (2020) 68:756–67. doi: 10.1002/glia.23725
59. Marchi N, Granata T, Ghosh C, Janigro D. Blood-brain barrier dysfunction and epilepsy: pathophysiologic role and therapeutic approaches. *Epilepsia*. (2012) 53:1877–86. doi: 10.1111/j.1528-1167.2012.03637.x
60. Marchi N, Lerner-Natoli M. Cerebrovascular remodeling and epilepsy. *Neuroscientist*. (2013) 19:304–12. doi: 10.1177/1073858412462747
61. Abbott NJ, Friedman A. Overview and introduction: the blood-brain barrier in health and disease. *Epilepsia*. (2012) 53:1–6. doi: 10.1111/j.1528-1167.2012.03696.x
62. Frigerio F, Frasca A, Weissberg I, Parrella S, Friedman A, Vezzani A, et al. Long-lasting pro-ictogenic effects induced *in vivo* by rat brain exposure to serum albumin in the absence of concomitant pathology. *Epilepsia*. (2012) 53:1887–97. doi: 10.1111/j.1528-1167.2012.03666.x
63. Hooper C, Taylor DL, Pocock JM. Pure albumin is a potent trigger of calcium signalling and proliferation in microglia but not macrophages or astrocytes. *J Neurochem*. (2005) 92:1363–76. doi: 10.1111/j.1471-4159.2005.02982.x
64. Nadal A, Fuentes E, McNaughton PA. Glial cell responses to lipids bound to albumin in serum and plasma. *Prog Brain Res*. (2001) 132:367–74. doi: 10.1016/S0079-6123(01)32088-5
65. Hooper C, Pinteaux-Jones F, Fry VAH, Sevastou IG, Baker D, Heales SJ, et al. Differential effects of albumin on microglia and macrophages; Implications for neurodegeneration following blood-brain barrier damage. *J Neurochem*. (2009) 109:694–705. doi: 10.1111/j.1471-4159.2009.05953.x
66. Nadal A, Fuentes E, Pastor J, Mcnaughton PA. Plasma albumin is a potent trigger of calcium signals and DNA synthesis in astrocytes. *Proc Natl Acad Sci USA*. (1995) 92:1426–30. doi: 10.1073/pnas.92.5.1426
67. Vega-Zelaya L, Ortega GJ, Sola RG, Pastor J. Plasma albumin induces cytosolic calcium oscilations and DNA synthesis in human cultured astrocytes. *Biomed Res Int*. (2014) 2014: 539140. doi: 10.1155/2014/539140
68. Weissberg I, Wood L, Kamintsky L, Vazquez O, Milikovsky DZ, Alexander A, et al. Albumin induces excitatory synaptogenesis through astrocytic TGF-β/ALK5 signaling in a model of acquired epilepsy following blood-brain barrier dysfunction. *Neurobiol Dis*. (2015) 78:115–25. doi: 10.1016/j.nbd.2015.02.029
69. Swissa E, Serlin Y, Vazana U, Prager O, Friedman A. Blood–brain barrier dysfunction in status epileptics: mechanisms and role in epileptogenesis. *Epilepsy Behav*. (2019) 101:106285. doi: 10.1016/j.yebeh.2019.04.038
70. Janigro D, Gasparini S, D'Ambrosio R, McKhann G, DiFrancesco D. Reduction of K+ uptake in gila prevents long-term depression maintenance and causes epileptiform activity. *J Neurosci*. (1997) 17:2813–24. doi: 10.1523/JNEUROSCI.17-08-02813.1997
71. Si QS, Nakamura Y, Kataoka K. Albumin enhances superoxide production in cultured microglia. *Glia*. (1997) 21:413–8. doi: 10.1002/(SICI)1098-1136(199712)21:4<413::AID-GLIA9>3.0.CO;2-3
72. Kreutzberg GW. Microglia: a sensor for pathological events in the CNS. *Trends Neurosci*. (1996) 19:312–8. doi: 10.1016/0166-2236(96)10049-7
73. Sierra A, de Castro F, del Río-Hortega J, Rafael Iglesias-Rozas J, Garrosa M, Kettenmann H. The "Big-Bang" for modern glial biology: translation and comments on Pío del Río-Hortega 1919 series of papers on microglia. *Glia*. (2016) 64:1801–40. doi: 10.1002/glia.23046
74. Sofroniew MV, Vinters HV. Astrocytes: biology and pathology. *Acta Neuropathol*. (2010) 119:7–35. doi: 10.1007/s00401-009-0619-8
75. Noè F, Cattalini A, Vila Verde D, Alessi C, Colciaghi F, Figini M, et al. Epileptiform activity contralateral to unilateral hippocampal sclerosis does not cause the expression of brain damage markers. *Epilepsia*. (2019) 0:1–16. doi: 10.1111/epi.15611

Conflict of Interest: The authors declare that the research was conducted in the absence of any commercial or financial relationships that could be construed as a potential conflict of interest.

The handling editor is currently organizing a Research Topic with one of the authors MC.

Peripheral blood mononuclear cell activation sustains seizure activity

Journal:	*Epilepsia*
Manuscript ID	EPI-00126-2021
Manuscript Type:	Full length original research paper
Date Submitted by the Author:	04-Feb-2021
Complete List of Authors:	Librizzi, Laura; Fondazione IRCCS Istituto Neurologico Carlo Besta, Epilepsy Unit Vila Verde, Diogo; Fondazione IRCCS Istituto Neurologico Carlo Besta, Epilepsy Unit Colciaghi, Francesca; Fondazione IRCCS Istituto Neurologico Carlo Besta, Epilepsy Unit Deleo, Francesco; Fondazione IRCCS Istituto Nazionale dei Tumori, Epilepsy Unit Regondi, Maria; Fondazione IRCCS Istituto Neurologico Carlo Besta, Epilepsy Unit Costanza, Massimo; Fondazione IRCCS Istituto Neurologico Carlo Besta, Molecular Neuro-Oncology Unit Cipelletti, Barbara; Fondazione IRCCS Istituto Neurologico Carlo Besta, Epilepsy Unit de Curtis, Marco; Fondazione IRCCS Istituto Neurologico Carlo Besta, Epilepsy Unit
Key Words:	Blood brain barrier damage, Serum albumin, Inflammatory mediators, Immune cells, microglia dysfunction

Peripheral blood mononuclear cell activation sustains seizure activity

Laura Librizzi[1*], Diogo Vila Verde[1], Francesca Colciaghi[1], Francesco Deleo[1], Maria Cristina Regondi[1], Massimo Costanza[2], Barbara Cipelletti[1] and Marco de Curtis[1]

(1) Epilepsy Unit and (2) Molecular Neuro-Oncology Unit, Fondazione IRCCS Istituto Neurologico *Carlo Besta*, via Amadeo 42, 20133 Milano, Italy

Running Title: PBMCs' role in ictogenesis

Key words: Serum albumin, inflammatory mediators, immune cells

Abstract: 232 words

Introduction: 465 words

Discussion: 1130 words

Manuscript's body: 3997 words

Number of figures: 6

Address for correspondence:

Laura Librizzi

laura.librizzi@istituto-besta.it

Tel +39 2023944519

ABSTRACT

Objective: The influx of immune cells and serum proteins from the periphery into the brain due to a dysfunctional blood-brain barrier (BBB) has been proposed to contribute to the pathogenesis of seizures in various forms of epilepsy and encephalitis.

We evaluated the pathophysiological impact of activated peripheral blood mononuclear cells (PBMCs) and serum albumin on neuronal excitability in an *in vitro* brain preparation.

Methods: A condition of mild endothelial activation induced by arterial perfusion of lipopolysaccharide (LPS) was induced in the whole brain preparation of guinea pigs maintained *in vitro* by arterial perfusion. The effects of co-perfusion of human recombinant serum albumin with human PBMCs activated with concanavalin A on neuronal excitability, BBB permeability (measured by FITC-albumin extravasation) and microglial activation was analyzed.

Results: Bioplex analysis in supernatants of concanavalin-A-stimulated PBMCs revealed increased levels of several inflammatory mediators, in particular IL-1β, TNF- α, INF-γ, IL-6, IL-10, IL-17A and MIP3α. LPS and human albumin arterially co-perfused with either concanavalin A-activated PBMCs or the cytokine-enriched supernatant of activated PBMCs i) modulated calcium-calmodulin-dependent protein kinase II at excitatory synapses, ii) enhanced BBB permeability, iii) induced microglial activation and iv) promoted seizure-like events. Separate perfusions of either non-activated PBMCs or concanavalin A-activated PBMCs without LPS/hALB failed to induce inflammatory and excitability changes.

Significance: Activated peripheral immune cells, such as PBMCs, and the extravasation of serum proteins in a condition of BBB impairment contribute to seizure generation.

Abbreviations:

human albumin = hALB; fluorescein-iso-thio-cyanate albumin= FITC-alb; blood-brain barrier = BBB; seizure-like events = SLEs; activated peripheral blood mononuclear cells = a-PBMCs; nonactivated peripheral blood mononuclear cells = na-PBMCs; peripheral blood mononuclear cells = PBMC; concanavalin A = ConA; lipopolysaccaride = LPS; medial entorhinal cortex = mEC; interleukin = IL; tumor necrosis factor =TNF,interferon =INF macrophage inflammatory protein = MIP.

Key Points

- Emerging data propose innate and adaptive immune cells as possible triggers of ictogenesis;
- Activated immune cells induce BBB premeability changes responsible for the extravasation into the brain parenchyma of serum proteins and other inflammatory mediators that promote neuroinflammation and seizures;
- The identification of cellular and soluble biomarkers that describe these processes is mandatory to better understand dysimmune encephalopathies with seizures.

INTRODUCTION

The neuro-centric view of epilepsy has been challenged by clinical and experimental evidence suggesting a prominent role of both immune and cerebrovascular systems in the pathogenesis of seizure disorders[1]. The blood-brain barrier (BBB) represents an initial defense of the central nervous system (CNS) and its impairment has been implicated in the induction of seizures and progression of epilepsy[2,3]. When there is a disruption in BBB, the extravasation of both plasma proteins and blood-borne immune cells into brain parenchyma, leads to the activation of pro-inflammatory pathways, neuronal dysfunction and seizure occurrence[4]. Interestingly, a positive correlation between the extent of BBB opening and the number of seizures has been established [2]. Rapid activation of pro-inflammatory cytokines, such as interleukin (IL)-1β, IL-6 and tumor necrosis factor- α (TNF-α), and danger signals, such as high mobility group box 1 (HMGB1), is observed after acute and chronic seizures in animal models of acquired epilepsies and in brain tissue obtained from patients with temporal lobe epilepsy or malformations of cortical development submitted to epilepsy surgery[5]. Alterations of cells of adaptive and innate immunity (T and B cells and NK cells, respectively) have been found in both serum and cerebrospinal fluid (CSF) of patients suffering from different forms of focal epilepsies[4,6]. Infiltration of blood-borne cells, micro and astrogliosis have been reported as hallmarks of an emerging group of epilepsies that feature seizures as a prominent clinical symptom[7,8]. In these, emerging data proposes innate and adaptive immune cells as possible triggers of ictogenesis[5]. Moreover, peripheral immune cell infiltration seems to be extremely abundant in encephalitis characterized by frequent seizures, in type IIB focal cortical dysplasia and tuberous sclerosis complex[5].

Although CNS-resident cells such as microglia and astrocytes are key modulators of neuroinflammation, the interaction between adaptive immune cells and intraluminal endothelial molecules triggers the release of diffusible inflammatory mediators into brain parenchyma (cytokines, chemokines) that are known to activate glial cells and increase neuronal excitability, along with serum albumin extravasation[4,9,10]. Also, extensive clinical and experimental evidence suggests that inflammatory processes play a role in the generation and recurrence of epileptic seizures[11].

In this study we aimed to investigate the specific role of peripheral blood mononuclear cells (PBMCs) in initiating brain inflammation and BBB damage, either autonomously or in cooperation with blood-borne molecules and microglial cells, to induce seizure-like events (SLE).

To pursuit this hypothesis, we utilized the *in vitro* isolated guinea pig brain preparation that retains the physiological interactions between neuronal, glial and vascular compartments in a close to *in vivo* condition[12,13] and lacks peripheral immune cells or blood-derived molecules. Understanding the impact of activated PBMCs on brain excitability might contribute to identify key mediators involved in seizure generation and provide additional treatment options for focal epilepsy.

MATERIALS AND METHODS

According with the ARRIVE guidelines, procedures were carried out to minimize discomfort and pain to treated rats, in compliance with National (D.L. 116 Suppl 40/1992 and D.L. 26/2014) and International guidelines and laws (2010/63/EU Legislation for the protection of animals used for scientific purposes). The experimental protocols were approved by the Ethics Committee the Fondazione IRCCS Istituto Neurologico Carlo Besta (DO-01-2020) and by the Italian Ministry of Health (Aut Min N° 271-2012/A).

Isolation of guinea pig brain

Brains were isolated from young adult Hartley guinea-pigs (n=35; 150–200g; Charles River Laboratories, Italy) according to the standard technique described elsewhere[12]. Human recombinant albumin (hALB; Sigma Aldrich, Italy; 4gr/L) and the non-specific endotoxin, lipopolysaccharide (LPS; Sigma Aldrich, Italy; 100 ng/ml), were applied by arterial perfusion[14,15].

Blood collection and peripheral blood mononuclear cells isolation and stimulation

Human PBMCs were obtained from healthy volunteers who undersigned informed consent in accordance with the Declaration of Helsinki and with approval from the Ethic Committee of the IRCCS Neurological Institute Foundation “Carlo Besta”. Human PBMCs were isolated from anticoagulated whole blood using a discontinuous density gradient (Lymphoprep, Nycomed,

Norway) as previously described[16]. Spleen cells were harvested from naïve female 3-weeks-old guinea pigs. Both PBMCs and splenocytes were treated with 1x RBC Lysis Buffer (eBioscience) for red blood cell lysis, according to the manufacturer's protocol. Immune cells were cultured in 24-well plates at a density of 2 x 10^6 cells/well in 1 ml RPMI 1640 (EuroClone) supplemented with L-glutamine (2 mM), sodium pyruvate (1 mM), nonessential amino acids (0.1 mM), penicillin (100 U/ml), streptomycin (0.1 mg/ml), HEPES buffer (0.01 M), and 10% FBS. Cells were cultured *in vitro* with ConA (2 μg/ml) or medium alone at 37°C with 5% CO_2[16]. After 48h of incubation, 5-10 x 10^6 cells and their supernatant were collected, the preparation was diluted to a final volume of 10 ml with phosphate buffer saline (PBS) without calcium and magnesium and it was perfused into the isolated guinea-pig brain for 30 min at the rate of 0.3 ml/min via a syringe-infuser (KD Scientific, USA) connected to the brain main arterial perfusion line[14]. In experiments with cell-free supernatants, PBMCs were previously pelleted by centrifugation at 370g for 8' at 4°C, supernatants were collected and diluted in 10 ml PBS before the injection in the brain arterial system.

At the end of each experiment, brain hemispheres were separated, and each hemisphere was either post-fixed by immersion into 4% paraformaldehyde in PBS (0.1M, pH 7.4) and processed for immunohistochemistry analysis or immediately snap-frozen with liquid nitrogen for subsequent biochemical analysis.

Electrophysiology

Simultaneous extracellular recordings were performed in the piriform cortex, in the medial entorhinal cortex and in hippocampal formation with glass micropipettes filled with a 0.9% NaCl solution (2–5 MOhm input resistance).

Biochemical analysis: subcellular fractioning and western blot

Hippocampi were used to obtain whole homogenates and crude cytosol/membrane fractions as previously reported[17]. Equal amount of proteins from different fractions were separated by SDS-PAGE (8%), were electroblotted onto nitrocellulose and then incubated with specific primary antibodies to detect both total calcium-calmodulin-dependent protein kinase II (dependent

prCaMKII; 1:2.000; mouse mAb #GTX22725 Genetex Int Corporation) and autophosphorylated CaMKII at Thr286 or p286-CaMKII (1:2.000; rabbit pAb, #V111A; Promega Corporation) in Odyssey® Blocking Buffer (LI-COR Biosciences, USA) and PBS (1:1) either for 4 hours at room temperature or overnight at 4°C. A monoclonal pan actin antibody was used as loading control. Primary antibodies were detected with IRDye (680 or 800 nm) labelled goat-anti-rabbit or goat-anti-mouse IgG (LI-COR Biosciences). Immunoreactive bands were visualized and quantified by means of Odyssey Infrared Imaging System (LI-COR Biosciences) and were normalized *vs* actin signals[17]. Ratio between p286-CaMKII/total CaMKII bands was used as a measure of the CaMKII activation in each fraction, in different experimental conditions (at least *n*=3 animals/each condition).

Evaluation of BBB permeability to albumin

The morphologic and functional integrity of the BBB in the *in vitro* isolated guinea pig brain preparation has been demonstrated[13,15]. We assessed the presence of BBB breakdown by perfusing fluorescein-iso-thio-cyanate (FITC)–albumin (50 mg/10 ml, Sigma- Aldrich) for 4 min immediately before the brains were fixed after the electrophysiological experiment for histologic analysis of FITC–albumin extravasation (at least *n*=3 for each protocol).

Immunohistochemistry

BBB permeability changes. Fifty µm thick coronal sections were cut by vibratome (VT 1000S Leica, Germany) throughout the extension of the hippocampus (plates A5.2–A7.4 of the guinea pig brain atlas by Luparello). Sections collected on gelatin-coated slides were mounted in Fluorosave (Calbiochem, USA) and were cover-slipped. Two sections corresponding to plates A5.40 and A5.76 were collected for each brain to assess the intraluminal *vs* extravascular FITC–albumin fluorescein signal. Slide-mounted sections were examined with a laser scanning confocal microscope using excitation light of 488 nm (Laser Ar). The quantification of parenchymal FITC–albumin was performed in the hippocampal formation. In each brain, three high–power, non-overlapping fields per section were acquired at 10x magnification. Laser intensity was set at 30–

35% power. Gain and photomultiplier were kept constant during the acquisition of all images. The BBB damage was evaluated using an image analysis system (Image-Pro Premier 9.1 software: Media Cybernetics). The percentage of FITC-albumin extravasation was estimated using densitometric analysis that combined user-defined color intensity threshold and size and shape parameters of the objects of interest. The area occupied by the parenchymal FITC signal (number of pixels) was quantified.

Immunostaining. A standardized protocol was used for immunohistochemical staining. After endogenous peroxidase inactivation (3% H_2O_2 in PBS) and non-specific antigen binding sites blocking (1% BSA/0.2% Triton-X 100 in PBS), free-floating sections were incubated overnight at 4° C with the desired primary antibody in 0.1% BSA/0.2% Triton-X 100 at 4° C. On the subsequent day, sections were incubated for 75 min in the correspondent secondary antibody diluted in 0.1% BSA. Tissue was washed in PBS 3 times and then rinsed, mounted, dehydrated and cover-slipped with fluorsave (Merck-Millipore, Germany). For tridimensional reconstruction of microglial cells, immunofluorescence for Iba-1 (1:200 – Abcam, United Kingdom) and To-PRO (1:5000) conjugated with Cy5 (1:600 – Neomarker-Invitrogen, USA) was performed on 50 µm thick coronal sections. For the detection of the blood-borne immune cells immunostaining for anti-CD4 and anti-CD8 (1:50- Dako, USA) was performed on 50 µm thick coronal sections. Immunoreactivity was tested by the avidin– biotin–peroxidase technique (Vector Labs), using DAB as chromogen. Sections were dried, then dehydrated in graded alcohols, and cover slipped.

Morphometric analysis of microglial cells. For tridimensional reconstruction of microglial structure, two coronal sections *per* animal were used and stained for Iba-1 and TO-PRO (cell nuclei) as described before. Sections were visualized using a Leica SP8 Confocal (Leica Microsystems, Germany), applying the LASX software (version 3.1.5.1). Previews of the whole section in wide-field (10X/0.3 dry) using TO-PRO channel were taken in order to choose areas of interest, namely ventral CA1 *stratum radiatum* that was further acquired at a higher resolution in the confocal mode. Two channel (Iba-1 and TO-PRO) Z-stack images (Z-step intervals of 0.3 µm) were acquired using a 63X/1.4 oil objective and a DFC365 FX CCD Camera (Leica) with a x-y

sampling of 72 nm. Cells were eligible for reconstruction if the following criteria were met: i) Iba-1 positive cell was surrounding a single TO-PRO-stained nucleus; ii) cell did not present truncated processes; iii) cell was sufficiently individualized from neighboring cells to ensure correct reconstruction. A total of 65 cells (5 cells *per* animal; *n*= 5) were selected for reconstruction performed using simple neurite tracer plugin available in FIJI-ImageJ software (v2.0.0)[18]. Microglial morphometric properties were evaluated by quantifying the number of processes, total length (in µm), sum of intersections. Sholl analysis[19] was used to quantify the number of intersections at radial intervals of 2 µm starting from the central point of the soma.

Bio-Plex Immunoassay

Supernatants derived from cultures of PBMCs treated with ConA or left untreated for 48h were tested in duplicate with the Bio-Plex Multiplex Immunoassay System (BioRad Laboratories, Hercules,USA), according to the manufacturer's protocol.

Statistical analysis

The normal distribution of samples was checked with Shapiro–Wilks test and the homogeneity of variances was evaluated with F test. When the equal variance criterion was violated, the Welch correction was used. The nonparametric tests Mann–Whitney tests and Kruskal-Wallis followed by Dunn's post-hoc test was chosen when data was not normally distributed. Otherwise, Student *t* test and ANOVA followed by Tukey's post-hoc test were used. All statistical tests were performed with Origin 9.0 (OriginLab Corporation, USA), and Prism 8.2 (GraphPad Software Inc., USA). The tests are two-sided and confidence interval of 95% ($p \leq 0.05$) was required for values to be statistically significant. Data are shown as mean ± standard deviation (SD).

RESULTS

Effect of blood-borne human immune cell perfusion

In order to respectively induce and mimic a mild BBB impairment, LPS and h-recombinant albumin (hALB) were injected into the arterial stream before performing immune cells perfusion. The

selective effect of blood-borne immune cells was investigated by perfusing the isolated *in vitro* brain with LPS and hALB together with either resting or ConA-activated PBMCs derived from healthy subjects (Figure1A-C).

The treatment with LPS and hALB (protocol A in Figure1A; *n*=3) occasionally induced short spreading depression phenomena in both PC and hippocampal formation (data not shown), and never induced epileptiform activity (graphic in Figure C). Neither arterial perfusion with LPS+hALB+na-PBMCs ($10x10^6$ cells, *n*=5; Fig 1A, C; protocol B) nor perfusion with a-PBMCs only ($10x10^6$ cells; *n*=4; Fig 1A,C; protocol C) induced electrophysiological alterations. Conversely, treatment with LPS+hALB+a-PBMCs ($10x10^6$ cells, n=8; Figure1A-C; protocol D) was able to evoke SLEs with a mean duration of 3.9±2.3 min, characterized by rhythmic discharges of fast activity initially at about 15Hz in the hippocampus/m-EC region.

Of note, the arterial perfusion of cell-free supernatants from a-PBMCs (*n*=4; Figure1A, protocol E) induced spontaneous SLEs with a mean duration of 2.1±0.6 min (Figure1B; see also below).

In order to exclude any involvement of Concanavalin A in seizure generation, in a separate set of experiments, LPS, hALB and ConA were co-perfused in the isolated *in vitro* brain. Neither changes in LOT-evoked potentials nor induction of SLEs occurred in medial entorhinal cortex and hippocampus (*n*=2; data not shown).

Modulation of αCaMKII activation

Next, we evaluated excitatory transmission changes with western blot (WB) analysis of CaMKII, a major component of excitatory synapses implicated in seizure activity[20]. The expression levels of total αCaMKII and active CaMKII phosphorylated in Thr^{286} (CaMKII-P^{286} or p286) in hippocampal homogenate, particulate (enriched membrane) and soluble (enriched cytosolic) fractions obtained from brains which either experienced or not SLEs, were analyzed. A reduction in CaMKII-P^{286} protein levels was observed in both total homogenate (Figure2A, B; H=6.71, p≤0.05) and membrane fractions (Figure 2C, B, H=6.71; p≤0.05) of brains in which hippocampal SLEs were recorded (protocol D and E) compared to conditions that had no epileptiform discharges (protocol B). Conversely, no differences in CaMKII-P^{286} protein levels were observed in the cytosolic

fractions (Figure 2B, D; H=4.38; p=0.112). On the other hand, total αCaMKII levels were not altered in any subcellular fractions analyzed. As expected, the comparison of protein ratio CaMKII-P^{286}/total CaMKII was decreased in both homogenate (H=6.62; p≤0.05) and membrane fractions (H=7; p≤0.05) of *in vitro* isolated brains that experienced SLEs (protocol D and E) *vs* basal conditions (protocol B). No differences in CaMKII-P^{286}/total CaMKII ratio was observed in cytosolic fractions among the different experimental groups (H= 3.08; p=0.2148).

BBB opening associated with activated human immune cells

The morphologic and functional integrity of BBB in the *in vitro* isolated guinea pig brain preparation has been previously demonstrated[13]. BBB permeability changes were evaluated in four groups of isolated brains: control brains maintained *in vitro* for the same time as experimental brains (*n*=4); FITC–albumin perfused brains 60 min after LPS and hALB perfusion (*n*=3); FITC–albumin perfused brains 60 min after ConA-activated PBMCs arterial perfusion (*n*=4) and FITC–albumin perfused brains after LPS, hALB and ConA-activated PBMCs perfusion (*n*=8). A significant leakage of arterial-injected FITC–albumin into the parenchyma of limbic regions compared to control and LPS+ hALB treated brains was observed in the FITC-albumin perfused brains after LPS,hALB and ConA-activated PBMCs. A weak extravasation was observed when a-PBMCs were applied without pre-activation of the endothelium with LPS (Figure 3; F (3) =38,7; p≤0.001). Interestingly, immune cells were occasionally detected within the brain parenchyma or inside the vessels (*n*=4; data not shown).

Morphological analysis and reconstruction of microglial cells

The morphological changes of microglia in cerebral tissue of brains after protocols B, C, D and E was evaluated (Figure 5; *n*= 5 for each protocol). Sholl analysis showed smaller values after LPS+hALB+a-hPBMC and LPS+hALB+supernatant treatments (protocols D and E, respectively) compared to LPS+hALB+na-hPBMC and a-hPBMC treatments (protocols B and C, respectively; Figure 5B, C). As expected, microglia cells had lower number of processes (Figure 5D; F(3)= 27.66; p≤0.001), total length (Figure 5E; F(3)= 38.99; p≤0.001) and sum of intersections (Figure 5F; F(3)= 19.22; p≤0.001)following LPS+hALB+a-hPBMC perfusion (protocol D) and

LPS+hALB+Supern. (protocol E; p≤0.001, p≤0.01 and p≤0.05, respectively) in comparison to LPS+hALB+na-hPBMC perfusion (protocol B). Furthermore, microglia cells with lower number of processes (p≤0.001), total length (p≤0.001) and sum of intersections (p≤0.01) were observed in LPS+hALB+a-hPBMC (protocol D) in comparison to a-hPBMC perfused animals (protocol C). The same trend in number of processes (p≤0.01) and total length (p≤0.05) was observed when LPS+hALB+Supern. (protocol E) was compared to a-hPBMC (protocol C) microglia cells.

Cytokine analysis

Next, we investigated the mediators released by a-PBMCs eventually involved in BBB opening and seizure precipitation (see Figure1A, protocol E), by measuring the levels of inflammatory cytokines and chemokines in supernatants of resting (*n*= 8) and ConA-activated (*n*= 5) PBMCs (Figure 4). High expression levels of inflammatory mediators were observed: IL-1β (1.612 ± 0.8372 ng/ml *vs* 0.007 ± 0.005 ng/ml; p≤ 0.001; ConA-activated *vs* resting hPBMCs, respectively, for this and the following measures); TNF-α (1.473 ± 1.426ng/ml *vs* 0.004 ± 0.005 ng/ml; p≤ 0.001), IL-6 (20.009 ± 11.8ng/ml *vs* 0.029 ± 0.02 ng/ml; p≤ 0.05), INF-γ (8.805 ± 4.395ng/ml *vs* 0.003 ± 0.008 ng/ml; p≤ 0.001), IL-10 (4.661 ± 3.274ng/ml *vs* 0.007 ± 0.007 ng/ml; p≤ 0.005), MIP3α (1.557 ± 1.479ng/ml *vs* 0.000 ± 0.000 ng/ml; p≤ 0.001) and IL-17A (3.341 ± 2.638ng/ml *vs* 0.000 ± 0.000 ng/ml; p≤ 0.001).

Effect of guinea pig splenocytes perfusion

To rule out the potential contribution of human cells in the results obtained, guinea pig spleen cells activated with ConA for 48h were used. As expected, evoked spontaneous ictal discharges with a mean duration of 2.65±1.1 min was recorded (*n*=3), whereas arterial perfusion of resting splenocytes (*n*=2) did not induce any spontaneous ictal activity (data not shown) Of note, activated or resting splenocytes infusion was preceded by LPS+hALB treatment.

DISCUSSION

Our study provides the first direct demonstration that in a condition of LPS-induced mild endothelium activation, arterial perfusion of a-PBMCs (and cytokine release) and serum albumin are able to induce microgliosis and seizure generation (illustrated in Figure 6).

In the isolated brain preparation, LPS, hALB and blood-borne cells can be perfused at any time, enabling us to discriminate the role of each molecule in a pathological process that cannot be otherwise individually or independently analyzed in other models.

Peripheral immune cell infiltration into the brain parenchyma has been shown to induce the activation of specific pro-inflammatory cascades[5]. We choose to focus on PBMCs since they represent an easy accessible source of immune cells, in particular T and B lymphocytes and monocytes[21]. Infiltration of lymphocytes has been observed in a variety of focal epilepsies such as autoimmune epilepsies (AE), focal cerebral dysplasias, tuberous sclerosis complex and Rasmussen encephalitis[5]. Interestingly, an increased frequency of epileptic events has also been reported in multiple sclerosis, a prototypical CNS inflammatory disorder characterized by extensive infiltration of T cells in both white and gray matter[22]. By assuming that PBMCs of AE patients display an active profile, we preliminarily utilized human PBMCs pre-treated with concanavalin A in our acute *in vitro* preparation to set the background for future studies aimed to directly evaluate the role of PBMCs and cytokines obtained from patients with inflammatory and immunomediated encephalitis associated with seizures.

As previously mentioned, BBB permeability leads to the extravasation into the brain parenchyma of serum proteins and immune cells, triggering inflammation and ictogenesis.

Serum albumin extravasation, due to its negative charge, alters the neuronal membrane charge, contributing to an acute increase in neuronal excitability[23] and, at the same time, is able to disrupt the neuronal and glial membrane homeostasis[15,24]. In our experimental conditions[15], hALB is perfused at 4mg/ml, which falls within the range associated with BBB damage occurring in a pathology associated condition[25]. Co-perfusion of LPS, hALB and na-PBMCs (and autologous resting guinea pig splenocytes) never generated SLEs or microgliosis. Interestingly, exclusive a-PBMCs perfusion induced an increase in the percentage of FITC-albumin extravasation and microglia activation compared to control or LPS+hALB+na-hPBMC condition, underlying the pivotal

role of a-PBMCs and the cytokines detected in their supernatant in affecting BBB permeability and microglia morphology. As expected, simultaneous injection of LPS, hALB and a-hPBMCs (or ConA activated autologous splenocytes) worsened BBB permeability, promoting hALB extravasation (phase 4 in Figure 6). As consequence, simultaneous perfusion of LPS, hALB and a-hPBMCs or LPS, hALB and supernatant was able to trigger microglial activation and seizure occurrence (phase 5 in Figure 6). This upholds the concept that co-activation of mononuclear cells and cerebral endothelium is an essential requirement for serum albumin extravasation, brain inflammation and excitability increase[4,26].

Surprisingly, few PBMCs were detected in the brain parenchyma or adhered to endothelial cells and since trans-endothelial migration of adherent leukocytes is a fast process that requires few minutes[27] and considering the established BBB impairment, we expected to observe transmigrated PBMCs. This evidence suggests that in our experimental conditions, missing blood-borne factors preclude PBMCs diapedesis. The most likely explanation for the absence of massive transmigration in our experimental conditions could be two-fold: the lack of signals originating from the circulating blood and the insufficient production of chemoattractants from brain parenchyma in response to PBMCs rolling and tethering the endothelium. Interestingly, cells of adaptive immunity such as T and B cells or NK cells were not detected in brain parenchyma in chronic rats or human epileptic tissue[28] , as well as in those AEs with antibodies against membrane antigens[5], revealing the strong impact of immune-derived factors on neuronal networks sustaining seizure activity.

Our study confirmed that PBMCs-secreted mediators, including IL-1β, TNF-α, IL-6, INF-γ, IL-10, IL-17A, MIP3α, were sufficient to compromise BBB permeability, to elicit serum albumin extravasation and to trigger seizure occurrence. In line with our observation many clinical and animal studies support the role of these specific cytokines in maintaining the complex relationship between seizure and the immune system[29,30,31,32,33,34]. The effects of serum albumin extravasation and a-PBMCs-induced release of inflammatory mediators was for the first time analyzed in regard to microglial activation. We observed that microglial cells promptly responded to these immunological triggers through a significant change in their morphological phenotype towards a more activated state demonstrated by their amoeboid shape[35]. Both proinflammatory cytokines and

chemokines released by a-PBMCs and hALB extravasation promote resident microglia activation[36], which in turn are expected to activate astrocytes and exacerbate reactive pathways[10]. In our experiments, microgliosis was evident when either ConA-activated hPBMCs or a-hPBMC supernatant only (both associated with LPS and hALB infusion) were perfused into the *in vitro* guinea pig brain. Glial cells have a plethora of housekeeping functions such as sensing and responding to alterations in energy supply, neuronal activity, extracellular ion concentrations, osmolarity, among many other processes. Their dysfunction has been linked to epilepsy mainly through hyperexcitability and inflammatory pathways[37]. Due to the acute nature of our experimental preparation, our study did not specifically show if this gliosis is permanent or transient, and if the latter was the case, for how long they remained in an activated-like phenotype state.

Lastly, we evaluated CaMKII expression in the different experimental protocols to verify if excitatory neurotransmission could be rapidly enhanced in our experimental conditions. A reduction in the activation of CaMKII has been demonstrated in a variety of *in vitro* and *in vivo* seizure/epilepsy models[38]. Here we showed a reduction of αCaMKII activity, as measured by CaMKII-P^{286} protein levels, in both whole hippocampal homogenate and membrane-enriched fractions obtained from guinea pig brains that experienced SLEs, compared to brains where no ictal activity was recorded. Decreased CaMKII activity was not accompanied by a significant loss of enzyme protein; this is in line with previous data suggesting that CaMKII inhibition and/or a modification of post-translational mechanism, possibly through NMDA receptor activation, may play a functional role in the expression of neuronal hyperexcitability and ictal activity[39]. It is now widely accepted that the pro-inflammatory cytokines, especially IL-1β, TNFα and IL-6, affect BBB permeability and also contribute to enhance excitatory transmission and decrease inhibitory transmission[40]. Since the occurrence of SLEs in our experimental setting is also associated with the release of inflammatory mediators from a-PBMCs, we can speculate that the modulation of αCaMKII activation in seizure-expressing brains may represent the expression of an effect of cytokines on CaMKII-mediated modulation of excitatory synaptic transmission.

CONCLUSIONS

Activated PBMCs and their secreted molecules seem to have an impact on neuro-vascular compartment and brain excitability. The present findings are preliminary to further *in vitro* studies on the pathogenic role of peripheral immune-mediated inflammation on ictogenesis. Our experiments might shed light on identifying key mediators involved in seizure generation in order to identify novel treatments in epilepsies due to inflammatory and dysimmune causes.

ACKNOWLEDGMENTS

The study was funded by the Fondazione Epilessia LICE - grant 2019, by the European Union's Horizon 2020 Research and Innovation Programme under the Marie Sklodowska-Curie grant agreement no. 722053 (EU-GliaPhD), by the Italian Health Ministry and by the EPICARE project of the Associazione Paolo Zorzi per le Neuroscienze. M.C. is supported by FISM – Fondazione Italiana Sclerosi Multipla – cod. 2019/R-Single/065 and by '5 per mille' public funding. We thank Paola Cavalcante for kind support in Bioplex samples processing and Francesca Andreetta and Emilio Ciusani for helpful scientific discussion.

DISCLOSURE OF CONFLICTS OF INTEREST

The authors have nothing to disclose.

ETHICAL PUBLICATION STATEMENT

All the authors confirm that they have read the Journal's position on issues involved in ethical publication and affirm that this report is consistent with those guidelines.

REFERENCES

1. Marchi N, Granata T, Janigro D. Inflammatory pathways of seizure disorders. Trends in Neurosciences 2014;37:55–65 .
2. van Vliet EA, da Costa Araujo S, Redeker S, van Schaik R, Aronica E, Gorter JA. Blood-brain barrier leakage may lead to progression of temporal lobe epilepsy. Brain

2007;130:521–534.

3. Swissa E, Serlin Y, Vazana U, Prager O, Friedman A. Blood–brain barrier dysfunction in status epileptics: Mechanisms and role in epileptogenesis. Epilepsy and Behavior 2019;101.

4. Fabene PF, Navarro MG, Martinello M, Rossi B, Merigo F, Ottoboni L, et al. A role for leukocyte-endothelial adhesion mechanisms in epilepsy. Nat Med 2008;14:1377–1383.

5. Bauer J, Becker AJ, Elyaman W, Peltola J, Rüegg S, Titulaer MJ, et al. Innate and adaptive immunity in human epilepsies. Epilepsia 2017;58:57–68.

6. Vezzani A, Granata T. Brain inflammation in epilepsy: experimental and clinical evidence. Epilepsia 2005;46:1724–1743.

7. Dalmau J, Graus F. Antibody-Mediated Encephalitis. New England Journal of Medicine 2018;378:840–851.

8. Bien CG, Granata T, Antozzi C, Cross JH, Dulac O, Kurthen M, et al. Pathogenesis, diagnosis and treatment of Rasmussen encephalitis: a European consensus statement. Brain 2005;128:454–471.

9. Marchi N, Granata T, Ghosh C, Janigro D. Blood-brain barrier dysfunction and epilepsy: Pathophysiologic role and therapeutic approaches. Epilepsia 2012;53:1877–1886.

10. Vila Verde D, Zimmer T, Cattalini A, Pereira MF, Vliet E, Testa G, et al. Seizure activity and brain damage in a model of focal non convulsive status epilepticus. Neuropathology and Applied Neurobiology 2021;nan.12693.

11. Vezzani A, Balosso S, Ravizza T. Neuroinflammatory pathways as treatment targets and biomarkers in epilepsy. Nature Reviews Neurology 2019;15:459–472.

12. de Curtis M, Biella G, Buccellati C, Folco G. Simultaneous investigation of the neuronal and vascular compartments in the guinea pig brain isolated in vitro. Brain Research Protocols 1998;3:221–228.

13. Librizzi L, Janigro D, De Biasi S, de Curtis M. Blood brain barrier preservation in the in vitro isolated guinea -pig brain preparation . Journal of Neuroscience Research 2001;66:289–297.

14. Librizzi L, Mazzetti S, Pastori C, Frigerio S, Salmaggi A, Buccellati C, et al. Activation of cerebral endothelium is required for mononuclear cell recruitment in a novel in vitro model of brain inflammation. Neuroscience 2006;137(4):1211-9.

15. Noé FM, Bellistri E, Colciaghi F, Cipelletti B, Battaglia G, De Curtis M, et al. Kainic acid-induced albumin leak across the blood-brain barrier facilitates epileptiform hyperexcitability in limbic regions. Epilepsia 2016;57(6):967-76.

16. Costanza M, Poliani PL, Portararo P, Cappetti B, Musio S, Pagani F, et al. DNA threads released by activated CD4+ T lymphocytes provide autocrine costimulation. Proceedings of the National Academy of Sciences of the United States of America 2019;116:8985–8994.

17. Colciaghi F, Nobili P, Cipelletti B, Cagnoli C, Zambon S, Locatelli D, et al. Targeting PSD95-nNOS interaction by Tat-N-dimer peptide during status epilepticus is neuroprotective in MAM-pilocarpine rat model. Neuropharmacology 2019;153:82–97.

18. Tavares G, Martins M, Correia JS, Sardinha VM, Guerra-Gomes S, das Neves SP, et al. Employing an open-source tool to assess astrocyte tridimensional structure. Brain Structure and Function 2017;222:1989–1999.

19. Schindelin J, Arganda-Carreras I, Frise E, Kaynig V, Longair M, Pietzsch T, et al. Fiji: An open-source platform for biological-image analysis. Nature Methods 2012;9: 676–682.

20. Yamagata Y, Imoto K, Obata K. A mechanism for the inactivation of Ca2+/calmodulin-dependent protein kinase II during prolonged seizure activity and its consequence after the recovery from seizure activity in rats in vivo. Neuroscience 2006;140:981–992.

21. Kleiveland C, Kleiveland C. Peripheral blood mononuclear cells. in The Impact of Food Bioactives on Health: In Vitro and Ex Vivo Models 2015;161–167 (Springer International Publishing).

22. Burman J, Zelano J. Epilepsy in multiple sclerosis: A nationwide population-based register study. Neurology 2017; 89(24):2462–8.

23. Frigerio F, Frasca A, Weissberg I, Parrella S, Friedman A, Vezzani A, et al. Long-lasting pro-ictogenic effects induced in vivo by rat brain exposure to serum albumin in the absence of concomitant pathology. Epilepsia 2012;53:1887–1897.

24. Marchi N, Angelov L, Masaryk T, Fazio V, Granata T, Hernandez N, et al. Seizure-promoting effect of blood-brain barrier disruption. Epilepsia 2007;48:732–742.

25. Hooper C, Pinteaux-Jones F, Fry VAH, Sevastou IG, Baker D, Heales SJ, et al. Differential effects of albumin on microglia and macrophages; Implications for neurodegeneration following blood-brain barrier damage. Journal of Neurochemistry 2009;109:694–705.

26. Fabene PF, Bramanti P, Constantin G. The emerging role for chemokines in epilepsy. Journal of Neuroimmunology 2010;224:22–27.

27. Muller WA. Leukocyte-endothelial-cell interactions in leukocyte transmigration and the inflammatory response. Trends Immunol 2003;24:327–334.

28. Ravizza T, Gagliardi B, Noe F, Boer K, Aronica E, Vezzani A. Innate and adaptive immunity during epileptogenesis and spontaneous seizures: evidence from experimental models and human temporal lobe epilepsy. Neurobiol Dis 2008;29:142–160.

29. Vezzani A, Balosso S, Ravizza T. The role of cytokines in the pathophysiology of epilepsy. Brain, behavior, and immunity 2008;22:797–803.

30. Stellwagen D, Beattie EC, Seo JY, Malenka RC. Differential regulation of AMPA receptor and GABA receptor trafficking by tumor necrosis factor-α. Journal of Neuroscience 2005;25: 3219–3228.

31. Getts DR, Matsumoto I, Müller M, Getts MT, Radford J, Shrestha B, et al. Role of IFN-γ in an experimental murine model of West Nile virus-induced seizures. Journal of Neurochemistry 2007;103:1019–1030.

32. Mao LY, Ding J, Peng WF, Ma Y, Zhang YH, Fan W, et al. Interictal interleukin-17A levels are elevated and correlate with seizure severity of epilepsy patients. Epilepsia. 2013;54(9):e142-5.

33. de Vries EE, van den Munckhof B, Braun KPJ, van Royen-Kerkhof A, de Jager W, Jansen FE. Inflammatory mediators in human epilepsy: A systematic review and meta-analysis. Neuroscience and Biobehavioral Reviews 2016;63:177–190.

34. Liu JX, Cao X, Liu Y, Tang FR. Altered expression of neuronal CCR6 during pilocarpine induced status epilepticus in mice. Epilepsy Research 2016;126:45–52.

35. Kreutzberg GW. Microglia: A sensor for pathological events in the CNS. Trends in Neurosciences 1996;19: 312–318.

36. Wesselingh R, Butzkueven H, Buzzard K, Tarlinton D, O'Brien TJ, Monif M. Innate Immunity in the Central Nervous System: A Missing Piece of the Autoimmune Encephalitis Puzzle? Frontiers in Immunology 2019;10:2066.

37. Devinsky O, Vezzani A, O'Brien TJ, Jette N, Scheffer IE, De Curtis M, et al. Epilepsy. Nature Reviews Disease Primers 2018;4:18024.

38. Dong Y, Rosenberg HC. Prolonged changes in Ca2+/calmodulin-dependent protein kinase II after a brief pentylenetetrazol seizure; Potential role in kindling. Epilepsy Research 2004;58:107–117.

39. Kochan LD, Churn SB, Omojokun O, Rice A, Delorenzo RJ. Status epilepticus results in an N-methyl-D-aspartate receptor-dependent inhibition of Ca2+/calmodulin-dependent kinase II activity in the rat. Neuroscience 1999;95:735–743.

40. Klement W, Garbelli R, Zub E, Rossini L, Tassi L, Girard B, et al. Seizure progression and inflammatory mediators promote pericytosis and pericyte-microglia clustering at the cerebrovasculature. Neurobiology of Disease 2018;11:70–81.

FIGURE LEGENDS

Figure 1. Schematic drawing of the different experimental protocols utilized in the study. **A)** The *in vitro* brain was arterially perfused with: (A) LPS and human recombinant albumin (hALB); (B) LPS, hALB and non-activated hPBMCs; (C) ConA-activated hPBMCs (a-hPBMC); (D) LPS, hALB and a-hPBMCs; (E) LPS, hALB and cell-free supernatants from a-hPBMC. At the end of each experiments the brains that underwent protocol A, C, D were perfused with a bolus of FITC-albumin to evaluate its diffusion in the brain. Each experimental protocol lasted 4 hours. **B)** Epileptiform discharges simultaneously recorded in medial entorhinal cortex (mEnt) and in hippocampal CA1. The simultaneous perfusion of LPS, hALB and a-hPBMCs (protocol C) and a-

hPBMCs supernatant (protocol E) shown in the left and in the right panel, respectively, induced one single seizure-like event. **C)** Mean values of seizures duration induced by the application of all experimental protocols. The application of protocols A, B and C did not induce SLEs.

Figure 2. Modulation of CaMKII activation in seizure-experienced brains. **A)** Western blot analysis of CaMKII and its active form phospho-thr286-CaMKII (p286) performed in whole hippocampal homogenates (A), membrane (C) and cytosolic fractions (D) obtained from three guinea-pig brains as treated with protocol B (non-activated PBMCs), protocol D (activated-PBMCs) and protocol E (supernatants from activated- PBMCs). Note the decreased expression of the activated p286 form in total homogenates (A) in protocol D and E vs protocol B brains, that was paralleled by similar expression of total CaMKII in all experimental group. A similar expression pattern of p286 form was obtained in membrane fractions (C), while no differences emerged in the cytosolic fractions (D) among groups, indicating a selective decrease of membrane recruitment of active p286-CaMKII in seizure-experienced brains. **B)** Bargrams showing the quantification of the immunoreactive ratio CaMKII/actin, p286/actin and p286/total CaMKII in all experimental conditions, in the different cellular fractions. All protein ratios were expressed as a percentage of Protocol B. p286/actin and p286/CamKII ratio were significantly decreased in both whole homogenates and in membrane fractions of brain treated with both protocol D and E when compared to Protocol B. Homogenate: *p≤0.05; Membranes: **p≤0.01 by Kruskall Wallis followed by post-hoc Dunn's test. No significant differences were obtained in the cytosolic fraction. Significant differences were never obtained between protocol D and E in all fractions. Similarly, significant differences were never obtained in CaMKII protein level in any subcellular fractions.

Figure 3. Effects of ictal activity on BBB permeability. A) Representative photomicrographs of intraparenchymal FITC–albumin signal in the hippocampal formation in control condition (ctr) and after the application of the experimental protocols C and D. Under control condition and after application of protocol C no BBB damage occurred. Brain sections showed exclusively intraluminal signal with scattered perivascular spots (white arrow). Areas of a wide FITC–albumin parenchymal

extravasation around vessels (white arrowheads) were detected after the application of protocol D. Calibration bar =100 μm. **B)** Quantification of parenchymal FITC–albumin leakage in the experimental conditions reported in Figure 1A. FITC-albumin leakage has been evaluated as spot area (number of pixels) and it is expressed as a percentage of values versus control experiments ***p ≤ 0.001 by ANOVA followed by post hoc Tukey's test.

Figure 4. Cytokine production by *in vitro* cultured PBMCs. PBMCs were isolated from healthy donors and stimulated *in vitro* with ConA (2 μg/ml) (n = 5) or left nonactivated (n=8) for 48h. Concentrations of inflammatory mediators in supernatants were evaluated with BioPlex Immunoassay (Bio-Rad). * p≤ 0.05 with Student *t* test (exclusively for IL-6), ** p≤ 0.005 and *** p≤ 0.001 with Mann-Whitney test.

Figure 5. Morphological analysis and reconstruction of microglial cells in ventral hippocampal CA1. **A)** Representative morphologies of microglial cells in Iba-1 immunofluorescence coronal sections in the ventral CA1 hippocampal regions are shown for LPS+hALB+na-hPBMC, a-hPBMC, LPS+hALB+a-hPBMC, LPS+hALB+Supernatant (Supern.); the correspondent reconstruction of the microglial cell is illustrated in the lower part of the panel. Calibration bar = 20 μm. **B)** Number of intersections per 2 μm radius plotted against the distance from the cell soma in ventral CA1 hippocampus. Grey line: LPS+hALB+na-hPBMC. Blue line: a-hPBMC. Red line: LPS+hALB+a-hPBMC. Purple line: LPS+hALB+Supern. **C)** Representative Sholl analysis setting of a manually reconstructed microglia cell from LPS+hALB+na-hPBMC (left) and LPS+hALB+a-hPBMC (right). The circles centered around the soma are separated by radial intervals of 2 μm. **D)** Number of processes per 2 μm radius of microglia cells in ventral CA1 hippocampal formation from LPS+hALB+na-hPBMC (*n*=15 cells), a-hPBMC (*n*=15 cells), LPS+hALB+a-hPBMC (*n*=20 cells) and LPS+hALB+Supern. (*n*=15 cells) guinea pigs (5 cells *per* animal). **E)** Total length *per* 2 μm radius of microglia cells in ventral CA1 region from LPS+hALB+na-hPBMC (*n*=15 cells), a-hPBMC (*n*=15 cells), LPS+hALB+a-hPBMC (*n*=20 cells) and LPS+hALB+Supern. (*n*=15 cells) guinea pigs (5 cells *per* animal). **F)** Sum of intersections per

2 µm radius of microglia cells in ventral hippocampal CA1 area from LPS+hALB+na-hPBMC (*n*=15 cells), a-hPBMC (*n*=15 cells), LPS+hALB+a-hPBMC (*n*=20 cells) and LPS+hALB+Supern. (*n*=15 cells) guinea pigs (5 cells *per* animal). *p≤0.05; ** p≤0.01; *** p≤0.001 by ANOVA followed by post hoc Tukey's test. For D, E and F: Grey plots: LPS+hALB+na-hPBMC; Blue plots: a-hPBMC; Red plots: LPS+hALB+a-hPBMC; Purple plots: LPS+hALB+Supern.

Figure 6. Proposed scheme of how activated PBMCs might cause microglia activation and seizure activity. 1-2) PBMCs' activation (from blue to red cells) produces the release of inflammatory cytokines (ck) into the bloodstream. **3)** Activated PBMCs (either free-floating or after endothelial adhesion) release cytokines that **4)** enhance BBB permeability and promote the extravasation of serum albumin into brain parenchyma. **5**) Pro-inflammatory cytokines and serum albumin diffusion into brain parenchyma activate resident microglia and stimulate seizure occurrence.

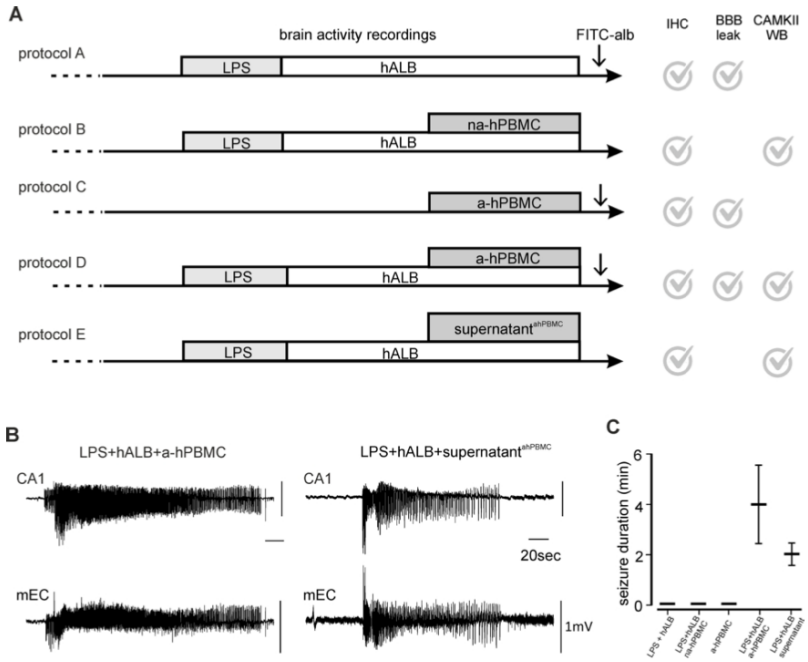

Figure 1. Schematic drawing of the different experimental protocols utilized in the study. A) The in vitro brain was arterially perfused with: (A) LPS and human recombinant albumin (hALB); (B) LPS, hALB and non-activated hPBMCs; (C) ConA-activated hPBMCs (a-hPBMC); (D) LPS, hALB and a-hPBMCs; (E) LPS, hALB and cell-free supernatants from a-hPBMC. At the end of each experiments the brains that underwent protocol A, C, D were perfused with a bolus of FITC-albumin to evaluate its diffusion in the brain. Each experimental protocol lasted 4 hours. B) Epileptiform discharges simultaneously recorded in medial entorhinal cortex (mEnt) and in hippocampal CA1. The simultaneous perfusion of LPS, hALB and a-hPBMCs (protocol C) and a-hPBMCs supernatant (protocol E) shown in the left and in the right panel, respectively, induced one single seizure-like event. C) Mean values of seizures duration induced by the application of all experimental protocols. The application of protocols A, B and C did not induce SLEs.

169x137mm (300 x 300 DPI)

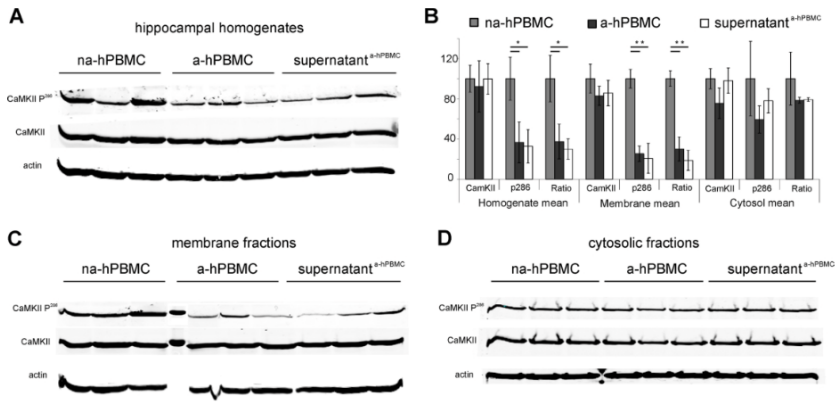

Figure 2. Modulation of CaMKII activation in seizure-experienced brains. A) Western blot analysis of CaMKII and its active form phospho-thr286-CaMKII (p286) performed in whole hippocampal homogenates (A), membrane (C) and cytosolic fractions (D) obtained from three guinea-pig brains as treated with protocol B (non-activated PBMCs), protocol D (activated-PBMCs) and protocol E (supernatants from activated- PBMCs). Note the decreased expression of the activated p286 form in total homogenates (A) in protocol D and E vs protocol B brains, that was paralleled by similar expression of total CaMKII in all experimental group. A similar expression pattern of p286 form was obtained in membrane fractions (C), while no differences emerged in the cytosolic fractions (D) among groups, indicating a selective decrease of membrane recruitment of active p286-CaMKII in seizure-experienced brains. B) Bargrams showing the quantification of the immunoreactive ratio CaMKII/actin, p286/actin and p286/total CaMKII in all experimental conditions, in the different cellular fractions. All protein ratios were expressed as a percentage of Protocol B. p286/actin and p286/CamKII ratio were significantly decreased in both whole homogenates and in membrane fractions of brain treated with both protocol D and E when compared to Protocol B. Homogenate: *p≤0.05; Membranes: **p≤0.01 by Kruskall Wallis followed by post-hoc Dunn's test. No significant differences were obtained in the cytosolic fraction. Significant differences were never obtained between protocol D and E in all fractions. Similarly, significant differences were never obtained in CaMKII protein level in any subcellular fractions.

165x79mm (300 x 300 DPI)

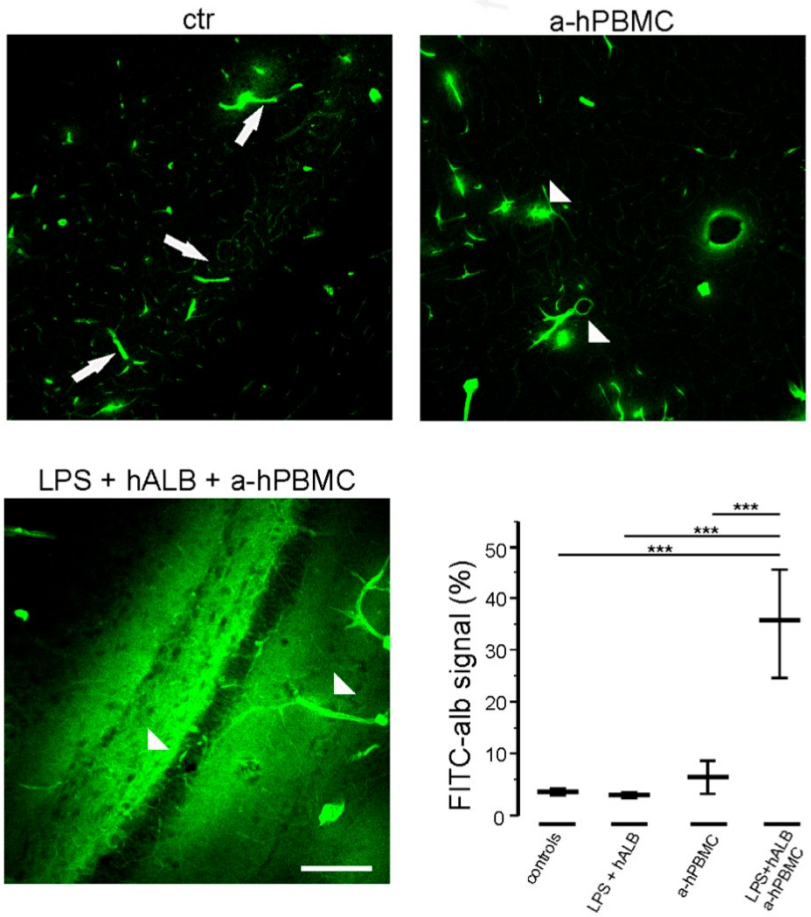

Figure 3. Effects of ictal activity on BBB permeability. A) Representative photomicrographs of intraparenchymal FITC–albumin signal in the hippocampal formation in control condition (ctr) and after the application of the experimental protocols C and D. Under control condition and after application of protocol C no BBB damage occurred. Brain sections showed exclusively intraluminal signal with scattered perivascular spots (white arrow). Areas of a wide FITC–albumin parenchymal extravasation around vessels (white arrowheads) were detected after the application of protocol D. Calibration bar =100 μm. B) Quantification of parenchymal FITC–albumin leakage in the experimental conditions reported in Figure 1A. FITC-albumin leakage has been evaluated as spot area (number of pixels) and it is expressed as a percentage of values versus control experiments ***p ≤ 0.001 by ANOVA followed by post hoc Tukey's test.

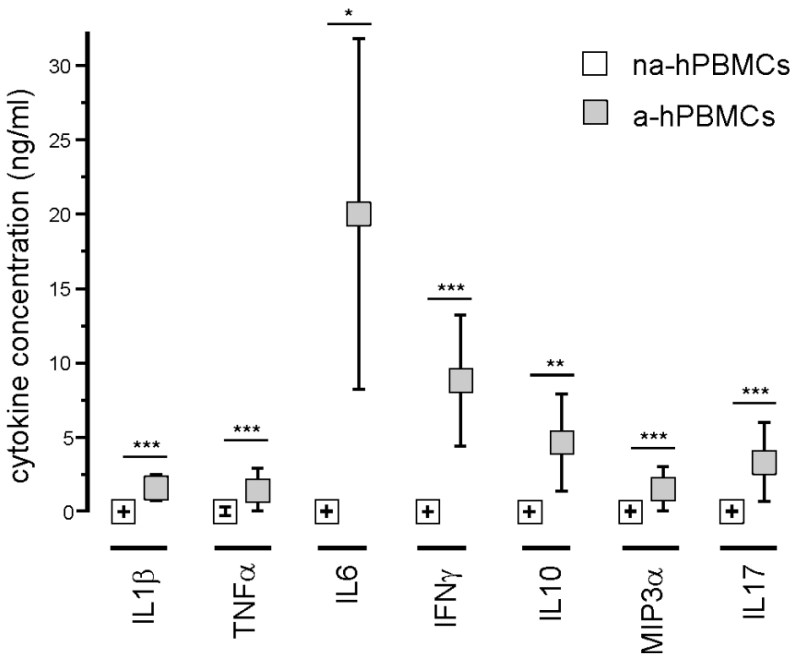

Figure 4. Cytokine production by in vitro cultured PBMCs. PBMCs were isolated from healthy donors and stimulated in vitro with ConA (2 □g/ml) (n = 5) or left nonactivated (n=8) for 48h. Concentrations of inflammatory mediators in supernatants were evaluated with BioPlex Immunoassay (Bio-Rad). * p≤ 0.05 with Student t test (exclusively for IL-6), ** p≤ 0.005 and *** p≤ 0.001 with Mann-Whitney test.

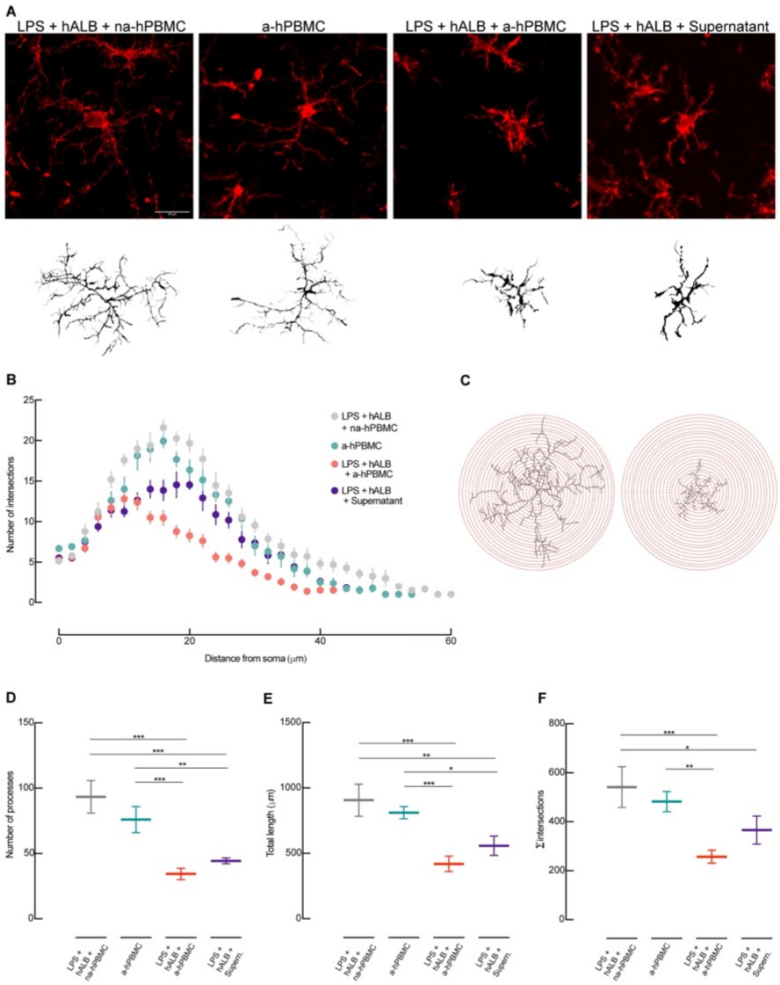

Figure 5. Morphological analysis and reconstruction of microglial cells in ventral hippocampal CA1. A) Representative morphologies of microglial cells in Iba-1 immunofluorescence coronal sections in the ventral CA1 hippocampal regions are shown for LPS+hALB+na-hPBMC, a-hPBMC, LPS+hALB+a-hPBMC, LPS+hALB+Supernatant (Supern.); the correspondent reconstruction of the microglial cell is illustrated in the lower part of the panel. Calibration bar = 20 μm. B) Number of intersections per 2 μm radius plotted against the distance from the cell soma in ventral CA1 hippocampus. Grey line: LPS+hALB+na-hPBMC. Blue line: a-hPBMC. Red line: LPS+hALB+a-hPBMC. Purple line: LPS+hALB+Supern. C) Representative Sholl analysis setting of a manually reconstructed microglia cell from LPS+hALB+na-hPBMC (left) and LPS+hALB+a-hPBMC (right). The circles centered around the soma are separated by radial intervals of 2 μm. D) Number of processes per 2 μm radius of microglia cells in ventral CA1 hippocampal formation from LPS+hALB+na-hPBMC (n=15 cells), a-hPBMC (n=15 cells), LPS+hALB+a-hPBMC (n=20 cells) and LPS+hALB+Supern. (n=15 cells) guinea pigs (5 cells per animal). E) Total length per 2 μm radius of microglia cells in ventral CA1 region from LPS+hALB+na-hPBMC (n=15 cells), a-hPBMC (n=15 cells), LPS+hALB+a-hPBMC (n=20 cells) and LPS+hALB+Supern. (n=15 cells) guinea pigs (5 cells per animal). F)

Sum of intersections per 2 µm radius of microglia cells in ventral hippocampal CA1 area from LPS+hALB+na-hPBMC (n=15 cells), a-hPBMC (n=15 cells), LPS+hALB+a-hPBMC (n=20 cells) and LPS+hALB+Supern. (n=15 cells) guinea pigs (5 cells per animal). *p≤0.05; ** p≤0.01; *** p≤0.001 by ANOVA followed by post hoc Tukey's test. For D, E and F: Grey plots: LPS+hALB+na-hPBMC; Blue plots: a-hPBMC; Red plots: LPS+hALB+a-hPBMC; Purple plots: LPS+hALB+Supern.

167x210mm (300 x 300 DPI)

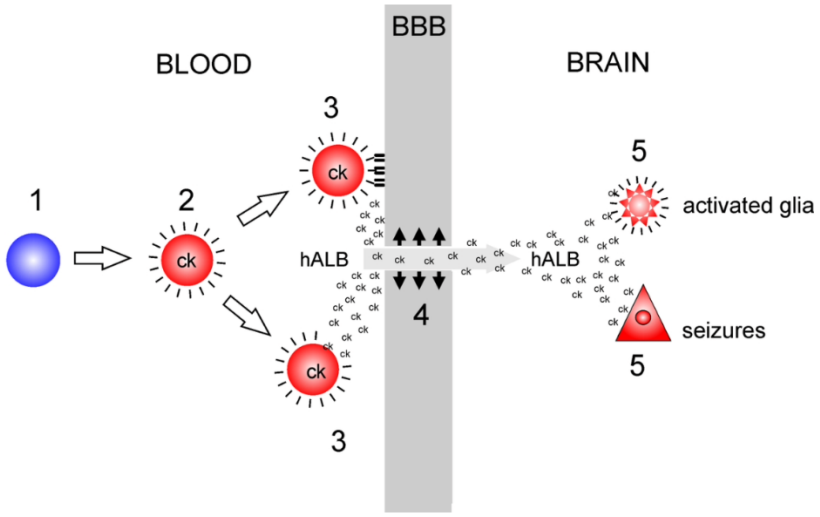

Figure 6. Proposed scheme of how activated PBMCs might cause microglia activation and seizure activity. 1-2) PBMCs' activation (from blue to red cells) produces the release of inflammatory cytokines (ck) into the bloodstream. 3) Activated PBMCs (either free-floating or after endothelial adhesion) release cytokines that 4) enhance BBB permeability and promote the extravasation of serum albumin into brain parenchyma. 5) Pro-inflammatory cytokines and serum albumin diffusion into brain parenchyma activate resident microglia and stimulate seizure occurrence.

113x71mm (300 x 300 DPI)

In submission

Brain pathology in focal *status epilepticus:* evidence from experimental models

Marco de Curtis[1], Andrea O. Rossetti[2], Diogo Vila Verde[1], Erwin A. van Vliet[3,4], Christine T Ekdahl[5,6]

(1) Epilepsy Unit, Fondazione IRCCS Istituto Neurologico *Carlo Besta*, Milano, Italy.

(2) Department of Clinical Neuroscience, University Hospital (CHUV) and University of Lausanne, Lausanne, Switzerland

(3) Swammerdam Institute for Life Sciences, Center for Neuroscience, University of Amsterdam, Science Park 904, P.O. box 94246, 1090 GE, Amsterdam, the Netherlands.

(4) Amsterdam UMC, University of Amsterdam, Department of (Neuro)Pathology, Amsterdam Neuroscience, Meibergdreef 9, Amsterdam, the Netherlands

(5) Division of Clinical Neurophysiology, Lund University, Sweden

(6) Lund Epilepsy Center, Dept Clinical Sciences, Lund University, Sweden

Correspondence to Marco de Curtis, Fondazione Istituto Neurologico *Carlo Besta*, Milano, Italy.

Abstract

Status Epilepticus (SE) is often a neurological emergency characterized by abnormally sustained, longer than habitual seizures. The new ILAE classification reports that SE "*…can have long-term consequences including neuronal death, neuronal injury…depending on the type and duration of seizures*". While it is accepted that generalized convulsive SE exerts a detrimental strain on the brain, it is not clear if other forms of SE, such as focal non-convulsive SE, produces brain pathology and contribute to long-term deficits in patients. Available clinical and experimental data struggle to discriminate the specific action of the underlying SE etiologies from that exerted by epileptiform activity. This information is clinically highly relevant for better stratification of treatment, which may include both medical and surgical intervention for seizure control. Here we reviewed experimental studies of brain tissue following focal SE, with emphasis on focal non-convulsive SE, as its subtle symptoms often delay clinical diagnosis and intervention. We present a broad repertoire of brain pathologies observed in the most commonly used animal models and highlight the need for more stringent description of seizure semiology and the duration of SE in order for higher accuracy in predicting clinical translation.

Abbreviations

blood-brain barrier = BBB; focal non-convulsive status epilepticus = FncSE; focal onset evolving into bilateral convulsive status epilepticus = FbcSE; focal status epilepticus = FSE; non-convulsive status epilepticus = ncSE; spontaneous recurrent seizures = SRS; status epilepticus = SE; pilocarpine = PILO; kainic acid = KA

Status Epilepticus (SE) is every so often a neurological emergency with considerable morbidity, characterized by continuous epileptic seizures and epileptic activity that persist without remission longer than a habitual seizure. SE may occur in patients with a pre-existing epileptic disorder or can be provoked by an acute *de novo* etiology. The current SE classification set by the International League Against Epilepsy (ILAE) defines two conceptual timelines for SE: a first threshold beyond which seizures are unlikely to stop (e.g., 5 minutes for generalized convulsive seizures, 10 minutes for focal seizures), and a second threshold after which the SE "*…can have long-term consequences…including neuronal death, neuronal injury…depending on the type and duration of seizures"*. For generalized convulsive SE, the latter has been estimated to about 30 minutes, mostly based on animal studies[2]. In addition, imaging studies revealed that structural alterations may occur in the brain of patients minutes/hours after SE resolution (Tien et al 1995; Fernandez-Torre et al. 2006). However, while it is generally accepted that prolonged and recurrent convulsive generalized seizures occurring during a SE have detrimental effects on the brain, it is not clear if focal SE (FSE) with mainly non-convulsive seizures and focal epileptiform discharges (a frequent human SE condition – see following paragraph) produce persistent epileptogenic brain pathology (Jableen et al., 2017; Szabo et al., 2005). Moreover, it remains controversial if epileptiform activities during focal SE exacerbate brain pathology per se (Shorvon and Sen 2020;) and contribute to the clinical outcome. Available clinical data are not enough to discriminate the specific actions of the underlying SE etiologies from that exerted by prolonged epileptiform activity. The distinction is clinically relevant, since swift and complete SE cessation is commonly enforced to prevent long-term consequences after both focal and generalized SE, in spite of the fact that aggressive anti-seizure treatment protocols may expose patients to potentially dangerous side effects (Kämppi et al 2015).

The correlation between FSE, with the emphasis on focal non-convulsive SE (FncSE), and brain pathology will here be reviewed and discussed in the light of *ad hoc* experiments performed in animal models presented in experimental studies. We highlight a need for stringent description of the epileptic seizures as well as duration of seizures in the experimental studies in order to increase the accuracy for predicting clinical translation.

1. What is a *focal status epilepticus*?

The ILAE classification categorizes SE semiology into either prominent motor symptoms (such as convulsive/ myoclonic/ focal motor/ tonic/ hyperkinetic behavior) or less prominent motor non-convulsive symptoms, according the predominant clinical manifestation (Table 1). The term *non-convulsive status epilepticus (ncSE*) includes SE with a variety of seizures that do not generate overt motor movements, and feature symptoms specifically generated by the recruited cortical region. The semiology of ncSE can be characterized by coma or more subtle clinical features, such as a change in behavior or mental status, aphasia or minimal motor symptoms (like the clonus of a finger) lasting longer than 10 min – often several hours/days. NcSE with this elusive symptomatology, is regularly diagnosed with the help of electroencephalogram (EEG) recordings that may demonstrate continuous epileptiform discharges (Trinka et al 2015, Kaplan PW 2000; Sutter and Kaplan 2013; Leitinger et al., 2016).

NcSE can be of generalized or focal origin. Primarily generalized ncSE typically occur in patients with genetic (idiopathic) epilepsy (*e.g.*, absence SE) and seems to carry few evident long-term morbidities and neuropathology. Indeed, absence SE may occur several times in patients without obvious clinical *sequelae*. However, rare examples of continuous non-convulsive generalized epileptiform activity associated with cognitive, neurological and psychiatric disorders exist, such electrical status epilepticus in slow wave sleep in children (Maltoni and Posar, 2016). Though, a clear delimitation of both the occurrence and consequences of generalized ncSE in children with epileptic encephalopathies are encumbered with difficulties (Hamad et al 2020). NcSE may also present as a focal non-convulsive status epilepticus (FncSE) in patients with i.e., a localized (focal) brain dysfunction or epilepsy syndrome, characterized by focal epileptiform EEG discharges. FncSE may or may not secondarily spread to both brain hemispheres and either remain as non-convulsive, or more often evolve into bilateral convulsive tonic-clonic seizures with diffuse bilateral synchronized EEG patterns (focal onset evolving into bilateral convulsive status epilepticus – FbcSE). Recent epidemiological assessments of SE that applied the new ILAE definition, indicate a prevalence of FncSE in 36 % of all SE cases. When FbcSE arising from an initial FncSE is included in the statistics, its prevalence increases to 65-85%, suggesting that FSE indeed represents the most frequent form of human SE. In addition, at the cessation of FbcSE, FncSE or electrographic seizures may continue with subtle or no overt

semiology, highlighting the value of continuous/repeated EEG recordings for correct diagnosis (Abend et al. 2014).

The majority of FSE etiologies in adults are related to acute brain injuries (such as cerebrovascular diseases, brain trauma, and infections) or progressive conditions (i.e, tumors and neurodegenerative diseases) associated with focal alterations in the brain. The most common causes of pediatric SE are fever, acute metabolic derangements, central nervous system infections, as well as suspected genetic causes (Zimmer and Korff 2020; Abend 2014). Several studies suggest that the underlying etiology, the age of onset, and pre-existing comorbidities represent the most important determinants of SE prognosis and long-term consequences. However, patients suffering from SE have a higher mortality than patients with the same underlying disease (stroke, anoxic-hypoxic encephalopathy, etc.) that do not experience a SE, especially in elderly (Canas et al 2018) and possibly in younger children (Zimmern and Korff 2020; Abend 2014). Clinical studies in adults suggest that FncSE may be associated with transient brain impairment and cognitive/neurological decline, followed by resolution and clinical remission within hours/days/weeks (Jabeen et al 2017, Szabo et al 2005; Verity and Golding 1993). Neuropsychological examinations performed before and after both FncSE and FbcSE in patients with pre-existing epilepsy has found divergent results in cognitive functions (Kaplan 2001). The lack of consensus regarding permanent neurological and psychiatric FncSE sequelae adds uncertainty to the prescription of aggressive treatment. Although the practical importance of treating timely and at sufficient doses to prevent SE refractoriness has been demonstrated [11], mortality does not seem to be affected by i.e., medical coma induction after adjusting for SE refractoriness (Alvarez et al., 2016).

Because of the intrinsic limitations of the studies performed on patient cohorts, clinical research has so far not reached a clear conclusion about how seizure activity occurring during FncSE may be related to brain pathology.

2. Animal models of focal status epilepticus

The broad criteria utilized for the ILAE clinical classification could also be applied to the studies performed in animal models of SE. Models of generalized, focal and multifocal SE have been developed to reproduce parts of the human conditions by pharmacological treatments, electrical stimulation and other lesional means. The most popular models of systemic pharmacological application of chemo-convulsants are the intra-peritoneal/subcutaneous pilocarpine (PILO) and kainic acid (KA) models (Sperk 1994; Curia et al., 2008; Levesque et al, 2013; Dudek and Staley 2017; Kelly and Coulter, 2017). With a few exceptions (Krsek et al 2001; 2004), systemic KA or PILO injections initiate focal and multifocal seizures that rapidly evolve into prolonged bilateral convulsive SE. In various animal species (rat, mouse, cat) these treatments induce a SE condition that results in multifocal lesions of cortical and subcortical brain structures, the latter most likely responsible for the overall relative high mortality observed in these models. PILO and KA systemic applications result in typical temporal-limbic pathology mimicking the pathology observed in human temporal lobe epilepsy with hippocampal sclerosis (Aronica et al., 2017). However, it is also associated with lesions outside the hippocampal region, in brain areas that are usually not affected in patients with temporal lobe epilepsy with hippocampal sclerosis (Falconer 1974; Engel 2001; Blümcke et al., 2012; Sloviter 2008). In addition, both PILO- and KA-induced SE are associated with prolonged bilateral convulsive SE, blood-brain barrier disruption leading to extravasation of plasma proteins, increased serum cytokines, brain potassium elevation and large variability of the multifocal brain pathology (Marchi et al.2007; van Vliet et al., 2014; Mendes et al., 2019). All these elements identify the systemic PILO and KA SE treatments as models of (multi)focal SE evolving into FbcSE, equivalent to the A1b sub-category from the clinical classification (Table 1). The accumulated burden of convulsive SE in these models results in a hypoxic heart insult, irregular breathing, altered autonomic activity or cardiac problems such as QT interval prolongation, that could be related to sudden unexpected death in epilepsy (SUDEP) and the relatively high mortality rate (Fabene et al., 2007; Lucchi et al 2015; Read et al, 2015; Auzmendu et al.). Therefore, systemic convulsant applications associated with primarily multifocal and convulsive SE represent conditions with several possible mechanisms leading to brain pathology and are excluded from further detailed analyses in the present review.

Intracerebral focal electrical stimulation (van Vliet and Gorter, 2017) and focal chemoconvulsant applications (Jefferys 2016; Henshall et al., 2017a; 2017b) have been utilized to induce a FSE primarily within the limbic system or the neocortex. A detailed description of the models is outlined in Tables 2 and 3. These procedures induce self-sustained focal seizures that can also evolve into bilateral convulsive seizures. Incidentally, since most FSE stimulation and drug application protocols involve temporal lobe areas, in the majority of animal's brain pathologies and spontaneous seizures with similarities to focal mesial TLE develop over weeks after the initial provoked FSE. In the subsequent chronic epileptic condition, the animals may exhibit both focal and focal evolving into bilateral convulsive seizures. The semiology of the FSE varies between animals as well as during the FSE *per se*, even if similar stimulation/chemical regime is applied. The behavior typically includes a combination of non-convulsive symptoms such as reduced alertness, explorative stereotypic automatisms, oral/facial twitches, chewing, salivation that over time may or may not evolve into brief or extensive periods of bilateral convulsive tonic-clonic movements (Nissinen et al 2000; Mohapel et al., 2004; Lothman et al 1989; McIntyre et al 1991; Goodman 1998). Seizure behavior are often graded in rodents according to a motor symptom-oriented severity scale (Racine scale - Racine 1972). The degree of different seizure semiology and electrographic activity (focal vs bilateral convulsive behavior and focal vs bilateral epileptiform activity) during the FSE may explain the variation of reported brain pathology in these FSE models (Sutula and Pitkanen 2002). In addition, the SE duration varies significantly between studies, from typically cessation after 2 hours by treatment intervention to self-termination of SE after several hours. Optimally, a FncSE model (equivalent to the B2 sub-category in Table 1) should be characterized by focal seizures and a minimal (if any) number of bilateral convulsive seizures. This aspect is important for clinical translation, since evolvement into prolonged periods of bilateral convulsive seizures and FbcSE (category A1.b in Table 1) is associated with more extensive brain damage compared to FncSE with only minimal bilateral convulsions (Mohapel et al 2004 Neurobiol Dis). In the following paragraphs, the reported brain pathology in animal models of FncSE and FbcSE will be analyzed in detail.

2.1 FncSE and FbcSE induced by intracerebral drug application

Chemoconvulsants have been applied focally to brain areas such as the hippocampus, amygdala, olfactory cortex, entorhinal cortex and motor cortex to induce a focal SE. Intracerebral injection of KA is the most widely used FSE model (Table 2). A small volume of KA (typically 50 nl- 0.5 µL, depending on both the animal species and the brain area) at a concentration that varies between 7 ng up to 0.4 µg is slowly injected through a cannula stereotactically inserted in the target region (Henshall, 2017). A KA injection is typically followed within a few minutes by continuous epileptiform activity in the injected region and the animal exhibits focal seizure semiology. Due to the presence of mainly non-convulsive seizures (> than 50% of the total duration of the provoked SE), these protocols have very low mortality rates and FSE typically recedes spontaneously within 20 hours. In few studies FSE was terminated at 2-10 hours with intraperitoneal injection of either benzodiazepines or barbiturates (Table 2). At present, diverse procedures are utilized in different centers; depending on the dose of KA, the site of injection and the animal species, local KA application can induce exclusively FncSE or focal motor SE or FbcSE. KA has most frequently been injected unilaterally into the CA1 and CA3 regions of the hippocampus. Administration of PILO has only been evaluated after injection into the dentate hilus of the hippocampus (Furtado et al., 2002; 2011). Different protocols utilized in mice, guinea pigs and cats are less likely to generate FbcSE (grey shading rows in Table 2), while both high and low doses of KA in rats are most likely associated with a FbcSE. The number/percentage of secondarily generalized convulsive seizures have been evaluated either with video and EEG monitoring or video alone (Table 2). In all reviewed studies, KA induced a localized excitotoxic damage at the site of injection (hippocampal CA1 and CA3 regions, amygdala or neocortex), regardless of FbcSE or FncSE associated semiology. In FbcSE conditions, markers of tissue pathology such as neuronal degeneration (evaluated with Fluoro-Jade, TUNEL staining or caspase immunostainings), neuronal loss (NeuN stainings), gliosis (GFAP, vimentin, CD11 b/c and/or Iba-1 immunostainings) were observed with variable intensity and expression, also in the contralateral and ipsilateral limbic regions remote from the KA injection site. Contralateral hippocampi and amygdala showed cell loss and gliosis in regions homologous to KA injection. Diffuse tissue alterations outside the limbic areas, such as thalamus (Moneta et al., 2002), amygdala (Ben-Ari et al., 1980; Tanaka et al., 1982; 1985), piriform cortex (Tanaka et al., 1985) and perirhinal cortex (Mouri et al., 2008) were also found when higher doses of KA were injected in the

hippocampus, long-lasting SE was generated and/or when convulsive seizures were prominent during FbcSE (Schwarcz et al., 1978; Schwob et al., 1980;Cavalheiro et al., 1982; Tanaka et al., 1982; Berger et al., 1989; Araki et al., 2002). Interestingly, contralateral pathology was not evident in more recent FbcSE studies when unilateral CA1 or amygdala KA injections were performed in mice (Schauwecker et al., 2002; Mouri et al., 2008; Pernot et al., 2011, Welzel et al., 2019) or rats (Rattka et al., 2013). However, Bragin (1999) reported hippocampal cell loss contralateral to hippocampal CA1 KA injection in rats, without giving details on the type of seizures observed during the SE. The progression of pathology in areas remote from the injection site were also observed in the FbcSE intra-amygdala KA model in the rat (Ben-Ari et al., 1980; Schwob et al 1980), cat (Tanaka et al., 1985) and mouse (Araki et al., 2002; Mouri et al., 2008) as well as in the intrahippocampal PILO rat model (Furtado et al., 2001; 2002).

Contralateral or remote cell death and gliosis outside the injection site were not detected in FncSE models in which bilateral convulsive seizures were occasionally observed in the late SE phases of self-termined SE and for less than 10% of the total FSE duration (French et al., 1982; Leite et al., 1996 Bouilleret et al., 1999; Moneta et al., 2000; Riban et al., 2002; Arabadzisz et al., 2005; Groticke et al., 2008;Carriero et al. 2012; Noè et al. 2019; Weitzel et al., 2019; Vila-Verde et al, 2021), with a few exceptions; Mathern and colleagues described bilateral sprouting of mossy fibers in the dentate gyrus after unilateral KA injection in the rat (Mathern et al., 1993). Magloczky and colleagues utilized focal KA injection in CA3 to generate a FncSE (and also FbcSE at higher doses) that was not monitored with video-EEG and that resulted in morphological alterations also within the contralateral hippocampus (Magloczky et al., 1993; 1995). No neuropathological changes in remote brain regions outside the limbic system were observed when FncSE was induced by local KA injection in the hippocampus (Tanaka et al., 1982; Riban et al., 2002). In the studies by Tanaka in the cat, mild secondary neuronal loss was observed in the amygdala following intrahippocampal injection of high doses of KA (Tanaka 1982) and in the piriform cortex, following intra-amygdala KA application (Tanaka 1985).

The intrahippocampal KA model (injection in CA1) applied to the guinea pig demonstrated cell loss, neuronal MAP staining changes, gliosis (both astro and micro), enhanced blood-brain barrier (BBB) permeability and apoptotic cell death in the KA injected hippocampus 3 days after FncSE. Gliosis and

neuronal cell loss, but not BBB changes, was confirmed at 1-2 months after FncSE (Carriero et al., 2012; Noè et al., 2019; Vila Verde et al., 2021). In this model, reactive gliosis associated with aquaporin 4 and Kir4.1 RNA expression transiently activated in the CA1 region contralateral to KA injection; these changes were not maintained 1 month after FncSE, suggesting that seizure activity during FncSE may transiently activate brain areas remote to the KA injection, but does not promote long-lasting detrimental changes (Vila Verde et al., 2021).

With the exception of the work by Tanaka in the cat (1985), most studies that utilized unilateral intra-amygdala KA protocols reported frequent convulsive seizures during SE, configuring a condition of FbcSE that correlated with contralateral and extralimbic neuropathological alterations. Berger demonstrated that intra-amygdala KA injection in rats was able to occasionally induce FncSE in a minority of animals that demonstrated local pathology and gliosis extended to the contralateral CA3 and to the ipsilateral piriform cortex (Berger et al., 1989). In this study, video-EEG monitoring was not performed. For the intracortical KA model, developed by Bedner et al. (2015) in the mouse, both FncSE and FbcSE was reported, without evidence of contralateral pathology.

Unilateral intrahippocampal injection of PILO (2.4 mg/μL, 1 μL) into the dentate *hilus* of rats leads to SE within 30 minutes in 76% of all animals (Furtado et al. 2011). SE was characterized by repeated cycles of head and forelimb myoclonus, rearing, and falling; the number of animals developing either FncSE or FbcSE was not reported (Furtado et al., 2002). Ninety minutes after SE onset, FSE was stopped by diazepam injection (5 mg/kg). About 71% of the animals develop recurrent spontaneous seizures after SE, but this may be an underestimation, since video recordings were performed only for 8 hours/day (Furtado et al., 2002; 2011). Neuropathological alterations included bilateral neurodegeneration as detected by Fluoro-Jade positive cells in the dentate *hilus*, CA3 and CA1 ipsi- and contralateral to PILO injection site, as well as in the amygdala 24 hours after FSE (Furtado et al., 2011).

2.2 FncSE and FbcSE induced by intracerebral electrical stimulation

Intracerebral high frequency electrical stimulation is an elegant and clinically relevant, but laborious procedure to induce FSE (Table 3). Since stimulation can be timely stopped, the severity of the SE is often better controlled in these models in comparison to the pharmacological models. Two main stimulation protocols are commonly utilized: high frequency (>20 Hz) tetanic stimulation for max 60-90 min with or without low frequency (<2Hz) prolonged stimulation, leading to a self-sustained SE (Bertram and Lothman 1993; Gorter and van Vliet, 2017). As for the intracerebral convulsant application models, these procedures lead to either FbcSE or FncSE.

In the electrical FSE rodent models, rats or mice are most often implanted stereotactically with isolated stainless-steel electrodes into the posterior ventral hippocampus, angular bundle or the amygdala. One to two weeks later, thresholds for electrographic after discharges can be assessed by 1 sec train of current square-wave biphasic pulses (1 ms durations, 50 Hz) with increased intensity by 10 μA increments at 1 min intervals until at least 5 sec duration of after discharge is evoked. This is followed by 60-90min of suprathreshold electrical stimulation with 10 sec of 1 ms 50 Hz square-wave biphasic pulses. A typical stimulation and recording pattern during this electrical provocation is a cycle of repeated continuous stimulation for 9 min, momentarily shut-off for 1 min to allow EEG recordings from the same or additionally implanted electrodes and then stimulation is again resumed for another 9 min etc. The stimulation period induces a subsequent self-sustained, prolonged electrographic seizure/FSE after stimulation has ended that can be further evaluated in terms of both semiology and EEG activity. The FSE was originally described to self-terminate after around 8 hours (Bertram and Lothman 1993) but has in several subsequent studies been interrupted after 90-120 min by benzodiazepines or general anesthesia with pentobarbital. Interestingly, when SE is stopped too late is becomes refractory to benzodiazepines, since the GABA receptors internalize.

The seizure semiology during the FSE varies between animals. Typically, three distinct behavioral types have been described: (1) impaired alertness and explorative/ambulatory automatisms, briefly interrupted by few bilateral convulsive seizures; (2) impaired alertness, masticatory behavior with oral/facial twitches, chewing, and salivation, briefly interrupted by few bilateral convulsive seizures; and (3) mainly focal evolving into bilateral convulsive seizures. The first two seizure types correspond predominantly

(>90% of the time) to FncSE, while the third type primarily mimics FbcSE (>70% of the time; Mohapel et al 2004).

The majority of animals exhibit acute symptomatic focal seizures within the first week post-FSE induced in the hippocampus (Avdic et al Ekdahl 2018) to an extent similar to patients with SE without previous known seizure history (30-80% described in Maytal et al 1989, Hauser et al 1990, Verity et al 1993) and in about two-thirds of both rats that experienced FncSE and FbcSE, spontaneous recurrent seizures (SRS) can be observed chronically (Bonde et al 2006). This percentage resembles figures presented in the study of Brandt and colleagues where about 80% of the rats developed a chronic epileptic condition with spontaneous recurrent seizures (SRS) after self-sustained FSE in the amygdala. The proportion of rats developing SRS depended on the type of self-sustained SE. Only 33% of the rats developed SRS after a self-sustained FncSE with primarily focal seizures, compared to >90% in case of FbcSE with bilateral convulsive seizures. Interruption of different forms of self-sustained FSE in amygdala with diazepam after 90 min prevented development of epilepsy, while a FbcSE duration of 4 h consistently produced chronic epilepsy in >90% of rats (Brandt et al., 2003).

In these FSE models, local pathology at the site of stimulation is apparent (Table 3). Following hippocampal FncSE contralateral hippocampal alterations is also evident, including neuronal pathology, microglial and astrocytic activation, neurogenesis and synaptic alterations (Ekdahl et al 2003, Avdic et al 2018, Mohapel et al 2004, Jackson et al 2012). Similar to the KA and PILO models of FSE, the pathology after electrically induced FSE becomes even more pronounced after FbcSE (Mohapel et al 2004, Brandt et al 2003). In addition, several reports have demonstrated that electrically induced FncSE and FbcSE can produce tissue alterations also outside limbic regions (Table 3), even as far as the retina (Avdic et al 2019), and the acute immune reaction is prominent both in epileptic brain tissue and systemically in blood samples (Avdic et al 2018, 2019). Evidently, FncSE leads to increased cytokine and chemokine levels, such as IL-6 and KC/GRO, within 6hrs in the hippocampus as well as in the blood (Avdic et al 2018).

At 1-week post-FSE, neurogenesis is evident and cell proliferation and neuroblast production is equally increased after FncSE and FbcSE, both ipsi- and contralateral to the stimulating electrode. However, the survival rate of the newborn neurons 1 month later is >100% higher after FncSE than FbcSE SE

(Mohapel et al 2004). Initially, the newborn neurons undergo a caspase/mitochondrial-dependent programmed cell death/apoptosis at 1-week post-SE to an equal extent following FncSE and FbcSE, but it continues particularly in rats that exhibited FbcSE. The cell death of newly formed neurons is partly due to the FSE-induced immune response (Ekdahl et al 2003, Iosif et al 2006, Ali et al 2015, Chugh et al 2016) rather than the subsequent SRS, since additional electrically provoked focal and focal evolving into bilateral convulsive seizures at 1-4 weeks post-FncSE do not affect the survival of the newborn neurons (Ekdahl et al 2002, Ekdahl et al 2003). However, an over-all large reduction in FSE-induced hippocampal neuronal cell loss following immune modulation post-FncSE has not been described (Ekdahl et al 2003, Ali et al 2015). Instead, NeuN protein levels within the hippocampus are particularly reduced in FncSE rats that develop SRS (Avdic et al 2018).

The striking regenerative neurogenesis can be observed within the hippocampus of both animals and humans (Eriksson et al 1998), though its production is several times increased after epileptic seizures. A cohort of newborn DG neurons generated for 2 weeks post-FncSE has been estimated to represent almost 10% of the total number of granule cells within the DG 6 months later, as compared to 2% in non-stimulated electrode-implanted control rats (Bonde et al 2006). In what way the production of new granule cells may compensate for the initial FSE-induced neuronal alterations and the loss of interneurons in particular within the DG, is still unclear (Jakobs et al 2006). Stereological cell counts of the entire population of mature NeuN+ granule cells have only shown increased tissue volume, compared to control animals 5 weeks post-FncSE, while a significant reduction in DG cell number was observed in FbcSE animals (Mohapel et al 2004). Both FncSE and FbcSE show similar reduction of DG neuropeptide Y interneurons 5 weeks post-SE, though only FbcSE leads to fewer parvalbumin interneurons. Necrosis of pyramidal cells and cell dispersion in CA1 and CA3 regions of the hippocampus are observed after both self-sustained FSE profiles, as early as 24hrs up to at least 6 months post-insult (Mohapel et al 2004; Bonde et al 2006; Avdic et al 2018).

To what extent the degree of cell death and other plastic structural changes such as mossy fiber sprouting post-FncSE is correlated to number of subsequent spontaneous seizures is also not clear (Nissinen et al 2000, Gorter et al van Vliet 2001). No such correlation was observed in studies of electrically induced FSE in the amygdala, except for the previously mentioned study by Brandt et al. (2003). Furthermore, the

average latency to the first spontaneous seizure tended to be longer after FncSE in amygdala (69 days) than after FbcSE (46 or 42 days, respectively; Brandt et al., 2003). When diazepam was given 60-90 min after FSE onset, chronic spontaneous seizures did not develop, which may be in contrast to FSE induced in the hippocampus or due to a high natural variation among the rats. Interruption of a FbcSE after 180 min was only performed in two rats, resulting in SRS in one of these rats. Self-sustained SE was interrupted after 240 min, resulting in SRS in 93% of the rats (Brandt et al., 2003).

A positive correlation between the diffusion of the epileptic discharge during the FSE and the development of chronic epilepsy was also suggested following electrical stimulation of the angle bundle, the fibre tract that contains fibers of entorhinal cortex neurons projecting to the hippocampus (Pitkanen et al 2002, Nissinen et al 2000, Gorter et al van Vliet 2001). Neither of these studies explicitly separated rats with FncSE from FbcSE semiology. Finally, MRI studies were developed to evaluate animals after FncSE in parallel with immunohistochemical analysis of both neuronal death and inflammatory-immune reaction. DTI did not reveal robust long-lasting changes in fractional anisotropy within the hippocampal epileptic focus (Avdic et al 2018).

2.3 Other models with FncSE features

Intracerebroventricular injection KA (2.5-100 ng) immediately leads to wet dog shake behaviour in rats and this lasts up to 2h after administration, depending on the dose (Kleinrok 1980), suggesting the occurrence of FncSE. However, EEG recordings were not performed, thus this cannot be confirmed. Higher doses (up to 800 ng) lead to convulsive SE (Nadler 1978). Neuronal damage is exclusively present within the hippocampus, but with increasing dose, neuronal damage is also evident in additional brain regions, including some of the thalamic nuclei, amygdala and deep layers of the cerebral neocortex (Nadler 1978). In another study, it was reported that neuronal degeneration appeared to be more closely related to total seizure duration than to the dose of KA (Sater 1987).

Bilateral and longitudinally extensive intrahippocampal microinjections of Stable Substance P–saporin conjugate (SSP-saporin) in rats was utilized to induce temporal lobe epilepsy (Martin and Sloviter

2001; Chum et al., 2019). The ribosome inactivating protein, saporin, specifically targets substance P receptor-expressing inhibitory interneurons that constitutively express the neurokinin-1 receptors and internalize this neurotoxin. The intrahippocampal injection of SSP-saporin virtually completely eliminate GABAergic interneurons and caused negligible nonspecific damage at the injection site. This selective neurotoxic treatment caused no obvious acute behavioral effects. However, 4 days post-injection, rats exhibited episodes of wet-dog shakes and focal motor seizures for a few days (Chun et al., 2019). Even though a clear FSE did not develop, this model could be interpreted as a mild and subtle form of FncSE. Epileptiform pathophysiology was consistently observed only within areas of SPR ablation, whereas relatively normal evoked responses were recorded from immediately adjacent and relatively unaffected regions.

Low doses (<0.3, 1 and 4 mg/kg) of KA given intravenously to rats caused a stereo-typed sequence of staring spells, wet dog shakes, automatisms over 1–2 h (Lothman and Collins, 1981) that correlated with electrographic seizures in limbic areas, mainly in the hippocampus. Higher doses (7 and 12 mg/kg) induced seizure activity in both limbic and cortical areas, coincident with severe convulsions. Quantitative 2-deoxyglucose autoradiography showed that the hippocampus, subiculum, piriform and entorhinal cortices, septum and amygdala were most sensitive to metabolic changes during mild limbic seizures. Neuronal damage was seen in these areas of intense seizure activity (Lothman and Collins 1981). Similarly, low doses KA (up to 6 mg/kg) given subcutaneously (Sperk 1985) or intraperitoneally (Schwob 1980; Koryntova 1997 and 1998), leads to automatisms (e.g., wet dogs shake) lasting for up to 2 h, while with higher doses (>6 mg/kg) generalized seizures start to occur. Behavioral analysis shows that a low dose KA induced changes in the structure of spontaneous behavior and impaired the processes related to maintenance of attention (Mikulecka 1999). Histological analysis did not reveal any pathological changes in the hippocampus for low doses of KA, while higher doses lead to neuronal damage, as well as decreased GAD activity in the hippocampus and Chat activity in the amygdala and piriform cortex (Sperk 1985, Schwob 1980; Koryntova 1997 and 1998). Doses of PILO (100-200 mg/kg) given intraperitoneally results in NCSE within 15 min (with automatisms, including eye-blinking, chewing and teeth chattering) lasting up to 2 h without any neuropathological alterations, while higher doses lead to convulsive SE and hippocampal, extrahippocampal as well as cortical neuronal damage (Turski 1983&1985). In later studies, an even lower dose of PILO (15

mg/kg) was used (Cook 1998, Mikulecka 2000, Krsek et al., 2001; 2004). Within the first minutes after injection of this dose hypersalivation, chewing, licking, tearing, face washing, piloerection, and creep walking was observed. The animals alternated creep walking with long periods of sitting with head nodding and chewing for approximately 70 min, followed by repeated episodes of exploration–searching activity and self-grooming that gradually disappeared within 2 h (Mikulecka 2000, Krsek et al., 2001; 2004). Epileptic EEG activity was observed both in the neocortex and, predominantly, in the hippocampus during this behavior (Krsek et al., 2001; 2004; Mikulecka et al., 2000). Animals with NCSE tested 5 days or 4 months after SE displayed memory deficits but not learning deficits (Cook 1998) as well as profound impairment of behavior as well as responsiveness to exteroceptive stimuli (Mikulecka 2000). In contrast to previous studies using higher doses of PILO, Nissl staining revealed neuronal damage (mainly pyramidal cells) in layer V of diverse neocortical fields 1-2 weeks after PILO injection (Mikulecka 2000, Krsek et al., 2001). Less pronounced neuronal damage was evident in piriform cortex layer II, as well as in the rostral striatum, thalamus, and substantia nigra pars reticulata (Krsek et al., 2001). Furthermore, the number of PV-IR and CB-IR neurons in the neocortical area was lower in PILO-treated animals as compared to controls (Krk et al., 2004).

Recently, it has been shown that rats have a non-convulsive SE after lateral-fluid percussion injury (Andrade et al., 2019), a model of traumatic brain injury (TBI; Pitkänen et al., 2017) that is evoked with a fluid percussion device via a brief (21-23 ms) focal pressure pulse to the exposed dura mater. During the first 72 hours after TBI, rats had seizures intermingled with other epileptiform EEG patterns suggestive of a FncSE, including occipital intermittent rhythmic delta activity, lateralized or generalized periodic discharges, spike-and-wave complexes, poly-spikes, poly-spike-and-wave complexes, generalized continuous spiking, burst suppression, or suppression (Andrade et al., 2019). Fifty-nine percent of electrographic seizures were not accompanied by behavioral manifestations (Andrade et al., 2019). A novel mouse model of FscSE has been developed recently (Singh et al., 2020) by administering homocysteine i.p. after cortical cobalt implantation. With homocysteine being an agonist of NMDA receptors combined with the decreased GABAergic inhibition caused by cobalt injection, this model induces a convulsive SE with neocortical edema and injury mimicking human SE following cortical injury induced by trauma or hemorrhage. FbcSE-

induced neuronal loss in the cortex, thalamus, and amygdala but not in the hippocampus. Of note, in the hemisphere contralateral to cobalt application, no neurodegeneration was present in any brain region.

3. Correlation with clinical findings and conclusions

The consequences of exhibiting a FncSE and subsequent seizures and brain pathology first become of clinical concern when they i) precede or induce cognitive, neurological or psychiatric dysfunction evident for the patient, ii) disrupt normal brain function leading to developmental delay, disrupted circadian rhythm or sleep architecture, iii) contribute to seizure progression in terms of seizure severity, frequency, involvement of additional epileptogenic brain areas, and treatment resistance, or iv) alter systemic body functions such as cardiorespiratory function and increase the risk of sudden unexpected death due to epilepsy (SUDEP). The fact that the patients are often also stigmatized by their seizures and develop additional co-morbidities, such as psychiatric disorders and non-epileptic psychogenic seizures, makes adequate level of seizure control even more delicate.

There has been a long-lasting effort starting in the early 19th century to determine when, how and to what extent prolonged or brief repeated seizures induce pathology to the brain (Sutula and Pitkanen 2002). There is even evidence that a brief single unilateral hippocampal electrical stimulation in rats, producing focal epileptiform activity lasting around 80 sec, induced programmed cell death bilaterally within the dentate gyrus 5 h later (Bengzon et al 1997, Bengzon et al 2002). However, the consequences of different types of seizures and SE may vary substantially, ranging from functional and structural changes in single neurons and glial cells, dysfunction of intracellular compartments/mitochondria, disturbed electrical and chemical activity in neural circuitries, altered systemic body functions, blood-brain barrier and immune reactions, to irreversible brain pathology with cell death and scar formation. The latter is most commonly ascribed to conditions of persistent seizure activity, such as during SE. The complexity increases when taking in to account the different triggering factors and origins of seizures, as well as the endogenous individual susceptibility for seizure induction, persistence and progression. In order to improve prediction of clinical outcome and sequelae following seizures or SE, a deeper knowledge in the seizure-induced

pathology stratified according to seizure type, etiology and endogenous individual vulnerability/comorbidities appears today as important as 100 years ago.

After reviewing the data available on animal models of FSE, we distinguished between FSE that feature focal seizures without and with bilateral convulsions. Both FncSEs and FbcSEs induce obvious neuropathological changes at the site of action of the primary epileptogenic agent, either local drug application or local electrical stimulation. Contralateral changes with direct contact to the epileptogenic focus, such as left and right hippocampus, also show long-lasting pathology, though often less prominent than the ipsilateral reaction. Remote changes have been sporadically described in FncSE, but it is more pronounced after FbcSE. On the other hand, convulsive generalized seizures during FbcSE are commonly associated to pathogenic and long-lasting alterations of brain tissue in regions contralateral and distant from the site of action of the focal epileptogenic agent. These data suggest that truly focal SEs do not generate secondary pathology outside the region of action of the *noxa patogena* and support the notion that the presence of convulsive seizures correlates with diffuse tissue neuropathology.

In Tables 2 and 3, we highlight manuscripts that have identified the methods for FncSE induction and presented during FSE at least 90% of focal seizures or <3 Racine score seizures verified by video-EEG monitoring. The revision of the literature has been facilitated when the description of the animal models provided the following details, that we strongly recommend to explicitly describe for the characterization of a SE model: 1) the induction and termination regime, e.g. chemical doses/stimulation parameters (intensity, frequency and duration)/location; 2) seizure semiology during FSE, differentiating and defining the duration of focal/multifocal/secondary generalized bilateral convulsive seizures; 3) EEG parameters during the FSE measured using i.e. 24/7hrs video-EEG recordings and whether intra or/and extracranial electrodes were utilized, in order to define spatial and temporal development of ictal and interictal epileptiform activity; 4) the presence of chronic cognitive consequences and epilepsy development after FSE. The degree of different seizure semiology and electrographic activity (focal vs bilateral convulsive behavior and focal vs bilateral epileptiform activity) during the FSE may explain the variation of reported brain pathology in these FSE models (Sutula and Pitkanen 2002) and need to be distinguished and taken into account when predicting pathophysiology following FncSE and FbcSE in patients.

Table 1: schematic overview of the ILAE SE semiology classification (after (2)**).**

Main category	Sub-categories	Comment
A.1 Convulsive SE	A.1.a Generalized convulsive A.1.b Focal onset evolving into bilateral convulsive A.1.c Unknown whether generalized or focal	Focal origin difficult to assess clinically; history is of great help
A.2 Myoclonic SE	A.2.a With coma A.2.b Without coma	Generalized
A.3 Focal motor SE	A.3.a Repeated focal motor seizures A.3.b Epilepsia partialis continua A.3.c Adversive status A.3.d Oculoclonic status A.3.e Ictal paresis	
A.4 Tonic SE		Generalized, rare, mostly in pt with developmental retardation
A.5 Hyperkinetic SE		Extremely rare, focal
B.1 Non convulsive SE with coma		May be generalized or focal
B.2 Non convulsive SE without coma	B.2.a. Generalized B.2.a.a Typical absence status B.2.a.b Atypical absence status B.2.a.c Myoclonic absence status	
	B.2.b. Focal B.2.b.a Without awareness impairment B.2.b.b Aphasic status B.2.b.c With awareness impairment	
	B.2.c Unknown B.2.c.a Autonomic SE	Very rare, focal

Table 2. Animal models of drug-induced focal status epilepticus. Fluoro jade: FJ; hematoxylin eosin: HE; parvalbumin: PV; calretinin: CR; calbindin: CB; [14C]2-Deoxyglucose: 2DG; video-EEG: VEEG; diazepam: DZP; phenobarbital: PB; amygdala: AMY; basolateral amygdala: BLA; entorhinal cortex: EC; perirhinal cortex: PRC; hippocampus: HPC; dose dependent: d.d.; not evaluated: n.e; 2-photon microscophy: 2PM.

author	year	specie	injected region	EEG	SE duration	SE terminatio	SE semeiology		stainings / markers / techniques	damage		
							focal	convulsive		ipsilat	contralat	extra-limbic
intrahippocampal KA												
Schwarcz	1978	rat	-	no	n.e	-	yes	yes (>7nM)	Nissl, GAD, CAT, Th hydroxylase muscarinic rec., GABA, ACH, NA, synaptosomal uptake	yes	no	d.d. > 20 nM
Ben-Ari	1979	rat	-	EEG	4-7h	DZP	-	yes	Nissl, Fink-heimer	yes	yes	yes,
Schwob	1980	rat	-	no	n.e	-	-	yes	Thionine, Nissl, cupric silver	yes	yes	yes
French	**1982**	**rat**	**CA3**	**VEEG**	**2-4h**	**-**	**yes**	**-**	**Nissl, Thionin**	**yes**	**no**	**n.e.**
Cavalheiro	1982	rat	CA1, CA3	VEEG	d.d.	-	-	yes	Nissl, Luxol fast blue	yes	d.d.	yes d.d.
Tanaka	**1982**	**cat**	**CA2**	**VEEG**	**d.d.**	**-**	**yes**	**-**	**Nissl, HE**	**yes**	**d.d.**	**yes d.d.**
Mathern	**1993**	**rat**	**-**	**VEEG**	**4-6h**	**-**	**yes**	**-**	**Timm, Nissl**	**yes**	**yes**	**n.e.**
Magloczky	1993 & 1995	rat	CA3	no	n.e	-	-	yes	PV, CB, CR, HSP, 5HT, Silver impregnation	yes	CA3 CA1	n.e.
Leite	**1996**	**rat**	**-**	**VEEG**	**5-6h**	**-**	**yes <PN14**	**yes >PN15**	**Timm, Nissl**	**yes**	**no**	**n.e.**
Bragin	1999	rat	-	VEEG	n.e	-	?	?	Timm, Nissl	yes	yes	n.e.
Bouilleret	**1999**	**mouse**	**-**	**VEEG**	**3-6h**	**-**	**yes**	**few**	**GFAP, Timm, E-NCAM, CV,2DG**	**yes**	**no**	**n.e.**
Moneta	2002	mouse		VEEG					Nissl, FJ	yes	no	thalamus
Schauwecker	2002	mouse	CA3	no	n.e	-	-	yes	Nissl, Fink-Heimer, FJ, GFAP	yes	no	no
Riban	**2002**	**mouse**	**-**	**EEG**	**<10h**	**-**	**yes**	**50%**	**Nissl**	**yes**	**no**	**no**
Arabadzisz	**2005**	**mouse**	**CA1**	**EEG**	**n.e**	**-**	**yes**	**-**	**Nissl, NeuN, CCK8, VIP, 5HT, NPY, CB, PV, Galanin, CR, Diasorin, EEG spectral analysis**	**yes**	**no**	**n.e.**
Grotcke	**2008**	**mouse**	**CA1**	**VEEG**	**9-17h**	**-**	**yes**	**in 11% mice**	**FJ, Thionine, behaviour**	**yes**	**no**	**n.e.**
Raedt	2009	rat	-	VEEG	9-10h	PB		yes	Vimentin, CD11 b/c, Timm	yes	n.e.	n.e.
Pernot	2011	mouse	-	VEEG	n.e	-	yes	rare	GFAP, GSA, lectin, (H&P),Tunel, mRNA for IL-1β, COX-2,cPLA2-α, SOCS3, IL-1Ra	yes	no	n.e.
Carriero	**2012**	**guinea pig**	**CA1**	**VEEG**	**n.e**	**-**	**yes**	**-**	**Timm, GFAP, Thionine**	**yes**	**no**	**n.e.**
Rattka	2013	rat	CA3	VEEG	4-20h	-	-	yes	Nissl,Thionin, Bahavior	yes	no	yes - mild
Noé	**2019**	**guinea pig**	**CA1**	**VEEG**	**<20 h**	**-**	**yes**	**<10% TCG**	**GFAP, IgG, MAP2, NeuN,FJ, Tunnel, MRI**	**yes**	**no**	**n.e.**
Welzel	**2019**	**mouse**	**CA1**	**VEEG**	**15-18h**	**-**	**yes**	**sporadic TCG**	**Thionine**	**yes**	**no**	**n.e.**
Vila-Verde	**2021**	**guinea pig**	**CA1**	**VEEG**	**<20 h**		**yes**	**<10%**	**Nissl, GFAP, IgG, MAP2; IL1β, COX2, HO1, cFos, AQP4 and Kir4.1 RNA expr.**	**yes**	**no ***	**n.e.**

intra-amygdala KA													
Ben-Ari	1980	rat	AMY	EEG	2-6h	DZP	-	yes	Nissl,Fink-heimer	yes	yes	yes	yes
Berger	1989	rat	AMY	**no**	n.e	DZP	yes	-	Nissl, HE, Giemsa, Van Giesson, Prussian blue, Kluver-Barrera, GFAP	yes	yes	yes	yes
Tanaka	**1985**	**cat**	**AMY**	**EEG**	**n.e**	**-**	**yes**	**sporadic TCG**	**Nissl, HE**	**yes**	**yes***	**yes - mild**	
Araki	2002	mouse	BLA	EEG	d.d.	DZP	-	yes	Tunel, Nissl, DAPI, Caspase-3,NeuN, Laser-Doppler flowmetry	yes	CA1,CA3	no	
Mouri	2008	mouse	AMY	VEEG	n.e	LRZP	-	yes	FJ, NeuN, GFAP, NPY	CA1, CA3	no	EC, PRC, temporal NC	
Welzel	2019	mouse	BLA	VEEG	12-13h	-	-	yes	Thionine	AMY, CA3,	no	n.e.	
intracortical KA													
Bedner	2015	mouse	-	VEEG	4.4 ± 2.4 h	-	-	yes	FJ, Tunel, GFAP, Iba1, NeuN,S100B, NG2, PDGFRA, GJB6,GJA1, 2PM	yes	no	n.e.	
intraventricular KA													
Nadler	1978	rat	-	no	3-4.5 h	no	-	yes	Nissl	yes	no	d.d.	
Sater	1978	rat	-	EEG HPC & AMY	n.e.	no	-	yes	Silver impregnation	yes	no	d.d.	
Kleinrok	1980	rat	-	no	2 h	no	yes?	no	n.e.	n.e.	n.e.	n.e.	
intrahippocampal PILOCARPINE													
Furtado	2002 & 2011	rat	Hilus	VEEG	n.e	DZP	-	yes	FJ, Timm, Nissl	yes	yes	n.e.	

Table 3. Animal models of electrical stimulation-induced focal status epilepticus. Video-EEG: VEEG; diazepam: DZP; phenobarbital: PB; amygdala: AMY; basolateral amygdala: BLA; olfactory bulbs: OB; entorhinal cortex: EC; perirhinal cortex: PRC; piriform cortex: PC; hippocampus: HPC; neocortex NC;

presubiculum: preS; parasubiculum: paraS; subiculum: S; thalamus: T; dose dependent: d.d.; not evaluated: n.e; 2-photon microscophy: 2PM.

author	year	specie	stimulation		EEG	SE duration	SE termination	SE semeiology		stainings / markers / techniques	damage		
			site	pattern				focal	convulsive		ipsi	contra	extra-limbic
McIntyre	1982	rat	BLA	kindling SSSE	EEG	-	PB			Nissl	yes	no	OB, T PC EC
Sloviter	1983	rat	PP	40ms, 2Hz x 2-24 h	no	-	-	-	-	Nissl, Timm, Electrophysiology, Rapid Golgi	yes	yes	n.e.
Lothman	1989	rat	HIP	10s, 50 Hz, 1 ms x 9 min	EEG		-			-	-	-	-
Handforth	1992	rat	AMY	5s, 60Hz, 1 ms	EEG		-		mostly	-	-	-	-
Marazati	1998	rat	PP	10s, 20 Hz, 0.1 ms x 30 min	EEG		-			HE	yes	yes	EC, PC, CC, S, septum, T
Nissinen	2000	rat	AMY	0.5s, 60 Hz, 1ms x 20-30 min	VEEG		-			Nissl, Timm, Morris water-maze	yes	yes	PC, EC
Gorter	2001	rat	PP	10s, 50-Hz , 1.5h, 10s on/ 3s off	EEG		PB		mostly	Nissl, Timm, PV, 5HT, NeuN	yes	yes - mild	PC, EC, T
Gorter	2002	rat	PP	10s, 50-Hz , 1.5h, 10s on/ 3s off	EEG		-			Timm, PV, GFAP, Vimentin, CD 11b/c, NaCh β1 Na-channel	yes	n.e.	β1+ astrocyte in EC
Pitkanen	2002	rat	AMY	2x 100 ms/s, 60-Hz , 20 min	VEEG		DZP			Thionine, FJ, Timm, MRI, Stereologic analysi	yes	n.e.	PC, T
Ekdahl	**2003**	**rat**	**HPC**	**50 Hz, 1-1.5h, every 9th 1 min on/off**	**EEG**	**2h**	**PB**	**81%**	**13%**	**NeuN, FJ, CD68, BrdUrd, Doublecortin, Ki67**	**yes**	**n.e.**	**n.e.**
Gorter	2003	rat	HPC	10s, 50-Hz , 1.5h, 10s on/ 3s off	VEEG	4h	PB			Nissl, TUNEL, FJ, NeuN, CD11b/c, GFAP	yes	no	ParaS, PC
Brandt	2003	rat	BLA	50 Hz, 1ms, 25 min	EEG		DZP			Thionine, Nissl	yes	d.d	PC,EC, T
Mohapel	**2004**	**rat**	**HPC**	**50 Hz, 1h, every 9th min 1 min off**	**EEG**	**3h**	**PB**	**93-94%**	**72%**	**NeuN, PV, NPY, FJ, Tunel, Ki 67, BrdU**	**yes**	**yes**	**n.e.**
Van Vliet	2004	rat	PP	10s, 50-Hz , 1.5h, 10s on/ 3s off	VEEG	4h	PB			Nissl, NeuN, PV, CR GABA, Timm	yes	n.e.	EC, perS, paraS, S
Pitkanen	2005	rat	AMY	0.5s, 60 Hz, 1ms, 20-30 min	VEEG	2-3h	DZP			Thionine, Timm	yes	yes	n.e.
Iosif	2006	mouse	HPC	50 Hz, 1h, every 9th min 1 min off		2h	PB	83-98%	2-17%	NeuN, S100β, Iba-1, FJ, BrdU, p-H3, PCNA,	yes	n.e.	n.e.
Kienzler	2006	mouse	PP	40ms, 2Hz x 2-24 h	EEG	-				NeuN, Nissl	yes	no	n.e.
Bumanglag	2008	rat	PP	40ms, 2Hz for 3h+10s 20 Hz once per min	VEEG	3h	Halot		yes	Nissl, FJ, NeuN	yes	yes	EC, PRC, T, septum, caudate
Norwood	2010	rat	PP	40ms, 2Hz, 30 min+10s, 20 Hz 2 dd, followed by 1d 8h	VEEG	3h	Halot		yes	Nissl, NeuN, FJ, Timm, MRI	yes	n.e.	EC, T, septum
Ahl	**2016**	**rats**	**HPC**	**50 Hz, 1h, every 9th min 1 min off**	**EEG**	**2h**	**PB**	**97%**	**3%**	**FJ, Iba1, GFAP, IL1β, TNFα, IFNγ, IL4/5/6/10/13, CD-45 GADPH, KC/GRO, PSD-95, CX3CR1, CD68/ED1, NG2**	**yes**	**yes**	**n.e.**
Lewczuk	2017	mouse	HPC	10s, 50-Hz , 1h, 10s on/ 5s off	VEEG	-	-			FJ, NeuN, EEG spectrum analysis	yes	n.e.	n.e.
Bumanglag	**2018**	**rat**	**PP**	**40ms, 2Hz fx 24h+10s 20 Hz**	**VEEG**		**Uret**	**yes**		**Nissl, FJ, Timm, fluoro gold**	**yes**	**n.e.**	**ParaS, EC, PRC, septum**
Avdic	**2018**	**rat mouse**	**HPC**	**50 Hz, 1h, every 9th min 1 min off**	**VEEG**	**2h**	**PB**	**94%**	**6%**	**MRI-DTI, FJ, HE, NeuN, Iba1, GFAP, S100β, PSD95, cadherin, gephyrin, NL-2, neurofascin, Synapsin**	**yes**	**yes**	**NC sub-cortex**

Table 4. Other models of focal status epilepticus.

author	year	specie	injected region	EEG	SE duration	SE termination	SE semeiology		stainings / markers / techniques	damage		
							focal	convulsive		ipsilat	contralat	extra-limbic
low dose PILO i.p.												
Turski	1983 & 1985	rat	i.p.	EEG HPC, AMY, ctx	2 h	no	yes	no	Nissl	no	no	no
Cook	1998	rat	i.p.	no	n.e.	no	yes	no	Behavioral test	n.e.	n.e.	n.e.
Mikulecka	2000	rat	i.p.	EEG HPC, ctx	<2.5 h		yes	no	Nissl, behavioral tests	n.e.	n.e.	yes
Krsek	2001 & 2004	rat	ip	EEG HPC & ctx	n.e		yes	no?	PV, CB, Nissl, Timm,	n.e.	n.e.	yes
low dose KA i.v. s.c. or i.p.												
Lothman	1981	rat	i.v.	EEG HPC, AMY, EC & striatum	2h	no	yes	no	Thionin, [14C]2-Deoxyglucose	no	no	no
Sperk	1985	rat	s.c.	no	n.e.	no	yes	no	Nissl, HE, Luxol, bodian, [14C]GAD-ChaT	no	no	no
Schwob	1980	rat	i.p.	no	n.e.	no	yes	no	Thionin, cupric silver method	no	no	no
Koryntova	1997 & 1998	rat	i.p.	EEG ctx	>2 h	no	yes	no	Nissl	no	no	no
Mikulecka	1999	rat	i.p.	no	n.e.	no	yes	no	Behavioral tests	n.e.	n.e.	n.e.
intrahippocampal SSP-saporin												
Martin	2001	rat	-	no	n.e	-	no	no	NeuN, GFAP, Zinc transporter 3, PV, CB, CR, GLUr 2, 5HT, GABA, SPr, CCK8, β-synuclein	yes	no	n.e.
Chun	**2019**	**rat**	**-**	**VEEG**	**n.e**	**-**	**yes?**	**-**	**PV, Neurokinin-1**	**yes**	**no**	**n.e.**
intracortical cobalt+homocysteine i.p.												
Singh	2020	mouse	cortex	Yes	1-2h	-	yes	yes	FJ, NeuN, MRI	yes	no	yes
Lateral fluid-percussion injury												
Andrade	2019	rat	cortex	VEEG	6-8h	-	yes	-	Thionin	yes	n.e.	n.e.

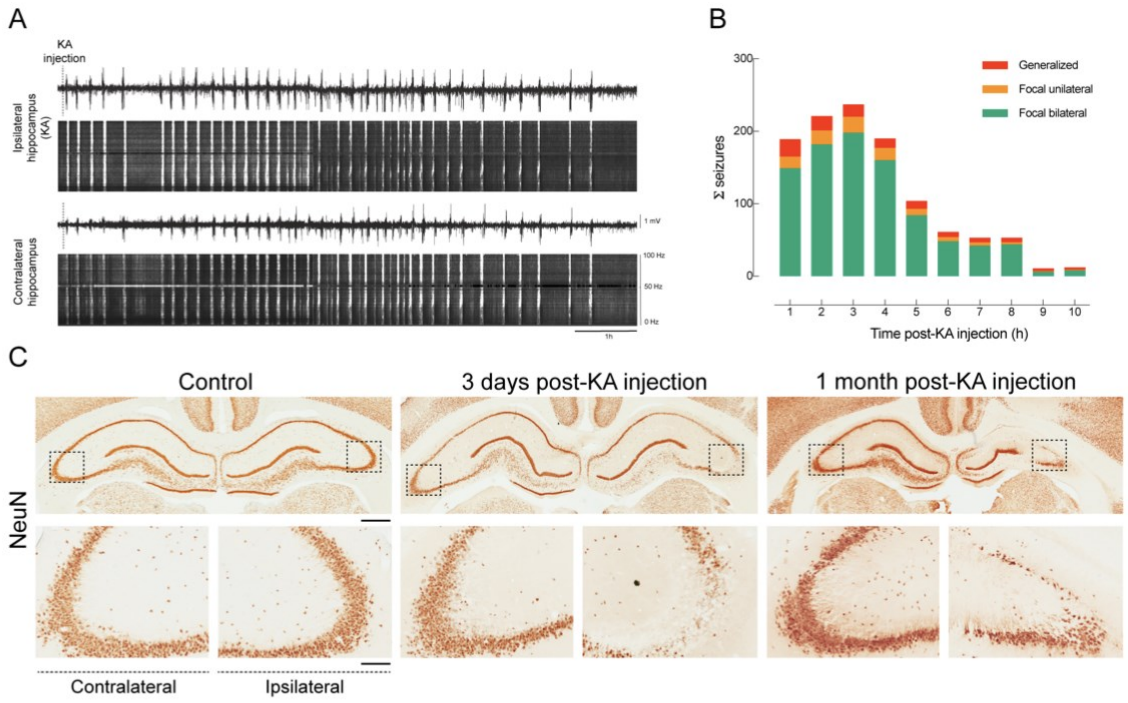

Figure 1. EEG and neuropathological changes in the guinea pig FncSE model induced by unilateral intra-hippocampal injection of kainic acid. A. percentage of convulsive generalized seizures (red) and focal seizures with unilateral (orange) and bilateral (grey) EEG discharges observed by video-EEG monitoring performed during the FSE. B. In vivo intrahippocampal recordings in the CA1 regions ipsilateral (lower trace) and contralateral (upper trace) to KA injection. The lower plot in each panel shows the complete spectrogram of the EEG trace. Typical example of the development of a FncSE characterized by bilateral hippocampal seizures (vertical lines in the spectrogram) with larger amplitude in the CA1 region injected with KA. C. NeuN-stained coronal sections of control sham-operated animals (left panels), 3 days after FncSE induced by KA injection in the right CA1 region (middle panel) and 1 month after right KA injection. In each panel high power magnifications of the region outlined by the dotted areas in the left and right hippocampi are illustrated.

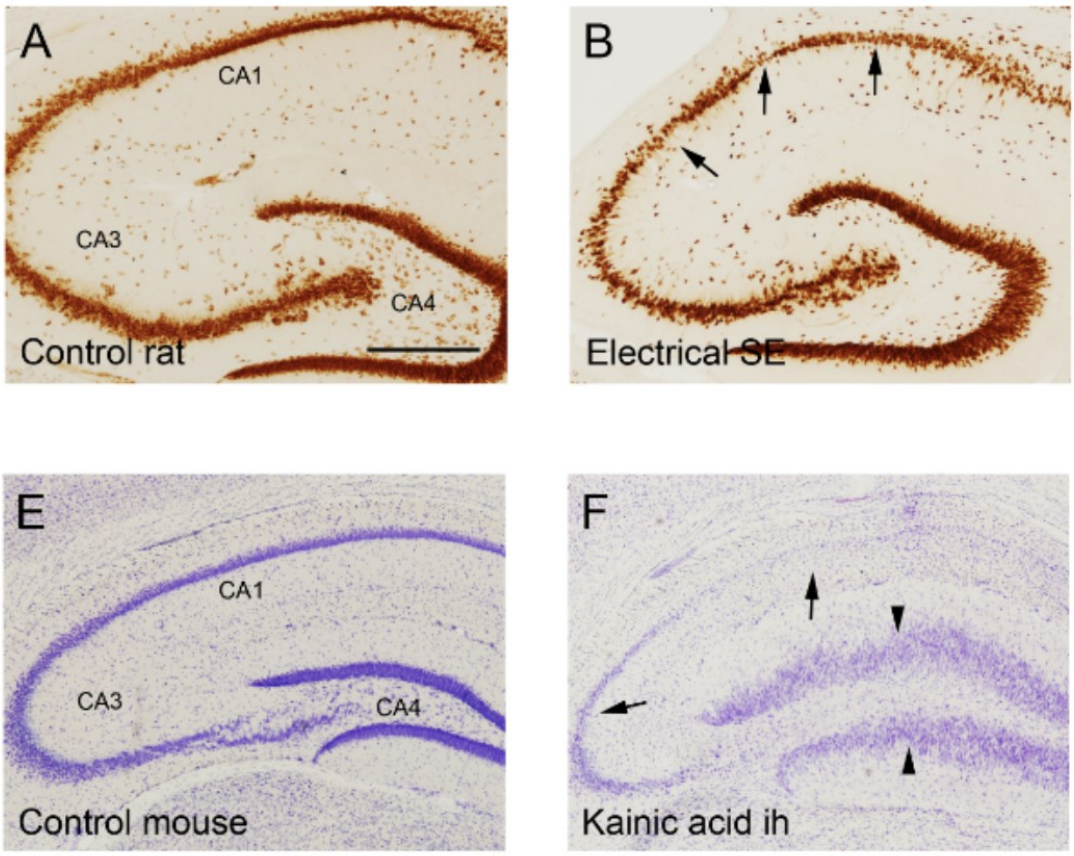

Figure 2. Neuropathological changes in FbcSE induced in the rat by electrical stimulation (A, B) and by intrahippocampal injection of KA in the mouse (E, F).

References

1. Neligan A, Noyce AJ, Gosavi TD, Shorvon SD, Kohler S, Walker MC. Change in Mortality of Generalized Convulsive Status Epilepticus in High-Income Countries Over Time: A Systematic Review and Meta-analysis. JAMA neurology 2019.

2. Trinka E, Cock H, Hesdorffer D, et al. A definition and classification of status epilepticus--Report of the ILAE Task Force on Classification of Status Epilepticus. Epilepsia 2015;56:1515-1523.

3. Young GB, Claassen J. Nonconvulsive status epilepticus and brain damage: further evidence, more questions. Neurology 2010;75:760-761.

4. Kaplan PW. No, some types of nonconvulsive status epilepticus cause little permanent neurologic sequelae (or: "the cure may be worse than the disease"). Neurophysiologie clinique = Clinical neurophysiology 2000;30:377-382.

5. Sutter R, Marsch S, Fuhr P, Kaplan PW, Ruegg S. Anesthetic drugs in status epilepticus: Risk or rescue?: A 6-year cohort study. Neurology 2014;82:656-664.

6. Bergin PS, Brockington A, Jayabal J, et al. Status epilepticus in Auckland, New Zealand: Incidence, etiology, and outcomes. Epilepsia 2019;60:1552-1564.

7. Leitinger M, Trinka E, Giovannini G, et al. Epidemiology of status epilepticus in adults: A population-based study on incidence, causes, and outcomes. Epilepsia 2019;60:53-62.

8. Rossetti AO, Trinka E, Stahli C, Novy J. New ILAE versus previous clinical status epilepticus semiologic classification: Analysis of a hospital-based cohort. Epilepsia 2016;57:1036-1041.

9. Sutter R, Kaplan PW, Ruegg S. Outcome predictors for status epilepticus--what really counts. Nature reviews Neurology 2013;9:525-534.

10. Alvarez V, Januel JM, Burnand B, Rossetti AO. Role of comorbidities in outcome prediction after status epilepticus. Epilepsia 2012;53:e89-92.

11. Kellinghaus C, Rossetti AO, Trinka E, et al. Factors predicting cessation of status epilepticus in clinical practice: Data from a prospective observational registry (SENSE). Annals of neurology 2019;85:421-432.

12. Rossetti AO, Alvarez V, Januel JM, Burnand B. Treatment deviating from guidelines does not influence status epilepticus prognosis. Journal of neurology 2013;260:421-428.

13. Rossetti AO, Logroscino G, Liaudet L, et al. Status epilepticus: an independent outcome predictor after cerebral anoxia. Neurology 2007;69:255-260.

14. Knake S, Rochon J, Fleischer S, et al. Status epilepticus after stroke is associated with increased long-term case fatality. Epilepsia 2006;47:2020-2026.

15. Logroscino G, Hesdorffer DC, Cascino G, Hauser WA. Status epilepticus without an underlying cause and risk of death: a population-based study. Arch Neurol 2008;65:221-224

Veni Vidi Vici